

10-27-2015

Elemental Analysis of Printing Inks Using Tandem Laser- Induced Breakdown Spectroscopy and Laser Ablation Inductively Coupled Plasma Mass Spectrometry

Kiran Subedi

Florida International University, ksube001@fiu.edu

DOI: 10.25148/etd.FIDC000153

Follow this and additional works at: <https://digitalcommons.fiu.edu/etd>

 Part of the [Analytical Chemistry Commons](#)

Recommended Citation

Subedi, Kiran, "Elemental Analysis of Printing Inks Using Tandem Laser- Induced Breakdown Spectroscopy and Laser Ablation Inductively Coupled Plasma Mass Spectrometry" (2015). *FIU Electronic Theses and Dissertations*. 2263.
<https://digitalcommons.fiu.edu/etd/2263>

This work is brought to you for free and open access by the University Graduate School at FIU Digital Commons. It has been accepted for inclusion in FIU Electronic Theses and Dissertations by an authorized administrator of FIU Digital Commons. For more information, please contact dcc@fiu.edu.

FLORIDA INTERNATIONAL UNIVERSITY

Miami, Florida

ELEMENTAL ANALYSIS OF PRINTING INKS USING TANDEM LASER-
INDUCED BREAKDOWN SPECTROSCOPY AND LASER ABLATION
INDUCTIVELY COUPLED PLASMA MASS SPECTROMETRY

A dissertation submitted in partial fulfillment of

the requirements for the degree of

DOCTOR OF PHILOSOPHY

in

CHEMISTRY

by

Kiran Subedi

2015

To: Dean Michael R. Heithaus
College of Arts and Sciences

This dissertation, written by Kiran Subedi, and entitled Elemental Analysis of Printing Inks Using Tandem Tandem Laser-Induced Breakdown Spectroscopy and Laser Ablation Inductively Coupled Plasma Mass Spectrometry, having been approved in respect to style and intellectual content, is referred to you for judgment.

We have read this dissertation and recommend that it be approved.

Yong Cai

Francisco Fernandez-Lima

Jaroslava Miksovska

Jin He

José R. Almirall, Major Professor

Date of Defense: October 27, 2015

The dissertation of Kiran Subedi is approved.

Dean Michael R. Heithaus
College of Arts and Sciences

Dean Lakshmi N. Reddi
University Graduate School

Florida International University, 2015

DEDICATION

This dissertation is dedicated to my family in Nepal for their unconditional support for my studies and for believing in me. I would also like to dedicate this work to my friends, football, and Anu. I could not have done this without you.

ACKNOWLEDGMENTS

I have been inspired by a lot of people throughout my life. My time at Florida International University (FIU) has been the most memorable. My family, teachers, and friends in Nepal have always encouraged me to work harder. Their unwavering love and motivation has been the driving force for my overseas study. I am very much thankful to FIU for granting me the Presidential Fellowship and with it, a golden opportunity to pursue my PhD in the Chemistry Department. I was also awarded the prestigious Dissertation Year Fellowship (DYF) by the University Graduate School at FIU during the final phase of my PhD career, and I feel very much privileged to receive such an honor. I would like to extend my sincere gratitude to my professors, colleagues, and friends who have contributed directly or indirectly for the completion of this degree.

Dr. Almirall, my supervisor, has always been an exemplary figure in my life. I feel honored to complete my research under his mentorship. I wish to extend my utmost gratitude to him for his patient guidance, encouragement, and advice through out my time as his student. I am thankful to my research committee members Dr. Yong Cai, Dr. Francisco Fernandez Lima, Dr. Jaroslava Miksovska, and Dr. Jin He for their valuable advisements and recommendations for my research. I would also like to take this opportunity to express my gratitude to Dr. James Curran for his inspiring guidance in statistical data analysis. I would like to thank GPSC (Graduate and Professional Student Council) and the Dean's Office for funding my travels to different conferences, which helped me to present my research and exchange ideas with great scientists across the world.

I have been extremely lucky to be a part of the Almirall research group (the A-team) where everyone has been very supportive of me, which has made me feel like I am at home. In particular, I am grateful to Dr. Tatiana Trejos, for her continuous support and encouragement. I have been inspired by her knowledge, experience, and commitment to the highest standards. I also extend my heartfelt gratitude to Pupi Tomassini, the senior secretary at IFRI (International Forensic Research Institute) for her support and care. Completing this work without all of your support and constant encouragement would have been very difficult. I believe the Lord will bless you all for the precious contributions you have made.

ABSTRACT OF THE DISSERTATION
ELEMENTAL ANALYSIS OF PRINTING INKS USING TANDEM LASER- INDUCED
BREAKDOWN SPECTROSCOPY AND LASER ABLATION INDUCTIVELY
COUPLED PLASMA MASS SPECTROMETRY

by

Kiran Subedi

Florida International University, 2015

Miami, Florida

Professor José R. Almirall, Major Professor

As a consequence of the widespread use of computers coupled to high-quality printers and different types of papers, forgery, counterfeiting, change of wills, anonymous letter writing and felonious use of the documents have become serious problems. Forensic analysts are always seeking methods that can provide reliable information on whether a specimen collected at the crime scene is linked to the crime or to a source of known origin. Sensitive methods that can provide more detailed characterization of natural or man-made materials or even provide information not previously available to forensic examiners.

Recent advances in rapid solid sampling of materials using laser ablation (LA) coupled to inductively coupled plasma mass spectroscopy (ICP-MS) have led to this analytical method to be regarded as the gold standard in the field of elemental analysis for trace level components in solids. Another, emerging, analytical technique that uses the same laser pulse to generate a plasma that can be interrogated with spectroscopy is laser induced break down spectroscopy (LIBS).

The analysis of ink and paper is also possible because of the surface removal effect of laser interactions with the samples. In the present study, printing inks were analyzed using LIBS, LA-ICP-MS and both of them in tandem mode. In the tandem setup, the light generated during the relaxation of the excited species (LIBS) was used to create a spectral signature of the elements, and the mass-to-charge ratio of the ejected particles (ICP-MS) was used to create a mass spectrum.

For a set of 319 printing ink samples, LA-ICP-MS alone provided discrimination greater than 99%. A subset of 43 printing inks, having a very similar elemental profile, was analyzed by tandem LIBS/LA-ICP-MS. The fusion of LIBS and LA-ICP-MS provided additional discrimination through the detection of elements like Ca, Si, Fe, and K by LIBS, that are difficult to detect and confirm using standalone ICP-MS because of the spectral interferences (isobaric and polyatomic) involved. The combination of these two sensors was found to minimize the individual limitations and provide a more complete and representative chemical characterization of printing inks.

TABLE OF CONTENTS

CHAPTER	PAGE
Chapter 1. Introduction	1
1.1 Motivation for Research	1
1.2 Goals of This Research	3
1.3 Introduction to Analytical Tools	4
1.3.1 LIBS	4
1.3.1.1 The Physics of Plasma in LIBS	6
1.3.2 LA-ICP-MS	8
1.4 Literature Review of LIBS and LA-ICP-MS on Ink Analysis	12
1.5 Tandem LIBS/LA-ICP-MS	12
1.5.1 Principles of Tandem LIBS/LA-ICP-MS	13
1.5.2 Significance of Tandem LIBS/LA-ICP-MS	15
1.5.3 Literature Review of LIBS and LA-ICP-MS Used Together	16
1.6 Introduction to Printing Inks	16
1.6.1 Types of Printing Inks	17
1.6.1.1 Inkjet Printing Inks	17
1.6.1.2 Toner Printing Inks	18
1.6.1.3 Intaglio Printing Inks	19
1.6.1.4 Offset Printing Inks	20
Chapter 2. Experimental and Materials for LA-ICP-MS	21
2.1 Sample Set Collection	21
2.1.1 Toner Collection Set	21
2.1.2 Inkjet Collection Set	22
2.1.3 Intaglio Collection set	23
2.1.4 Offset Collection Set	24
2.2 Sample Preparation	25
2.1.2.1 Sample Preparation for Toner Printing Inks	26
2.1.2.3 Sample Preparation for Inkjet Printing Inks	26
2.1.2.4 Sample Preparation for Intaglio Printing Inks	27
2.1.2.5 Sample Preparation for Offset Printing Inks	28
Chapter 3. Method Development and Optimization of Standalone LA-ICP-MS	29
3.1 Experimental for LA-ICP-MS	29
3.2 Method Development and Optimization	30
3.2.1 Optimization of Parameters for Toner Printing Inks	31
3.2.2 Optimization of Parameters for Inkjet Printing Inks	32
3.2.3 Optimization of Parameters for Intaglio Printing Inks	33
3.2.4 Optimization of Parameters for Offset Printing Inks	34
Chapter 4. Data Acquisition, Analysis and Results by Standalone LA-ICP-MS	35

4.1. Data Reduction and Comparison Strategies for LA-ICP-MS.....	35
4.2 Match Criteria	36
4.2.1 Spectral Overlay.....	36
4.2.2 Univariate Statistics (Significance Testing for Pairwise Comparisons).....	37
4.2.2.1 Analysis of Variance (ANOVA).....	38
4.2.2.2 Tukey’s Honestly Significant Difference Test	38
4.2.3 Multivariate Statistics	39
4.2.3.1 Principal Component Analysis (PCA).....	39
4.2.3.2 Linear Discriminant Analysis (LDA)	40
4.2.3.3 Cluster Analysis.....	40
4.3 Results for comparison of Toner Printing Inks.....	40
4.3.1 Black Toner Printing Inks.....	44
4.3.2 Cyan Toner Printing Inks.....	44
4.3.3 Yellow Toner Printing Inks	45
4.3.4 Magenta Toner Printing Inks	46
4.3.5 Overall Discrimination for Toner Printing Inks.....	47
4.3.6 Multivariate Analysis of Toner Printing Inks	51
4.3.6.1 Principal Component Analysis of Toner Printing Inks.....	51
4.3.6.2 Principal Component Analysis by Brand.....	53
4.3.6.3 Linear Discriminant Analysis (LDA) of Toner Printing Inks.....	54
4.3.6.4 Partial Least Squares Discriminant Analysis (PLS-DA) for Toner Printing Inks.....	56
4.3.6.5 K- Nearest Neighbor analysis (KNN classification) for Toner Printing Inks.....	58
4.4 Results for Comparison of Inkjet Printing Inks	59
4.4.1 Black Inkjet Printing Inks	62
4.4.2 Cyan Inkjet Printing Inks.....	62
4.4.3 Yellow Inkjet Printing Inks.....	63
4.4.4 Magenta Inkjet Printing Inks	64
4.4.5 Overall Discrimination for Inkjet Printing Inks.....	64
4.4.6 Multivariate Analysis of Inkjet Printing Inks	67
4.4.6.1 Principal Component Analysis of Inkjet Printing Inks	67
4.4.6.2 Linear Discriminant Analysis of Inkjet Printing Inks.....	70
4.4.6.3 Partial Least Squares Discriminant Analysis of Inkjet Printing Inks ...	72
4.4.6.4 K-Nearest Neighbor Analysis of Inkjet Printing Inks.....	73
4.5 Results for Comparison of Offset Printing Inks	74
4.5.1 Black Offset Printing Inks	76
4.5.2 Cyan Offset Printing Inks	77
4.5.3 Yellow Offset Printing Inks.....	77
4.5.4 Blue Offset Printing Inks	77
4.5.5 Magenta Offset Printing Inks.....	78
4.5.6 Red Offset Printing Inks	79
4.5.7 Different Colored Offset Printing Inks	80
4.5.8 Overall Discrimination for Offset Printing Inks	81
4.5.9 Multivariate Analysis of Offset Printing Inks.....	83

4.5.9.1 Principal Component Analysis of Offset Printing Inks	83
4.5.9.2 Linear Discriminant Analysis of Offset Printing Inks	86
4.5.9.3 Partial Least Square Discriminant Analysis of Offset Printing Inks	88
4.5.9.4 K-Nearest Neighbor Analysis of Offset Printing Inks	89
4.6 Results for Comparison of Intaglio Printing Inks	89
4.6.1 Aqua Intaglio Printing Inks.....	92
4.6.2 Gold Intaglio Printing Inks	93
4.6.3 Black Intaglio Printing Inks	93
4.6.4 Yellow Intaglio Printing Inks.....	94
4.6.4 Blue Intaglio Printing Inks.....	95
4.6.5 Brown Intaglio Printing Inks	95
4.6.6 Red Intaglio Printing Inks	96
4.6.6 Green Intaglio Printing Inks.....	97
4.6.7 Purple Intaglio Printing Inks.....	97
4.6.8 Maroon Intaglio Printing Inks.....	98
4.6.9 Orange Intaglio Printing Inks.....	99
4.6.10 Overall Discrimination for Intaglio Printing Inks.....	99
4.6.11 Multivariate Analysis of Intaglio Printing Inks	102
4.6.11.1 Principal Component Analysis of Intaglio Printing Inks	102
4.6.11.2 Linear Discriminant Analysis of Intaglio Printing Inks.....	106
4.6.11.3 Partial Least Square Discriminant Analysis of Intaglio Printing Inks.....	107
4.6.11.4 K-Nearest Neighbor Analysis of Intaglio Printing Inks	108
4.7 Canonical Discriminant Analysis of Intaglio Printing Inks	108
4.8 Conclusion	111
Chapter 5. Analysis of Ink Samples by LIBS	112
5.1 Instrumentation of LIBS	112
5.2 Sample Preparation for Analysis by LIBS	113
5.3 Optimization of LIBS for the Analysis of Inks.....	113
5.3.1 Use of Argon as an Ambient Gas	114
5.4 Data Analysis of LIBS for the Analysis of Printing Inks (Intaglio)	116
5.4 Conclusion	119
Chapter 6. Analysis of Printing Inks by Tandem LIBS/LA-ICP-MS and Normalization study.....	120
6.1 Sample selection for Tandem LIBS/LA-ICP-MS Analysis.....	121
6.2 Analysis of toner printing inks by tandem LIBS/LA-ICP-MS	121
6.2.1 Optimization of Tandem LIBS/LA-ICP-MS for the Analysis of Toners ..	123
6.2.2 Results from the Tandem LIBS/LA-ICP-MS Analysis of Toners.....	124
6.2.3 3 Multivariate Analysis of the Tandem LIBS/LA-ICP-MS data for Toners	126
6.2.3.1 Principal Component Analysis of Toners by LA-ICP-MS Spectrum.	126
6.2.3.2 Principal Component Analysis of Toners by LIBS Spectrum	127

6.2.3.3 Principal Component Analysis of Toners by the Fusion of LIBS and LA-ICP-MS Spectrum	129
6.2.3.4 Linear Discriminant Analysis of Toners by LIBS	130
6.2.3.5 Linear Discriminant Analysis of Toners by LA-ICP-MS.....	131
6.2.3.6 Linear Discriminant Analysis of Toners by the Fusion of LIBS and LA-ICP-MS	132
6.2.3.7 Canonical Discriminant Analysis of Toners by Tandem LIBS/LA-ICP-MS.....	133
6.2.3.8 Cluster Analysis of Toners by Tandem LIBS/LA-ICP-MS.....	134
6.3 Analysis of Inkjet Printing Inks by Tandem LIBS/LA-ICP-MS	136
6.3.1 Optimization of Tandem LIBS/LA-ICP-MS for the Analysis of Inkjets ..	137
6.3.2 Results for the Tandem LIBS/LA-ICP-MS Analysis of Inkjets	138
6.3.3 Multivariate Analysis of the Tandem LIBS/LA-ICP-MS data for Inkjets	139
6.3.3.1 Principal Component Analysis of Inkjets by LA-ICP-MS	139
6.3.3.2 Principal Component Analysis of Inkjets by LIBS.....	141
6.3.3.3 Principal Component Analysis of Inkjets by the Fusion of LIBS and LA-ICP-MS.....	142
6.3.3.4 Linear Discriminant Analysis of Inkjet Printing Inks by Tandem LIBS/LA-ICP-MS.....	144
6.3.3.4.1 Linear Discriminant Analysis using LA-ICP-MS for inkjets	144
6.3.3.4.2 Linear Discriminant Analysis Using LIBS for Inkjets	146
6.3.3.5 Linear Discriminant Analysis of Inkjets by the Fusion of LIBS and LA-ICP-MS.....	148
6.3.3.6 Cluster Analysis for Inkjet Printing Inks	150
6.4 Analysis of Intaglio Printing Inks by Tandem LIBS/LA-ICP-MS	152
6.4.1 Optimization of Tandem LIBS/LA-ICP-MS for the Analysis of Intaglio Printing Inks.....	153
6.4.2 Results from Tandem LIBS/LA-ICP-MS Analysis of Intaglio Printing Inks.....	153
6.4.3 Multivariate Analysis of Intaglio Printing Inks by Tandem LIBS/LA-ICP-MS.....	155
6.4.3.1 Principal Component Analysis of intaglio printing inks by LIBS.....	155
6.4.3.2 Principal Component Analysis of Intaglio Printing Inks by LA-ICP-MS	156
6.4.3.3 Principal Component Analysis of Intaglio Printing Inks by the Fusion of LIBS and LA-ICP-MS.....	158
6.4.3.4 Linear Discriminant Analysis of Intaglio Printing Inks by LIBS.....	160
6.4.3.5 Linear Discriminant Analysis of Intaglio Printing Inks by LA-ICP-MS	160
6.4.3.6 Linear Discriminant Analysis of Intaglio Printing Inks after the Fusion of LIBS and LA-ICP-MS.....	161
6.4.3.7 Cluster Analysis of Intaglio Printing Inks by Tandem LIBS/LA-ICP-MS.....	163
6.5 Analysis of Offset Printing Inks by Tandem LIBS/LA-ICP-MS.....	165
6.5.1 Optimization of Tandem LIBS/LA-ICP-MS for the Analysis of Offset	

Inks.....	166
6.5.2 Results from Tandem LIBS/LA-ICP-MS Analysis of Offset Printing Inks.....	167
6.5.3 Multivariate Analysis of Offset Printing Inks by tandem LIBS/LA-ICP-MS.....	168
6.5.3.1 Principal Component Analysis of Offset Printing Inks by LIBS.....	168
6.5.3.2 Principal Component Analysis of Offset Printing Inks by LA-ICP-MS	170
6.5.3.3 Principal Component Analysis of Offset Printing Inks by tandem LIBS/ LA-ICP-MS.....	171
6.5.3.4 Linear Discriminant Analysis of Offset Printing Inks by LIBS	173
6.5.3.5 Linear Discriminant Analysis of Offset Printing Inks by LA-ICP-MS	173
6.5.3.6 Linear Discriminant Analysis of Offset Printing Inks after the Fusion of LIBS and LA-ICP-MS.....	174
6.5.3.7 Cluster Analysis of Offset Printing Inks by LIBS	177
6.6 Analysis of Controls in Tandem LIBS/LA-ICP-MS Study	179
6.7 Calibration Curves and Limit of Detections	181
6.8 Data Fusion Using Machine Learning Algorithm and Chemometrics	183
6.8 Overall Results from Tandem LIBS/LA-ICP-MS Study of Printing Inks.....	185
6.9. Normalization of LA-ICP-MS Spectrum Using LIBS Spectrum	186
6.9.1 Optimization of Tandem LIBS/LA-ICP-MS for the Analysis of Glass Samples.....	187
6.9.2 Silicon as an Internal Standard	189
6.9.3 Normalization of LA-ICP-MS Spectra Using Si 288.1nm	190
6.9.4 Comparison with the Standard Test Method for Glass Analysis by LA-ICP-MS	191
6.9.5 Conclusion	193
Chapter 7. Contamination Study Using Tandem LIBS/LA-ICP-MS	194
7.1 Sample Preparation	194
7.2 Method Optimization.....	195
7.3 Results and Discussion	195
7.4 Statistical Analysis of Contaminated and Clean Printing Inks.....	198
7.4.1 One-Way ANOVA for Contaminated and Clean Printing Inks.....	198
7.4.2 Principal Component Analysis of Contaminated and Clean Printing Inks.....	201
7.4.3 Cluster Analysis for contaminated and clean printing inks	201
7.4.3 Canonical Correlation Analysis of Contaminated and Clean Printing Inks.....	202
7.5 Conclusion	203
Chapter 8. Summary	204
8.1 Future Directions of the Research Work	206

REFERENCES	208
VITA.....	214

LIST OF TABLES

TABLE	PAGE
Table 1. Optimized parameters for the analysis of toners by LA-ICP-MS.	31
Table 2. Optimized parameters for the analysis of inkjet printing inks by LA-ICP-MS.	32
Table 3. Optimized parameters for the analysis of intaglio printing inks by LA-ICP-MS.	33
Table 4. Optimized parameters for the analysis of offset printing inks by LA-ICP-MS.	34
Table 5. List of elements detected in toner printing inks by LA-ICP-MS.	41
Table 6. Discrimination capability of LA-ICP-MS for the analysis of toner printing inks.	47
Table 7. List of toner pairs that were indistinguishable by LA-ICP-MS.	48
Table 8. Overall Discrimination for toners in CMYK colors.	49
Table 9. PCA scores for first three components.	51
Table 10. Misclassified pairs by linear discriminant analysis	55
Table 11. List of common toner pairs that were not distinguished by Spectral Overlay and were also misclassified by LDA.	56
Table 12. List of elements detected in inkjet inks.	59
Table 13. Discrimination capability of LA-ICP-MS for inkjet inks.	65
Table 14. List of indistinguishable inkjet pairs by LA-ICP-MS.	65
Table 15. Discrimination capability of LA-ICP-MS in CMYK inkjets.	65
Table 16. PCA scores for the first three principal components in inkjets.	67
Table 17. List of inkjet pairs misclassified by LDA.	71
Table 18. List of common pairs indistinguishable by Spectral Overlay and LDA.	72

Table 19. List of elements detected in offset samples.	74
Table 20. Discrimination capability of LA-ICP-MS for the analysis of offset printing inks.	81
Table 21. List of offset printing ink pairs that were not distinguishable by LA-ICP-MS.	82
Table 22. PCA scores for the first three PCs in offset printing inks.	83
Table 23. List of misclassified offset pairs by LDA.	87
Table 24. Common offset pair that was indistinguishable (Spectral Overlay) and also misclassified (LDA).	88
Table 25. List of elements detected by LA-ICP-MS in 86 intaglio inks.	90
Table 26. List of indistinguishable intaglio pairs by LA-ICP-MS.	99
Table 27. Overall discrimination capability of LA-ICP-MS for the analysis of intaglio printing inks.	100
Table 28. PCA scores for the first three Principal Components in intaglio inks.	103
Table 29. List of intaglio printing ink pairs misclassified by LDA.	106
Table 30. Common intaglio pairs indistinguishable by Spectral Overlay and LDA. .	107
Table 31. Overall discrimination of four inks by LA-ICP-MS ⁶	111
Table 32. Optimized parameters for the analysis of intaglio inks by LIBS.	116
Table 33. List of elements detected by standalone LIBS.	117
Table 34. List of toner pairs used for the tandem LIBS/LA-ICP-MS study.	122
Table 35. List of toner pairs that were indistinguishable by LA-ICP-MS.	122
Table 36. Optimized parameters for the analysis of toners by tandem LIBS/LA-ICP-MS.	123
Table 37. List of elements detected in toners by LA-ICP-MS and LIBS in tandem mode ⁴¹	125
Table 38. Variances explained by the first three Principal Components.	126

Table 39. Variances explained by the first three PCs (LIBS).....	128
Table 40. Variances from the first three PCs after the fusion of LIBS and LA-ICP-MS.....	130
Table 41. Confusion matrix obtained from LDA of toners using LIBS only.....	131
Table 42. Misclassified toner pair by LDA using data from LIBS.....	131
Table 43. Confusion matrix from LDA for toners using LA-ICP-MS only.....	132
Table 44. Misclassified toner pair by LDA using data from LA-ICP-MS only.....	132
Table 45. Confusion matrix from LDA for toners after fusion of LIBS and LA-ICP-MS.....	132
Table 46. List of inkjet printing inks used for the tandem LIBS/LA-ICP-MS study.	137
Table 47. List of indistinguishable inkjet pairs when analyzed by standalone LA-ICP-MS.....	137
Table 48. Optimized parameters for the analysis of inkjets by tandem LIBS-LA-ICP-MS.....	138
Table 49. List of elements detected by LIBS and LA-ICP-MS in inkjets in tandem mode.....	139
Table 50. Variances explained by first three PCs using LA-ICP-MS.....	141
Table 51. Variances explained by the first three PCs.....	141
Table 52. Variances explained by the first three PCs after the fusion of LIBS and LA-ICP-MS.....	143
Table 53. Confusion matrix from LDA for inkjets using LA-ICP-MS.....	145
Table 54. Confusion matrix from LDA for inkjets using LIBS.....	147
Table 55. Confusion matrix from LDA for inkjets after data fusion of LIBS and LA-ICP-MS.....	149
Table 56. List of intaglio inks selected for tandem LIBS/LA-ICP-MS study.....	152
Table 57. List of indistinguishable pairs for standalone LA-ICP-MS.....	152

Table 58. Optimized parameters for the analysis of intaglio inks by tandem LIBS/LA-ICP-MS.....	153
Table 59. List of elements detected by LA-ICP-MS and additional elements detected by LIBS for intaglio printing inks.	154
Table 60. Variances explained by the first three PCs for intaglio inks by LIBS.....	156
Table 61. Variances explained by first three PCs for intaglio inks by LA-ICP-MS. .	157
Table 62. Variances explained by first three PCs after fusion of LIBS and LA-ICP-MS.....	158
Table 63. Confusion matrix for intaglio printing inks by LDA using LIBS.....	160
Table 64. Confusion matrix for intaglio by LDA using LA-ICP-MS.....	161
Table 65. Confusion matrix from LDA for intaglio after fusion of LIBS and LA-ICP-MS.	162
Table 66. List of offset printing inks used for tandem LIBS/LA-ICP-MS study.	166
Table 67. List of indistinguishable pairs of offset inks when analyzed by LA-ICP-MS.....	166
Table 68. Optimized parameters for the analysis of offsets by tandem LIBS/LA-ICP-MS.	167
Table 69. List of elements detected in offset printing inks by LIBS and LA-ICP-MS in tandem mode ⁴¹	168
Table 70. Variances explained in offset samples by first three PCs using LIBS.....	169
Table 71. Variances explained in offset samples by first three PCs using LA-ICP-MS.....	170
Table 72. Variances explained in offset samples by first three PCs after fusion of LIBS and LA-ICP-MS	171
Table 73. Confusion matrix from LDA for offset samples by LIBS	173
Table 74. Confusion matrix for offset inks from LDA by LA-ICP-MS.....	174
Table 75. Confusion matrix for offset inks from LDA after fusion of LIBS and LA-ICP-MS.	174

Table 76. Limits of detection for LIBS and LA-ICP-MS in tandem mode ⁴¹	182
Table 77. Overall discrimination for LIBS and LA-ICP-MS and their fusion for four printing ink types ⁴¹	186
Table 78. Optimized parameters for the analysis of glass by tandem LIBS/LA-ICP- MS.	189
Table 79. Optimized parameters for the analysis of toners and inkjets by tandem LIBS/LA-ICP-MS.	195

LIST OF FIGURES

FIGURE	PAGE
Figure 1. A 266nm laser focused on the surface of an ink sample placed inside an ablation chamber, produces a microplasma in the Argon atmosphere, the light emitted by the elements present in the ink sample are collected using Silica lens and transported by fiber optic cables to a spectrometer where the light is separated into spectral components and the signal is displayed as a function of wavelength.	5
Figure 2. Temporal evolution of LIBS plasma ²²	7
Figure 3. Various components inside an ICP torch.	9
Figure 4. A pulsed laser (266nm) is focused on an ink sample, which ablates a small amount of the sample. These fine particles are transported to the ICP by using Helium gas, where they get ionized. The ions are separated on the basis of their m/z ratio by a quadrupole mass analyzer and detected by using an Electron Multiplier Tube.....	11
Figure 5. Schematic of tandem LIBS/LA-ICP-MS. Two sensors, LIBS and LA-ICP-MS are performed simultaneously on the same printing ink ⁴¹	14
Figure 6. Liquid droplets are generated through the nozzle of ink reservoir, which wet the substrate on contact. Evaporation, of the solvent takes place followed by penetration and absorption of ink on to the paper fibers. Finally the ink is fixed and dried.	18
Figure 7. The drum inside the printer is negatively charged by a corona wire. A tiny laser light shone on the drum where the image is to be formed, discharges the negative charge. The toners stick to the image part, which is transferred to the paper using heat and pressure.	19
Figure 8. An image is itched into the surface of printing plate, which is then covered with intaglio ink. A paper is pressed against the plate, to force the ink into the grooves on paper. The final appearance is a raised print surface on the paper.....	20
Figure 9. Schematic of offset printing.	20
Figure 10. Pie chart (left) and bar graph (right) showing the distribution of printing inks.....	21
Figure 11. Pie Chart showing the distribution of different brands in the toner set.....	22

Figure 12. Pie chart showing the distribution of different colors in the toner set.....	22
Figure 13. Pie Chart showing the distribution of four colors in inkjet samples.	23
Figure 14. Pie Chart showing the distribution of various colors in intaglio set.....	23
Figure 15. Pie Chart showing the distribution of intaglio inks collected from different countries.	24
Figure 16. Pie Chart showing the distribution of sources for the offset collection set.	25
Figure 17. Pie Chart showing the distribution of colors in offset sample set.	25
Figure 18. Intaglio ink present in a United States 1-dollar currency.	27
Figure 19. Example of an offset sample cut from an expired US passport.	28
Figure 20. Spectral Overlay Comparison showing two different inks (left) differing by Mg concentration and two similar inks by Sb.	37
Figure 21. Bar graph showing the distribution of elements in toner printing inks.	43
Figure 22. Bar graph showing discrimination capability of different elements in toners.	43
Figure 23. Bar graph showing the distribution of elements (in %) in black toners.	44
Figure 24. Chemical structure of Cu Pthalocyanine.	45
Figure 25. Bar graph showing the distribution of elements in cyan toners.	45
Figure 26. Bar graph showing the distribution of elements in yellow toners.	46
Figure 27. Bar graph showing the distribution of elements in the magenta toners.	46
Figure 28. Spectral Overlay showing overlapping of different replicates of control TN 37.	50
Figure 29. One Way ANOVA for Sn isotopes (^{116}Sn on the left and ^{117}Sn on the right) for TN 37 (Control).	50
Figure 30. Two-dimensional PCA plot for toners.	52
Figure 31. Three-dimensional PCA plot for 77 toners.	52

Figure 32. Two-dimensional PCA plot for 77 toners by brand.	53
Figure 33. Three-dimensional PCA plot for 77 toners by brand.	54
Figure 34. PLS-DA plot showing the correct association of a duplicate toner control with the same toner ink in the database.....	57
Figure 35. KNN plot for duplicate control TN 34 showing the correct association in the ink database.....	58
Figure 36. Bar graph showing the distribution of elements in inkjet inks.....	61
Figure 37. Bar graph showing the contribution of each element for pairwise comparison of inkjet printing inks.	61
Figure 38. Bar graph showing the distribution of elements in black inkjets.	62
Figure 39. Bar graph showing the distribution of elements for cyan inkjets.....	63
Figure 40. Bar graph showing the distribution of elements in yellow inkjets.	63
Figure 41. Bar graph showing the distribution of elements in magenta inkjets.	64
Figure 42. Spectral Overlay Analysis of Mg isotopes in inkjet controls.	66
Figure 43. One-Way ANOVA with Tukey’s HSD plot for ²⁴ Mg (left) and ²⁵ Mg (right) in inkjet control (IJ 25)	66
Figure 44. Two-dimensional PCA plot for inkjets by LA-ICP-MS.....	68
Figure 45. Three-dimensional PCA plot for inkjets by LA-ICP-MS.....	68
Figure 46. Two-dimensional PCA plot showing different brands of inkjets.....	69
Figure 47. Three-dimensional PCA plot for inkjets showing different brands.....	70
Figure 48. Pie chart showing the percentage of misclassified pairs in four different colors.....	72
Figure 49. PLS-DA plot showing the correct matching of IJ 25 in the ink database. .	73
Figure 50. K-NN plot for IJ 25 showing the first 10 nearest neighbors.	73
Figure 51. Bar graph showing the distribution of elements in offset samples.....	76

Figure 52. Bar graph showing the distribution of elements in black offset inks.	76
Figure 53. Bar graph showing the distribution of elements in cyan offset samples.	77
Figure 54. Bar graph showing the distribution of elements in Yellow offset samples.....	78
Figure 55. Bar graph showing the list of elements detected in blue offset samples.	78
Figure 56. Bar graph showing the list of elements detected in magenta offset samples.....	79
Figure 57. Bar graph showing the list of elements present in red offset samples.....	79
Figure 58. List of elements present in Bronze, Brown and Orange offset inks.....	80
Figure 59. Bar graph showing the list of elements detected in pink and purple offsets.....	81
Figure 60. Spectral Overlay showing Tungsten peaks in offset control (OF-7).....	82
Figure 61. One Way ANOVA for Tungsten (W) isotopes in offset control (OF-7).....	83
Figure 62. Two--dimensional PCA of offset samples by LA-ICP-MS.	84
Figure 63. Three-dimensional PCA of offset inks by LA-ICP-MS.....	85
Figure 64. Two-dimensional PCA plot (by brand) for offset samples.	85
Figure 65. Three-dimensional PCA plot (by brand) for offset samples.	86
Figure 66. Pie chart showing the distribution of misclassified offset pairs in different brands.	87
Figure 67. PLSD-DA plot showing correct association of offset control 7 to the same sample in the database.	88
Figure 68. KNN-plot for OF-70 showing correct association to in the database.	89
Figure 69. Bar graph showing the distribution of elements in the intaglio ink set.	92
Figure 70. Bar graph showing the distribution of elements in aqua intaglio inks.	92
Figure 71. Bar graph showing the list of elements detected in gold intaglio inks.....	93

Figure 72. Bar graph showing the list of elements detected in black intaglio inks.	94
Figure 73. Bar graph showing the list of elements detected in yellow intaglio inks. ...	94
Figure 74. Bar graph showing the list of elements detected in blue intaglio inks.	95
Figure 75. Bar graph showing the list of elements detected in brown intaglio inks.	96
Figure 76. Bar graph showing the list of elements detected in red intaglio inks.	96
Figure 77. Bar graph showing the list of elements detected in green intaglio samples.	97
Figure 78. Bar graph showing the list of elements detected in purple intaglio.	98
Figure 79. Bar graph showing the list of elements detected in maroon intaglio inks. ...	98
Figure 80. Bar graph showing the list of elements detected in orange intaglio samples.	99
Figure 81. Spectral Overlay comparison for two Intaglio Controls on the right (IT 06) and left (IT 04) by Mn.	101
Figure 82. Spectral Overlay comparison for two intaglio controls (IT 06 on right and IT 04 on left) by Co.	101
Figure 83. One Way ANOVA with Tukey's HSD test for the analysis of ⁵⁵ Mn in intaglio controls.	102
Figure 84. One Way ANOVA with Tukey's HSD test for the analysis of ⁵⁹ Co in intaglio controls.	102
Figure 85. Two-dimensional PCA plot for intaglio printing inks by LA-ICP-MS.	103
Figure 86. Three-dimensional PCA plot for intaglio printing inks by LA-ICP-MS. ...	104
Figure 87. Two-dimensional PCA plot obtained from LA-ICP-MS data for intaglio samples by country.	105
Figure 88. Three-dimensional PCA plot for intaglio inks by country.	105
Figure 89. Pie chart showing the percentage of misclassified pairs from different sources.	106

Figure 90. PLS-DA plot for IT04 showing the correct association in the ink database.....	107
Figure 91. PLS-DA plot for IT06 showing the correct association in the ink database.....	107
Figure 92. K-NN plot for IT06 showing the correct association with itself in the ink database.....	108
Figure 93. Two-dimensional Canonical Plot for 391 ink samples from four different groups.....	109
Figure 94. Three-dimensional Canonical plot for 319 different types of inks.....	110
Figure 95. A LIBS spectrum for a 10,000ppm standard sample.	112
Figure 96. Intaglio ink present in a United States banknote.....	113
Figure 97. Effect of increasing laser energy and the extent of paper damage ¹¹	114
Figure 98. Effect of Helium (left) and Argon (right) as ambient gas on the intensity of emission lines in LIBS.....	115
Figure 99. Effect of Argon gas flow on the precision of peak intensity in LIBS.	115
Figure 100. LIBS spectra for ink and paper.....	117
Figure 101. Multiple Ti emission lines detected by LIBS in intaglio ink.....	118
Figure 102. Ca emission lines detected in ink and paper by LIBS.....	118
Figure 103. Bar graph showing the distribution of four printing inks for the tandem LIBS/LA-ICP-MS study.....	121
Figure 104. Si peaks for TN 12 and TN 77 detected in LIBS spectrum ⁴¹	124
Figure 105. Two-dimensional PCA plot for toners from data obtained by LA-ICP-MS.....	126
Figure 106. Three-dimensional PCA plot using data obtained from LA-ICP-MS.	127
Figure 107. Two-dimensional PCA plot for toners using data obtained from LIBS..	128
Figure 108. Three-dimensional PCA plot for toners obtained by using LA-ICP-MS data.....	128

Figure 109. Two-dimensional PCA plot for toners after fusion of LIBS and LA-ICP-MS.	129
Figure 110. Three-dimensional PCA plot obtained after the fusion of LIBS and LA-ICP-MS.	130
Figure 111. Canonical plots for toners using a) LIBS b) LA-ICP-MS and c) fusion of LIBS and LA-ICP-MS.	133
Figure 112. Three-dimensional Canonical Plot for toners using a) LIBS b) LA-ICP-MS, c) fusion of LIBS and LA-ICP-MS.	134
Figure 113. Hierarchical cluster Analysis for toners using a) LIBS b) LA-ICP-MS c) Fusion of LIBS and LA-ICP-MS.	135
Figure 114. Constellation plot for toners using a) LIBS b) LA-ICP-MS and c) fusion of LIBS and LA-ICP-MS.	136
Figure 115. K peaks for IJ 9 and IJ 10 detected by LIBS ⁴¹	138
Figure 116. Two-dimensional PCA plot for inkjets by LA-ICP-MS.	140
Figure 117. Three-dimensional PCA plot for inkjets by LA-ICP-MS.	140
Figure 118. Two-dimensional PCA plot for inkjets using LIBS.	141
Figure 119. Three-dimensional PCA plot for inkjets using LIBS.	142
Figure 120. Two-dimensional PCA plot for inkjets from the fusion of LIBS and LA-ICP-MS.	143
Figure 121. Three-dimensional PCA plot for inkjets from the fusion of LIBS and LA-ICP-MS.	143
Figure 122. Two-dimensional Canonical Plot for inkjets from LA-ICP-MS data.	144
Figure 123. Three-dimensional Canonical plot for inkjets based on LA-ICP-MS spectrum.	145
Figure 124. Two-dimensional PCA plot for inkjets using LIBS data.	146
Figure 125. Three-dimensional Canonical plot for inkjets by LIBS.	147

Figure 126. Two-dimensional Canonical Plot for inkjets from the fusion of LIBS and LA-ICP-MS.....	148
Figure 127. Three-dimensional Canonical plot for inkjets after data fusion of LIBS and LA-ICP-MS.....	149
Figure 128. Hierarchical cluster analysis for inkjets by a) LIBS b) LA-ICP-MS c) fusion of LIBS and LA-ICP-MS.....	150
Figure 129. Constellation plot for inkjets by a) LIBS b) LA-ICP-MS c) fusion of LIBS and LA-ICP-MS.....	151
Figure 130. Spectral Overlay of two intaglio samples discriminated by K emission lines in LIBS spectrum ⁴¹	154
Figure 131. Two-dimensional PCA plot for intaglio inks by LIBS.....	155
Figure 132. Three-dimensional PCA plot for intaglio printing inks by LIBS.....	156
Figure 133. Two-dimensional PCA plot for intaglio by LA-ICP-MS.....	157
Figure 134. Three-dimensional PCA plot for intaglio by LA-ICP-MS.....	158
Figure 135. Two-dimensional PCA plot for intaglio after the fusion of LIBS and LA-ICP-MS.	159
Figure 136. Three-dimensional PCA plot for intaglio after the fusion of LIBS and LA-ICP-MS.	159
Figure 137. Two dimensional Canonical plot for intaglio by LIBS (top left), LA-ICP-MS (top right) and the fusion of LIBS and LA-ICP-MS (bottom).	162
Figure 138. Three-dimensional Canonical plot for intaglio by LIBS (top left), LA-ICP-MS (top right) and the fusion of LIBS and LA-ICP-MS (bottom).	163
Figure 139. Hierarchical cluster analysis for intaglio inks by a) LIBS b) LA-ICP-MS c) Fusion of LIBS and LA-ICP-MS.....	164
Figure 140. Constellation plot for intaglio inks by LIBS (top-left), LA-ICP-MS (top-right) and fusion of LIBS and LA-ICP-MS (bottom).	165
Figure 141. Spectral Overlay of Ca emission lines obtained through LIBS spectrum for two offset printing inks ⁴¹	167
Figure 142. Two-dimensional PCA plot for offset samples by LIBS.....	169

Figure 143. Three-dimensional PCA plot for offset samples by LIBS.....	169
Figure 144. Two-dimensional PCA plot for offset samples after fusion of LIBS and LA-ICP-MS.	170
Figure 145. Three-dimensional PCA plot for offset samples after fusion of LIBS and LA-ICP-MS.....	171
Figure 146. Two-dimensional PCA plot for offset inks from the fusion of LIBS and LA-ICP-MS.....	172
Figure 147. Three-dimensional PCA plot for offset inks after fusion of LIBS and LA-ICP-MS.	172
Figure 148. Two dimensional Canonical plot for offset samples by a) LIBS b) LA- ICP-MS c) fusion of LIBS and LA-ICP-MS.	175
Figure 149. Three dimensional Canonical plot for offset samples by a) LIBS b) LA-ICP-MS c) fusion of LIBS and LA-ICP-MS.....	176
Figure 150. Hierarchical cluster analysis of offset samples by a) LIBS b) LA-ICP- MS c) fusion of LIBS and LA-ICP-MS.....	177
Figure 151. Constellation plot for offset samples by a) LIBS b) LA-ICP-MS c) fusion of LIBS and LA-ICP-MS.....	178
Figure 152. One-Way ANOVA for two controls for ^{86}Sr from mass spectrum.	179
Figure 153. One-Way ANOVA for two controls for ^{88}Sr from mass spectrum.	179
Figure 154. One-Way ANOVA for two controls for Sr 421nm emission line from LIBS.....	180
Figure 155. One Way ANOVA for two controls based on Sr 407.8nm emission line from LIBS	180
Figure 156. Calibration curves for Mg (top) and Al (bottom) from LA-ICP-MS and LIBS respectively in the tandem mode.....	181
Figure 157. PLSDA plot showing the discrimination by LIBS (top), LA-ICP-MS (middle) and the fusion of LIBS and LA-ICP-MS (bottom).	184
Figure 158. Variation of emission intensities with gate delay for LIBS.	188

Figure 159. Optimization of Helium gas flow through precision analysis.	188
Figure 160. Correlation plot for a) ^{27}Al b) ^{39}K c) ^{24}Mg d) ^{88}Sr with Si (I) 288.1 line.....	189
Figure 161. Bar graph showing the Relative Standard Deviations before and after normalization for elements in mass spectrum for NIST 1831.	190
Figure 162. Bar graph showing the Relative Standard Deviations before and after normalization for elements in mass spectrum for NIST 610.	191
Figure 163. Comparison of RSDs obtained from Tandem method with the Standard method for NIST 1831 by LA-ICP-MS.....	191
Figure 164. Comparison of RSDs obtained from Tandem method with the Standard method for FGS1 glass analysis.	192
Figure 165. Bar graph showing the Relative Standard Deviations for elements in LIBS spectrum for NIST and FGS glass standards.	192
Figure 166. Spectral Overlay of ^{23}Na peaks for contaminated and clean toners (right) and inkjets (left).	196
Figure 167. Spectral Overlay of K emission lines for contaminated and clean toners.	196
Figure 168. Variation of ^{48}Ti peaks in contaminated and pristine toners.	197
Figure 169. Ti peaks in contaminated and clean toners after removing the contribution from Na and K.	198
Figure 170. One Way ANOVA plot for contaminated and clean toner by ^{23}Na	199
Figure 171. One Way ANOVA plot for contaminated and clean inkjet samples by ^{23}Na	199
Figure 172. One Way ANOVA plot for contaminated and clean toner inks by ^{48}Ti	200
Figure 173. One Way ANOVA plot for contaminated and clean toner inks by ^{48}Ti after removing the contribution from Na and K.	200
Figure 174. Three-dimensional PCA plot for contaminated and clean inkjets.	201
Figure 175. Hierarchical cluster analyses for contaminated and clean inkjet printing inks.	202

Figure 176. Three-dimensional Canonical Plot for toners and inkjets. 202

ABBREVIATIONS AND ACRONYMS

ANOVA- Analysis of Variance

ARG- Argentina

BAR- Barbados

BR- Brother

BR- Brother Brand

C EP- Epson Brand

C- Cyan Color

CAN- Canada

CAY- Cayman Islands

CCD- Charge Coupled Device

CHI- China

CMYK- Cyan, Magenta, Yellow, and Black Color

CN- Cannon Brand

CTR- Costa Rica

CUB- Cuba

CZE- Czech Republic

DART- Direct Analysis in Real Time

DG- DayGlo Brand

DL- Dell Brand

ECK- Eckart Brand

EDS- Energy Dispersive Spectroscopy

EP- Epson Brand

EUR- Europe

FG- Flint Group Brand

GI- Graphic Ink Co. Brand

GUA- Guatemala

GC-MS- Gas Chromatography Mass Spectrometry

HAI- Haiti

HP- Hewlett Packard Brand

HPCN- HB (HP/Canon) "Hummingbird" Brand

ICP- Inductively Coupled Plasma

ICCD- Intensified Charge Coupled Device

IJ- Inkjet

IMX- IMEX 2300 Brand

IN- Intaglio

JAM- Jamaica

K- Black Color

K-NN- K Nearest Neighbor

KD- Kodak Brand

KN- Konica Brand

LA-ICP-MS- Laser Ablation Inductively Coupled Plasma Mass Spectrometry

LDA- Linear Discriminant Analysis

LIBS- Laser-Induced Breakdown Spectroscopy

LIVI- Lincoln Visa

LOD- Limit of Detection

LTE- Local Thermodynamic Equilibrium

LX- Lexmark Brand

M- Magenta Color

NEP- Nepal

Nd:YAG- Neodymium-doped yttrium aluminum garnet

NZE- New Zealand

NIST- National Institute of Standards and Technology

OD- Office Depot Brand

OF- Offset

OKI- OKI Brand

OL- Olivetti Brand

KOR- Korea (South)

PCA- Principal Component Analysis

PER- Peru

PLS-DA- Partial Least Squares Discriminant Analysis

PMT- Photomultiplier Tube

ppm- Parts per million

ppb- Parts per billion

PN- Panasonic Brand

RC- RICOH Brand

RIT- RIT sample

RSD- Relative Standard Deviation

RUS- Russia

SC- Sunchemicals Brand
SEM- Scanning Electron Microscopy
SH- Sharp Brand
SM- Samsung Brand
TLC- Thin Layer Chromatography
TI- Toyo Ink Brand
TN- Toner
TRI- Trinidad and Tobago
TUN- Tunisia
UAE- United Arab Emirates
UB- Unibrilliant (Germany)
UKR- Ukraine
USA- United States
USPB- United States Passport Bio Section
USPNB- United States Passport Non-Bio-Section
UZB- Uzbekistan
VSC- Video Spectral Comparator
XK- Xeikon Brand
XR- Xerox Brand
XRF- X- Ray- Fluorescence Spectrometry
Y- Yellow Color

Chapter 1. Introduction

1.1 Motivation for Research

Ink and paper have been widely used in criminal cases in the form of counterfeit currencies, changed wills, ransom letters, and altered checks. Various techniques have been developed to analyze ink and paper. Non-destructive tools like the optical microscopy, Video Spectral Comparator (VSC), X-Ray Fluorescence (XRF)^{1,2}, Thin Layer Chromatography (TLC)³, and Scanning Electron Microscopy (SEM)⁴⁻⁶ are usually the tools of choice. But these tools have a high limit of detection (LOD), which make it impossible when trace elements (present below 1 part per million) have to be detected. Elemental analysis of microscopic evidence present at trace levels (low parts per million in a matrix) can provide a very high degree of discrimination between samples suspected of sharing the same source of origin. The two of the commonly used laser based analytical tools are LIBS and LA-ICP-MS that provide elemental information of inks⁷⁻¹². Both these sensors have benefits and limitations. The present study focuses on combining the two techniques into one setup that minimizes their individual drawbacks and provides complementary information for both sensors.

Both LIBS and LA-ICP-MS use a laser beam to ablate small amounts of solid particles from the sample. Qualitative and semi-quantitative analysis can be performed using these two sensors. The typical limits of detection are in the order of sub ppm to ppb for LIBS, and LA-ICP-MS, respectively for the analysis of solid samples. These two methods have intrinsic benefits for document analysis, especially the ability for spatial resolution and quasi-non destructive nature of the lasers commercially available. The spot

size of the laser can be varied from a few microns to hundreds of microns, which permits to remove ink from a single letter in a document if necessary and also to study the sample homogeneity. LA-ICP-MS is the instrument of choice for any analyst looking for trace elements in different matrices. Also the time for analysis is very short, usually 30 seconds per replicate. The major limitations of LA-ICP-MS include the high cost, the presence of isobaric and polyatomic interferences making some of the elements very difficult to detect. LIBS is a simple to use, cost-effective instrument, having a wide range of applications. The tedious and complicated acid digestion step for extremely hard materials can be avoided by the use of laser. Almost nothing touches the sample, which decreases the chances of any sample contamination. Nevertheless, it is accompanied by some drawbacks such as higher limits of detections, which makes the detection of trace elements very challenging. It complements LA-ICP-MS by providing interference free emission lines for elements suffering from isobaric and polyatomic interferences in ICP-plasma.

The common drawback for both LIBS and LA-ICP-MS is the unavailability of suitable matrix matched standards for different matrices including inks. Matrix effects are reported in literature for laser-induced plasmas¹³⁻¹⁶. Physical matrix effects depend on the concentration of the samples. It is found to be more pronounced in concentrated samples than in dilute samples, even though the laser energy is constant throughout¹⁴. Similarly the detection limit of the elements have been reported to vary depending on the morphology (coarse/fine) of the solid sample¹⁷. Some of the solutions to the matrix effect are the application of matrix-matched standards, use of a suitable internal standard or normalization of the spectrum.

1.2 Goals of This Research

The goals of the research were to design and develop analytical tools, LIBS and LA-ICP-MS for the chemical characterization of printing inks, and build an ink database. A novel tandem method was designed and developed for the elemental and isotopic analysis of printing inks by combining LIBS and LA-ICP-MS in a single set up. The goals were based on the following facts.

- 1) Elements such as S, K, Ca, Fe, are very difficult to detect using a quadrupole ICP-MS because of the spectral interferences (isobaric and polyatomic). Interference free emission lines of these elements, obtained from LIBS spectrum could be used as points of comparison.
- 2) Elements present at trace levels (<10 ppm) are difficult to detect using standalone LIBS while LA-ICP-MS has detection limits in sub ppm levels. Therefore, trace elements can be detected using LA-ICP-MS, while major elements that are present at higher concentrations (%wt.) can be monitored using LIBS instead of LA-ICP-MS to protect the ICP-MS detector from saturation.
- 3) The application of tandem LIBS/LA-ICP-MS will minimize the amount of sample consumed as compared to the amount when two separate samples are introduced to LIBS and LA-ICP-MS in two standalone experiments. In real cases, the amount of sample (as evidence) is usually very small and could be insufficient for the analysis by two instruments. Tandem LIBS/LA-ICP-MS can be an ideal tool in such circumstances.
- 4) Tandem experiment also saves the total analysis time, as it is shorter compared to the analysis by two individual instruments.

- 5) LIBS can be used for the rapid screening of the ink sample while LA-ICP-MS can be used for the confirmation of the elements. Thus LIBS can be used to create an element menu for LA-ICP-MS.
- 6) A suitable element from LIBS can be used to normalize the LA-ICP-MS signals and vice-versa. Glass is a solid matrix that contains approximately 70% of Silicon dioxide (SiO₂). Any laser shot to shot fluctuation can be accounted by measuring the amount of Silicon ablated. A suitable interference free Silicon emission line obtained in LIBS can be used to normalize the mass spectrum.

1.3 Introduction to Analytical Tools

1.3.1 LIBS

Laser Induced Breakdown Spectroscopy (LIBS) uses a laser of suitable wavelength that is focused on the surface of a solid surface to create a plasma that can be analyzed. The laser interacts with the sample and ablates a small amount of sample, and if the laser power density is greater than the breakdown threshold value of the solid surface, it creates a micro plasma plume just above the irradiated spot¹⁸. Inside the micro plasma, an electron absorbs a photon, in doing so, it reaches a higher energy quantum mechanical level. The higher energy state or the excited state of the atom is an unstable state, so it tries to return back to the ground state. In doing so, it releases energy in the form of characteristic photon energies. The energy associated with a photon is given by equation (1).

$$E_{photon} = h\nu \quad (1)$$

$$\nu = c/\lambda \quad (2)$$

$$E_{\text{photon}} = hc/\lambda \quad (3)$$

Where E_{photon} , h and ν correspond to the energy, plank's constant and the frequency associated with the photon. Similarly, energy of the photon is related to its wavelength by equation (3).

These photons are collected using fused silica lenses coupled onto a fiber-optic cable, which transports the light to a spectrometer. The spectrometer consists of a Czerny Turner Spectrograph with dual gratings, which separate the photons into wavelengths. The light obtained from the excited species in the plasma provides elemental signature of the material. The intensity of the peak at a particular wavelength reflects the concentration of that element. Figure 1 shows the schematic of LIBS where a 266nm wavelength laser is focused on a sample containing a standard solution (10,000ppm) of various elements spiked on paper.

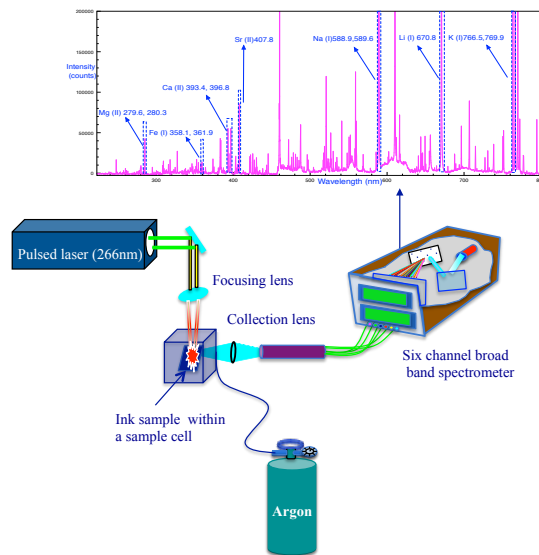


Figure 1. A 266nm laser focused on the surface of an ink sample placed inside an ablation chamber, produces a microplasma in the Argon atmosphere, the light emitted by the elements present in the ink sample are collected using Silica lens and transported by fiber optic cables to a spectrometer where the light is separated into spectral components and the signal is displayed as a function of wavelength.

1.3.1.1 The Physics of Plasma in LIBS

The plasma formed after the laser interaction with the sample is short lived. Figure 2 shows the evolution of plasma across different time regimes. A white light or continuum dominates the plasma light in the beginning, which is because of the free-free (bremsstrahlung) and free-bound (recombination) transitions¹⁸. Bremsstrahlung occurs when free electrons collide to produce photons, similarly when an atom or an ion captures an electron, some photons are emitted, which is called the recombination event¹⁹. As the plasma expands away from the surface of the material, it starts to cool, and line emission from ions, atoms and molecules dominate. The continuum emission, because of the hot plasma decays at a faster rate than the line emission (ions, atoms and neutrals) from the cold plasma as shown in Figure 2.²²

Due to the high electron density in the LIBS plasma, and the dominant collisional processes over the radiative processes, Local Thermodynamic Equilibrium (LTE) is assumed to exist in local regions of the plasma²⁰. Two commonly used equations to study the population distribution of excited species and ions inside the plasma are the Boltzmann equation and the Saha equation²¹. The Boltzmann equation is used to calculate the differences in distributions of excited species in the plasma²². It can be described by equation 4.

$$\frac{N_1}{N_0} = \frac{g_1}{Z} \exp\left(\frac{-E_1}{kT}\right) \quad (4)$$

Where N_1 and N_0 is the number of atoms in the excited and ground state respectively. Similarly g_1 represents the degeneracy at excited state, while Z denotes the partition function at the ground state, K is the Boltzmann's constant, and T is the temperature.

The Saha equation can also be used to calculate the ionization temperature inside the LIBS plasma^{23,24}. It is given by equation 5.

$$\frac{n_i n_e}{n_a} = \left(\frac{2\pi m k T}{h^2} \right)^{\frac{3}{2}} \left(\frac{2Z_i}{Z_a} \right) \exp\left(\frac{-E_i}{kT} \right) \quad (5)$$

where n_i is the density of atoms in the i -th state of ionization,

n_e is the electron density, n_a is the density of atoms, Z is the partition function

m is the mass of electron, and E_i is the ionization energy of the species²¹.

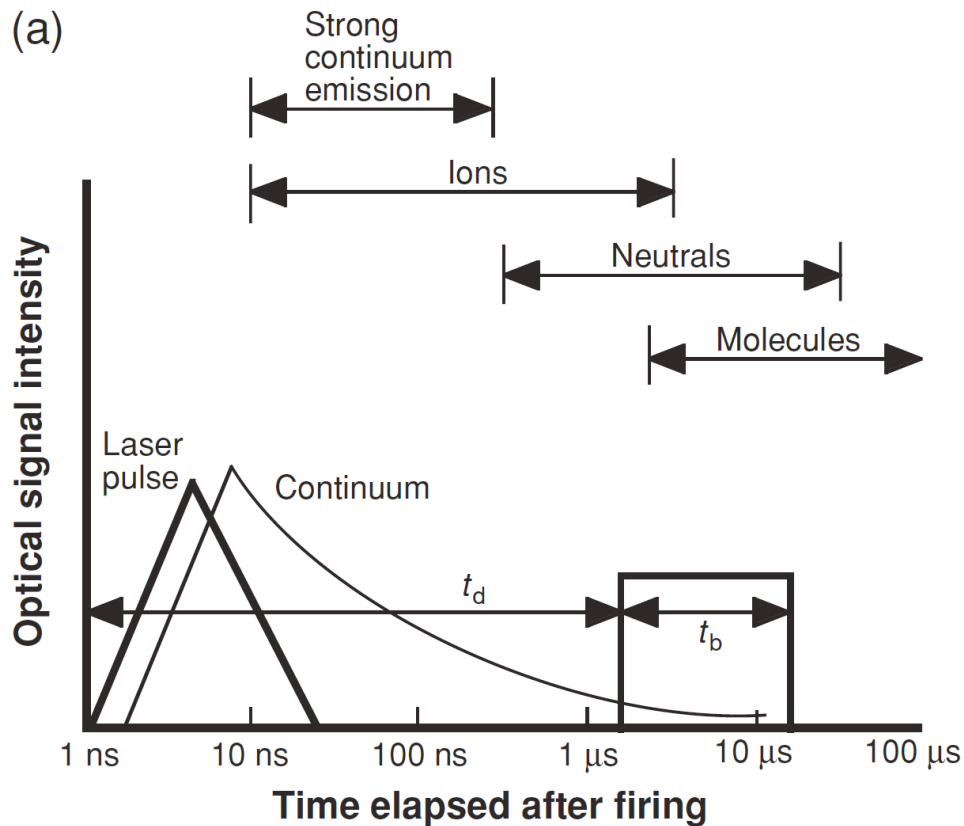


Figure 2. Temporal evolution of LIBS plasma²².

The detector in LIBS has to be gated to avoid the continuum and to capture the light emitted by the ions and excited atoms which are of analytical interest.

1.3.2 LA-ICP-MS

Laser Ablation Inductively Coupled Plasma Mass Spectrometry is an analytical technique that uses laser as a sampling tool. In LA-ICP-MS, a high-energy (10^9 - 10^{11} W/cm²) short (ns) laser pulse (in the IR 1064 nm, VIS 532 nm or UV 266 nm) is focused on the surface of the material to generate small particles that are transferred to the ICP-MS for analysis. A typical LA-ICP-MS includes a laser, a camera (CCD), an ablation chamber, and a ICP-MS. A CCD camera helps to locate the sampling spot and focus the laser on the surface of the sample. The laser ablates a small amount of material, which is carried by a carrier gas to the ICP, where it gets atomized and ionized. The ions are analyzed on the basis of their mass to charge (m/z) ratios by a quadrupole mass analyzer and finally detected by a detector, Electron Multiplier Tube (EMT). The use of laser makes it possible to analyze solid samples without tedious sample preparation. Lower limits of detection (below parts per million) is another important feature of LA-ICP-MS that has attracted the trace-element community. Inductively Coupled Plasma Mass Spectrometry (ICP-OES) is another technique that offers multi-element detection but the detection capability is not as good as compared to ICP-MS. Electro-thermal Atomization (ETA) offers lower detection limits but does not provide the sample throughput compared to ICP-MS and ICP-OES²⁵. The isotopic signature of the elements obtained from ICP-MS provides an unambiguous identity of the elements. The other notable feature of ICP-MS is the analytical range, which is nine orders of magnitude. However, ICP is plagued by the presence of isobaric and polyatomic interferences, which make it difficult to analyze elements like S, K, Ca, and Fe.

The ICP consists of three main parts: a torch, a radiofrequency (RF) coil and a power supply. The torch is made of quartz and consists of three concentric tubes. Argon gas is introduced between the two outlets, which helps to keep the outer tube from melting. The auxiliary gas, which is usually Argon, is used to keep the plasma from getting too close and it also prevents the injector tip from melting. Nebulizer gas passes along with the sample through the central tube. The radiofrequency coil is made of Cu tubing, which is coiled around the outer tube of the torch. This coil is held grounded and AC (Alternate Current) RF power is applied. This causes an electromagnetic field to the torch. A spark then supplies a few seed electrons, which are accelerated by the RF field. These electrons collide with the Argon atoms in the torch knocking off more electrons from the outermost orbit of Argon atoms resulting in a chain reaction, which sustains the plasma (hence the name inductively coupled plasma with RF)²⁶. Energy supplied to the coil by the RF generator couples with free electrons to produce plasma. Plasma temperature is around 10,000K on the outer side while it is from 5000 to 7000 in the center where the sample is introduced. Figure 3 shows the different parts of an ICP torch.

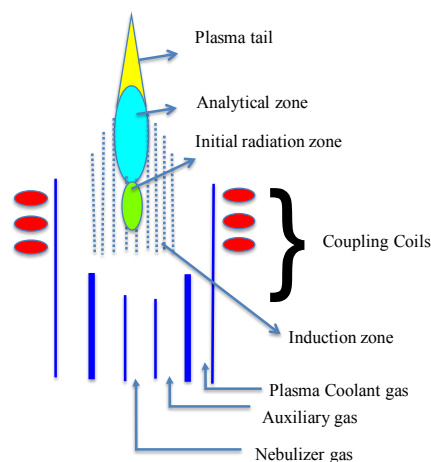


Figure 3. Various components inside an ICP torch.

Argon is usually used as fuel gas because of its high ionization potential (15.8eV), which is greater than the first ionization potential for most of the other elements, thus most of the elements can be ionized. However the ionization potential of Argon is lower than the second ionization energy of other elements which helps to minimize the doubly charged ions²⁵. As soon as the sample is introduced into the ICP, the solvent is dried off in the pre-heating zone, atomization occurs in the initial radiation zone, and ionization occurs in the analytical zone. Once the ions are formed at atmospheric pressure (760 Torr), they must be directed to the mass spectrometer that is under vacuum. The pressure reduction is done by the application of an interface, which helps to filter out the undesired chemical species namely photons, particles and neutral species from reaching the mass spectrometer. Two cones (namely sampler cone and skimmer cone) are placed inside the interface region with a design for down streaming focusing of ion beams. The sampler cone (1mm in diameter) allows only a narrow beam of ions to pass through it and the vacuum is reduced to 1-2 Torr. The skimmer cone (0.5mm in diameter) is placed immediately after the sampling cone which allows an even smaller beam of ions to pass through and reduces the vacuum to 10^{-3} - 10^{-6} Torr²⁵. A photon stop prevents photons and neutral species from entering to the detector²⁶. There is no ideal voltage that can produce the maximum transport efficiency for all ions when multiple elements are being measured. The voltages are scanned in concert with the mass spectrometer, which helps provide the optimal lens voltage for the isotope being analyzed²⁷. The quadrupole is the most commonly used mass analyzer with a unit mass resolution. It consists of four parallel rods, each usually 25cm in length, with two adjacent rods having opposite polarity. The separation and filtration of ions occurs through the application of a dc

potential and an oscillating radiofrequency (RF) potential applied to the pair of rods. At a specific potential, ions with particular m/z can only pass through it, while others are either destabilized or discharged by collision with rods²⁸. The ions finally reach the detector, which is usually an EMT (Electron Multiplier Tube), where the signal is magnified to 10^6 fold. Figure 4 shows the schematic of LA-ICP-MS for a standard sample containing 500 ppm of various elements like Li, Na, Al, Mn, Fe, Cu, and Sr.

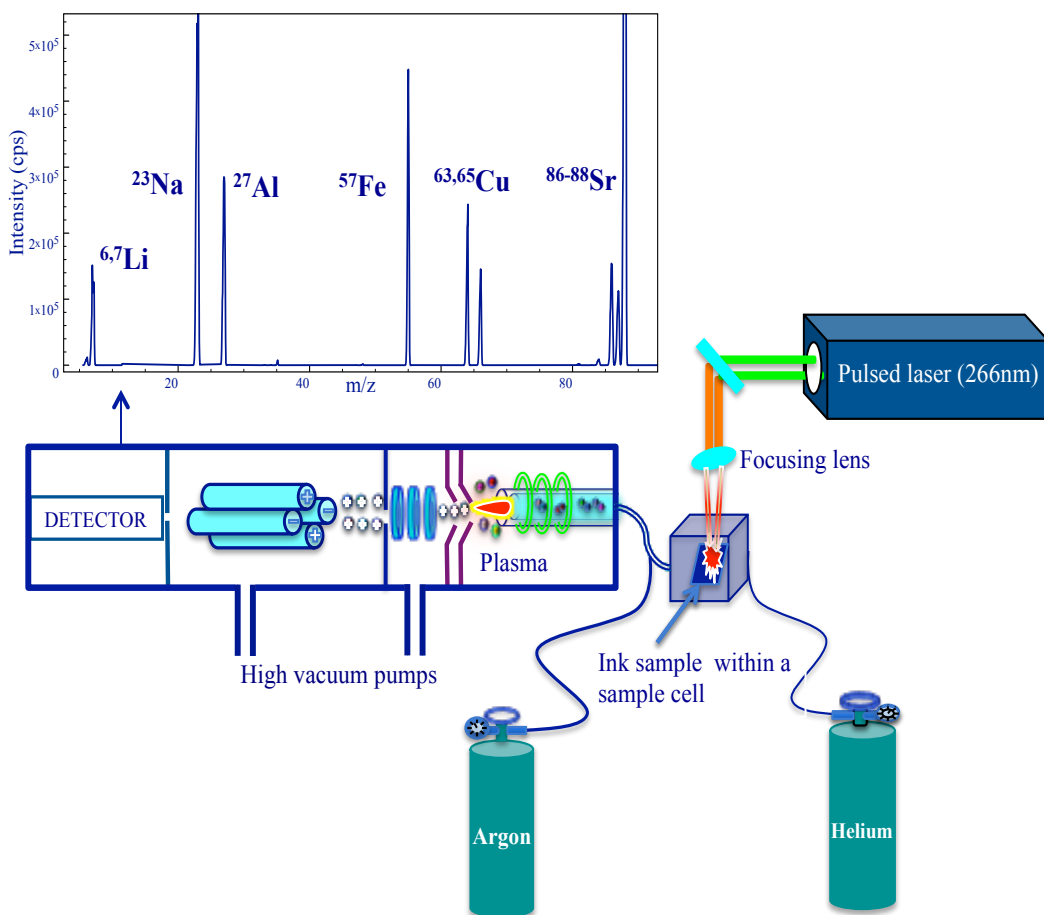


Figure 4. A pulsed laser (266nm) is focused on an ink sample, which ablates a small amount of the sample. These fine particles are transported to the ICP by using Helium gas, where they get ionized. The ions are separated on the basis of their m/z ratio by a quadrupole mass analyzer and detected by using an Electron Multiplier Tube.

1.4 Literature Review of LIBS and LA-ICP-MS on Ink Analysis

Most of the methods used for the analysis of documents involve the analysis of ink and paper by their physical properties, microscopic and optical examination, Thin Layer Chromatography (TLC)³, X-ray fluorescence (XRF)²⁹, Raman Spectroscopy^{2,30-35}, FTIR², and Desorption/Ionization Mass Spectrometry^{32,36}.

LIBS has been used for a wide range of applications like remote analysis of rocks on Mars³⁷, chemical mapping³⁸, high spatial resolution,³⁹ and also for in situ analysis⁴⁰. It has also been used for the inorganic analysis of printing inks. LIBS has been used to classify the pigments and pen inks³³, gel inks¹² and recently toners and inkjets⁴¹. It has also been used for the identification of inks used in artistic prints⁹, the examination of writing inks for forensic purposes^{42,43}, the rapid characterization of Parchment⁴⁴, and the quantitative analysis of silver nanoparticle inks⁷. LIBS has been carried out using different excitation wavelengths (at 532 nm and 1064 nm) for questioned documents analysis⁴⁵. LIBS has been successfully used for the analysis of white office paper, ballpoint inks (blue and black), black inkjet inks and black toners⁴⁶. Multivariate statistical analysis using LIBS has been performed for the discrimination of paper types and prints made by various printers⁴⁷.

ICP-MS has also been used in the study of ink and paper. Koenig has used LA-ICP-MS for the analysis of inkjet inks⁸. Wagner et al⁴⁸ have shown the use of LA-ICP-MS for the investigation of the written heritage by investigating the distribution of elements like Fe, Cu, and Mn. Elements like Fe and Cu have also been determined in old manuscripts by the application of LA-ICP-MS⁴⁹. Isotope ratio mass spectrometry (IRMS) has been used for the analysis of stable isotopes of Nitrogen, Carbon, Hydrogen and

Oxygen to characterize ballpoint ink and also gel inks⁵⁰. LA-ICP-MS has been used with for the analysis of different types of printing inks, and it was found that the fusion of SEM and LA-ICP-MS provided additional discrimination⁵¹. Szyrkowska et al. have used LA- ICP-TOF-MS for the identification and discrimination of toners from different producers on the basis of their elemental composition⁵². Data fusion from different sensors has also been performed for the analysis of printing inks. Our group has performed data fusion for 319 different printing inks obtained from five different sensors namely, Infrared Spectroscopy (IR), SEM-EDS, Pyrolysis GC-MS, LA-ICP-MS and Direct Analysis in Real Time Mass Spectrometry (DART)⁶.

1.5 Tandem LIBS/LA-ICP-MS

1.5.1 Principles of Tandem LIBS/LA-ICP-MS

LIBS and LA-ICP-MS are combined in a single set up. Two phenomena take place simultaneously from the same sample. Figure 5 shows the schematic of tandem LIBS/LA-ICP-MS for a standard sample containing 10,000ppm of elements like Li, Na, Al, Mg, K, Sc, Ti, Mn, Fe, Cu, Zn, Pb⁴¹. A laser is focused on the surface of a sample; it ablates a small amount of sample and a micro-plasma is formed on top of the sample, where the neutral and ionic species are excited to a higher energy state. LIBS utilizes the characteristic photons emitted from the excited species (neutral and ionic) to create a spectral signature of the elements. The particles ejected from the same laser sample interaction are then transferred to the ICP using a tubing with a flow gas at 0.9L/min to an ICP. Argon is used as a carrier gas, which also acts as an ambient gas for LIBS, and increases the lifetime of excited species in the LIBS plasma.

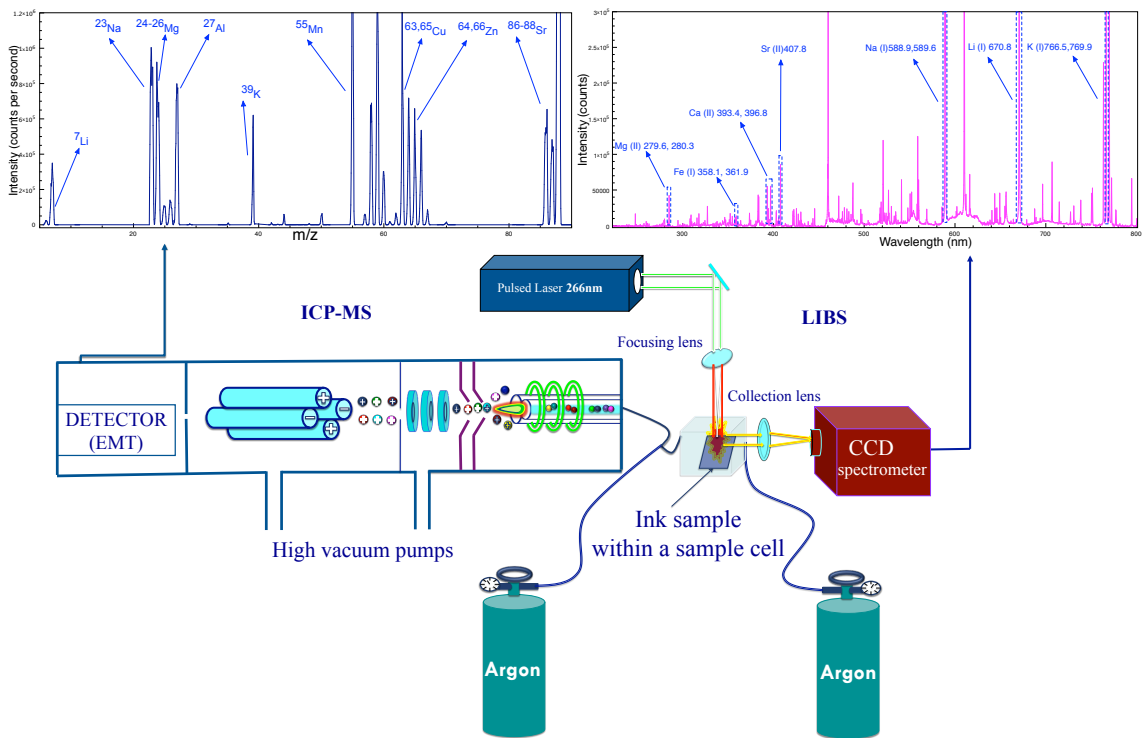


Figure 5. Schematic of tandem LIBS/LA-ICP-MS. Two sensors, LIBS and LA-ICP-MS are performed simultaneously on the same printing ink⁴¹.

LIBS utilizes the characteristic photons emitted from the excited species (neutral and ionic) to create a spectral signature of the elements present in the ink sample. Once the particles reach the ICP, they are atomized, and ionized. The ions are analyzed by a quadrupole mass analyzer, and detected by EMT. The same laser performs micro sampling and acts as an agent that breaks down material to feed the ICP, while it acts as a plasma-forming agent in LIBS. In this way the two techniques, ICP-MS and LIBS can be performed simultaneously on the same sample⁴¹. The laser parameters like the laser energy, the laser frequency, the laser spot-size, and the scanning speed have to be optimized in a way that it favors both the techniques.

1.5.2 Significance of Tandem LIBS/LA-ICP-MS

There are several notable benefits of using a tandem LIBS/LA-ICP-MS. The tandem technique allows the rapid screening of elements using LIBS, and further confirmation can be achieved using LA-ICP-MS. Since the LIBS spectrum and the mass spectrum are created from the same sample, there is a correlation between the two⁵³. A number of factors affect the ablation yield such as the variation in the laser's power and in the laser's temporal and spatial profiles. Similarly, the transportation of the ablated particles to the ICP may vary depending on the ablated particle size distribution⁵⁴. To account for the laser shot to shot fluctuation and any differences in the amount of mass ablated during the laser ablation, a suitable element (usually present in higher concentration) from LIBS can be used as an internal standard to normalize the LA-ICP-MS spectrum and vice versa. In a realistic case, the amount of sample for forensic analysis is usually low and may not be sufficient for two different instruments. In such a case, a tandem mode is favorable as the sample is the same for both instruments. Also the time to analyze the ink samples in a tandem mode is shorter than its analysis by two different instruments. Thus it saves the amount of sample consumed and the analysis time as well. These two methods also complement each other in several ways. Elements like S, Ca, Fe, and K are very difficult to detect and confirm using a standalone LA-ICP-MS because of the spectral interferences (polyatomic and isobaric) involved. These problematic elements emit multiple emission photons, in LIBS and the interference free wavelengths can be used to confirm these elements. The major drawback of LIBS is the sensitivity. Trace elements present below 10 ppm are very difficult to detect using LIBS while LA-ICP-MS has detection limits in sub ppm level, which makes the detection of

trace elements feasible. Alternatively, major elements present at higher concentration (% Wt.) can be monitored using LIBS alone, which saves the mass detector from saturation. Isotopic information obtained from mass spectrum further provides unambiguous identification of the elements⁴¹. Thus the combination of these two sensors in a single setup allows the detection of most of the elements in the periodic table and also expands the dynamic range of the analysis.

1.5.3 Literature Review of LIBS and LA-ICP-MS Used Together

The combination of LIBS and LA-ICP-MS is fairly a novel concept. Kaiser et al, used LIBS and LA-ICP-MS for the chemical mapping of Pb, Mg and Cu accumulated in plant tissues⁵⁵. Novotny et al, also used these two sensors for the mapping of different structures on a large area of granite samples. Latkcozy et al, used LIBS and LA-ICP-MS simultaneously for the analysis of industrial samples⁵³. Chirinos et al, used LIBS and LA-ICP-MS for the three dimensional elemental mapping of rocks⁵⁶. The first use of LIBS and LA-ICP-MS in tandem was done by Latkcozy et al⁵³. The present research is the first time a tandem LIBS/LA-ICP-MS has been used for the analysis of printing inks.

1.6 Introduction to Printing Inks

Printing inks can be solid (usually toners), liquid (inkjets) or a paste (offset, intaglio), which are used to color the surface of any substrate or produce a design or text. There are basically three ingredients in ink⁵⁷.

1) Pigments and dyes

Pigments can be organic (containing Carbon and Hydrogen and made from petroleum) or inorganic (containing elements besides Carbon and Hydrogen) formed by

precipitation. The function of pigments is to impart color to the ink. Pigments are insoluble while dyes are soluble.

2) Vehicles (Resin and solvent)

The liquid portion of the ink that holds and binds the pigment to the substrate is called vehicle. Vehicles are usually made with resins and solvents.

3) Ink Additives

Several additives are used in ink for different purposes. Varnishes or oils are used to reduce the stickiness of ink and for better ink penetration and setting. Metallic salts are used as driers to speed the oxidation and drying of the oil vehicle⁵⁸. Alternatively antioxidants are used to prevent ink on ink rollers from skinning and drying in the form of anti-skinning agents⁵⁹.

1.6.1 Types of Printing Inks

The current study focuses on the following four main types of printing inks.

1.6.1.1 Inkjet Printing Inks

In the inkjet printing methodology, a digitally controlled print head is used to eject very small droplets of ink on to a substrate which can be either continuous (CIJ) or drop on demand (DOD)⁶⁰. The first method ejects the drops continuously which are charged according to the image to be printed and then controlled electronically. The un-deflected droplets which cannot make up to the paper substrate are then redirected to a circulation container so that they can be reused⁶¹. In DOD inkjets, the ejection is done only when required. The method used to eject the ink for DOD could be heat (thermal inkjet), pressure (piezoelectric inkjet), or electrostatic field (Electrostatic inkjet).

Figure 6 shows the schematic of inkjet printing. Inkjet formulations could be one of these four types: solvent-based, water-based, UV curable and phase change⁶². Dyes are preferred over pigments for inkjets, and when pigments have to be used, the particle size of the pigment should be less than $1\mu\text{m}$ ⁶³. The major applications include marking of packages or products, graphics for signs and posters, trade show displays, billboards, banners etc⁶⁰.

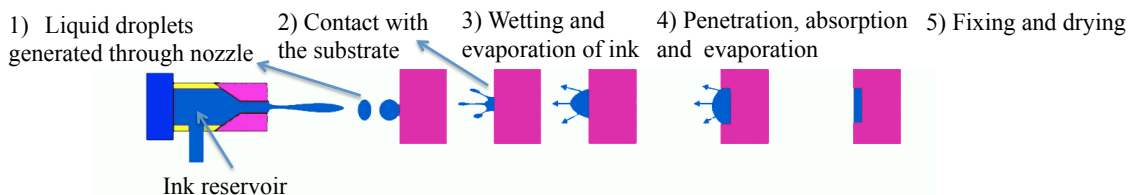


Figure 6. Liquid droplets are generated through the nozzle of ink reservoir, which wet the substrate on contact. Evaporation, of the solvent takes place followed by penetration and absorption of ink on to the paper fibers. Finally the ink is fixed and dried.

1.6.1.2 Toner Printing Inks

A toner is usually a solid powder, but can also be in liquid form. It is an electrostatically charged powder containing a pigment, a resin and some charge control agents. The typical resins are styrene acrylic polymers⁵⁷. The laser printing mechanism can be explained as below^{64,65}.

A corona wire/roller charges the drum inside the printer. As the drum rolls, a tiny laser light shines on the charged drum and discharges the negative charge on a certain portion of the drum where the image is to be formed⁶⁵. Thus an image is formed in static electricity on the surface of the photoconductive drum. The drum is then exposed to toners (negatively charged). The toners stick only to that part which contains the opposite charge (neutralized negative charge) while the negatively charged drum is left unaffected.

The image is then transferred to the paper. Heat (up to 200 degree centigrade) and pressure is applied to fuse the plastic toner to the paper. Figure 7 shows the general schematic of toner printing.

- 1) Generation of negative ions on corona wire
- 2) Negatively charged toner particles are adhered on the image
- 3) The paper passes through rollers in the fuser assembly (200 °C and pressure) binds the plastic powder to the paper.

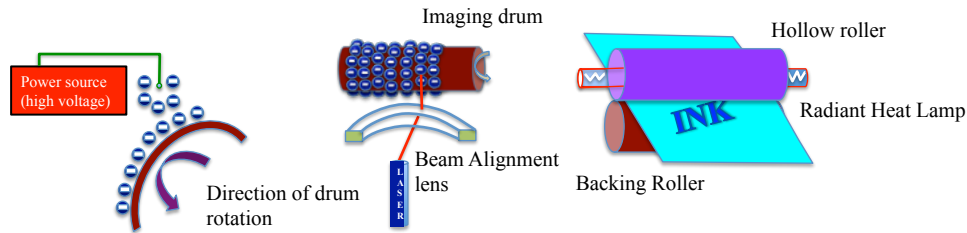


Figure 7. The drum inside the printer is negatively charged by a corona wire. A tiny laser light shone on the drum where the image is to be formed, discharges the negative charge. The toners stick to the image part, which is transferred to the paper using heat and pressure.

1.6.1.3 Intaglio Printing Inks

Intaglio printing is a relatively more complex and expensive. It is used specially for printing high security documents. Most of the banknotes and visas have intaglio printing inks. The intaglio inks are printed in a different way compared to toners and inkjets. First, master plates are prepared, which contain grooves where the images to be printed are incised. The grooves are filled with highly viscous ink⁶⁶. The dampened paper and the roller are made to roll over the plates, exerting a heavy pressure (7,500 to 15,000 psi) that helps transfer the ink and emboss the paper⁶⁷. Figure 8 shows the schematic of intaglio printing.

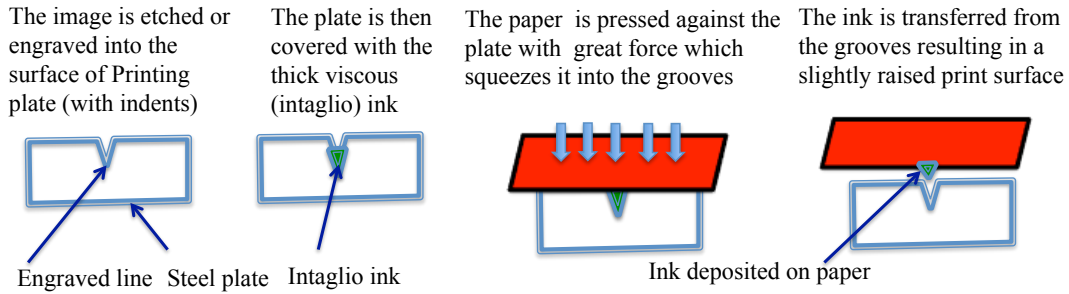


Figure 8. An image is itched into the surface of printing plate, which is then covered with intaglio ink. A paper is pressed against the plate, to force the ink into the grooves on paper. The final appearance is a raised print surface on the paper.

1.6.1.4 Offset Printing Inks

The technique is usually employed for mass production printing like in the production of newspapers. Here the images are transferred from metal plates first to rubber blankets or rollers and then subsequently to the paper⁵⁷ as shown in Figure 9. The paper does not come directly in contact with the metal plates, which make the plates long lasting. Newspapers, magazines, brochures, flyers are some of the examples of offset printing.

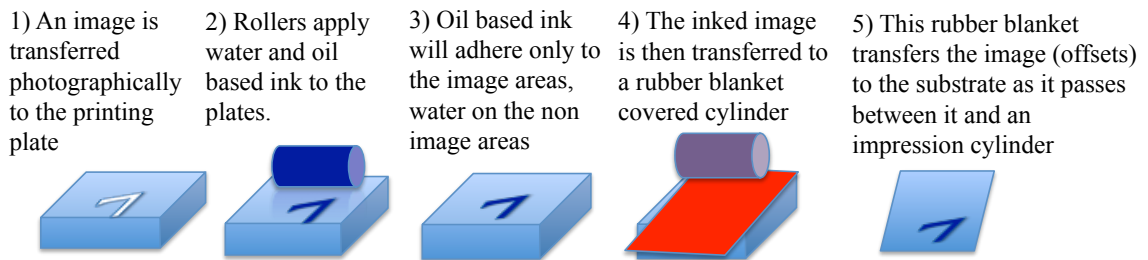


Figure 9. Schematic of offset printing.

Chapter 2. Experimental and Materials for LA-ICP-MS

2.1 Sample Set Collection

Four main types of printing inks, namely toners, inkjet, intaglio and offset were used for this study. A total of 319 samples of printing inks were collected and analyzed. Figure 10 shows the distribution of four inks in this set of printing inks.

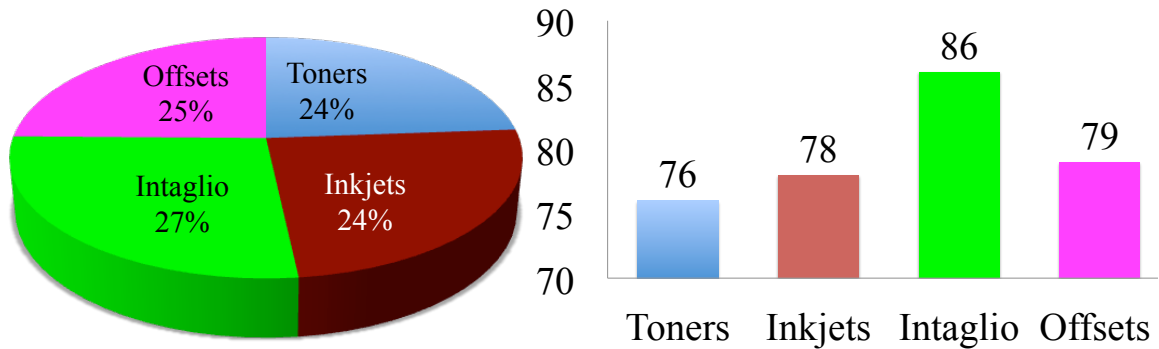


Figure 10. Pie chart (left) and bar graph (right) showing the distribution of printing inks.

2.1.1 Toner Collection Set

A total of 76 toner samples belonging to 16 different brands were used in the study. Figure 11 shows the distribution of different brands of inks for the toner set. The majority of toner samples were from Hewlett Packard (HP), constituting of 33% of the total set. There was an equal number of toners (six) that belonged to Canon and OKI brands. There was one toner from each of the brands Sharp, Toshiba and Office Depot. Three of the toners from the RICOH brand, which were in liquid form, were deposited in Whatman filter paper.

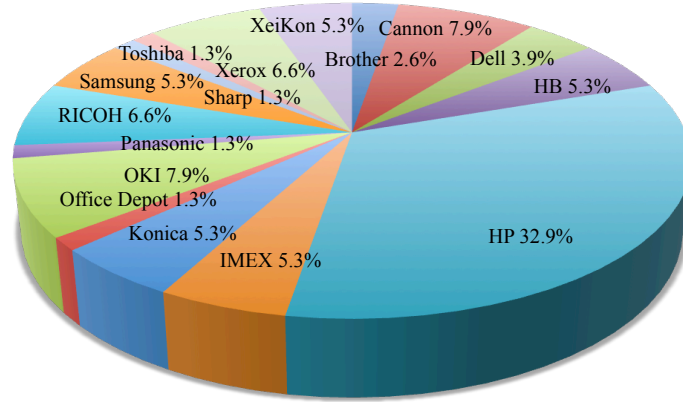


Figure 11. Pie Chart showing the distribution of different brands in the toner set.

All of the toners had one of the four colors (Cyan, Magenta, Yellow, Black). Black toners dominated the collection set. Figure 12 shows the distribution of four different colors in the toner set.

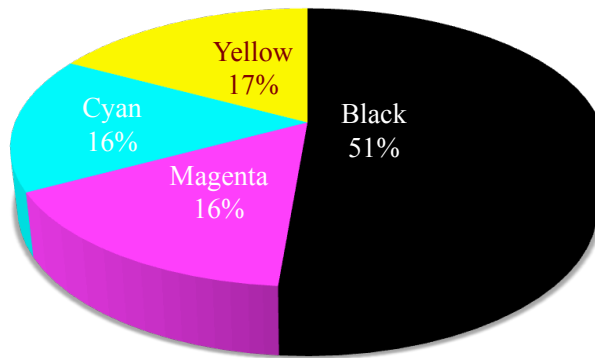


Figure 12. Pie chart showing the distribution of different colors in the toner set.

2.1.2 Inkjet Collection Set

A variety of brands were included in the inkjet collection set. It consisted of nine different brands and represented four colors. The four colors were Cyan, Magenta, Yellow and Black (CMYK) as shown in figure 13. A total of 31% of the inkjets were from HP. The three most commonly used brands were HP, Cannon, and Epson.

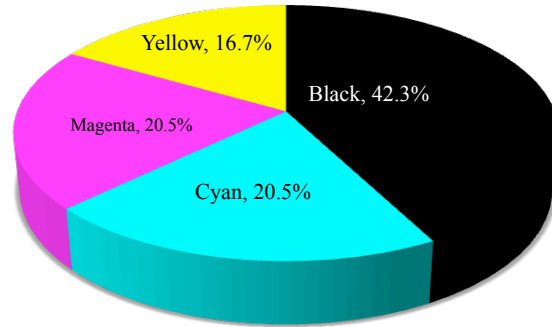


Figure 13. Pie Chart showing the distribution of four colors in inkjet samples.

2.1.3 Intaglio Collection set

Intaglio set was not limited to CMYK colors. Most of the intaglio samples were green, followed by blue and black. Some of the intaglio printing inks were maroon, purple, gold, brown, orange and aqua in color. Figure 14 shows the distribution of colors in intaglio printing inks. Intaglio printing inks were collected from the banknotes of different countries. A total of 86 intaglio ink samples were collected from 24 countries around the world. Two of the samples were collected from a training business card while three of the collection sets were from a Lincoln Visa document provided by the HSI lab.

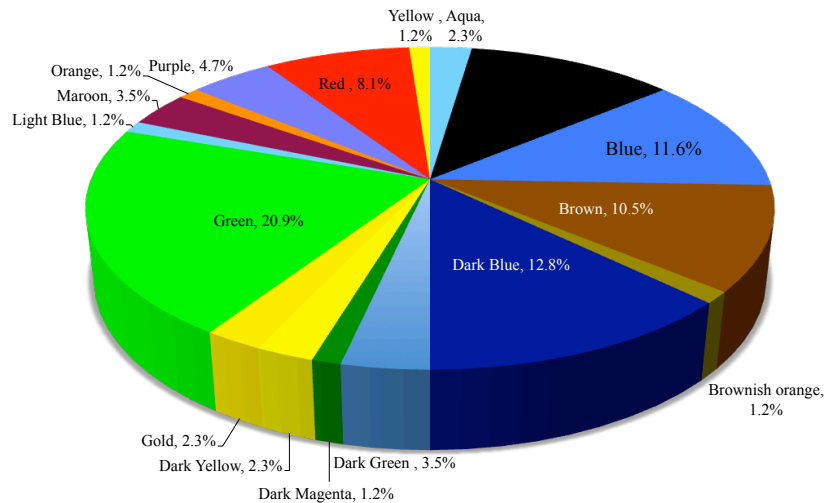


Figure 14. Pie Chart showing the distribution of various colors in intaglio set.

Most of the samples were from Costa Rica (14%) followed by Italy, Russia, and the United States (each 7%). Figure 15 shows the percentage of the intaglio samples belonging to 24 different countries. The country of origin for five samples was unknown, but they were identified as intaglio printing inks.

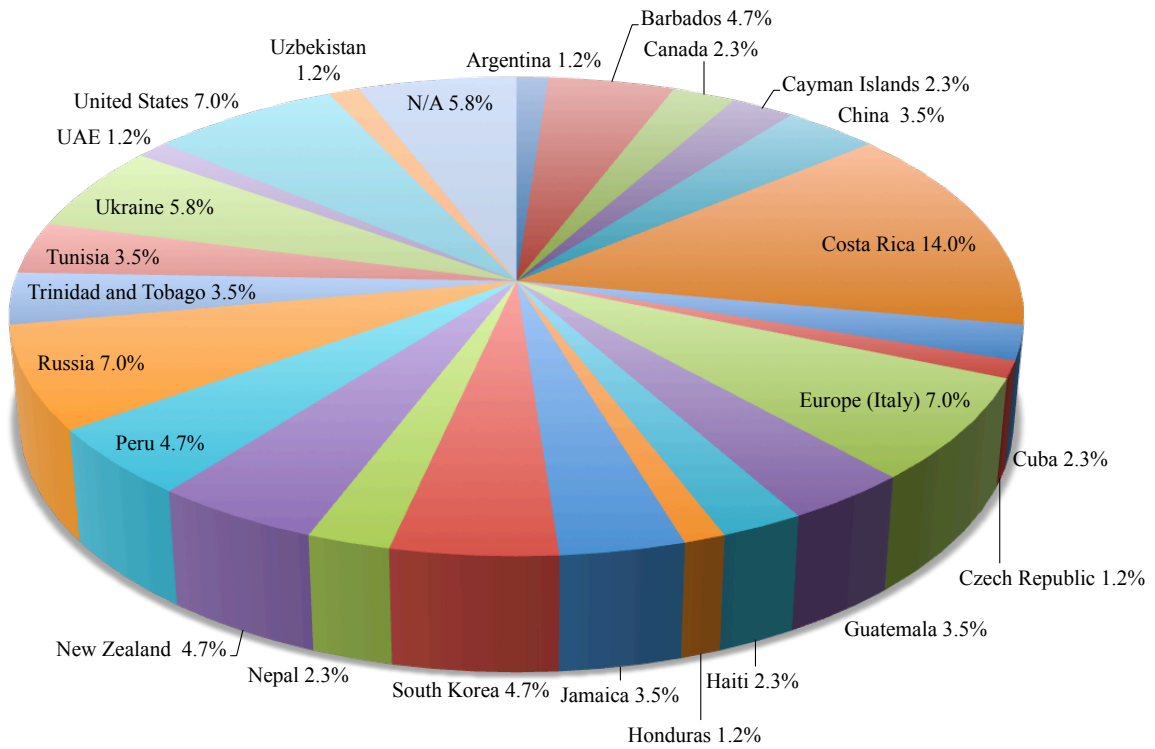


Figure 15. Pie Chart showing the distribution of intaglio inks collected from different countries.

2.1.4 Offset Collection Set

A total of 79 offset samples were collected for analysis. The set contained 39 printouts from 5 different manufacturers, 16 raw paste inks obtained from 2 different manufacturers, 8 print outs from Lincoln Visa, 15 printouts from a US passport, and 1 from a training business card. Figure 16 shows the distribution of offset samples (in percentage) collected from different types of manufacturers.

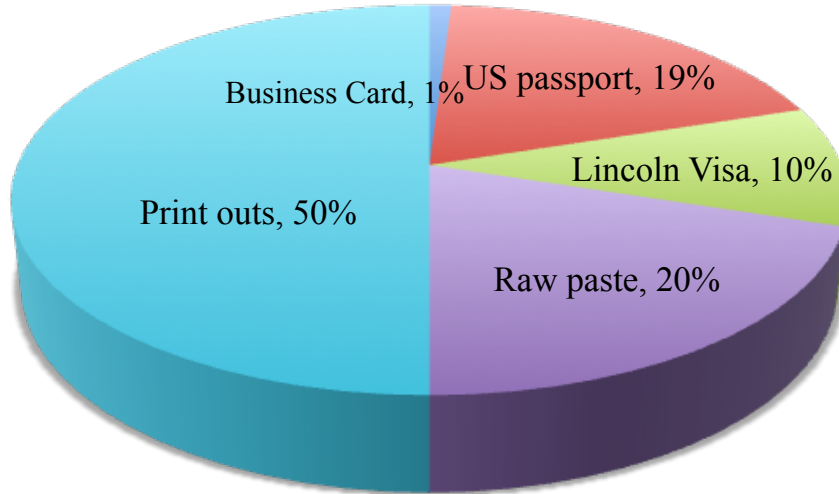


Figure 16. Pie Chart showing the distribution of sources for the offset collection set.

The offset collection set had a variety of colors besides CMYK. The most frequently appearing color was black, followed by Yellow, Cyan, Magenta and Red.

Figure 17 shows the distribution of different colors in the offset collection set.

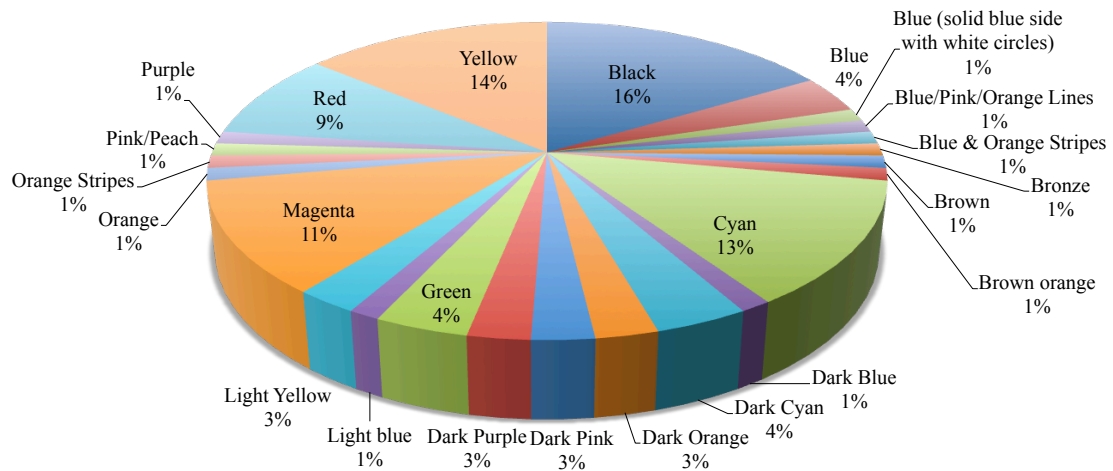


Figure 17. Pie Chart showing the distribution of colors in offset sample set.

2.2 Sample Preparation

The four types of printing ink were prepared using different methods. The sample preparation for each of the set is described below.

2.1.2.1 Sample Preparation for Toner Printing Inks

The deposition of the ink above the paper in toner printing inks makes it easier to remove only the ink using a laser. Whatman Grade 42 paper (Whatman Ltd, NJ) was cut into 8.5 by 11 inch pieces and used as a substrate for toner inks. Letters and numbers were used for each print out with the cartridge and printer information. For making a thick layer of ink on the paper some of the inks were printed several times on the same place (10 layers). In order to ensure there was no mixture of colors, the printouts were examined through Keyence 3d microscope, which showed only one of the four (CMYK) colors was present for each of the ink samples. One of the toners was selected as a control (TN 37) and was used before and after the end of the experiment, so as to examine the overall performance of the instrument. For those toners, which did not have a known printer model, sample preparation was done by a deposition method to simulate the printout samples. The following steps were followed for the sample preparation^{41,51}.

The toner powder was extracted from the ink cartridge in its pure form. About 0.1gms of powder was rolled on the paper substrate atop a clean microscope glass slide. The glass slide was placed on the surface of a hot block and heated till the toner began to melt (140-180⁰C). The molten toner was smeared homogeneously on the Whatman paper using a glass cover slide. The sample was allowed to cool. Thus prepared samples were affixed to the stage within the ablation chamber using a double-sided tape.

2.1.2.3 Sample Preparation for Inkjet Printing Inks

Similar to the toner inks, inkjet inks were also printed directly whenever the printer model was available and examined through the Keyence 3d microscope. Pure

color ink was extracted from those inkjet cartridges lacking a printer model. About 5 μ l of the inkjet ink was then carefully pipetted and spiked directly to Whatman paper (3 x 4 cm). A smaller piece was cut with a blade and placed inside the ablation chamber.

2.1.2.4 Sample Preparation for Intaglio Printing Inks

Most of the intaglio samples came from bank notes. The intaglio regions were first confirmed using Keesing Documentchecker (Keesing reference systems Inc.) and for further verification a microscope was used. For most of the intaglio inks, the ink part was slightly elevated from the paper. Figure 18 shows an example of intaglio ink present in the coat of George Washington in a one-dollar United States currency.

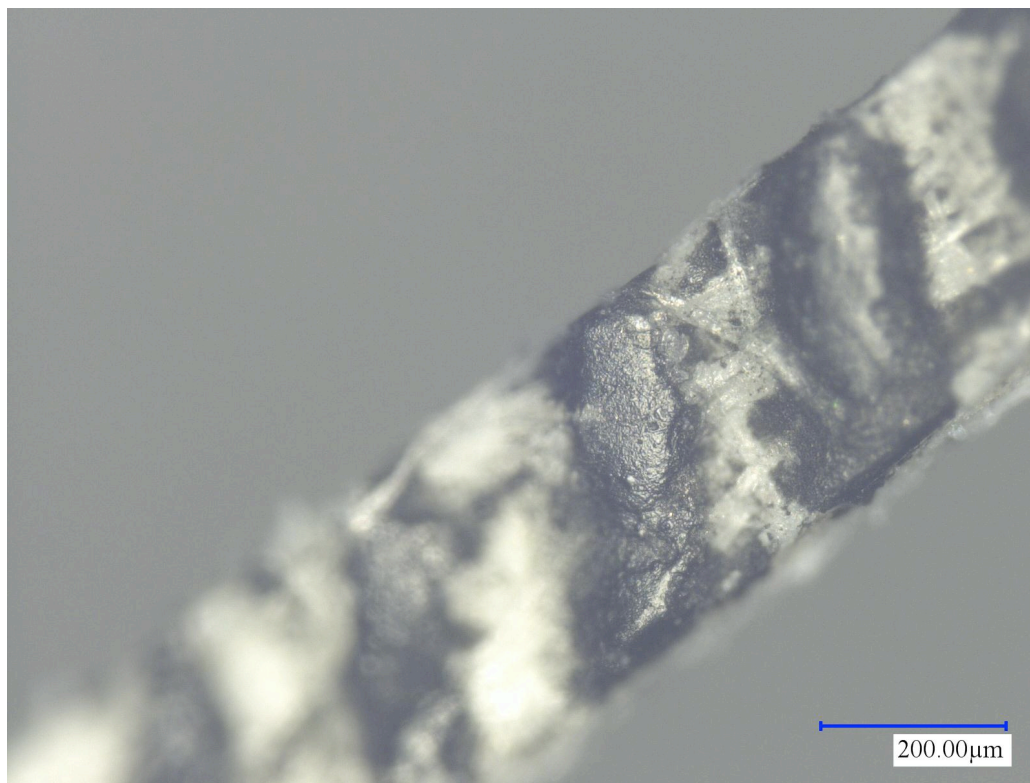


Figure 18. Intaglio ink present in a United States 1-dollar currency.

2.1.2.5 Sample Preparation for Offset Printing Inks

For print out offset samples, no sample preparation was done. The offset part of the print out was carefully cut and analyzed directly.

Figure 19 shows an example of offset printing ink. For raw paste offset samples, they were first homogenized with a vortex mixer, and deposited onto Whatman paper forming a thin layer on the paper. These samples were then dried at room temperature and analyzed.

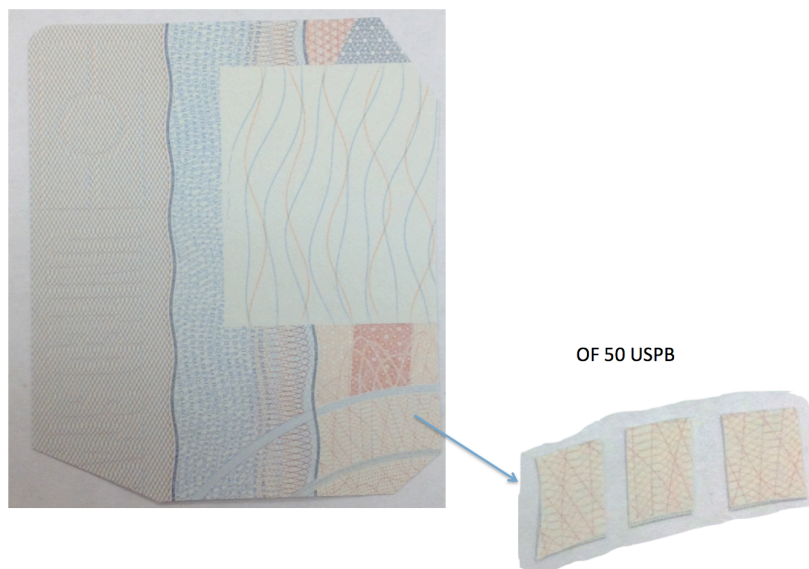


Figure 19. Example of an offset sample cut from an expired US passport.

Chapter 3. Method Development and Optimization of Standalone LA-ICP-MS

Method development and optimization was aimed at characterization of the ink precisely and accurately, while minimizing damage to the paper. Different parameters like laser energy, laser frequency, scan speed, were optimized. Similarly the nature of the carrier gas, and the gas flow were also optimized.

3.1 Experimental for LA-ICP-MS

Two different types of laser systems were coupled to ICP-MS. A 213 nm ns-ND: YAG laser ablation system (NW UP 213, New Wave, CA) and a 266nm ns-ND: YAG (J200, Tandem LA-LIBS, Applied Spectra, CA) were used for ink sampling. The laser power of UP-213 nm laser was 3mJ (at 100% Energy) while the J200 had a power of 18mJ at full power. Both systems had a CCD camera for visualization and focusing of the sample, automated valves and controllers for carrier gas introduction into the sample cell, automated x-y-z stages for rastering the laser beam across the sample. The J200 LIBS system had a micro camera and a macro camera for achieving better positioning of the sample with respect to the focused laser beam. The J200 laser ablation also consisted of 6 channel broad band spectrograph (190nm to 1040 nm) with a spectral resolution $> 0.1\text{nm}$ for UV to VIS and < 0.12 for VIS to NIR for LIBS system. A quadrupole ELAN DRC II (Perkin Elmer LAS, Shelton CT USA) was the mass analyzer used.

The ink samples were carefully cut into small pieces so as to accommodate inside the ablation chamber. The ink samples were securely attached to the surface of the ablation chamber by using a double-sided tape.

3.2 Method Development and Optimization

The four ink types have different physical properties and differ in the way they are deposited on paper, so each of these inks were optimized independently. The parameters affecting the laser ablation are the laser energy, frequency, scanning speed, and the mode of ablation. Because of the relatively thin layer of ink over paper, spot mode was not favorable for laser ablation, as it would create deep craters and ablate through paper. So a line mode of laser ablation was used. Different laser frequencies were tested ranging from 2 Hz to 10 Hz. Similarly different laser spot sizes were tested ranging from 100 μm to 250 μm . The best spot size was that which provided good sensitivity and provided representative composition of the bulk. Similarly the scanning speed of the laser was varied from 10 μms^{-1} to 35 μms^{-1} . A lower scan speed rate allowed firing more shots per location, thus shortening the ablation line but in the mean time it created deeper craters with significant amount of paper contribution. The flash lamp voltage was varied from 20% to a maximum of 80%. The combination of laser parameters (energy, frequency, and spot size), that provided the best precision, the highest signal, signal to noise ratio and caused least damage to the paper substrate were used as the final optimized parameters. The ablated craters were examined through Keyence 3d microscope. There is always some paper contribution despite the mild ablation conditions, so the analysis of paper was also done simultaneously and the paper background was subtracted: the final result being the only contribution from the ink⁴¹.

3.2.1 Optimization of Parameters for Toner Printing Inks

Usually toners are solid powders, although some liquid toners were also collected in the present study. The thickness of the print out was <100 μm . The parameters that were optimized were the signal intensity, signal to noise ratio and the precision. As the laser energy increased, so did the signal of the elements but at the cost of higher paper contribution. The laser energy was varied from 10% to 80%. It was found that the background noise was prominent at lower laser energies, which also suppressed the peaks at lower wavelength. The laser output energy at 70% was found to be optimum for toners. To account for the sample heterogeneity, a larger spot size (200 μm) was used. The flow of Helium gas (carrier gas) was also optimized. The optimized parameters for the analysis of toner printing inks are listed in Table 1.

Table 1. Optimized parameters for the analysis of toners by LA-ICP-MS.

Parameter	Toners
Laser wavelength	213 nm
Spot size	190 μm
Laser energy	40% (0.3mJ)
Ablation mode	Line
Stage speed	25 $\mu\text{m/s}$
Repetition rate	10 Hz
Carrier gas	He (0.9 L/min)
Ablation length	950 μm
Data acquisition mode	Mass scan m/z 7-238
Elements in ink	(Al, Ba, Ca, Cr, Cu, Fe, Hf, K, Mg, Mn, Mo, Na, Nb, Sb, Si, Sn, Sr, Ti, W,
Elements in paper substrate	Ba, Ca, Na, Si, Zn

3.2.2 Optimization of Parameters for Inkjet Printing Inks

As inkjet printing inks are embedded with the paper fiber, they are distributed more homogeneously compared to toners. The thickness of ink is minimal compared to the toners. This makes the laser ablation of inkjet printing ink without damaging the paper substrate a more challenging task when compared to toners. Different laser parameters and the gas flow were optimized for inkjet printing ink analysis by LA-ICP-MS. A mass scan method starting from m/z 7 (Li) to m/z 238 (U) was applied throughout the inkjet analysis. Table 2 lists the optimized parameters for the analysis of inkjet printing inks by LA-ICP-MS.

Table 2. Optimized parameters for the analysis of inkjet printing inks by LA-ICP-MS.

Parameter	Inkjets
Laser wavelength	213 nm
Spot size	190 μm
Laser energy	40% (0.3mJ)
Ablation mode	Line
Stage speed	25 $\mu\text{m/s}$
Repetition rate	10 Hz
Carrier gas	He (0.9 L/min)
Ablation length	950 μm
Data acquisition mode	Mass scan m/z 7-238
Elements in ink	(Al, B, Ba, Cu, Hf, K, Li, Mg, Na, S, Sn, Zr)
Elements detected in paper substrate	Ba, Ca, Na, Si, Zn

3.2.3 Optimization of Parameters for Intaglio Printing Inks

During intaglio printing, ink is deposited on to the substrate. Ink is slightly embossed above the paper substrate, which makes the removal of ink, by laser ablation without causing any damage to the paper substrate more convenient in intaglio inks compared to other three types of printing inks. Figure 18 shows an example of intaglio ink elevated above paper. As the paper in intaglio inks (usually currencies) has security features inside them, it also contains a wide variety of elements. To ensure that there is no background contribution from paper, the paper was also analyzed and was subtracted from all the intaglio inks. Thus paper background subtracted intaglio printing inks were used for the discrimination purpose. Table 3 summarizes the optimized parameters for the analysis of intaglio inks.

Table 3. Optimized parameters for the analysis of intaglio printing inks by LA-ICP-MS.

Parameter	Intaglio
Laser wavelength	213 nm
Spot size	190 μm
Laser energy	35% (0.3mJ)
Ablation mode	Line
Stage speed	25 $\mu\text{m/s}$
Repetition rate	10 Hz
Carrier gas	He (0.9 L/min)
Ablation length	800 μm
Data acquisition mode	Mass scan m/z 7-238
Element menu for ink	(Al, Ba, Bi, Ca, Co, Cu, Fe, Hf, K, Mg, Mn, Mo, Na, Nb, Pb, Sb, Si, Sn, Sr, Ti, W, Zn, Zr)
Elements in paper substrate	Co, Cu, Eu, Fe, Hg, Hf, Ho, K, Na, Pb, Sn, Sm, Sr, Ti, U, W, Zr

3.2.4 Optimization of Parameters for Offset Printing Inks

The thickness of offset print out is less than that of toners and intaglio and is similar to inkjets. During the offset printing, a thin film of ink is partially embedded into the paper fibers. Laser energy was reduced to 25% (0.1mJ) to reduce the extent of paper damage. Various kinds of papers are used in offset printing inks. The current set of offset printing inks also had a wide variety of paper. The paper contribution was also taken into account during the analysis. The ink ablation was followed by paper ablation and the contribution of different elements in the paper was subtracted from the ink. The final result provided the net contribution for elements present only in the ink. Table 4 summarizes the optimized parameters for the analysis of offset printing inks.

Table 4. Optimized parameters for the analysis of offset printing inks by LA-ICP-MS.

Parameter	Offset printing ink
Laser wavelength	213 nm
Spot size	190 μm
Laser energy	25% (0.1mJ)
Ablation mode	Line
Stage speed	25 $\mu\text{m/s}$
Repetition rate	10 Hz
Carrier gas	He (0.9 L/min)
Ablation length	800 μm
Data acquisition mode	Mass scan m/z 7-238
Element menu for ink	22 elements (Al, Ag, Ba, Ca, Ce, Co, Cu, K, Mg, Mn, Mo, Na, Nb, Rh, S, Si, Sn, Sr, Ti, W, Zn, Zr)
Element menu for paper substrate	Al, Ba, Ca, Mg, Na, Ti, Si, Sr, Eu, Zn

Chapter 4. Data Acquisition, Analysis and Results by Standalone LA-ICP-MS

The obtained LA-ICP-MS spectra were used for data analysis. The scan method provided the m/z of elements from Li ($m/z= 6$) to U ($m/z =238$). As the resolution of the quadrupole mass spectrometer is one atomic mass unit, certain isotopes (^{40}Ca , ^{32}S , ^{56}Fe) could not be resolved from their interferences: namely (^{40}Ar , ^{32}O , $^{40}\text{Ar}^{16}\text{O}$). These mass regions, dominated by isobaric and polyatomic interferences, were avoided to protect the detector from saturation. Also isotopes of elements like Carbon (^{12}C), Nitrogen isotopes (^{14}N , ^{15}N , $^{14}\text{N}^{14}\text{N}$), Oxygen isotopes (^{16}O , ^{17}O , ^{18}O , $^{16}\text{O}^{16}\text{O}$), Argon isotopes (^{36}Ar , ^{38}Ar , ^{40}Ar) and major polyatomic interferences ($^{40}\text{Ar}^{16}\text{O}$, $^{40}\text{Ar}^{40}\text{Ar}$ and all the $^n\text{Ar}^n\text{Ar}$ isotopic combinations from $m/z^{n+n} 72$ to 80) were not selected for detection, during the scanning method to prevent detector saturation^{11,41}.

Potassium, being an important discriminator, was also included in the elemental menu. The resolution of the ^{39}K peak was customized to 0.4amu (atomic mass units) to minimize interferences from Ca and Ar isotopes. For the rest of the elements and their isotopes the default quadrupole resolution of 0.7amu was used^{11,41}. The intensity of the elements reflected the concentration of the element in the ink sample. The presence and absence of elements and the difference in the intensity of the element peaks were used to distinguish between different ink samples.

4.1. Data Reduction and Comparison Strategies for LA-ICP-MS

Two different data acquisition modes were tested during the present study. The first approach was using a transient mode, where a list of elements was selected to create a menu, and then the intensity of these elements were measured with respect to time. The

area under the curve reflected the concentration of the element. However, to use this method, a list of the elements present in the ink had to be known previously. One element menu does not work for 319 different inks as they have different elements. The other mode of data acquisition was a scan mode. This consisted of scanning the elements from ${}^7\text{Li}$ to ${}^{248}\text{U}$ so that no element is left out or missed and no prior knowledge of the elemental composition of the ink is required. Also the scan mode is suitable in circumstances when multiple comparisons are needed or when a certain database has to search for a possible match. Due to the unavailability of a single internal standard that works for all four types of inks, the total sum of the peaks was used to normalize each peak in the spectrum. This approach has already been described in literature^{41,68,69}.

4.2 Match Criteria

The data analysis was done using different match criteria. Spectral Overlay, Univariate and Multivariate Statistics were applied for the association and discrimination of printing inks.

4.2.1 Spectral Overlay

Four replicates of two inks were overlaid and compared using the Plot software (Plot 2 Version 2.0.8). Comparing the variation within replicates to the variation between replicates, a decision was made. If the variance within the replicates was similar to or less than the variance between replicates, then two samples were concluded to be indistinguishable. If the variance between replicates was larger than the variance within replicates, then the two samples were concluded to be distinguishable. In Figure 20, two types of inks are different by Mg isotopes while they are similar by Antimony isotopes.

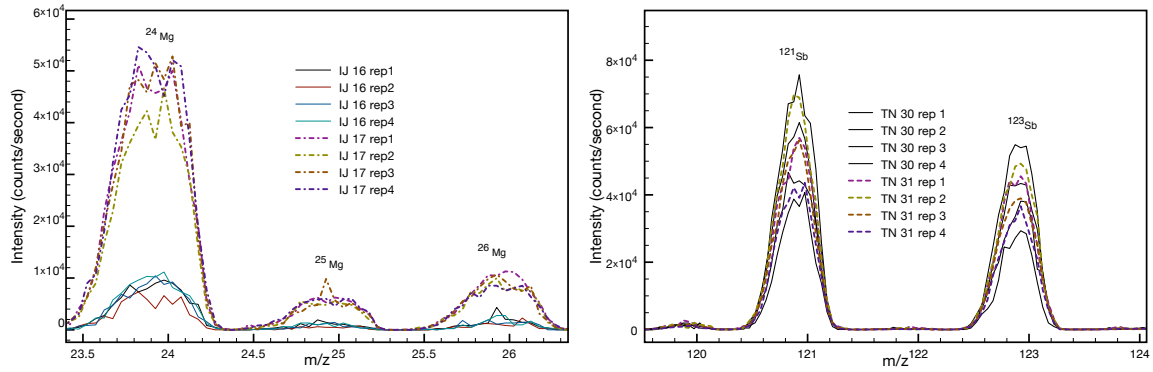


Figure 20. Spectral Overlay Comparison showing two different inks (left) differing by Mg concentration and two similar inks by Sb.

4.2.2 Univariate Statistics (Significance Testing for Pairwise Comparisons)

In univariate analysis, a single variable is under study. Two hypotheses are tested using a statistical test, to make a decision if there is any significant difference between the pairs or not. The number of possible pairs is given by equation (6),

$$\text{Number of possible pairs} = \frac{n(n-1)}{2} \quad (6)$$

Where n = total number of specimens under study. The means of two populations are compared using a t-test under the assumption that the data are normally distributed. Using a suitable test such as a 't' test, a 'p' value is calculated, and the value is compared to a pre-determined tabulated value for that fixed degree of freedom at a certain significance level ($\alpha = 0.01$ for 99% confidence level or $\alpha = 0.05$ for 95% confidence level). α is the level of significance. If the calculated p value is less than the Table value, the null hypothesis is rejected or vice versa⁷⁰. In an ideal case, a null hypothesis would be rejected when it is false, and would always be accepted when it is true. But this is not always the case. There are some errors associated with the hypothesis testing as well. The

incorrect rejection of a true null hypothesis is known as Type I or false positive error. Contrarily, another type of error that can occur during the hypothesis testing is Type II error, which is failing to reject a null when it is not true. The probability of a Type II error occurring is given by β . Power of sensitivity of a test is measured as $1-\beta$.

4.2.2.1 Analysis of Variance (ANOVA)

The comparison between two means can be done using a ‘t’ test, but when there are more than two means, ANOVA is used. It is because the chances of committing type I error increases with the increase in the number of comparison pairs when a ‘t’ test is used. So ANOVA is a statistical test used to determine any significant differences between three or more means. It is based on the comparison of variation between groups and the variation within groups⁷⁰.

The ANOVA F statistic is calculated using equation 7.

$$F = \frac{\text{Between group variance}}{\text{Within group variance}} \quad (7)$$

Between group variance and within group variances are calculated as shown in equation 8 and 9 respectively.

$$\text{Between group variance} = (\bar{X}_i - \bar{X})^2 \quad (8)$$

$$\text{Within group variance} = (\bar{X}_{ij} - \bar{X}_j)^2 \quad (9)$$

4.2.2.2 Tukey’s Honestly Significant Difference Test

The ANOVA test can determine if the means differ significantly but it alone cannot determine which means are significantly different. When the alternate hypothesis is accepted, it means that there is a significant difference between the groups in the sample, but the question still remains, which groups in the sample differ significantly. In

such a case, Tukey's Honestly Significant Difference Test is performed to determine which means significantly differ.

4.2.3 Multivariate Statistics

Mass spectrometry and emission spectroscopy provide spectra that are rich in information about different elements present in the matrix. Each of these elements can be considered as a variable. Multivariate statistics takes into account more than one variable at a time. This helps to visualize the contribution of all the elements at once. To simplify the visualization, the contribution of different elements is represented in 2 dimensions (using x and y axis) or in 3 dimensions (using x, y and z axis) after data reduction. Principal Component Analysis (PCA), Linear Discriminant Analysis (LDA), Partial Least Square Discriminant Analysis (PLS-DA), K-NN (K Nearest Neighbor Classification), and Cluster Analysis are some of the commonly used multivariate statistical tools.

4.2.3.1 Principal Component Analysis (PCA)

It is an unsupervised visualization technique. A set of linear combinations, also known as Principal Components (PCs), is created by the linear combination of the variables. A total of $N-1$ principal components that are orthogonal to each other are generated where N is the total number of variables. The first Principal Component provides the maximum variance, followed by second and third components. Since it is an unsupervised technique, prior knowledge of the samples is not required. It can be used as a classification and an exploratory technique. PCA helps to find out which group the unknown sample would be more similar to⁷⁰.

4.2.3.2 Linear Discriminant Analysis (LDA)

Unlike PCA, Linear Discriminant Analysis is a supervised technique, where the identity of all the samples is known. Two datasets, a training dataset and a test dataset, are required for this analysis. LDA builds a model based on training data set and uses the model to predict the test data set whose identity is already known. Cross validation is done using a Jackknife or leave one out method. The final result is presented in the form of a matrix, which shows the total percentage of correct classification and mis-classifications. This matrix is also known as confusion matrix⁷⁰.

4.2.3.3 Cluster Analysis

As the name implies, cluster analysis is a technique that divides samples into groups. Samples that exhibit similar properties are clustered into a group, while samples that are entirely different from each other are in separate groups. Hierarchical Cluster Analysis is one of the widely used cluster analysis methods. The clustering begins from each row, and builds up by combining the clusters together that are closest to each other based on their Euclidean distance⁷¹. The final result is a dendrogram, which shows the tree structure of different clusters.

4.3 Results for comparison of Toner Printing Inks

LA-ICP-MS provided a very good discrimination for toners belonging to different brands. The applicability of LA-ICP-MS was evaluated on the basis of its distinguishing power for samples originating from different sources, and also for its associating ability for the samples sharing a common origin. Type I and type II errors were evaluated.

Table 5. List of elements detected in toner printing inks by LA-ICP-MS.

TN	Na	Mg	Al	Si	K	Ca	Ti	Cr	Mn	Fe	Cu	Zn	Sr	Zr	Nb	Mo	Sn	Sb	Ba	Hf	W
1							Ti										Sn	Sb			
2		Mg	Al		K						Cu			Zr							
3		Mg	Al								Cu						Sn				
4	Na	Mg	Al								Cu										
5		Mg	Al								Cu						Sn				
6		Mg	Al				Ti								Nb						
7		Mg	Al				Ti							Zr			Sn				
8	Na	Mg	Al		K		Ti							Zr			Sn				
9			Al						Mn	Fe		Zn	Sr								
10		Mg	Al				Ti				Cu			Zr							
11																					
12									Mn	Fe		Zn									
13									Mn	Fe		Zn									
14						Ca															
15									Mn	Fe											
16			Al				Ti		Mn	Fe											
17									Mn	Fe											
18									Mn	Fe		Zn									
19									Mn	Fe											
20									Mn	Fe											
21		Mg	Al	Si			Ti							Zr	Nb						
22		Mg	Al				Ti				Cu										
23		Mg	Al								Cu										
24		Mg	Al				Ti							Zr	Nb						
25			Al	Si			Ti					Zn									
26		Mg	Al	Si			Ti								Nb						
27			Al	Si								Zn									
28							Ti					Zn					Sn	Sb	Ba		
29							Ti				Cu	Zn						Sb	Ba		
30							Ti					Zn						Sb	Ba		
31							Ti					Zn						Sb	Ba		
32	Na	Mg					Ti						Sr								
33		Mg					Ti				Cu		Sr								
34		Mg					Ti						Sr	Zr							W
35	Na	Mg					Ti						Sr		Nb						
36										Fe											
37																	Sn				
38																	Sn				
39											Cu	Zn					Sn				
40												Zn					Sn		Ba		
41												Zn					Sn				
42							Ti							Zr			Sn				
43							Ti				Cu				Nb		Sn				
44						Ca	Ti						Sr		Nb		Sn				

TN	Na	Mg	Al	Si	K	Ca	Ti	Cr	Mn	Fe	Cu	Zn	Sr	Zr	Nb	Mo	Sn	Sb	Ba	Hf	W
45						Ca	Ti						Sr		Nb		Sn				
46			Al								Cu						Sn	Sb			
47			Al								Cu						Sn	Sb			
48			Al														Sn	Sb			
49			Al														Sn	Sb			
50			Al														Sn				
51								Cr													
52							Ti							Zr	Nb		Sn			Hf	
53							Ti							Zr	Nb		Sn			Hf	
54		Mg	Al		K		Ti														
55			Al	Si								Zn									
56		Mg	Al		K		Ti							Zr	Nb						
57							Ti						Sr	Zr			Sn			Hf	
58			Al				Ti		Mn	Fe		Zn	Sr								
60			Al				Ti			Fe	Cu		Sr				Sn				
61												Zn					Sn				
62												Zn					Sn				
63		Mg	Al				Ti				Cu										
64		Mg	Al				Ti								Nb						
65		Mg	Al				Ti								Nb						
66			Al		K		Ti			Fe											
67	Na		Al				Ti				Cu				Nb		Sn				
68	Na		Al				Ti										Sn				
69										Fe							Sn				
70	Na										Cu		Sr			Mo					
71	Na	Mg	K																		
72	Na																				
73							Ti								Nb		Sn	Sb			
74							Ti				Cu		Sr					Sb			
75							Ti						Sr					Sb			
76					K		Ti										Sn	Sb			
77									Mn	Fe											

A total of 21 elements were detected in toners. The detailed list of elements is tabulated in Table 5. Elements like Ti, Al, and Sn were found in more than 10% of the toner samples. Figure 21 shows that Ti was found in most of the toners (13.6%), while Cr, Mo, and W were found in only a few toners (0.3% each). Elements like Zr, Hf, Mo,

and W are rarely found in the ink samples. The use of these elements can be found in literature. For example, Zr has been found to be used in inks to promote adhesions to metals and plastics and as cross linkers, and Zr has also been found to be the primary source of Hafnium⁷². Tungsten (W) has been found to be used in the fixing of ink toners as substrate⁷³. Similarly, Molybdenum is another useful element used in electrostatic toners. It has been found to be used as a charge controlling agent specially in blue toners⁷⁴.

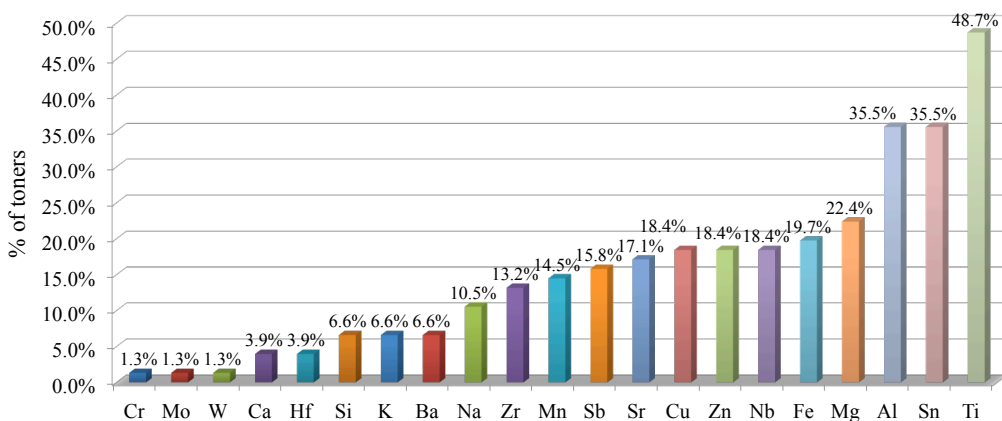


Figure 21. Bar graph showing the distribution of elements in toner printing inks.

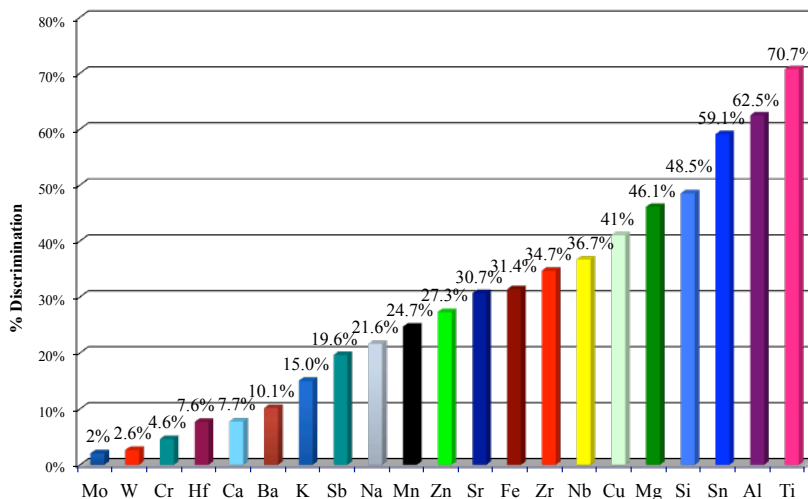


Figure 22. Bar graph showing discrimination capability of different elements in toners.

Different elements had different contribution in discrimination. Elements like Ti and Al were able to discriminate 70.7% and 62.5% of the comparison pairs, while Mo and W were only able to discriminate 2% and 2.6% of the pairs, as shown in Figure 22.

4.3.1 Black Toner Printing Inks

Most of the toner inks were black in color. A total of 19 elements were detected in this subset. Most of the black toners contained Ti (48.7%), followed by Sn (41%). Elements like Si, Ca, Cr, and Ba were detected in less than 5% of the black toners, while elements like W and Mo were completely absent. Figure 23 shows the distribution of elements in black toners.

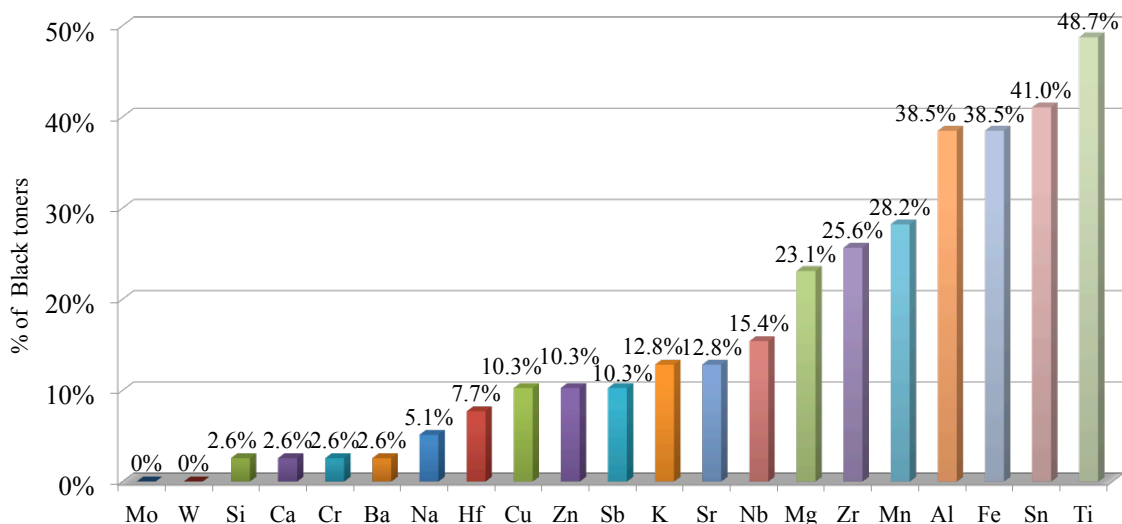


Figure 23. Bar graph showing the distribution of elements (in %) in black toners.

4.3.2 Cyan Toner Printing Inks

A total of 16% of the toners were cyan in color. Cu was the only element that was present in all cyan colors. It has been reported in the literature that Cu phthalocyanines is the most widely used pigment in blue inks⁷⁵. The chemical structure of Cu phthalocyanine is shown in Figure 24.

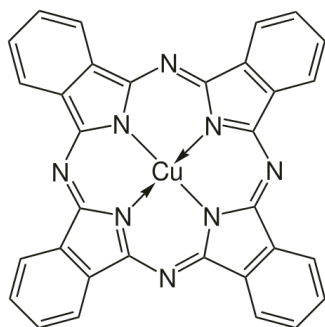


Figure 24. Chemical structure of Cu Pthalocyanine.

Similarly, Ti and Aluminum were present in 58% and 50% of the cyan toners respectively. Molybdenum and Ba were present in only two of the cyan toners. Some elements, like Si, K, Ca, Cr, Mn, Fe, Zr, Hf, and W, were completely absent in this subset. Figure 25 shows the detection of different elements in cyan toners.

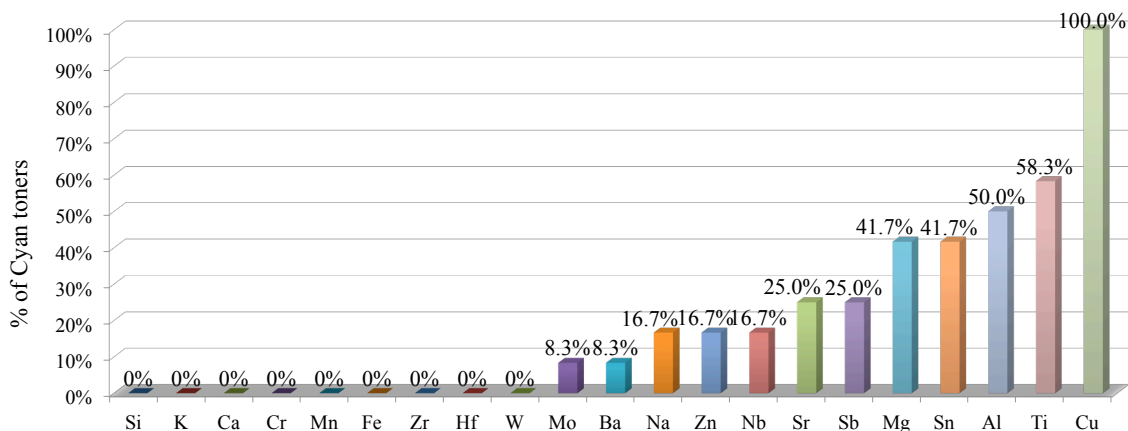


Figure 25. Bar graph showing the distribution of elements in cyan toners.

4.3.3 Yellow Toner Printing Inks

A total of 14 elements were detected in yellow toners. Aluminum, Ti, and Tin were present in 46.2% of the yellow toners, while elements like Cr, Mn, Fe, Zr, Mo, Hf, and W were completely absent. Similarly, 7.7% of the yellow toners had K, Ca, Cu, and Ba. Figure 26 shows the distribution of different elements in yellow toners.

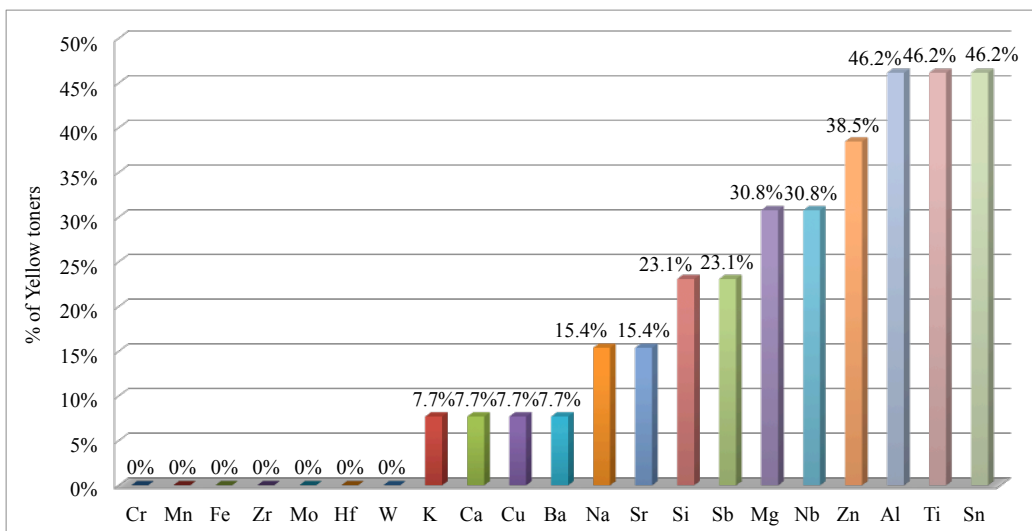


Figure 26. Bar graph showing the distribution of elements in yellow toners.

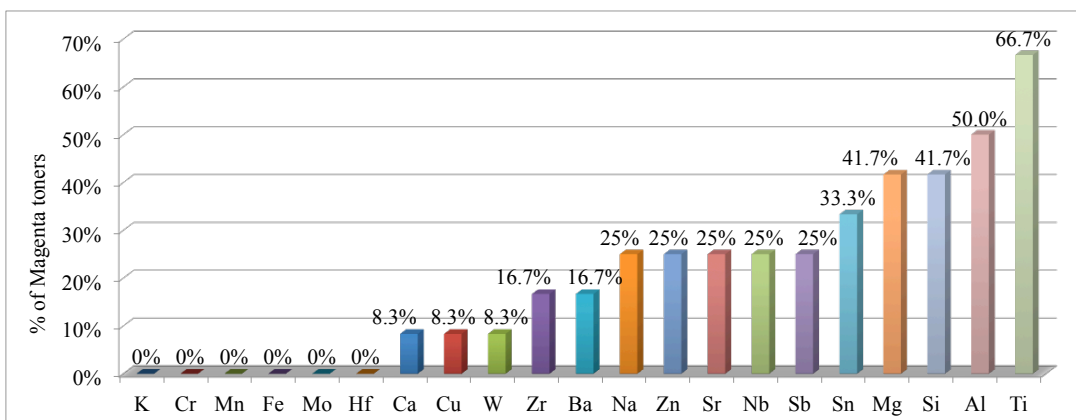


Figure 27. Bar graph showing the distribution of elements in the magenta toners.

4.3.4 Magenta Toner Printing Inks

Figure 27 shows the percentage of magenta toners containing different elements. Titanium was the most frequently detected element in magenta toners. It was detected in eight out of twelve magenta toners ($2/3^{\text{rd}}$). Elements like K, Cr, Mn, Fe, Mo, and Hf were completely absent in this set. Cu, Ca, and W were detected in 8.3% of the magenta toners. Na, Zn, Sr and Nb were detected in one-fourth of this set. Similarly Ba and Zr

were the other rare elements that were detected in this set. Aluminum was detected in 50% of magenta toners.

4.3.5 Overall Discrimination for Toner Printing Inks

Overall discrimination using LA-ICP-MS was found to be 99.1% with 0.9% false exclusion. Out of the 25 indistinguishable pairs, 14 of them shared the same brand. The indistinguishable toner pairs were mostly from HP brand. The remaining nine of them were Hewlett Packard versus Sharp and Cannon. The overall discrimination is summarized in Table 6. Table 7 shows the list of indistinguishable pairs.

Table 6. Discrimination capability of LA-ICP-MS for the analysis of toner printing inks.

# Samples	76
# Samples from different sources	76
# Comparison Pairs	(2850 comparison pairs)
Duplicate controls from same sources	4 quality controls, 20 duplicate controls (26 comparison pairs)
% Discrimination	99.1% (2825 out of 2850)
% False exclusions	7.7% (2 out 26)
% False inclusions	0.9% (25 out of 2850)

Of these 25 indistinguishable pairs, 18 pairs were black, 2 pairs were yellow, and 4 pairs were of different colors (magenta Vs. yellow), as shown in Table 7. Of these 4 pairs with different colors, 3 pairs shared a common brand. These indistinguishable pairs were found to have a very similar elemental profile. Four of the pairs were discriminated by either Na or K or both. These elements are sometimes transferred through contamination by hands. The discrimination of toners without taking Na and K as discriminators is 98.98% (2821 out of 2850).

Table 7. List of toner pairs that were indistinguishable by LA-ICP-MS.

Indistinguishable Pairs	Color	Brand
12TN Vs. 13TN	Black	HP
12TN Vs. 19TN	Black	HP
13TN Vs. 19TN	Black	HP
13TN Vs. 18TN	Black	HP
15TN Vs. 17TN	Black	HP
15TN Vs. 18TN	Black	HP
17TN Vs. 18TN	Black	HP
17TN Vs. 20TN	Black	HP
18TN Vs. 19TN	Black	HP
37TN Vs. 38TN	Black	OKI
54TN Vs. 56TN	Black	HP
52TN Vs. 53TN	Black	RICOH
12TN Vs. 77TN	Black	HP Vs. SH
13TN Vs. 77TN	Black	HP Vs. SH
14TN Vs. 77TN	Black	HP Vs. SH
17TN Vs. 77TN	Black	HP Vs. SH
18TN Vs. 77TN	Black	HP Vs. SH
19TN Vs. 77TN	Black	HP Vs. SH
22TN Vs. 63 TN	Cyan	HP Vs. CN
27TN Vs. 55 TN	Yellow	HP
27TN Vs. 65 TN	Yellow	HP Vs. CN
30TN Vs. 31 TN	Magenta	IM
44TN Vs. 45 TN	Magenta	XR
64TN Vs. 26 TN	Magenta	CN Vs. HP
64TN Vs. 65 TN	Magenta	CN

Table 8. Overall Discrimination for toners in CMYK colors.

	Black	Cyan	Magenta	Yellow
# Samples	39	12	12	13
# Samples from different sources	39	12	12	13
# Comparison pairs	741	66	66	78
% Discrimination	97.6%(723/741)	98.5% (65/66)	100% (66/66)	97.4 (76/78)
% False inclusions	2.4% (18/741)	1.5% (1/66)	0 (0/20)	2.6% (2/78)

The discrimination capability of LA-ICP-MS for toners across four different colors is shown Table 8. Only one of the pairs (Toner 64 and Toner 26) was from different brands, CN and HP, respectively. Similarly, Toner 52 and Toner 53 were from two cartridges that were part of the same package and batch. Besides discrimination, association of the controls was also studied to ensure that the experimental conditions remained the same between days and within days. Toner 37 was used at the beginning and end of the day as a control. The replicates were compared using Spectral Overlay and One-Way ANOVA to validate the performance of the instrument. Tin was the only element found in Toner 37 and all the isotopes of Sn were monitored for inter-day and intra-day variation as shown in Figure 28. The overlapping of the replicates was detected through spectral overlay, which meant that TN 37 remained constant throughout the experiment. It meant that the overall experimental conditions remained constant. Similarly, One-Way ANOVA with Tukey's HSD was also performed for the integrated peaks of Sn isotopes. Figure 29 is the One-Way ANOVA with Tukey's HSD plot for the toner controls, which shows no significant difference between the Sn isotopes.

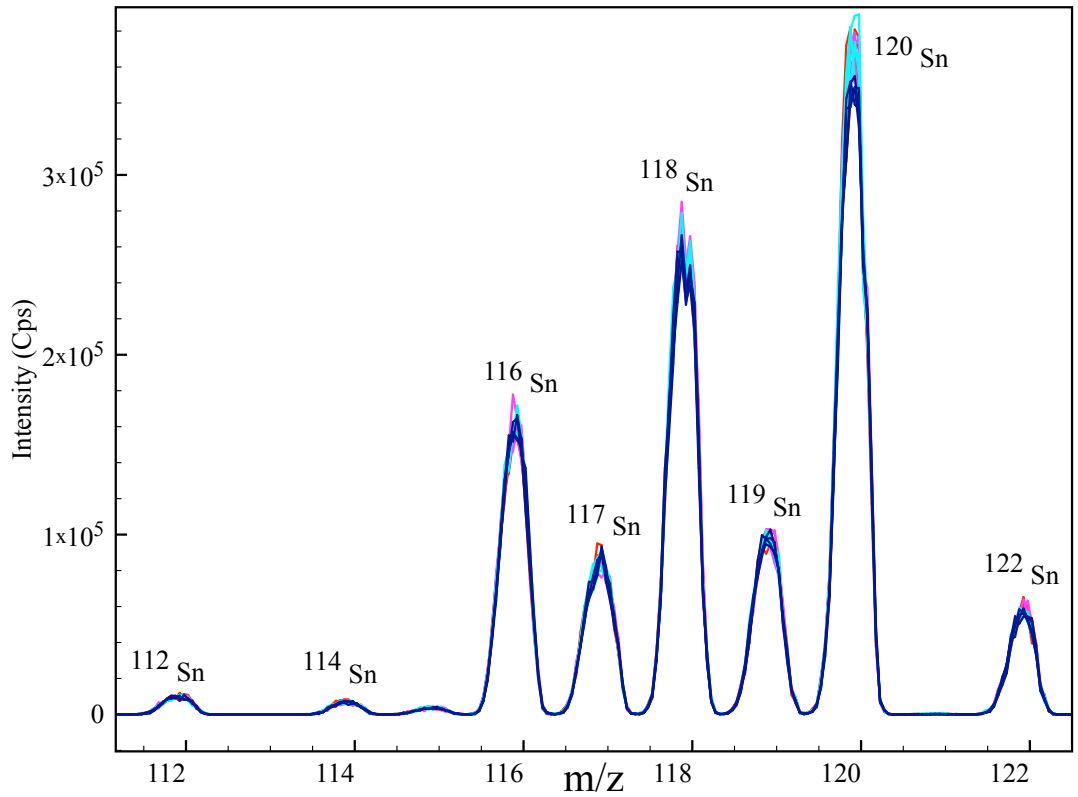


Figure 28. Spectral Overlay showing overlapping of different replicates of control TN 37.

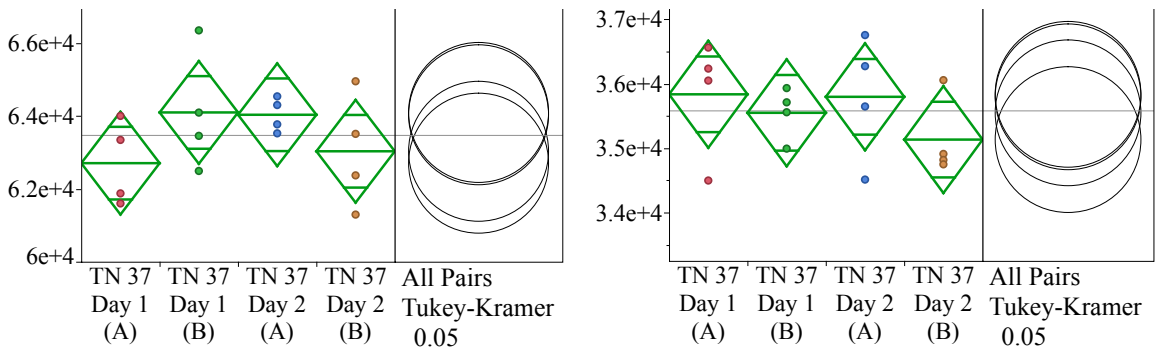


Figure 29. One Way ANOVA for Sn isotopes (^{116}Sn on the left and ^{117}Sn on the right) for TN 37 (Control).

4.3.6 Multivariate Analysis of Toner Printing Inks

The multivariate analysis of inkjet samples was performed by the application of Linear Discriminant Analysis and Principal Component Analysis. There were a total of 3635 data points in the entire mass spectrum. All the regions in the mass spectrum were not significant; hence, only those elements that were significantly higher than the noise (three times the intensity of paper) were used for statistical analysis. The peaks for the corresponding elements were integrated using Plot software (Plot 0.997). Thus, the obtained peak areas were used as variables for the multivariate analysis.

4.3.6.1 Principal Component Analysis of Toner Printing Inks

The visualization of 76 toners was done with Principal Component Analysis. A total of 21 elements were detected in the toner set. PCA was performed using these 21 different variables, which reduced the dimensionality of the analysis to three major Principal Components (PCs). Figure 30 shows the PCA plot for toner samples in two dimensions. Similarly, Figure 31 is the three dimensional PCA plot for toners that shows the classification of 76 different toner printing inks. The variance explained by the first three Principal Components, using 21 different elements, is summarized in Table 9.

Table 9. PCA scores for first three components.

PC1	PC2	PC3	Cumulative variance
16.7%	14.6%	12.9%	44.2%

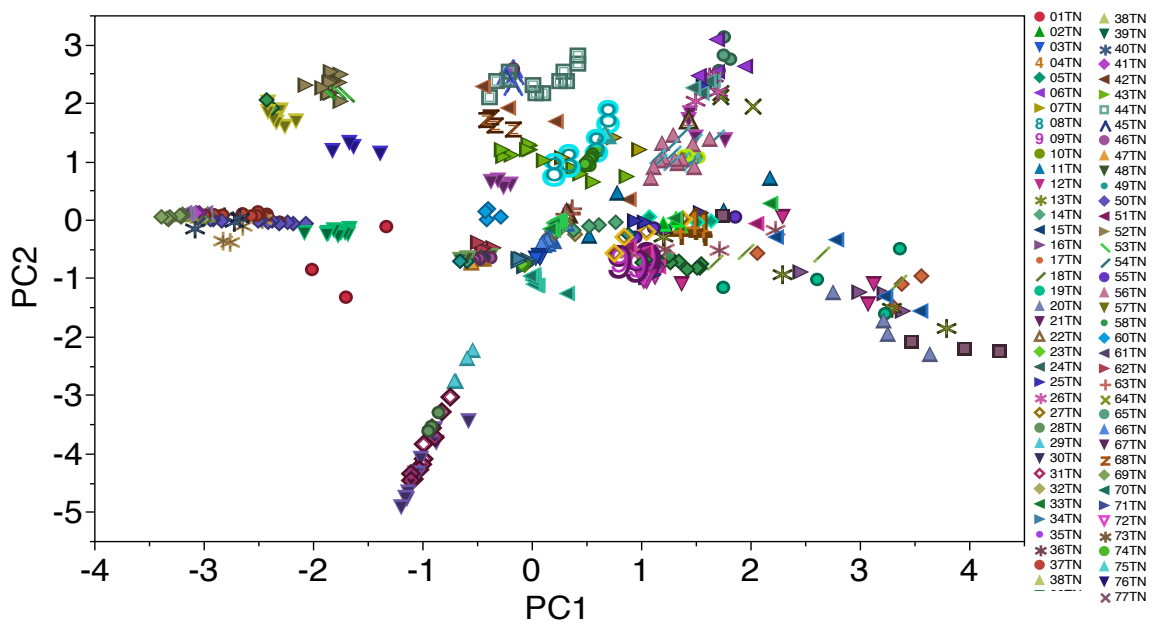


Figure 30. Two-dimensional PCA plot for toners.

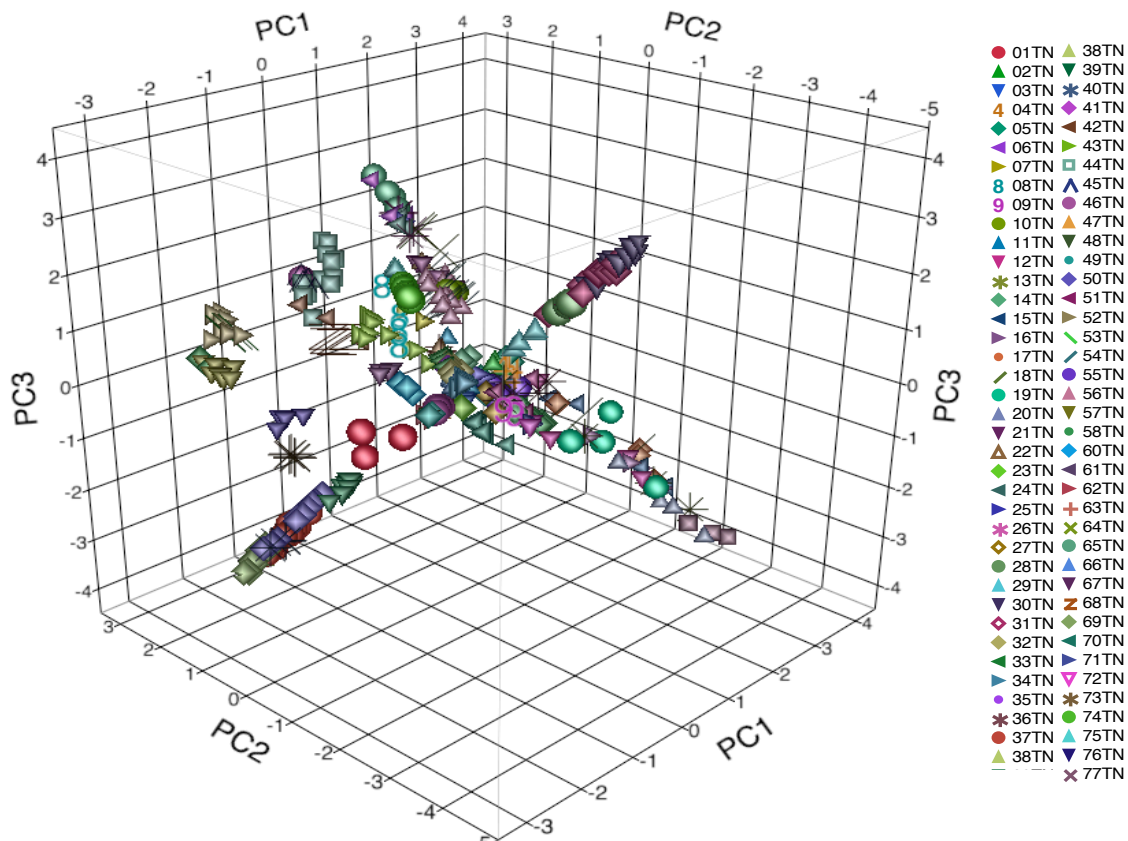


Figure 31. Three-dimensional PCA plot for 77 toners.

4.3.6.2 Principal Component Analysis by Brand

All the toners belonged to one of the sixteen brands. The classification of the brands can be visualized in Figure 32. The HP brand were randomly spread all over the PCA plot which accounted for almost one third (32.8%) of the total toner samples. XR (Xerox), and OD (office Depot), and RC (Ricoh) brands were clearly separated from the remaining toners. Sixteen different brands can be visualized through the two-dimensional and three-dimensional PCA plots as shown in Figure 32 and 33 respectively.

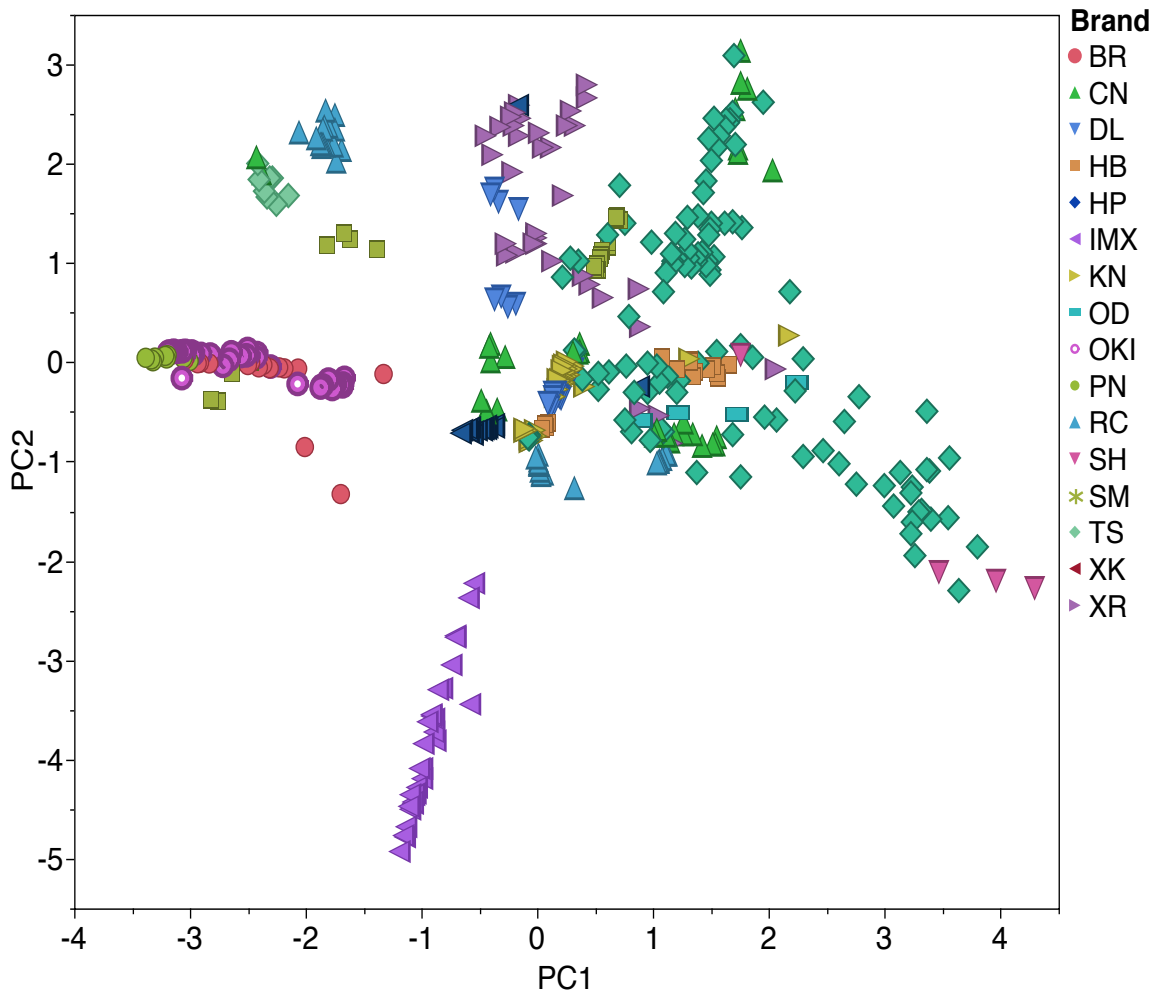


Figure 32. Two-dimensional PCA plot for 77 toners by brand.

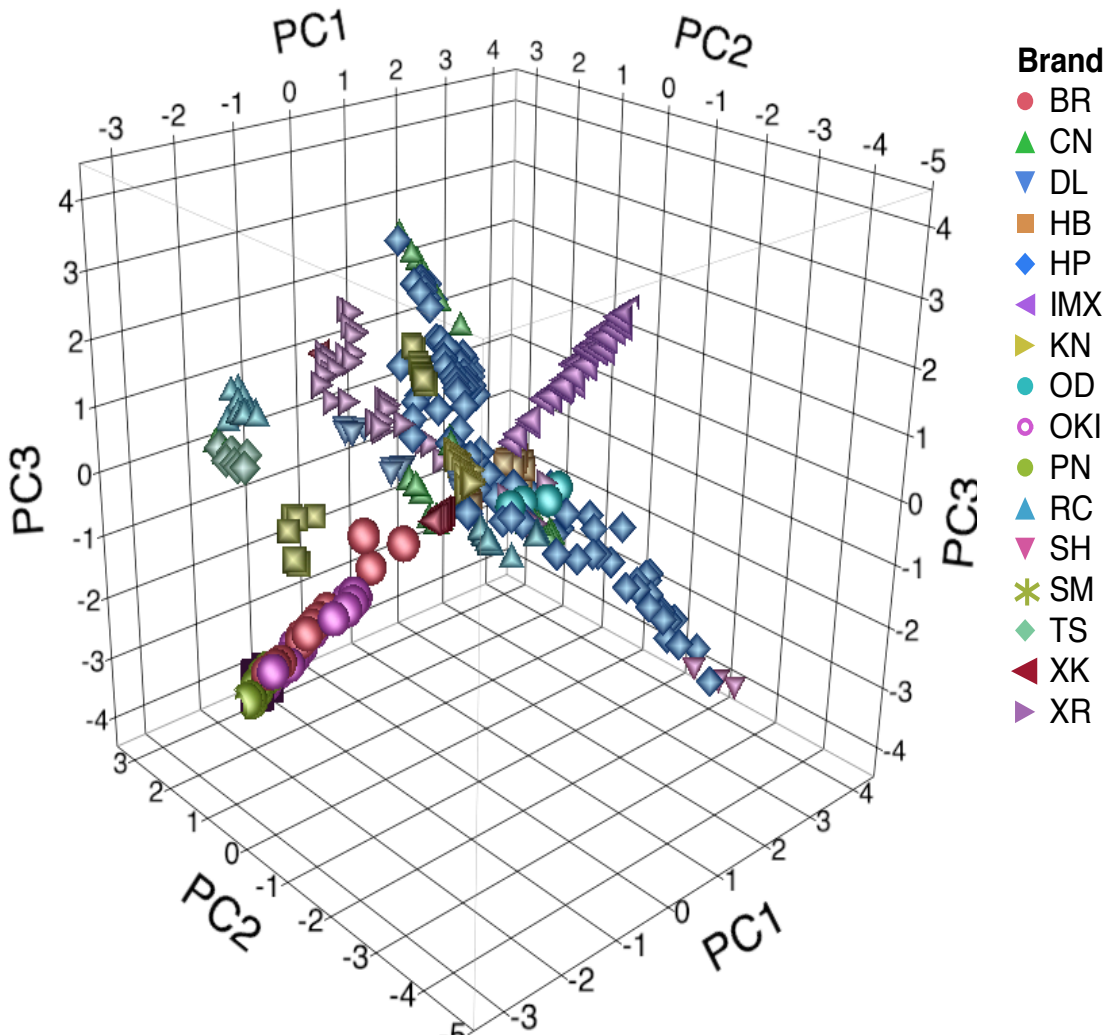


Figure 33. Three-dimensional PCA plot for 77 toners by brand.

4.3.6.3 Linear Discriminant Analysis (LDA) of Toner Printing Inks

Linear Discriminant Analysis was used for discrimination of 76 toner printing inks using leave-one-out cross validation. A total of 41 pairs were misclassified by LDA, resulting in 98.48% of total correct classification. Table 10 lists the misclassified pairs. Out of the 41 pairs, 9 pairs were also found to be indistinguishable by Spectral Overlay. These common pairs are listed in table 11.

Table 10. Misclassified pairs by linear discriminant analysis

Toner Pairs	Color	Brand
TN 12 Vs. TN 55	Black Vs. Yellow	HP
TN 12 Vs. TN 72	Black Vs. Yellow	HP Vs. RC
TN 13 Vs. TN 19	Black	HP
TN 15 Vs. TN 58	Black	HP Vs. CN
TN 15 Vs. TN 36	Black	HP Vs. OD
TN 18 Vs. TN 36	Black	HP Vs. OKI
TN 18 Vs. TN 9	Black	HP
TN 18 Vs. TN 15	Black	HP
TN 19 Vs. TN 15	Black	HP
TN 20 Vs. TN 18	Black	HP
TN 22 Vs. TN 17	Cyan Vs. Black	HP
TN 22 Vs. TN 63	Cyan	HP Vs. CN
TN 25 Vs. TN 21	Magenta Vs. Black	HP
TN 27 Vs. TN 26	Magenta Vs. Yellow	HP
TN 30 Vs. TN 72	Magenta Vs. Yellow	IMX Vs. RC
TN 31 Vs. TN 30	Magenta Vs. Yellow	IMX
TN 31 Vs. TN 28	Black Vs. Yellow	IMX
TN 33 Vs. TN 28	Cyan Vs. Black	KN Vs. IMX
TN 33 Vs. TN 55	Cyan Vs. Yellow	KN Vs. HP
TN 33 Vs. TN 35	Cyan Vs. Yellow	KN
TN 36 Vs. TN 35	Yellow Vs. Black	KN Vs. OD
TN 37 Vs. TN 51	Black	OKI Vs. XR
TN 38 Vs. TN 37	Black	OKI
TN 40 Vs. TN 61	Magenta Vs. Yellow	OKI
TN 41 Vs. TN 37	Yellow Vs. Black	OKI
TN 42 Vs. TN 38	Black	XR Vs. OKI
TN 42 Vs. TN 44	Black Vs. Magenta	XR
TN 46 Vs. TN 44	Black Vs. Magenta	XK Vs. XR
TN 46 Vs. TN 47	Black Vs. Cyan	XK
TN 46 Vs. TN 45	Black Vs. Yellow	XK Vs. XR
TN 49 Vs. TN 47	Yellow Vs. Cyan	XK
TN 49 Vs. TN 48	Yellow Vs. Magenta	XK
TN 49 Vs. TN 62	Yellow Vs. Black	XK Vs. CN
TN 49 Vs. TN 48	Magenta Vs. Yellow	XK
TN 51 Vs. TN 48	Black Vs. Magenta	XR Vs. XK
TN 54 Vs. TN 72	Black Vs. Yellow	HP Vs. RC
TN 61 Vs. TN 54	Yellow Vs. Black	OKI Vs. HP
TN 64 Vs. TN 38	Magenta Vs. Black	CN Vs. OKI
TN 74 Vs. TN 24	Magenta Vs. Cyan	SM Vs. HP
TN 77 Vs. TN 74	Black Vs. Magenta	SH Vs. SM
TN 77 Vs. TN 20	Black	SH Vs. HP

Table 11. List of common toner pairs that were not distinguished by Spectral Overlay and were also misclassified by LDA.

	Toner Pairs	Color	Brand	Elements detected
1)	TN 12 K HP	Black	HP	(Mn, Fe)
	TN 19 K HP	Black	HP	(Mn, Fe)
	TN 15 K HP	Black	HP	(Mn, Fe)
2)	TN 17 K HP	Black	HP	(Mn, Fe)
	TN 15 K HP	Black	HP	(Mn, Fe)
3)	TN 18 K HP	Black	HP	(Mn, Fe)
	TN 17 K HP	Black	HP	(Mn, Fe)
4)	TN 20 K HP	Black	HP	(Mn, Fe)
	TN 18 K HP	Black	HP	(Mn, Fe)
5)	TN 19 K HP	Black	HP	(Mn, Fe)
	TN 54 K HP	Black	HP	(Mg, Al, K, Ti, Zr, Nb)
6)	TN 56 K HP	Black	HP	(Mg, Al, K, Ti, Zr, Nb)
	TN 22 C HP	Cyan	HP	(Mg, Al, Ti, Cu)
7)	TN 63 C CN	Cyan	CN	(Mg, Al, Ti, Cu)
	TN 22 C HP	Cyan	HP	(Mg, Al, Ti, Cu)
8)	TN 63 C CN	Cyan	CN	(Mg, Al, Ti, Cu)
	TN 30 M IMX	Magenta	IMX	Ti, Zn, Sb, Ba)
	TN 31 Y IMX	Yellow	IMX	Ti, Zn, Sb, Ba)
9)	TN 63 C CN	Cyan	CN	(Mg, Al, Ti, Cu)
	TN 22 C HP	Cyan	HP	(Mg, Al, Ti, Cu)

Most of the indistinguishable pairs in Spectral Overlay and also the misclassified pairs by Linear Discriminant Analysis were either of the same color or were of the same brand as shown in Table 10 and 11.

4.3.6.4 Partial Least Squares Discriminant Analysis (PLS-DA) for Toner Printing Inks

An ink database was created with 76 toner printing inks. The replicates of ink were divided into two parts: one for training the database and the other for testing the database. The training or the reference database provides the background information about different kinds of available samples, while the testing database contains the information about a new or unknown ink sample. Spectral classification was done by

PLS-DA by using LIA-GIU (Laser Induced Acoustics- Graphic User Interface) software developed by CoVar technology in collaboration with Applied Spectra. This software performs PLS-DA using chemometrics and machine learning algorithm. For the 20 duplicate controls, PLS-DA showed a very good agreement between the reference database and the test database. If the correct duplicate was listed as one of top five selections provided by the PLS-DA algorithm, then it was predicted to be a match. For very similar inks coming from the same manufacturer, the rationale was that the correct matches could be multiple and be listed as second, third or fourth.

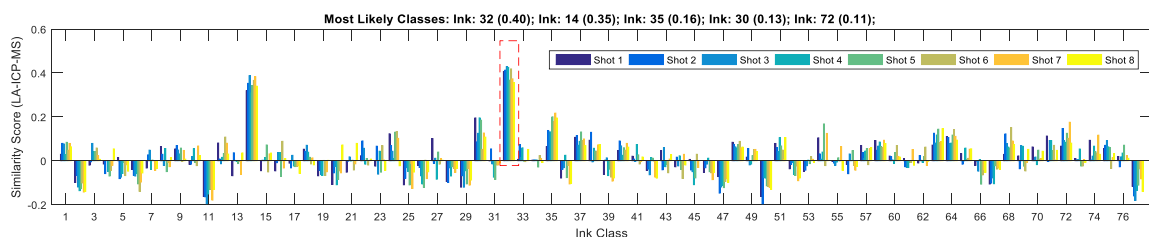


Figure 34. PLS-DA plot showing the correct association of a duplicate toner control with the same toner ink in the database.

From Figure 34, it can be seen that the duplicate control of toner 32 correctly matches to toner 32 in the database. In the Y-axis positive value shows the extent of similarity between the test sample (in this case duplicate controls of Toner 32 and the ink samples in the database). The similarity score on the Y-axis for TN 32 in the database is 0.4, which is the highest out of five possible matches, as shown in Figure 34. Eight duplicates (controls) of TN 32 correctly associate with the TN 32 in the database. The PLS-DA algorithm showed that 18 out of 20 duplicate controls were correctly associated with their respective sources in the ink database providing 90% correct classification.

4.3.6.5 K- Nearest Neighbor analysis (KNN classification) for Toner Printing Inks

The number of neighbors taken for classification was ten. So a classification was said to be correct if any of the top 10 similar spectra identified by KNN as a possible match for the test sample was correctly identified.

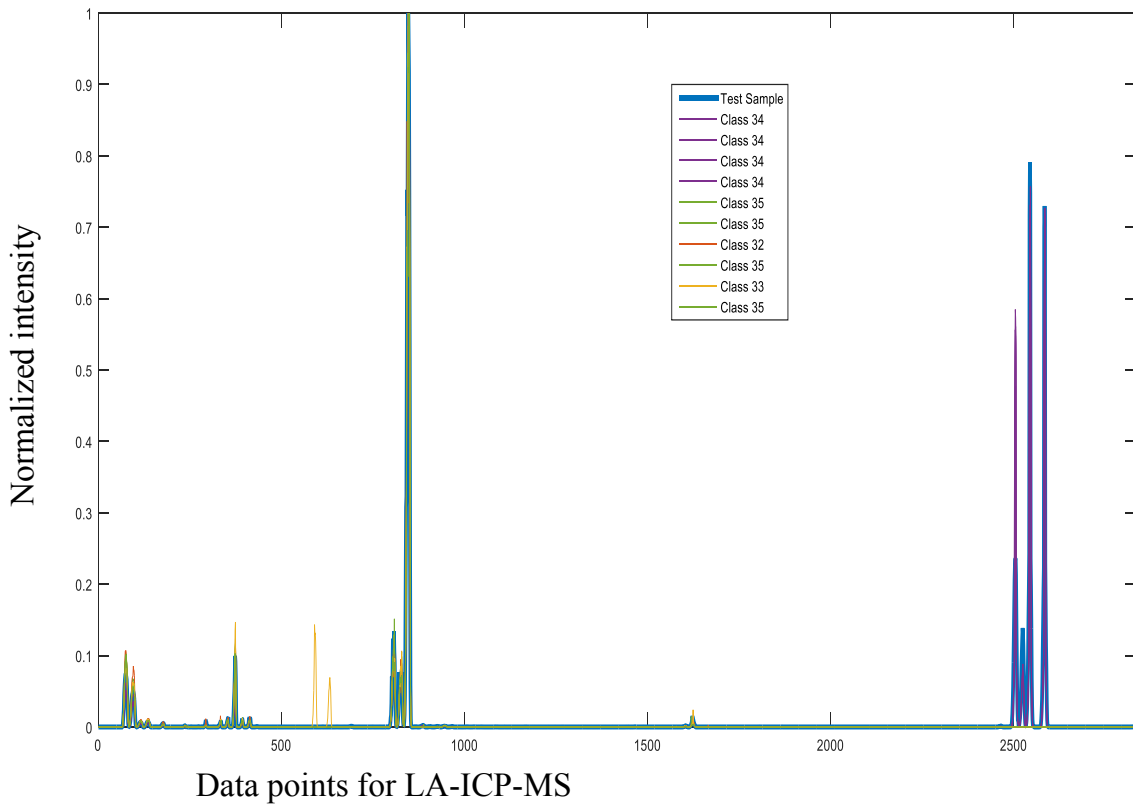


Figure 35. KNN plot for duplicate control TN 34 showing the correct association in the ink database.

Figure 35 shows that Toner 34 by KNN approach is correctly listed in the first four neighbors pulled out by the algorithm from the database. Only two of the duplicate toners were incorrectly classified, providing a correct classification of 90% for the 20 duplicate controls.

4.4 Results for Comparison of Inkjet Printing Inks

The number of elements detected in inkjet inks was relatively lower as compared to toners. However, a very good discrimination was detected for the pairwise comparison of inkjet inks. The element that was only detected in inkjet printing inks was Li. It is used as a conductive element in the form of Lithium nitrate and also as a drier. Elements like Mg and Zr are used as extenders and driers, respectively, for some inkjets⁵⁷.

Table 12. List of elements detected in inkjet inks.

Inkjets	Li	Na	Mg	Al	S	K	Cu	Fe	Zr	Sn	Ba	Hf
1.	Li	Na				K						
2.												
3.		Na				K						
4.		Na										
5.		Na										
6.		Na					Cu					
7.		Na				K						
8.		Na					Cu		Zr		Ba	
9.		Na										
10.		Na										
11.		Na				K			Zr			
12.	Li	Na	Mg			K	Cu					
13.		Na				K						
14.	Li	Na	Mg			K	Cu					
15.	Li	Na	Mg			K	Cu					
16.	Li	Na	Mg			K						
17.		Na	Mg			K	Cu					
18.		Na	Mg				Cu					
19.	Li	Na	Mg				Cu					
20.		Na				K						
21.		Na	Mg		S		Cu					
22.		Na	Mg		S							
23.		Na	Mg		S	K						
24.		Na				K						
25.		Na	Mg		S		Cu					
26.		Na	Mg		S							
27.		Na	Mg		S							
28.		Na				K			Zr			
29.		Na				K				Sn		
30.		Na				K	Cu		Zr	Sn		Hf
31.		Na				K	Cu		Zr	Sn		Hf
32.		Na				K			Zr	Sn		Hf

33.		Na				K			Zr	Sn		
34.		Na			S		Cu			Sn		
35.		Na			S					Sn		
36.		Na			S					Sn		
37.		Na				K						
38.	Li	Na			S	K						
39.	Li	Na			S							
40.		Na			S		Cu					
41.		Na				K						
42.		Na			S		Cu	Fe				
43.		Na				K						
44.		Na										
45.		Na				K	Cu					
46.		Na				K						
47.		Na										
48.	Li	Na										
49.		Na				K			Zr			
50.		Na				K			Zr	Sn		
51.		Na				K			Zr			
52.		Na				K			Zr			
53.		Na					Cu					
54.		Na										
55.		Na										
56.		Na		Al		K						
57.		Na		Al		K						
58.				Al		K	Cu		Zr			
59.		Na		Al	S	K						
60.				Al		K						
61.		Na				K						
62.		Na			S							
63.		Na			S	K						
64.		Na										
65.		Na			S							
66.		Na			S		Cu					
67.		Na			S							
68.	Li	Na										
69.		Na				K						
70.		Na			S		Cu					
71.		Na			S							
72.		Na			S							
73.		Na				K						
74.		Na				K						
75.		Na	Mg		S		Cu					
76.		Na			S							
77.		Na			S		Cu					
78.	Li	Na				K	Cu					

A total of 12 elements were detected for the inkjet set. Sodium was present in almost all of the inkjets (94.9%) and K was present in half of the samples as shown in figure 36. Table 12 shows the list of elements that were detected in inkjet set.

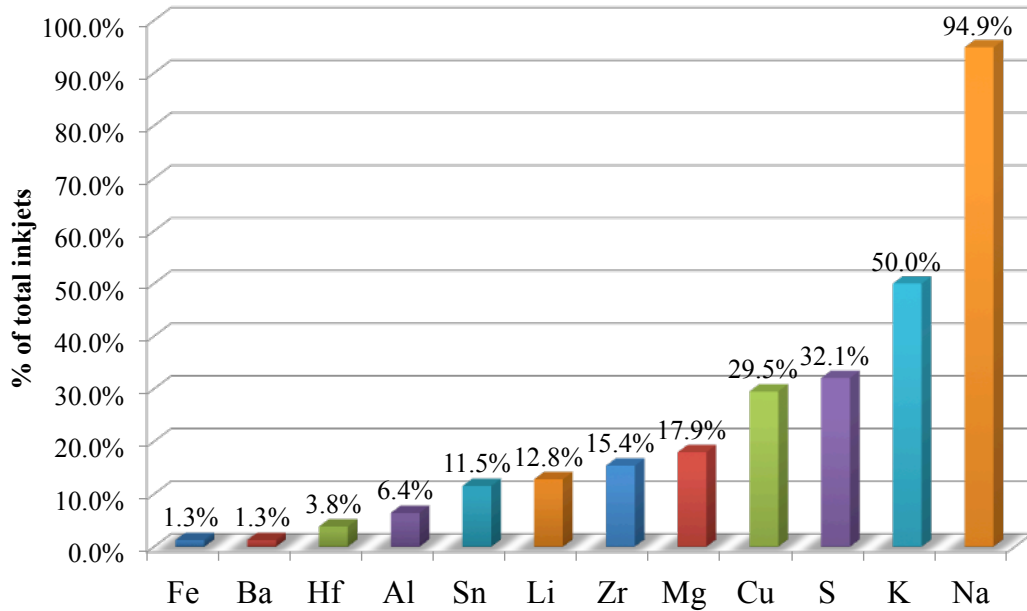


Figure 36. Bar graph showing the distribution of elements in inkjet inks.

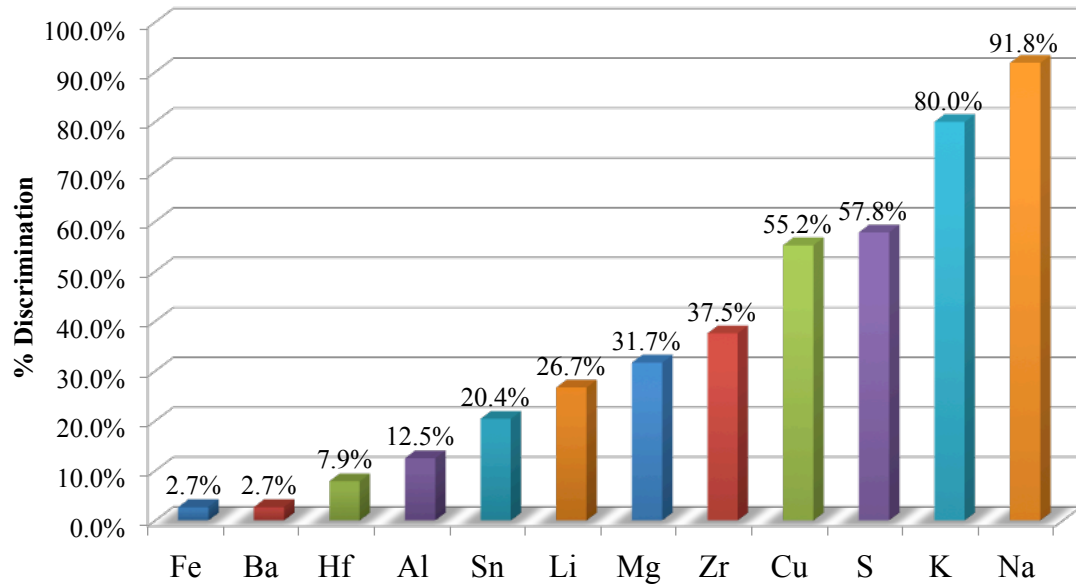


Figure 37. Bar graph showing the contribution of each element for pairwise comparison of inkjet printing inks.

The contribution of each individual element was also analyzed. It was found that Na and K were the most useful in discriminating the inkjet inks. Figure 37 shows the contribution of each element for the discrimination of 78 inkjet printing inks.

4.4.1 Black Inkjet Printing Inks

Almost all of the black inkjets (31 out of 32) contained Na. The other elements that were present were Al, Sn, Cu, Mg, Zr, Li, and K. Elements like S, Fe, Ba, and Hf were absent in black inkjets. The percentage of different elements is shown in Figure 38.

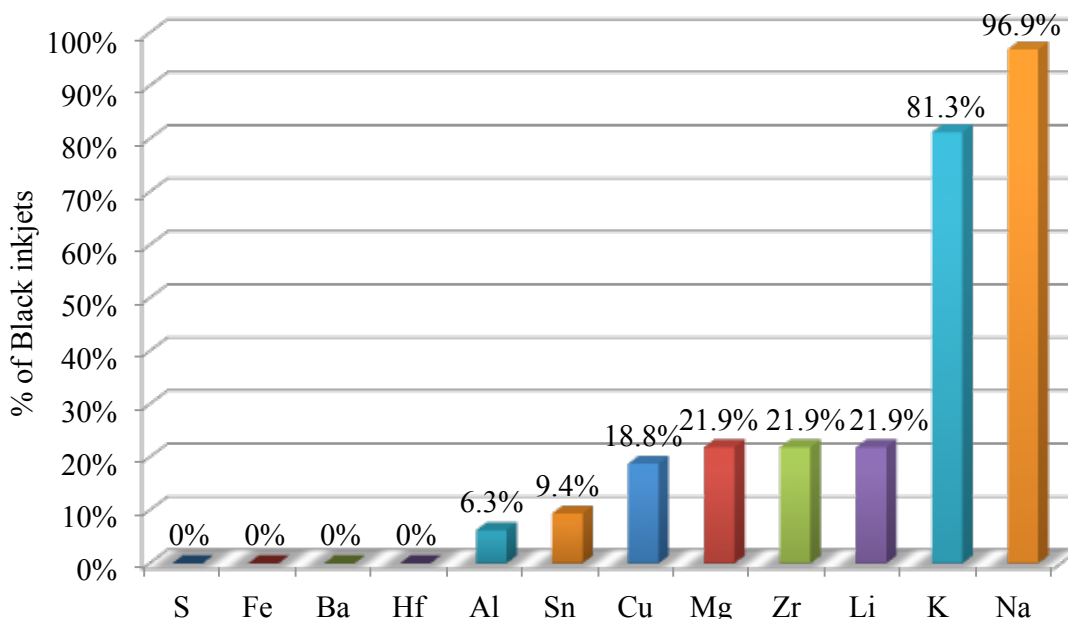


Figure 38. Bar graph showing the distribution of elements in black inkjets.

4.4.2 Cyan Inkjet Printing Inks

Like toners, all of the cyan inkjets also contained Cu. Similarly; Na was also present in all the cyan inkjet samples. At least one element from the element menu of inkjet set was present in all of the cyan inkjets. Figure 38 shows that Al, Fe, Ba, Hf, and Li were detected in only 6.7% of the total cyan inkjets.

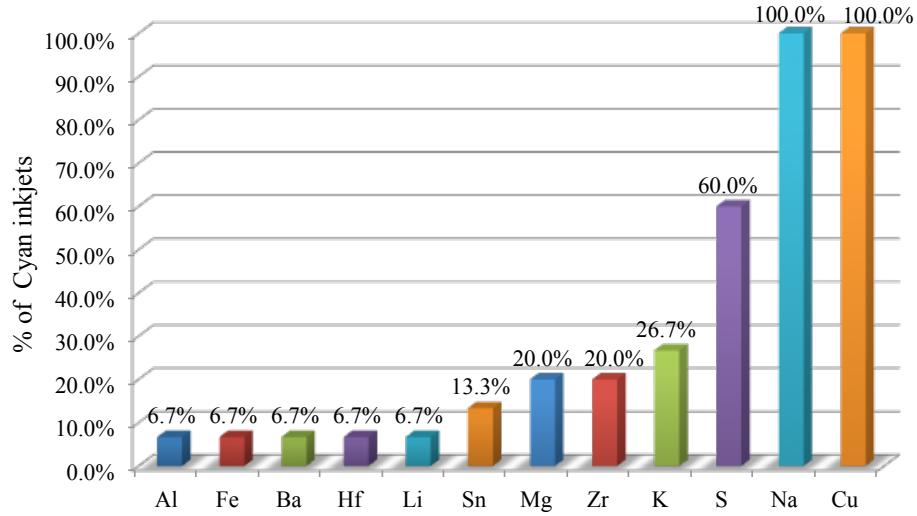


Figure 39. Bar graph showing the distribution of elements for cyan inkjets.

4.4.3 Yellow Inkjet Printing Inks

Sodium was the detected in most of the yellow inkjets (13 out of 14). Elements like Cu, Fe, Ba, and Li were not detected in yellow inkjets. Figure 40 shows the distribution of different elements in yellow inkjets.

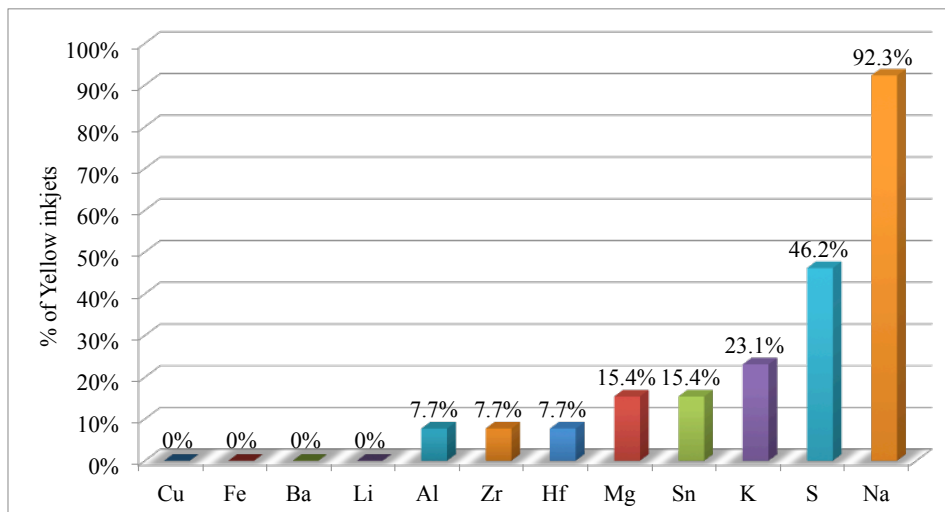


Figure 40. Bar graph showing the distribution of elements in yellow inkjets.

4.4.4 Magenta Inkjet Printing Inks

Sodium was present in all of the magenta inkjets. Elements like Iron and Ba were not detected in this subset. Elements like Al, Zr, and Hf were detected only in 6.3% of the magenta inkjets while Mg, Cu, Sn, and Li were detected in 12.5% of the samples, as shown in Figure 41.

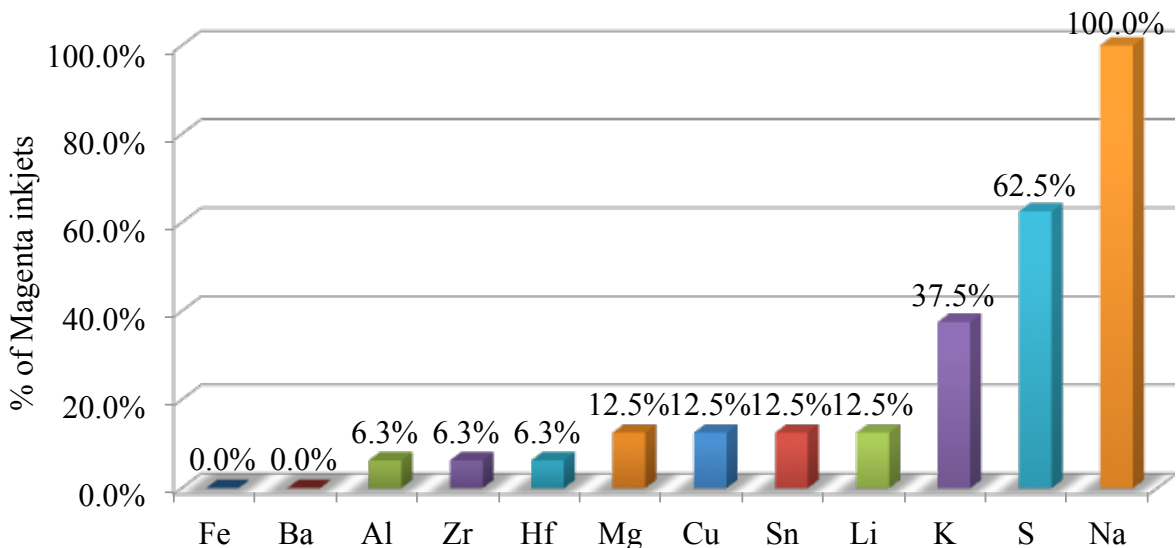


Figure 41. Bar graph showing the distribution of elements in magenta inkjets.

4.4.5 Overall Discrimination for Inkjet Printing Inks

Similar to toners, the discrimination capability of LA-ICP-MS for inkjets was also very high. Despite the lesser number of elements detected, a total of 99.6% discrimination was detected for inkjet printing inks. Only 13 pairs of the inkjet printing inks were not distinguishable out of a total of 3003 pairs. Table 13 shows the overall discrimination for inkjet samples using LA-ICP-MS. Most of these indistinguishable pairs were either from the same manufacturer (brand) or were of same color as shown in Table 14. The discrimination capability for each color of inkjets is shown in the Table 15.

Table 13. Discrimination capability of LA-ICP-MS for inkjet inks.

Number of samples	78
Number of samples from different sources	78 (3003 comparison pairs)
Duplicate controls from same sources	3 quality controls (3 comparison pairs)
% Discrimination	99.64% (2992 out of 3003)
% False exclusions	0% (0 out of 3)
% False inclusions	0.36% (11 out of 3003)

Table 14. List of indistinguishable inkjet pairs by LA-ICP-MS.

Indistinguishable Pairs	Color	Brand
56IJ Vs. 57IJ	Black	KD
05IJ Vs. 54IJ	Magenta	CN
05IJ Vs. 44IJ	Magenta Vs. Yellow	CN Vs. OL
04IJ Vs. 10IJ	Yellow	CN Vs. EP
05 IJ Vs. 55IJ	Magenta Vs. Yellow	CN
54IJ Vs. 55IJ	Magenta Vs. Yellow	CN
65IJ Vs. 67IJ	Yellow Vs. Magenta	BR
71IJ Vs. 72IJ	Yellow Vs. Magenta	BR
26IJ Vs. 27IJ	Magenta Vs. Yellow	HP
09IJ Vs. 10IJ	Magenta Vs. Yellow	EP
04IJ Vs. 09IJ	Yellow Vs. Magenta	CN Vs. EP

Table 15. Discrimination capability of LA-ICP-MS in CMYK inkjets.

	Black	Cyan	Magenta	Yellow
# Samples	33	16	16	13
# Samples from different sources	33	16	16	13
# Comparison pairs	528	120	120	78
% Discrimination	99.8% (527/528)	100% (120/120)	99.2% (119/120)	98.7% (77/78)
% False inclusions	0.2%(1/528)	0 (0/120)	0.8%(1/120)	1.3% (1/78)

Controls were used at all times during the analysis of inkjets to ensure the optimum instrument performance. All the controls were correctly associated, resulting in 100% correct association. Figure 42 shows the spectral overlay for inkjet controls.

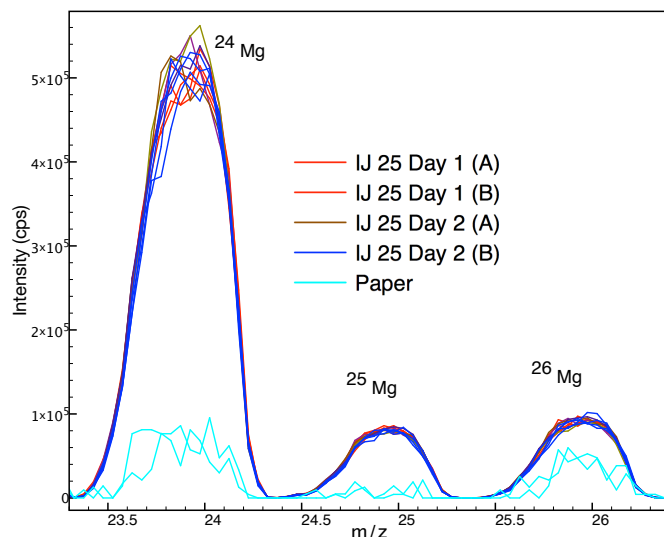


Figure 42. Spectral Overlay Analysis of Mg isotopes in inkjet controls.

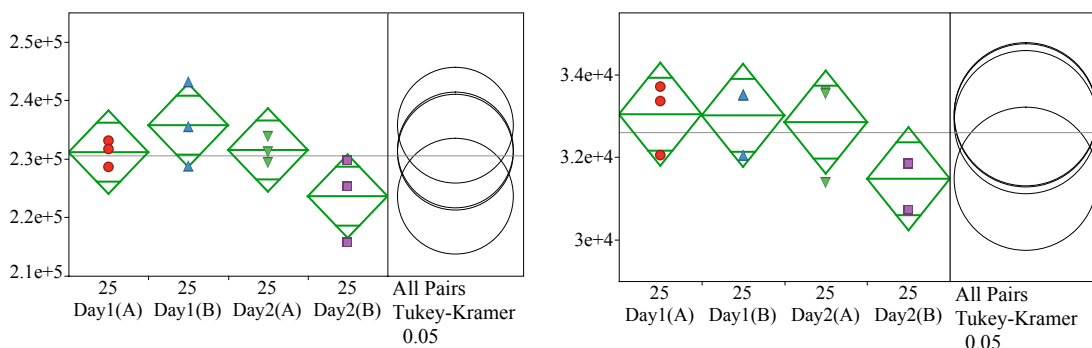


Figure 43. One-Way ANOVA with Tukey's HSD plot for ^{24}Mg (left) and ^{25}Mg (right) in inkjet control (IJ 25).

Similarly the statistical analysis also showed that the controls used on a daily basis were not significantly different. Figure 43 is the One-Way ANOVA with Tukey's HSD plot shows considerable overlapping of the controls and no significant difference between the controls.

4.4.6 Multivariate Analysis of Inkjet Printing Inks

4.4.6.1 Principal Component Analysis of Inkjet Printing Inks

All the peaks, that were at least three times greater than in the paper (background) were integrated and used for statistical analysis. A total of 12 elements were detected in the inkjet printing inks. Principal Component Analysis of inkjets was performed using these 12 variables. The total dimensionality was reduced to three components by PCA. The first three principal components provided the maximum variance between the inkjet printing inks. Table 16 shows the variance explained by each of the first three principal components.

Table 16. PCA scores for the first three principal components in inkjets.

PC1	PC2	PC3	Cumulative Variance
23%	18.80%	15%	57%

Inkjet 30 and 31 are grouped in a different region compared to other inkjets as shown in Figure 44. It might be a result of the fact that the largest number of elements was detected in these two inks. They both have Na, K, Cu, Zr, Sn, and Hf. They are grouped closer to each other and farther from the remaining inks. Figure 44 shows the two-dimensional PCA plot of inkjets. A total of 57% of the total variance was explained by the first three principal components as shown in Table 16.

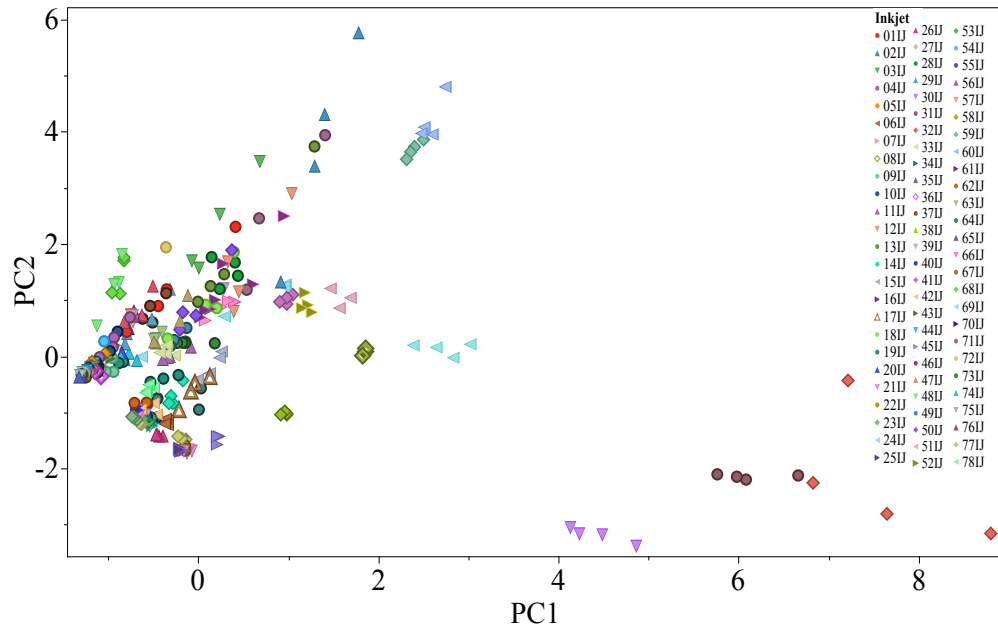


Figure 44. Two-dimensional PCA plot for inkjets by LA-ICP-MS.

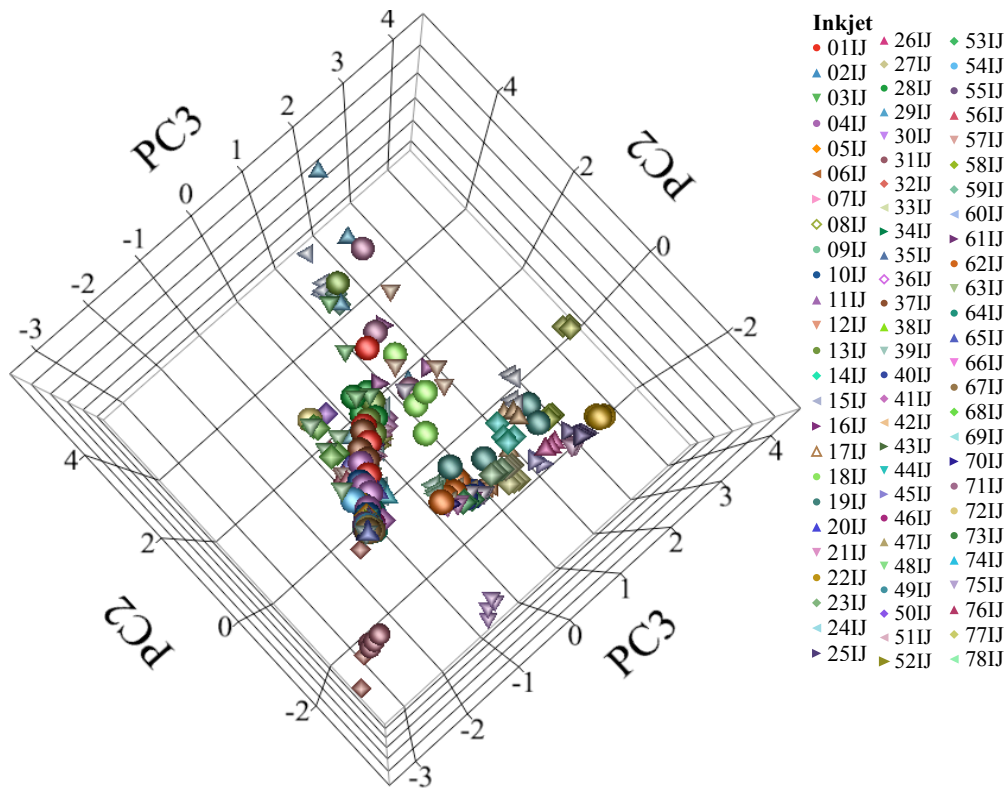


Figure 45. Three-dimensional PCA plot for inkjets by LA-ICP-MS.

The three dimensional PCA plot for inkjet printing inks is shown in Figure 45. The PCA plot on the basis of brands also showed classification of nine different brands. Brand HP had features similar to most of the inks, and it was also the largest brand (in quantity) for inkjet set. Figure 45 shows HP brand scattered all over the plot. Brand Lexmark is grouped distinctly from all other groups. Similarly, Kodak brand can also be discriminated visually from all other brands as shown in Figure 46. Figure 47 is the three dimensional PCA plot for inkjets based on their brands. The three-dimensional plot also shows that Hewlett Packard (HP) brand, which is the manufacturer for most of the inkjets, is scattered throughout the plot. Kodak (KD) brand can be seen to be in a group different from other brands. Similarly Olivetti brand (OL) and Lexmark (LX) also have distinct groups as shown in Figure 46 and Figure 47.

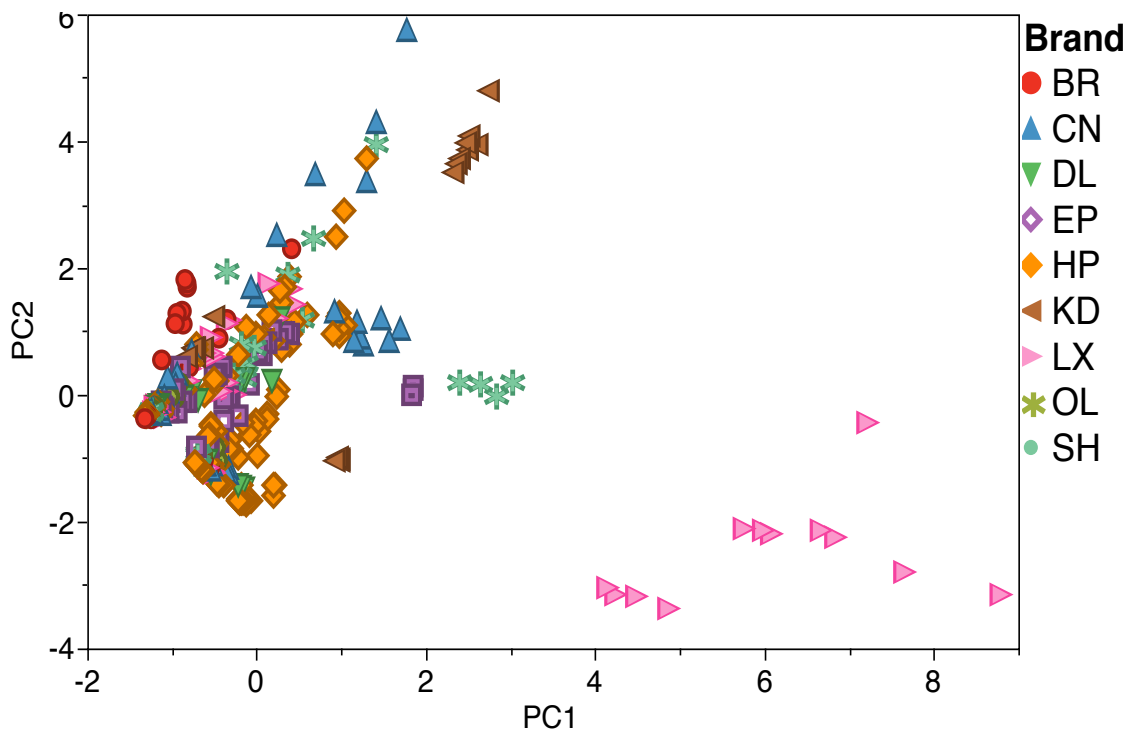


Figure 46. Two-dimensional PCA plot showing different brands of inkjets.

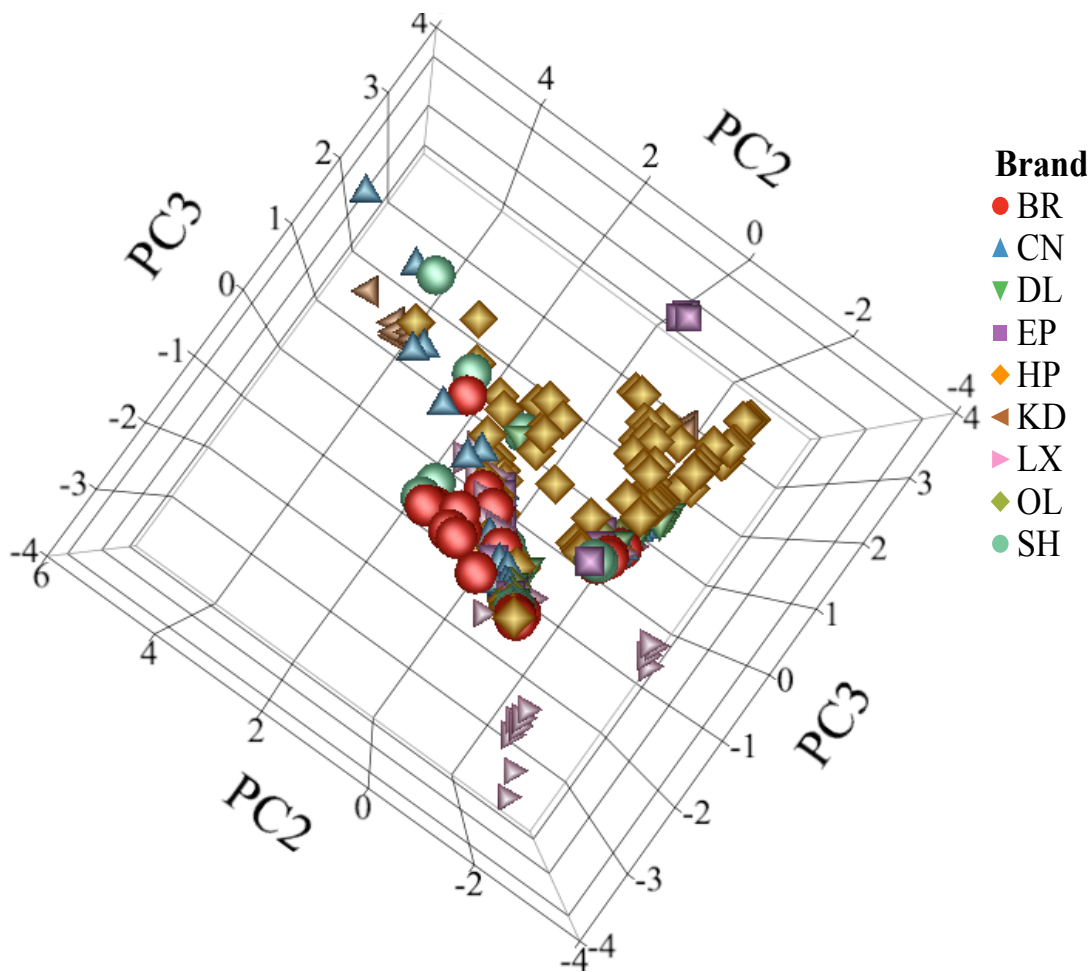


Figure 47. Three-dimensional PCA plot for inkjets showing different brands.

4.4.6.2 Linear Discriminant Analysis of Inkjet Printing Inks

A total of 45 pairs of inkjet printing inks were misclassified using LDA. These 45 pairs are shown in Table 17. It was found that most of the indistinguishable pairs were of the same color. Only 16 of the misclassified pairs were of two different colors. Of those same colored indistinguishable inkjet pairs, 27% were black and also 27% were cyan. There were three yellow colored indistinguishable inkjet samples and two magenta colored samples. Figure 48 shows the total percentage of indistinguishable pairs in four different colors.

Table 17. List of inkjet pairs misclassified by LDA.

Number	Misclassified pairs	Color	Brand
1	03 IN Vs.37 IN	Black	Cannon
2	04 IN Vs.10 IN	Yellow	CN Vs. EP
3	04 IN Vs.05 IN	Yellow Vs. Magenta	CN
4	05 IN Vs.65 IN	Magenta Vs. Yellow	CN Vs. BR
5	11 IN Vs.33 IN	Black	LX
6	15 IN Vs.14 IN	Black	HP
7	19 IN Vs.18 IN	Black	HP
8	19 IN Vs.15 IN	Black	HP
9	20 IN Vs.04 IN	Black Vs. Yellow	HP Vs. CN
10	24 IN Vs.74 IN	Black	HP vs. DL
11	24 IN Vs.41 IN	Black	HP
12	29 IN Vs.46 IN	Black Vs. Magenta	LX Vs. HP
13	34 IN Vs.53 IN	Cyan	LX Vs. CN
14	36 IN Vs.67 IN	Yellow Vs. Magenta	LX Vs. BR
15	37 IN Vs.20 IN	Black	CN Vs. HP
16	40 IN Vs.34 IN	Cyan	HP Vs. LX
17	40 IN Vs.53 IN	Cyan	HP Vs. CN
18	42 IN Vs.70 IN	Cyan	HP Vs. SH
19	42 IN Vs.40 IN	Cyan	OL Vs. HP
20	44 IN Vs.76 IN	Yellow	OL Vs. DL
21	44 IN Vs.67 IN	Yellow Vs. Magenta	OL Vs. BR
22	48 IN Vs.68 IN	Black	BR
23	49 IN Vs.33 IN	Black	SH Vs. LX
24	49 IN Vs.50 IN	Black	SH
25	50 IN Vs.47 IN	Black	CN Vs. HP
26	53 IN Vs.42 IN	Cyan	CN Vs. OL
27	54 IN Vs.72 IN	Magenta	CN Vs. SH
28	54 IN Vs.65 IN	Magenta Vs. Yellow	CN Vs. BR
29	55 IN Vs.67 IN	Yellow Vs. Black	CN Vs. KD
30	54 IN Vs.55 IN	Magenta vs. Yellow	CN
31	56 IN Vs.57 IN	Black	KD
32	62 IN Vs.42 IN	Cyan	EP Vs. OL
33	62 IN Vs.78 IN	Cyan	EP Vs. HP
34	66 IN Vs.70 IN	Cyan	BR Vs. SH
35	66 IN Vs.40 IN	Cyan	BR Vs. HP
36	66 IN Vs.62 IN	Cyan	BR Vs. EP
37	67 IN Vs.36 IN	Magenta Vs. Yellow	BR Vs. LX
38	65 IN Vs.67 IN	Yellow vs. Magenta	BR
39	65 IN Vs.71 IN	Yellow	BR Vs. SH
40	56 IN Vs.72 IN	Black Vs. Magenta	KD Vs. SH
41	44 IN Vs.72 IN	Yellow Vs. Magenta	OL Vs. SH
42	72 IN Vs.67 IN	Magenta	SH Vs. BR
43	65 IN Vs.72 IN	Yellow Vs. Magenta	BR Vs. SH
44	73 IN Vs.33 IN	Black	DL Vs. LX
45	78 IN Vs.70 IN	Cyan	HP Vs. SH

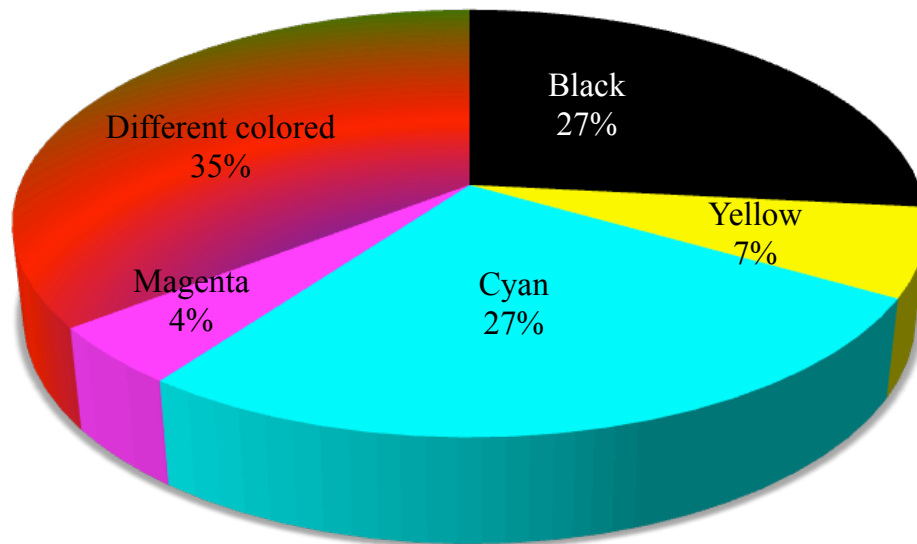


Figure 48. Pie chart showing the percentage of misclassified pairs in four different colors.

Four of the misclassified pairs were also indistinguishable by Spectral Overlay.

These common pairs are listed in Table 18.

Table 18. List of common pairs indistinguishable by Spectral Overlay and LDA.

Indistinguishable Pairs	Color	Brand
56IJ Vs. 57IJ	Black	KD
04IJ Vs. 10 IJ	Yellow	CN vs. EP
54IJ Vs. 55IJ	Magenta vs. Yellow	CN
65IJ Vs. 67IJ	Yellow vs. Magenta	BR

4.4.6.3 Partial Least Squares Discriminant Analysis of Inkjet Printing Inks

Inkjet 25 was chosen as the quality control for the analysis of inkjet printing inks. The database was populated with 77 inkjets. When duplicates of IJ 25 were searched through the entire database of 77 inkjets, it correctly associated with IJ 25 from the database. Figure 49 shows the PLS-DA plot for IJ 25. The other closely related inkjet

samples are IJ 26, IJ 21, IJ 23, and IJ 22, but the similarity score for IJ 25 (0.28) is the highest compared to other four possible inks.

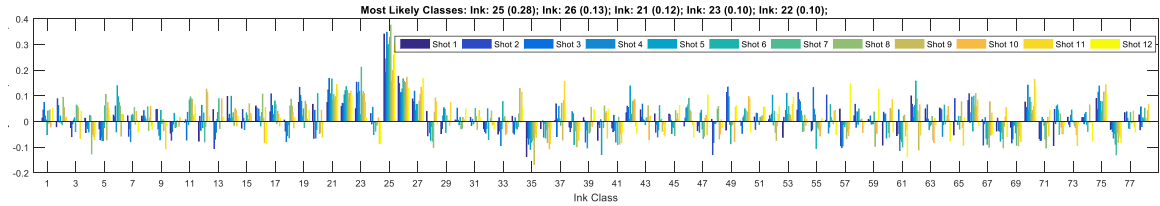


Figure 49. PLS-DA plot showing the correct matching of IJ 25 in the ink database.

4.4.6.4 K-Nearest Neighbor Analysis of Inkjet Printing Inks

When IJ 25, a quality control was searched through the database using the KNN algorithm, all the four replicates of IJ 25 were shown to be the first four closest neighbors. This provided a 100% correct association for the three IJ 25 controls. Figure 49 shows the K-NN plot for IJ 25. Of the ten closest spectra for IJ 25, its four replicates that were in the database as sample (not controls) were predicted as the nearest neighbors by the algorithm as shown in Figure 50.

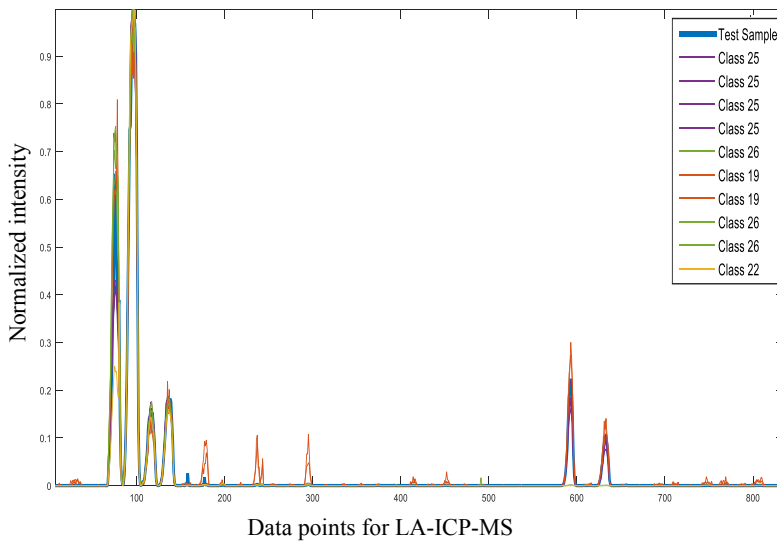


Figure 50. K-NN plot for IJ 25 showing the first 10 nearest neighbors.

4.5 Results for Comparison of Offset Printing Inks

Similar to inkjet samples, offset samples were also embedded into the paper fibers. There was always some paper contribution due to the thin layer of offset ink on paper, so the paper background was subtracted from the offset inks.

Table 19. List of elements detected in offset samples.

OF	Na	Mg	Al	Si	S	K	Ca	Ti	Mn	Co	Cu	Zr	Zn	Sr	Nb	Mo	Rh	Ag	Sn	Ba	Ce	W
1									Mn	Co	Cu											
2					S				Mn	Co	Cu											
3	Na			Si					Mn	Co												
4									Mn	Co	Cu											
5										Co	Cu		Zn				Rh					
6		Mg		Si					Mn	Co												
7			Al						Mn	Co	Cu					Mo						W
8					S				Mn		Cu					Mo					Ce	
9									Mn	Co	Cu							Ag				
10									Mn	Co	Cu					Mo		Ag				
11				Si					Mn	Co								Ag				
12									Mn	Co								Ag				
13	Na								Mn	Co										Sn		
14									Mn	Co	Cu											
15			Al	Si					Mn	Co										Sn		
16	Na		Al	Si	S				Mn	Co												
17									Mn	Co	Cu									Sn		
18									Mn	Co	Cu											
19	Na			Si	S				Mn	Co										Sn		
20	Na			Si					Mn	Co											Sn	
21									Mn	Co											Sn	
22									Mn	Co											Sn	
23					S				Mn	Co				Sr						Sn	Ba	
24	Na								Mn	Co	Cu											
25									Mn	Co	Cu					Mo						
26									Mn	Co											Sn	
27									Mn	Co											Sn	
28									Mn	Co												Ba
29										Co												Ba
30									Mn	Co											Sn	Ba

OF	Na	Mg	Al	Si	S	K	Ca	Ti	Mn	Co	Cu	Zr	Zn	Sr	Nb	Mo	Rh	Ag	Sn	Ba	Ce	W
31									Mn	Co	Cu			Sr								
32									Mn	Co											Ba	
33									Mn													
34	Na	Mg	Al						Mn	Co				Sr						Sn		
35									Mn	Co						Mo						
36									Mn	Co	Cu					Mo						
37									Mn	Co	Cu									Sn		
38									Mn	Co	Cu					Mo						W
39									Mn	Co	Cu									Sn		
40	Na	Mg				K			Mn	Co			Zn									
41											Cu					Mo						W
42											Cu					Mo						W
43																Mo						W
44					Si						Cu					Mo						W
45																						W
46									Mn													W
47	No elements detected																					
48							Ca				Cu		Zn									W
49											Cu											
50	No elements detected																					
51		Mg					Ca			Co										Sn		
52				Si				Ti														
53				Si			Ca				Cu											
54											Cu							Ag				
55								Ti	Mn													
56				Si							Cu											
57				Si							Cu											W
58	Na			Si					Mn													
59				Si			Ca				Cu											
60										Co												W
61				Si	K						Cu											
62				Si							Cu		Zn		Nb	Mo						W
63				Si																		
64							Ca															
65									Mn	Co	Cu											
66			Al						Mn	Co												
67		Mg	Al						Mn	Co												
68		Mg	Al								Cu											
69		Mg	Al								Cu											
70		Mg									Cu			Sr							Ba	
71		Mg	Al																			
72		Mg									Cu	Zr										
73		Mg									Cu											
74		Mg	Al											Sr							Ba	
75		Mg	Al																			
76		Mg	Al								Cu											W
77		Mg									Cu											
78		Mg	Al											Sr							Ba	
79		Mg																				

Table 19 lists all the different elements present in offset ink. A total of 22 elements were detected in offset samples. Elements like W and Ba were detected in some

of the offset samples. Figure 51 shows the distribution of different elements in the offset samples. Elements like Co and Mn were the elements found in more than half of the offset samples while elements like Zr, Nb, Rh and Ce were present in 1% of the total samples as shown in Figure 51.

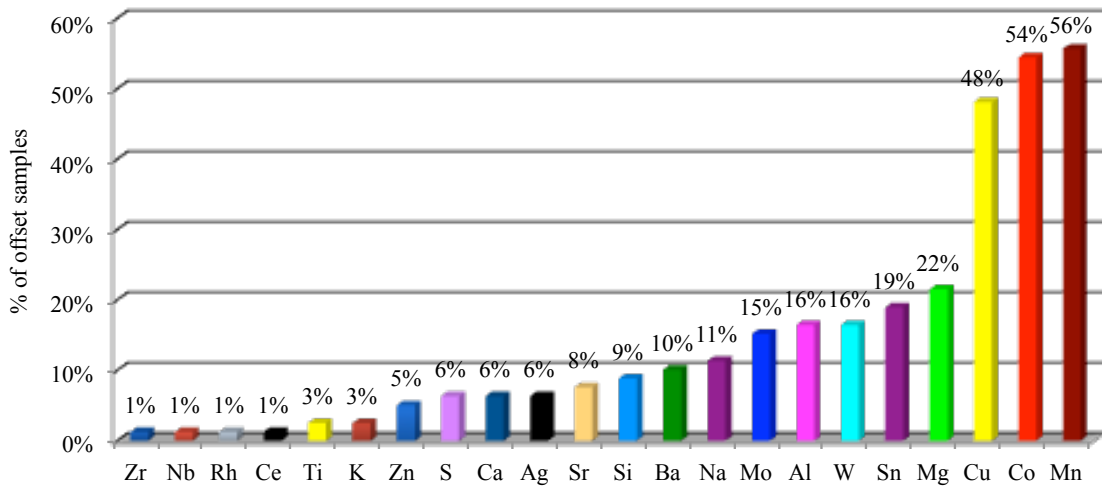


Figure 51. Bar graph showing the distribution of elements in offset samples.

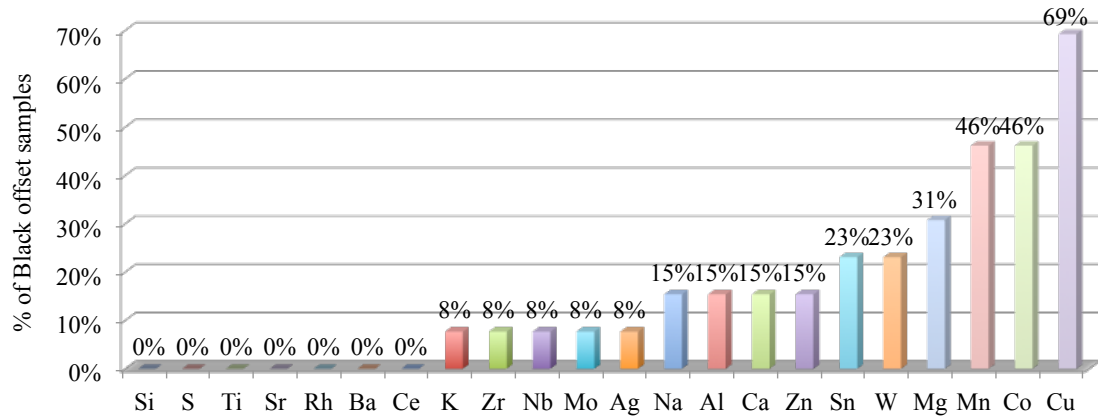


Figure 52. Bar graph showing the distribution of elements in black offset inks.

4.5.1 Black Offset Printing Inks

There were 13 offset samples that were black. Cu was detected in most of these black colored samples whereas elements like S, Si, Ti, Sr, Rh, Ba and Ce were absent.

Figure 52 shows the distribution of different elements in 13 black offset samples.

4.5.2 Cyan Offset Printing Inks

A total of 11 elements were detected in cyan offset samples. Copper was found in most of the cyan inks (toners and inkjets). It was also found in all of the cyan offsets. Another element that was most frequently detected was Mn. Some cyan offsets had Mo, Ce and W, which were not detected in toners or inkjets. Elements like Si, K, Ca, Ti, Zr, Zn, Sr, Nb, Rh, Sn, and Ba were not detected in this subset. Figure 53 shows the list of elements and their relative frequency (in terms of percentage) in offset samples.

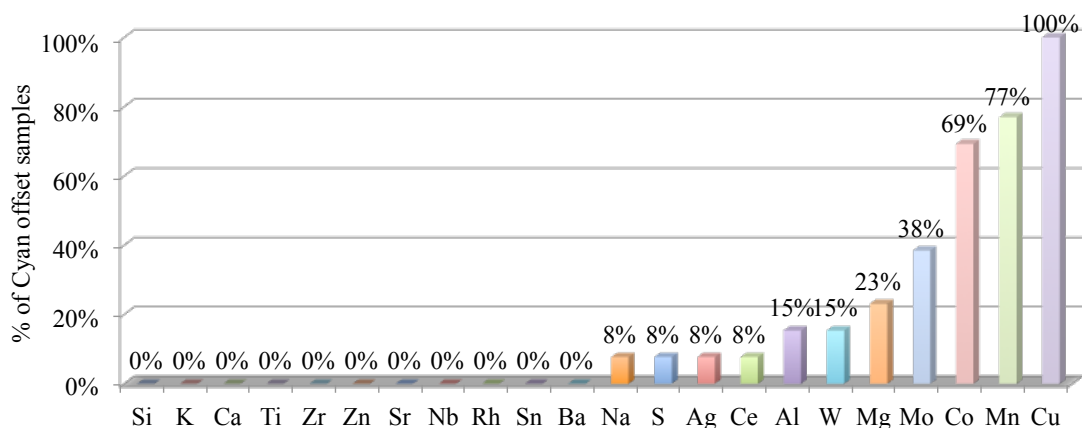


Figure 53. Bar graph showing the distribution of elements in cyan offset samples.

4.5.3 Yellow Offset Printing Inks

Two kinds of yellow color were seen in the offset samples. Some of the samples were light yellow while some were dark yellow. A total of nine elements were detected. Mn and Co were the two most frequently detected elements in yellow offset samples. Figure 54 shows the distribution of elements in yellow offset samples.

4.5.4 Blue Offset Printing Inks

Offset samples were not limited to CMYK colors. Some of the samples collected were either light blue or dark blue or had stripes of yellow, and orange color.

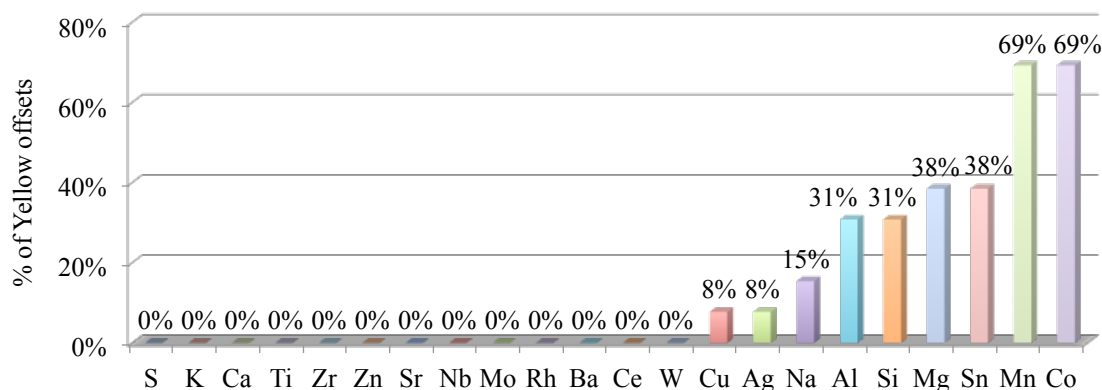


Figure 54. Bar graph showing the distribution of elements in Yellow offset samples.

A total of six elements were detected in this subset. Mn, Cu and W were detected in 25% of the total set while Na, K and Mo were detected in 13% of the samples. All other elements listed in the element menu for offset inks were completely absent as shown in Figure 55.

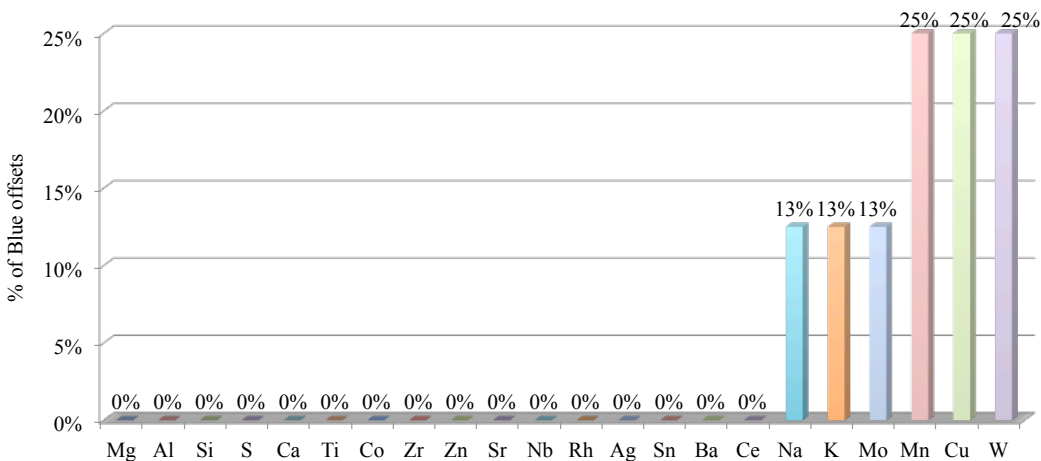


Figure 55. Bar graph showing the list of elements detected in blue offset samples.

4.5.5 Magenta Offset Printing Inks

A total of 12 elements were detected in magenta offset samples. Similar to the yellow offsets, Mn and Co were the elements most frequently detected in this subset. Various elements like K, Ca, Ti, Zr, Zn, Nb, Mo, Rh, Ce, and W were completely absent.

Figure 56 shows the list of elements that were detected in the magenta offset printing inks.

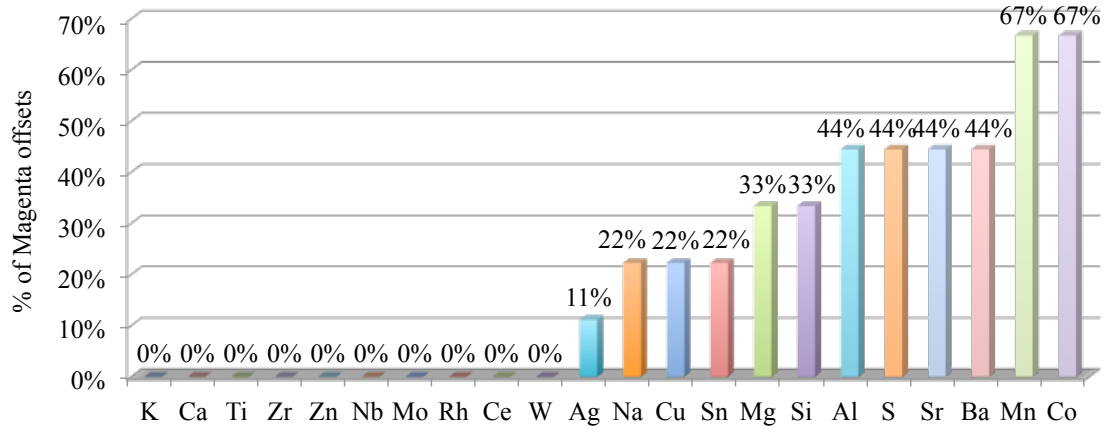


Figure 56. Bar graph showing the list of elements detected in magenta offset samples.

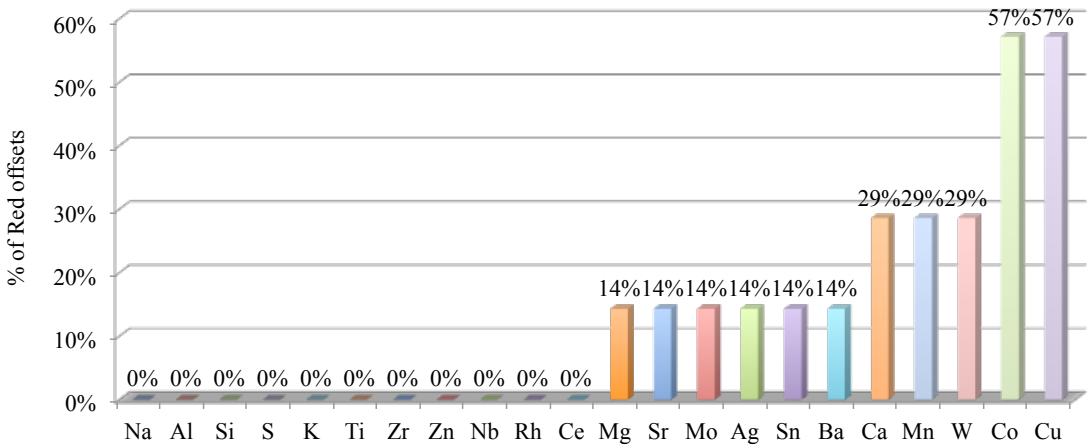


Figure 57. Bar graph showing the list of elements present in red offset samples.

4.5.6 Red Offset Printing Inks

There were seven offset samples that were red. A total of 11 elements were detected in these set. Co and Cu were the two most frequently encountered elements. Elements like Na, Al, Si, S, K, Ti, Zr, Zn, Nb, Rh, and Ce weren't detected in the red offset samples. Figure 57 shows the percentage of different elements detected in this set.

4.5.7 Different Colored Offset Printing Inks

This subset of printing inks was composed of many colors like bronze, brown, orange, pink, purple and green. There was only one offset sample that was bronze. Only two elements, Mn and W were detected. Similarly, there were two brown offsets. Ca, Co, Rh, W, Cu, Zn were the elements detected in these offset samples. Cu and Zn were present in all of the brown offsets. For four orange offset samples only four elements were detected; Sn, Mn, Co, and Ba. The list of elements along with their frequency of occurrence (in terms of percentage) is illustrated in Figure 58.

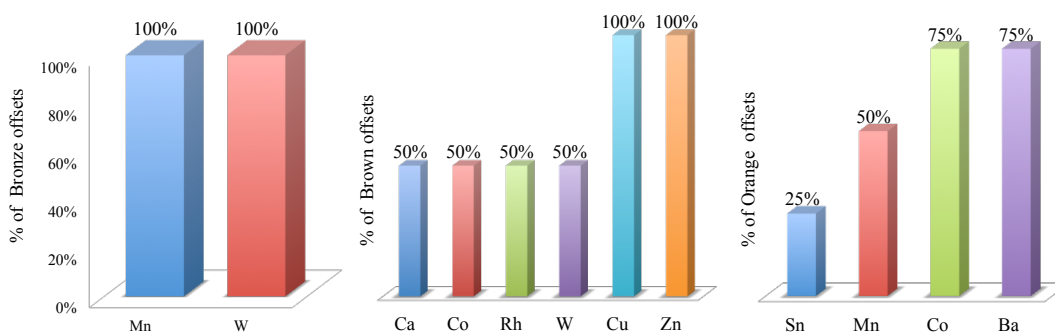


Figure 58. List of elements present in Bronze, Brown and Orange offset inks.

Similarly, the offset set also contained three pink and three purple inks. For pink offset samples, Mn was the element that was detected in two-thirds of the samples.

One third of the samples contained elements like Na, Mg, Al, Co, Cu, Sr, Mo, Sn, W, Mn. In purple inks, Mn and Co was detected in all three inks. Elements like Sn, Cu, and Mo were also detected in some of the purple inks. Figure 59 shows the presence of these elements in pink and purple offset samples.

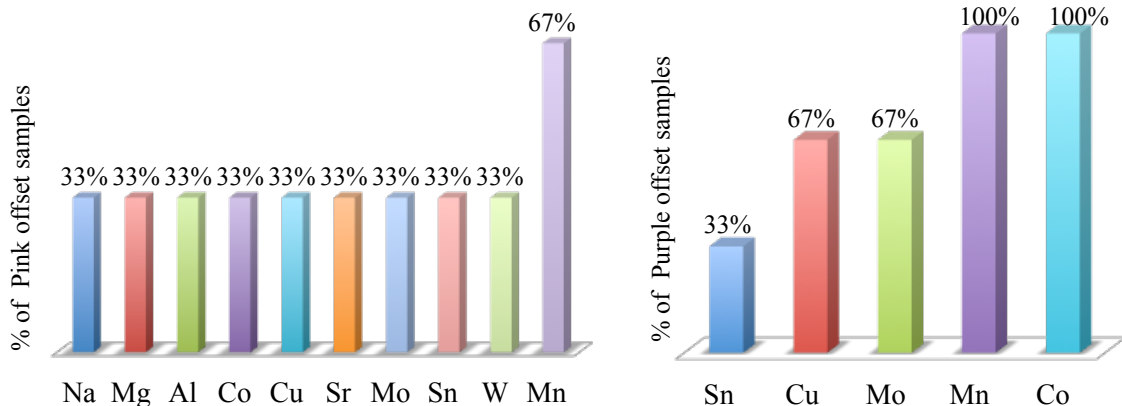


Figure 59. Bar graph showing the list of elements detected in pink and purple offsets.

4.5.8 Overall Discrimination for Offset Printing Inks

The overall discrimination for offset samples was found to be 99.8%. Only six pairs of samples were not distinguished by LA-ICP-MS⁷. Table 20 summarizes the discrimination potential of LA-ICP-MS for the analysis of offset printing inks.

Table 20. Discrimination capability of LA-ICP-MS for the analysis of offset printing inks.

# Samples	79
# Samples from different sources	79 (3081 comparison pairs)
Duplicate controls from same sources	7 quality controls, 16 duplicate controls (37 comparison pairs)
% Discrimination	99.8% (3075 out of 3081)
% False exclusions	0 (0 out of 37)
% False inclusions	0.2% (6 out of 3081)

A closer look at the indistinguishable pairs reveals that most of the inks were either of the same color or were manufactured by the same manufacturer. Table 21 shows the list of the offset pairs that were not distinguished by LA-ICP-MS. One of the pairs, OF 18 and OF 65, were of different colors and belonged to different manufacturers, while the other pairs either shared the same manufacturer or the same color.

Table 21. List of offset printing ink pairs that were not distinguishable by LA-ICP-MS.

Indistinguishable Pairs	Color	Source
21OF vs. 27OF	Black vs. Yellow	Graphic Ink Co.
47OF vs. 50OF	Green vs. Orange	Lincoln visa vs. US passport
18OF vs. 65OF	Cyan vs. Black	Sunchemicals (USA) vs. Brilliant (Germany)
71OF vs. 75OF	Yellow	Sunchemicals
73OF vs. 77OF	Cyan	Sunchemicals
74OF vs. 78OF	Magenta	Sunchemicals

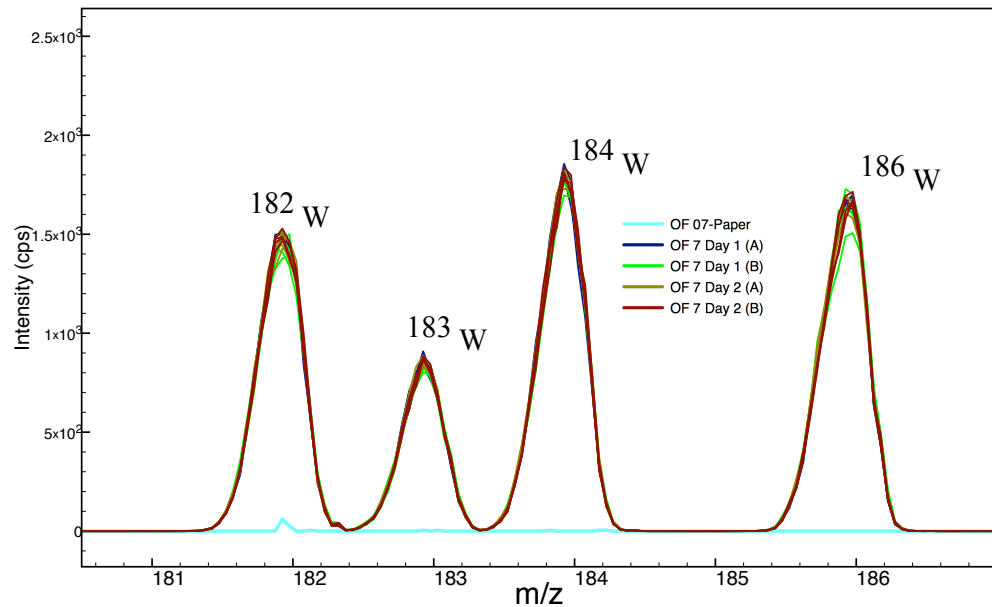


Figure 60. Spectral Overlay showing Tungsten peaks in offset control (OF-7).

The association of controls was also confirmed using spectral overlay and One-Way ANOVA. Figure 60 shows well-overlapped Tungsten peaks for each of the isotopes. Similarly statistical comparison of the controls was performed. One Way ANOVA with Tukey's HSD test showed no significant difference between the controls, as shown in Figure 61.

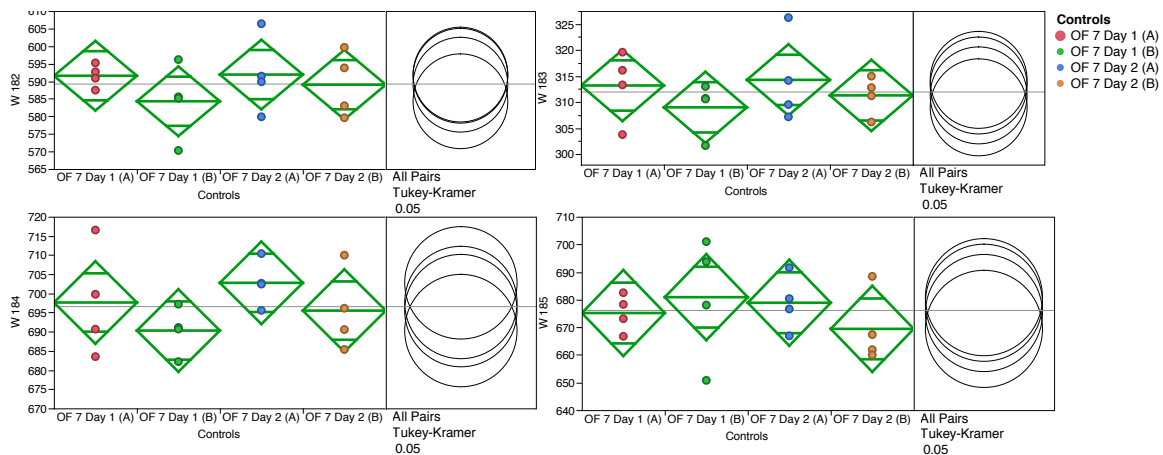


Figure 61. One Way ANOVA for Tungsten (W) isotopes in offset control (OF-7).

4.5.9 Multivariate Analysis of Offset Printing Inks

Principal Component Analysis and Linear Discriminant Analysis were performed using the integrated areas of the detected elements in LA-ICP-MS spectrum. The area under the peak reflected the concentration of the elements in the ink sample.

4.5.9.1 Principal Component Analysis of Offset Printing Inks

Principal Component Analysis showed the classification of 79 offset samples based on the integrated areas of the detected elements. The total variance explained by the first three principal components is 34.23% as shown in table 22. Figure 62 and Figure 63 show the two-dimensional and three-dimensional PCA of offset samples.

Table 22. PCA scores for the first three PCs in offset printing inks.

PC1	PC2	PC3	Cumulative variance
14.50%	11.50%	8.23%	34.23%

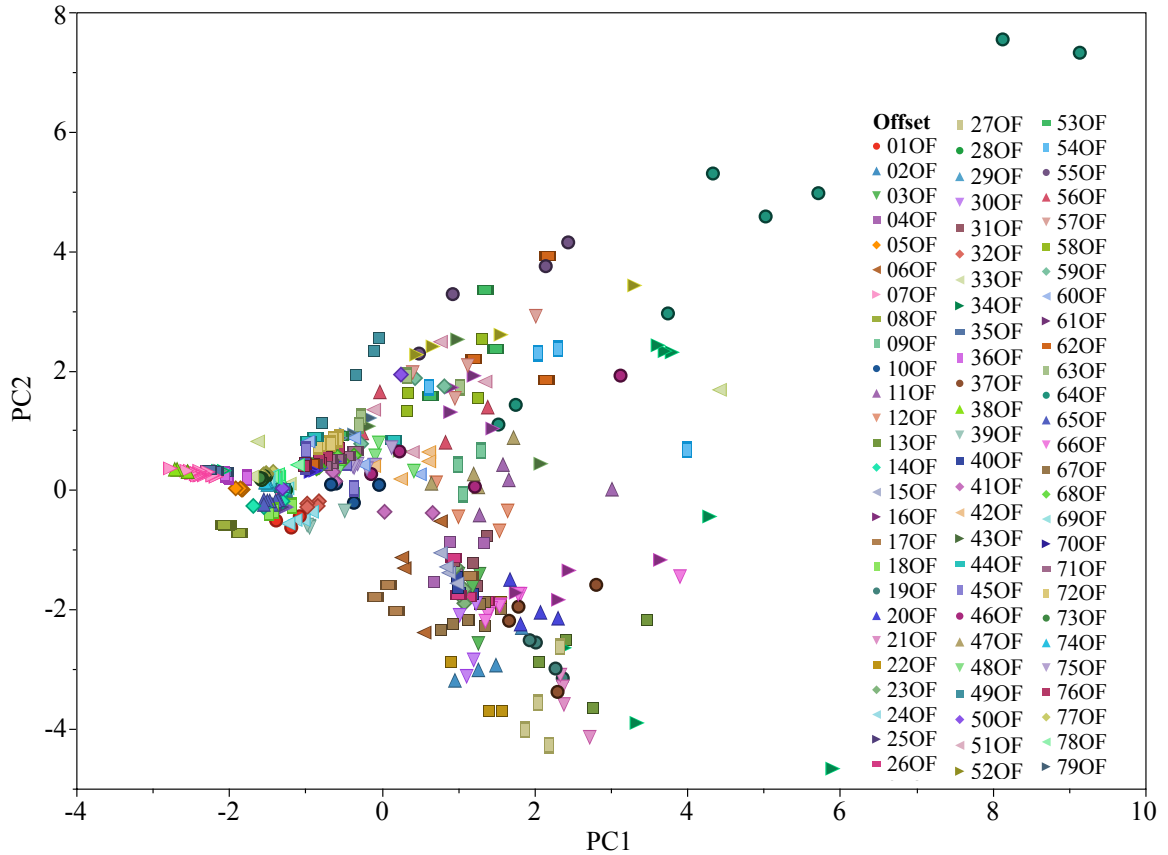


Figure 62. Two-dimensional PCA of offset samples by LA-ICP-MS.

Principal Component Analysis of offset samples by brand showed classification of 10 different brands. Offset inks manufactured from GI (Graphic Ink Company) are similar to most of the other inks in terms of elemental profile. They can be seen scattered all over the PCA plot. Offset inks with USPN brand are grouped very close to each other, as shown in PCA plots in Figure 64 and Figure 65.

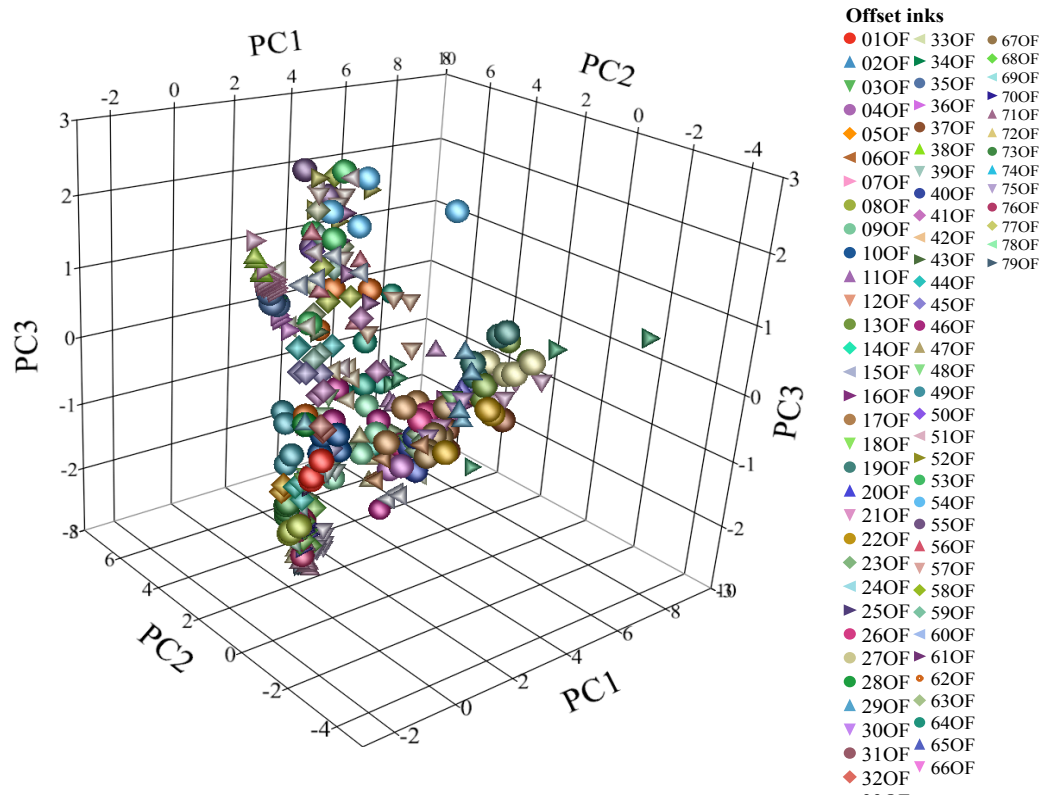


Figure 63. Three-dimensional PCA of offset inks by LA-ICP-MS.

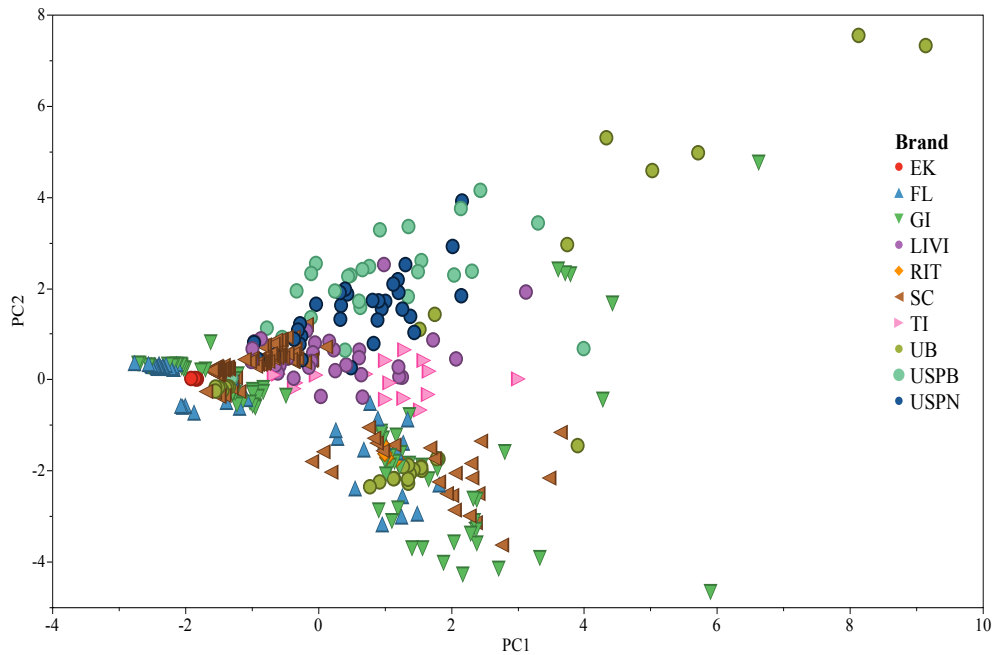


Figure 64. Two-dimensional PCA plot (by brand) for offset samples.

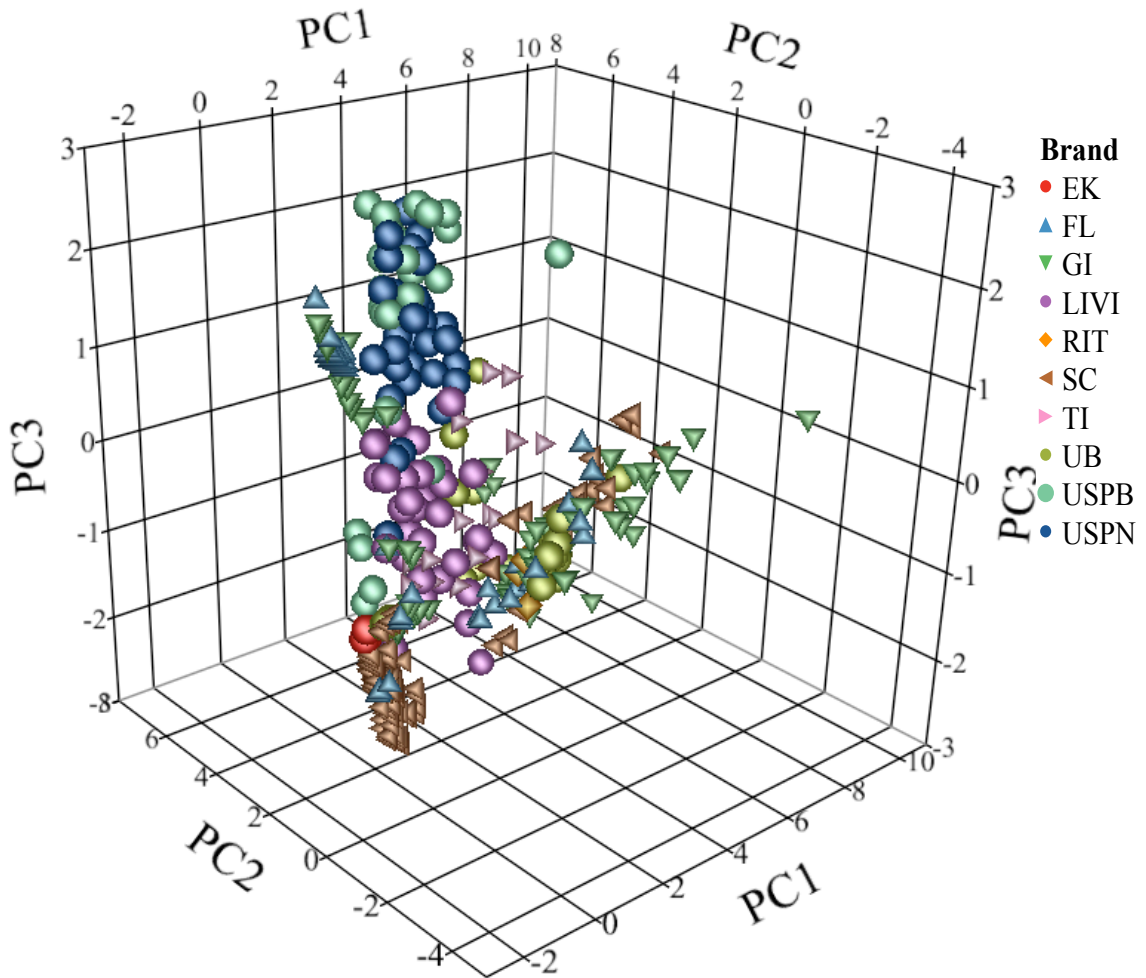


Figure 65. Three-dimensional PCA plot (by brand) for offset samples.

4.5.9.2 Linear Discriminant Analysis of Offset Printing Inks

Linear Discriminant Analysis showed a misclassification of 23 pairs of offset samples. These pairs are listed in Table 23. Sample OF 07 that was used as a control was also misclassified (correctly associated) with the offset sample OF 07.

Table 23. List of misclassified offset pairs by LDA.

Misclassified pairs	Source/Brand	Color
06OF Vs. 04OF	FG	Yellow Vs. Black
07OF Vs. 50OF	FG Vs. USPB	Cyan Vs. Orange
14OF Vs. 01OF	SC Vs. FG	Cyan
18OF Vs. 01OF	SC Vs. FG	Cyan
22OF Vs. 37OF	GI	Yellow Vs. Purple
28OF Vs. 29OF	GI	Orange
32OF Vs. 28OF	GI	Red Vs. Orange
34OF Vs. 35OF	GI	Pink Vs. Purple
40OF Vs. 15OF	RIT Vs. SC	Black Vs. Yellow
41OF Vs. 45OF	LIVI	Green Vs. Blue
43OF Vs. 42OF	LIVI	Blue & Orange Stripes Vs. Pink
43OF Vs. 44OF	LIVI	Blue & Orange Stripes Vs. Red
44OF Vs. 50OF	LIVI Vs. USPB	Red Vs. Blue/Pink/Orange Lines
48OF Vs. 45OF	LIVI	Brown/Orange vs. Red
50OF Vs. 63OF	USPN	Orange Vs. Blue
52OF Vs. 51OF	USPB	Red Vs. Blue
53OF Vs. 63OF	USPB Vs. USPN	Red Vs. Blue
57OF Vs. 63OF	USPN	Black Vs. Blue
58OF Vs. 56OF	USPN	Blue Vs. Yellow
59OF Vs. 50OF	USPN Vs. USPB	Black Vs. Orange
62OF Vs. 50OF	USPN Vs. USPB	Black Vs. Blue/Pink/Orange
69OF Vs. 73OF	SC	Cyan
73OF Vs. 77OF	SC	Cyan

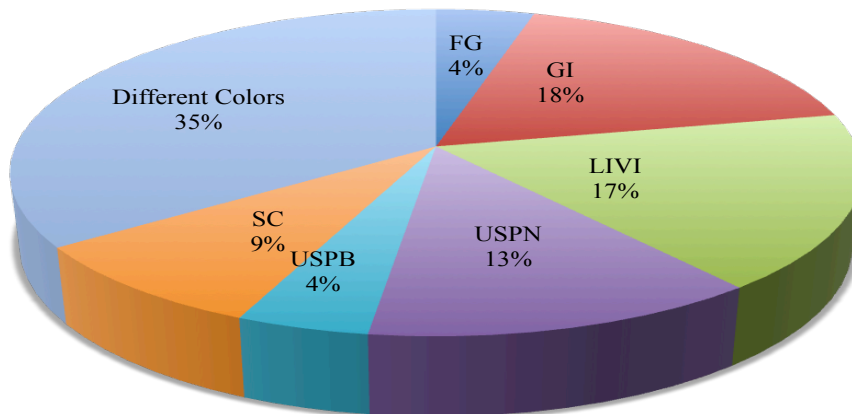


Figure 66. Pie chart showing the distribution of misclassified offset pairs in different brands.

Linear Discriminant Analysis showed that one of the indistinguishable pairs (by Spectral Overlay) was also misclassified. The pair common to both LDA and Spectral Overlay is listed in Table 24. This pair was of same color and also belonged to same manufacturer. Out of the 23 misclassified pairs, 8 pairs were from different sources, while the remaining 15 shared the same manufacturer as shown in Figure 66.

Table 24. Common offset pair that was indistinguishable (Spectral Overlay) and also misclassified (LDA).

Indistinguishable Pair/ Misclassified pair	Color	Source
73OF vs. 77OF	Cyan	Sunchemicals

4.5.9.3 Partial Least Square Discriminant Analysis of Offset Printing Inks

A total of 17 controls were used during the offset printing ink analysis by LA-ICP-MS. Only one of the controls was not correctly associated with the correct offset ink from the database. Figure 66 is a PLS-DA plot that shows the correct classification of offset control 7 to the same sample in the database. When the entire database is searched for that particular control, OF 7 is shown to be the closest one with the highest similarity index (0.52) as shown in Figure 67.

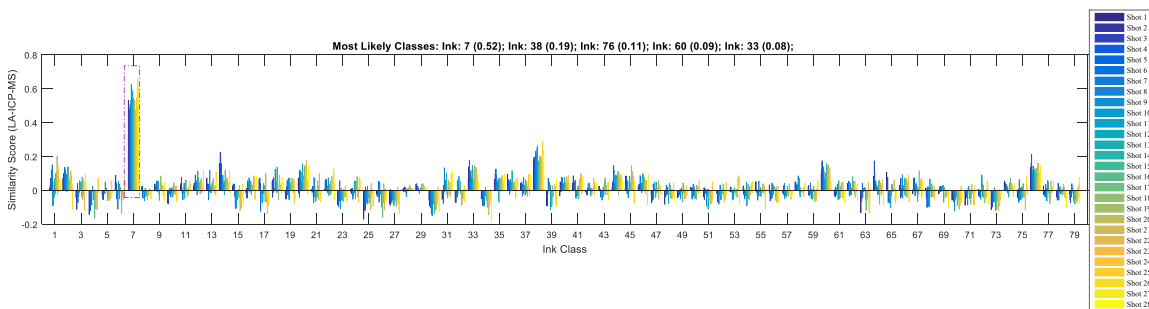


Figure 67. PLSD-DA plot showing correct association of offset control 7 to the same sample in the database.

4.5.9.4 K-Nearest Neighbor Analysis of Offset Printing Inks

The K-NN analysis also provided similar results to PLS-DA. Only one of the offset duplicate controls was incorrectly associated with a different offset sample from the database. The K-NN analysis provided 94.1% correct association between the duplicate controls and the quality controls. Figure 68 shows the correct association of a duplicate control, OF 70 to itself in the database. All the four replicates of sample OF 70 in the database were the first four nearest neighbors for the test sample.

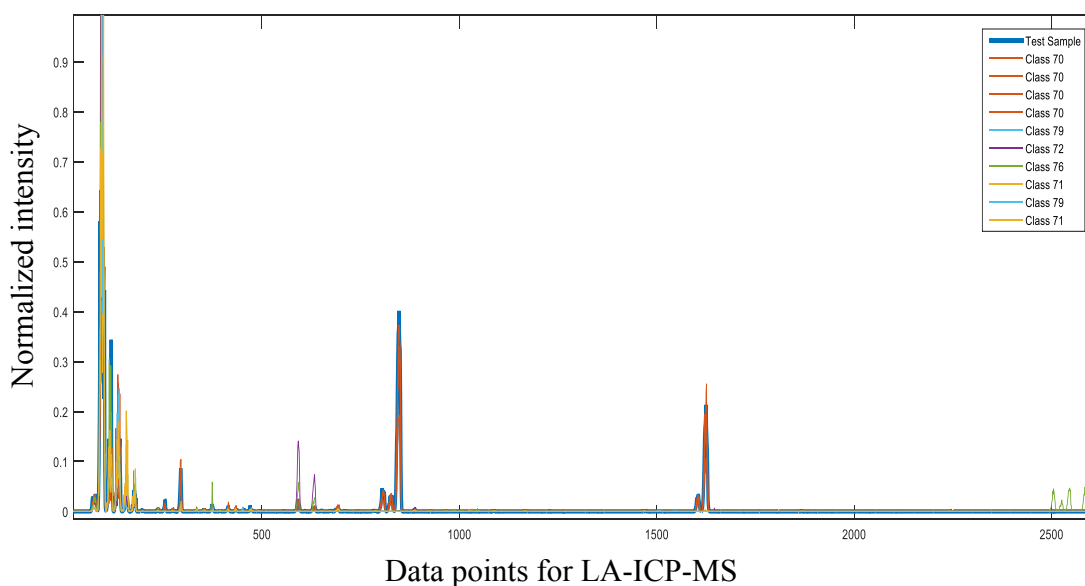


Figure 68. KNN-plot for OF-70 showing correct association to in the database.

4.6 Results for Comparison of Intaglio Printing Inks

Intaglio inks had a wide variety of elements. Twenty-three elements were detected in eighty-six inks. Table 25 shows the complete list of elements detected in all intaglio inks by LA-ICP-MS. Manganese was most frequently detected in the intaglio samples while elements like W, Sb, and Mo were detected only in a few inks. Figure 69 shows the distribution of different elements detected in intaglio inks in terms of percentage.

Table 25. List of elements detected by LA-ICP-MS in 86 intaglio inks.

IN	Na	Mg	Al	Si	K	Ca	Ti	Mn	Fe	Co	Cu	Zn	Sr	Zr	Nb	Mo	Sn	Sb	Ba	Hf	W	Pb	Bi
1		Mg	Al			Ca	Ti	Mn	Fe	Co	Cu		Sr	Zr					Ba	Hf			
2	Na	Mg			K	Ca																	
3		Mg	Al			Ca		Mn	Fe	Co	Cu	Zn	Sr	Zr			Sn			Hf		Pb	
4		Mg				Ca	Ti	Mn		Co	Cu		Sr	Zr						Hf			
5		Mg	Al					Mn		Co	Cu			Zr						Hf			
6		Mg	Al					Mn	Fe	Co				Zr						Hf			
7		Mg	Al		K	Ca		Mn	Fe	Co	Cu	Zn	Sr	Zr						Hf			
8		Mg	Al			Ca		Mn	Fe	Co	Cu		Sr	Zr						Hf			
9		Mg	Al			Ca		Mn	Fe	Co			Sr	Zr						Hf			
10		Mg	Al			Ca		Mn		Co			Sr	Zr						Hf			
11		Mg	Al			Ca		Mn		Co			Sr	Zr						Hf			
12	Na	Mg			K		Ti					Zn											
13						Ca		Mn		Co	Cu		Sr	Zr					Ba	Hf			
14		Mg	Al			Ca		Mn	Fe	Co	Cu		Sr	Zr					Ba				
15		Mg	Al		K	Ca		Mn	Fe	Co	Cu	Zn	Sr	Zr			Sn		Ba	Hf		Pb	
16		Mg			K	Ca		Mn	Fe	Co	Cu		Sr	Zr						Hf		Pb	
17	Na	Mg			K	Ca		Mn	Fe	Co	Cu		Sr	Zr						Hf			
18		Mg				Ca		Mn	Fe	Co	Cu			Zr					Ba	Hf			
19		Mg			K	Ca		Mn	Fe	Co	Cu	Zn	Sr	Zr					Ba	Hf			
20		Mg				Ca		Mn	Fe	Co	Cu	Zn	Sr		Nb	Mo			Ba	Hf			
21		Mg				Ca		Mn		Co	Cu		Sr	Zr	Nb		Sn		Ba	Hf			
22		Mg				Ca		Mn		Co	Cu		Sr	Zr	Nb		Sn		Ba	Hf		Pb	
23		Mg				Ca		Mn	Fe	Co	Cu		Sr	Zr	Nb		Sn			Hf		Pb	
24	Na		Al	Si		Ca		Mn	Fe	Co	Cu		Sr	Zr	Nb					Hf			
25		Mg	Al	Si		Ca		Mn	Fe	Co	Cu		Sr	Zr	Nb					Hf		Pb	
26	Na	Mg	Al		K	Ca		Mn		Co	Cu	Zn	Sr	Zr	Nb		Sn		Ba	Hf	W	Pb	
27		Mg				Ca		Mn	Fe	Co			Sr	Zr	Nb					Hf			
28		Mg	Al	Si		Ca		Mn	Fe	Co	Cu	Zn	Sr	Zr	Nb					Hf			
29		Mg	Al	Si		Ca		Mn	Fe	Co	Cu	Zn	Sr	Zr	Nb					Hf			
30		Mg	Al	Si		Ca		Mn		Co	Cu		Sr	Zr	Nb					Hf			
31		Mg	Al			Ca		Mn		Co			Sr	Zr	Nb					Hf			
32		Mg				Ca	Ti	Mn		Co	Cu		Sr	Zr	Nb					Hf			
33		Mg						Mn		Co	Cu		Sr	Zr	Nb					Hf		Pb	
34		Mg		Si		Ca		Mn		Co			Sr	Zr	Nb					Hf			
35		Mg				Ca	Ti	Mn		Co	Cu			Zr	Nb					Hf			
36		Mg				Ca	Ti	Mn		Co	Cu			Zr	Nb					Hf			
37		Mg				Ca			Fe	Co			Sr	Zr	Nb					Hf			
38		Mg		Si		Ca		Mn	Fe	Co	Cu		Sr	Zr	Nb		Sn			Hf			
39		Mg		Si		Ca		Mn			Cu		Sr	Zr	Nb					Hf			
40		Mg				Ca		Mn	Fe	Co	Cu		Sr	Zr	Nb					Hf			Bi
41		Mg				Ca		Mn	Fe		Cu		Sr	Zr	Nb			Sb		Hf		Pb	
42		Mg		Si		Ca		Mn			Cu		Sr	Zr	Nb					Hf		Pb	
43		Mg				Ca		Mn			Cu		Sr	Zr	Nb					Hf		Pb	
44		Mg				Ca		Mn			Cu		Sr	Zr	Nb					Hf		Pb	Bi

IN	Na	Mg	Al	Si	K	Ca	Ti	Mn	Fe	Co	Cu	Zn	Sr	Zr	Nb	Mo	Sn	Sb	Ba	Hf	W	Pb	Bi
45		Mg				Ca		Mn		Co			Sr	Zr	Nb					Hf			
46		Mg				Ca		Mn		Co			Sr	Zr	Nb					Hf			Bi
47		Mg	Al	Si		Ca		Mn	Fe	Co	Cu		Sr	Zr			Sn					Pb	Bi
48						Ca		Mn					Sr	Zr	Nb					Hf			Bi
49						Ca		Mn		Co	Cu					Mo		Sb					
50						Ca	Ti	Mn	Fe		Cu		Sr			Mo		Sb					
51						Ca	Ti	Mn	Fe		Cu					Mo		Sb					
52		Mg	Al	Si	K	Ca		Mn	Fe	Co	Cu		Sr	Zr			Sn			Hf			
53	Na	Mg	Al	Si		Ca		Mn	Fe	Co	Cu	Zn	Sr	Zr								Pb	Bi
54		Mg	Al	Si		Ca		Mn	Fe	Co			Sr										Pb
55		Mg						Ti	Mn	Fe	Co		Zn	Sr					Ba				Pb
56								Ti	Mn		Co	Cu			Zr			Sn			Hf		
57								Ti	Mn		Co				Zr						Hf		
58		Mg	Al	Si				Mn		Co				Zr			Sn	Sb		Hf			
59		Mg		Si		Ca		Mn	Fe	Co	Cu		Sr	Zr						Hf			
60		Mg	Al			Ca		Mn	Fe	Co	Cu	Zn	Sr	Zr						Hf			Pb
61		Mg	Al			Ca		Mn	Fe	Co	Cu	Zn	Sr	Zr						Hf			
62		Mg	Al			Ca		Mn	Fe	Co	Cu	Zn	Sr	Zr						Hf			Pb
63	Na	Mg	Al		K	Ca		Mn	Fe	Co	Cu		Sr	Zr									
64	Na	Mg	Al	Si	K	Ca		Mn	Fe	Co	Cu		Sr	Zr								Pb	Bi
65	Na	Mg	Al		K	Ca		Mn		Co	Cu		Sr	Zr								Pb	Bi
66						Ca		Mn		Co	Cu		Sr	Zr						Hf			
67	Na					Ca		Mn		Co	Cu	Zn	Sr	Zr						Hf			Pb
68		Mg				Ca	Ti	Mn		Co	Cu		Sr	Zr						Hf			
69		Mg				Ca		Mn		Co	Cu		Sr	Zr						Hf			
70		Mg	Al	Si		Ca		Mn		Co	Cu	Zn	Sr	Zr			Sn		Ba	Hf	W		
71		Mg	Al	Si		Ca		Mn	Fe	Co	Cu		Sr	Zr			Sn			Hf			Pb
72		Mg	Al		K	Ca		Mn		Co	Cu		Sr	Zr					Ba	Hf			Bi
73			Al			Ca		Mn	Fe	Co			Sr	Zr					Ba	Hf			
74			Al			Ca		Mn		Co			Sr	Zr					Ba	Hf			
75		Mg		Si	K	Ca		Mn	Fe		Cu	Zn	Sr	Zr									Bi
76		Mg	Al	Si		Ca		Mn	Fe		Cu		Sr	Zr			Sn						
77		Mg				Ca		Mn			Cu		Sr						Ba				Pb
78		Mg	Al	Si		Ca		Mn	Fe		Cu	Zn	Sr				Sn						Pb
79	Na	Mg	Al		K	Ca		Mn	Fe	Co	Cu		Sr				Sn						
80		Mg				Ca		Mn	Fe	Co	Cu		Sr	Zr			Sn						Pb
81						Ca					Cu	Zn	Sr						Ba		W		
82		Mg	Al			Ca		Mn	Fe	Co	Cu		Sr	Zr			Sn			Hf			Pb
83						Ca		Mn		Co	Cu		Sr	Zr					Ba	Hf			
84		Mg			K	Ca		Mn	Fe	Co	Cu	Zn	Sr	Zr			Sn		Ba				Pb
85		Mg	Al			Ca		Mn		Co	Cu		Sr	Zr						Hf			
86		Mg	Al	Si		Ca	Ti	Mn		Co			Sr				Sn						

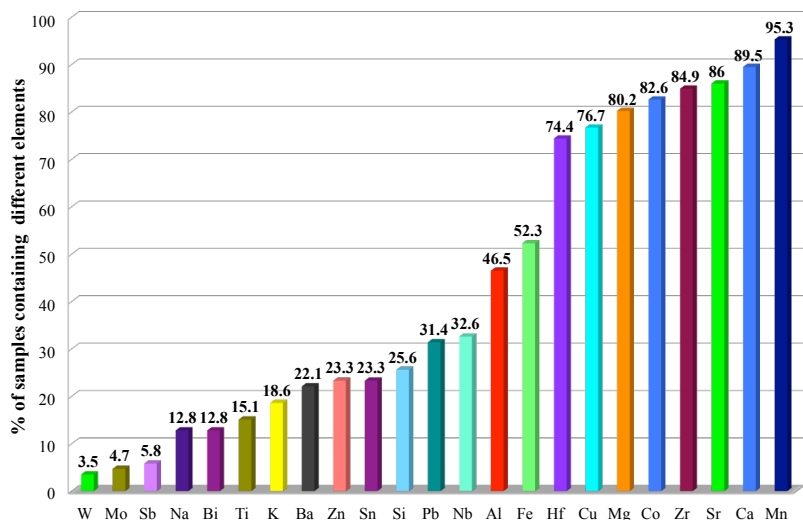


Figure 69. Bar graph showing the distribution of elements in the intaglio ink set.

4.6.1 Aqua Intaglio Printing Inks

There were two aqua intaglio samples. Three elements, Mn, Co, and Cu, were always present in this subset. Elements like Mg, Al, Ca, Zr, Mo, Sb, and Hf were detected in one or the other aqua intaglio ink. All other elements were either not detected or below the detection limit in this subset. Figure 69 shows the list of elements that were detected in the aqua subset.

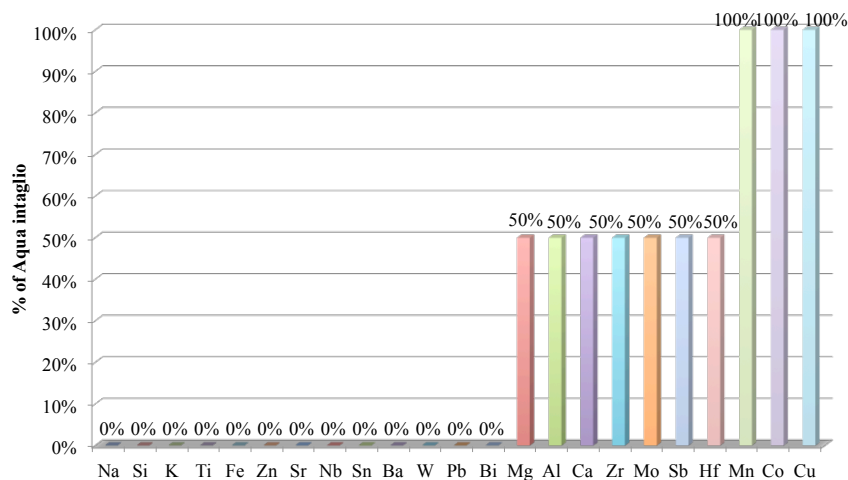


Figure 70. Bar graph showing the distribution of elements in aqua intaglio inks.

4.6.2 Gold Intaglio Printing Inks

There were two gold-colored inks in the intaglio set. In all of these inks, Mg, Al, Mn, Co, Zr, and Hf were detected. Si, Ca, Sr, Sn and Sb were present in half of this subset. The remaining elements in the element menu for intaglio inks were absent in gold intaglio inks. Figure 71 shows the list of elements detected in gold intaglio inks in terms of percentage.

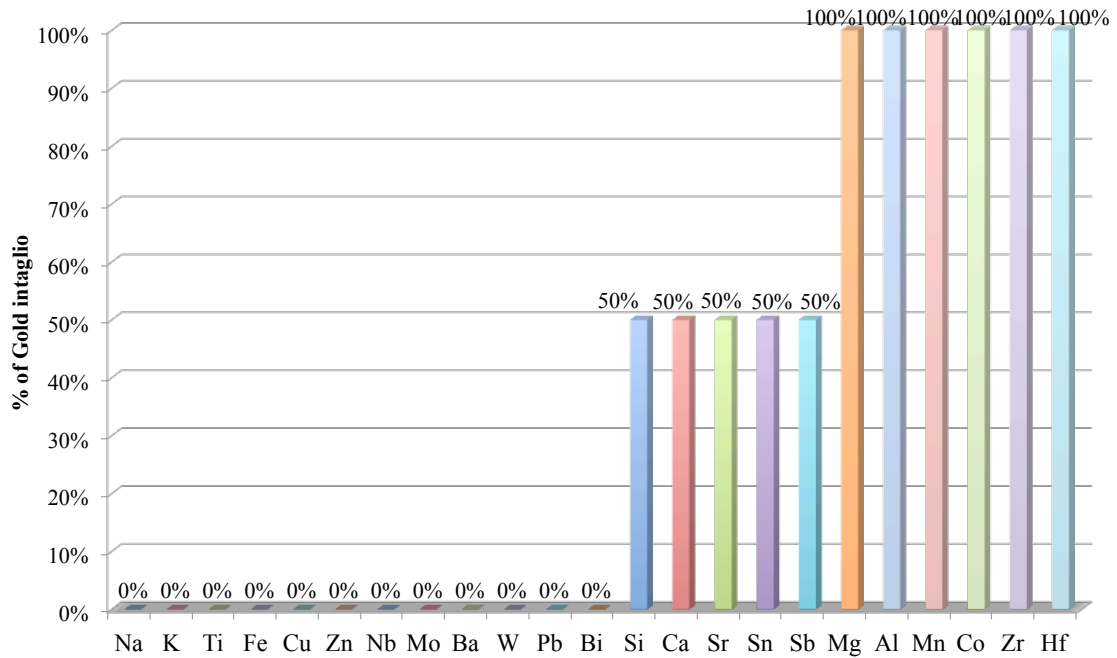


Figure 71. Bar graph showing the list of elements detected in gold intaglio inks.

4.6.3 Black Intaglio Printing Inks

A total of 19 elements were detected in ten black intaglio inks. Mn and Sr were present in nine of the black intaglio samples. Elements like Nb, Mo, Sb and W were completely absent in this set. Figure 72 shows the list of elements that were present in the black intaglio inks in terms of percentage.

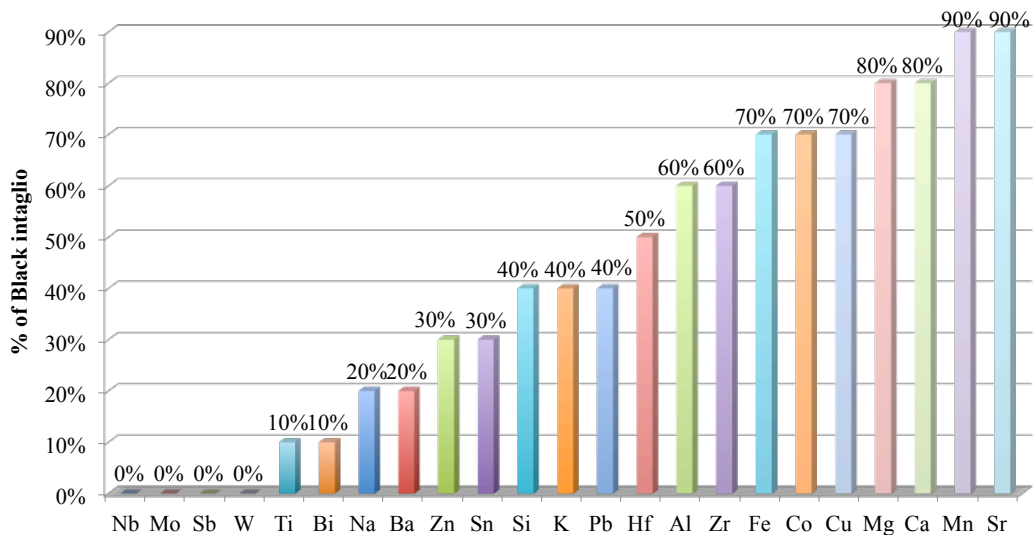


Figure 72. Bar graph showing the list of elements detected in black intaglio inks.

4.6.4 Yellow Intaglio Printing Inks

Three of the samples from Costa Rica were Yellow in color. In all of these samples Mg, Ca, Mn, Sr, Zr, Nb, and Hf were detected. Cu, Pb, and Bi were detected in only one the samples. Co was detected in two-thirds of Yellow intaglio samples. Other elements were absent in this subset as shown in Figure 73.

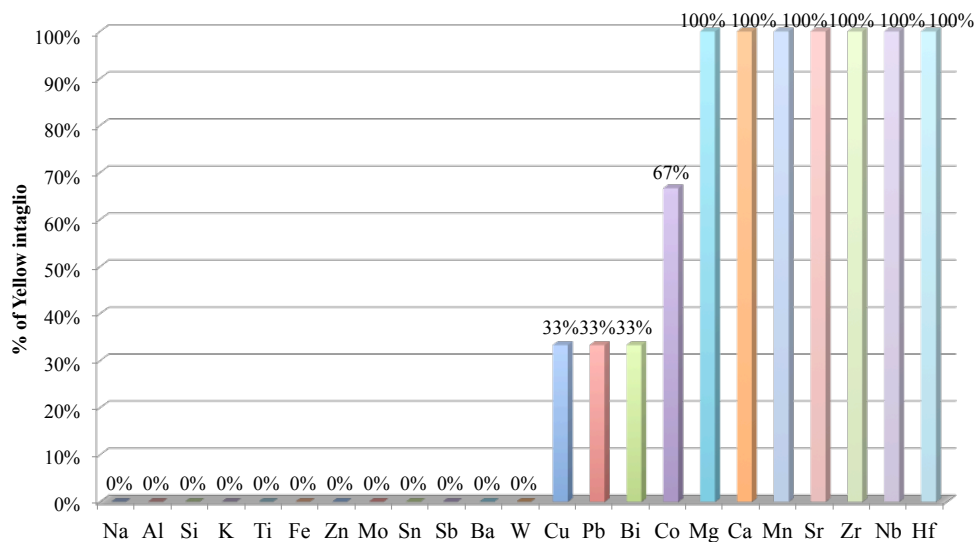


Figure 73. Bar graph showing the list of elements detected in yellow intaglio inks.

4.6.4 Blue Intaglio Printing Inks

A total of 22 of the intaglio printing inks were blue in color. All of them had Mn and Cu. Except W all other elements in the element menu for intaglio inks were present in the blue intaglio. Figure 74 shows the total number of elements present in the blue intaglio inks along with their percentage.

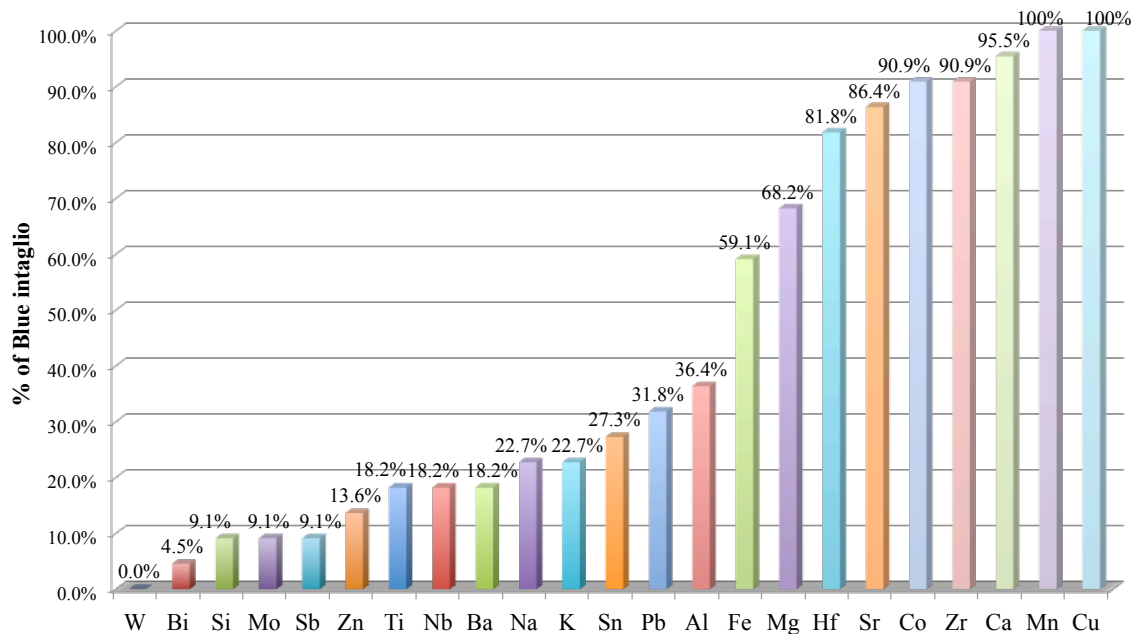


Figure 74. Bar graph showing the list of elements detected in blue intaglio inks.

4.6.5 Brown Intaglio Printing Inks

There were a total of nine brown intaglio samples. Ca was the only element that was detected in all of these inks. Mo, Sb and W were the only elements from the element menu that were not detected in this subset. Figure 75 shows the list of elements that were detected in brown intaglio samples and their relative percentage in the total set.

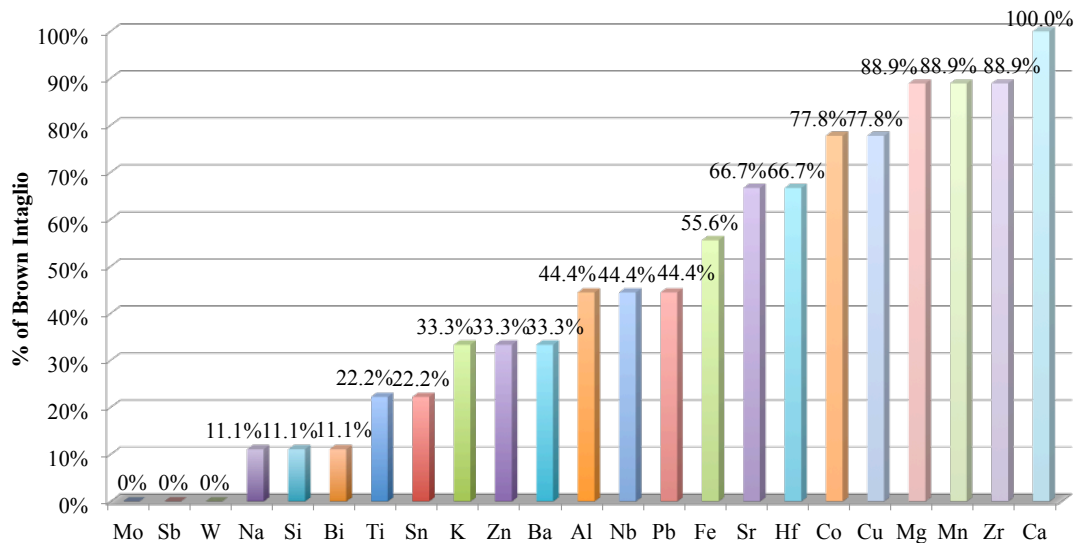


Figure 75. Bar graph showing the list of elements detected in brown intaglio inks.

4.6.6 Red Intaglio Printing Inks

A total of seven red intaglio inks were present in the set. Co was the only element that was detected in all of these inks. Elements like Na, K, Mo, Sb, Ba, W, Pb, and Bi were completely absent in this subset. Figure 76 shows the list of elements present in this subset.

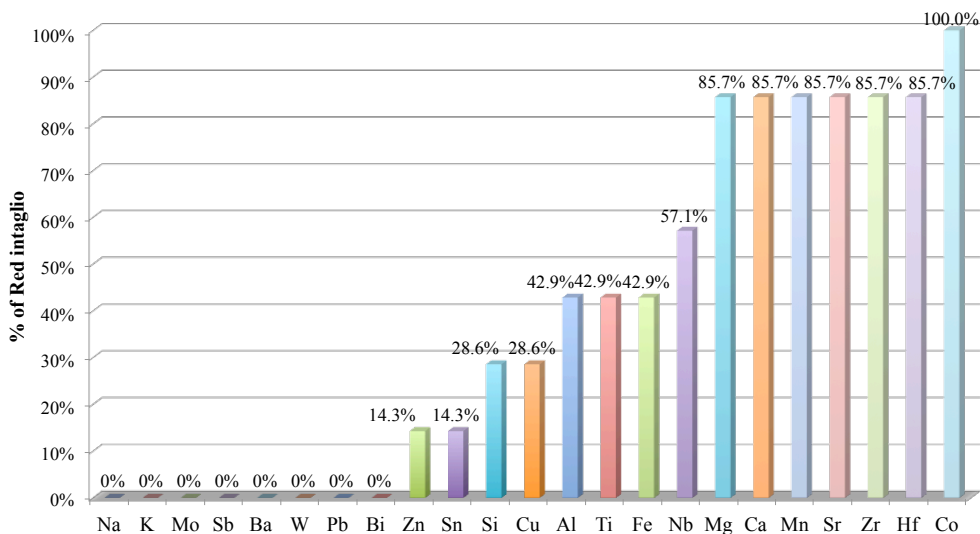


Figure 76. Bar graph showing the list of elements detected in red intaglio inks.

4.6.6 Green Intaglio Printing Inks

A total of 21 intaglio samples were green in color. Mn and Sr were detected in all of the green intaglio samples. The only element that was not detected was Mo out of the element menu. Figure 77 summarizes the list of elements detected in green intaglio samples.

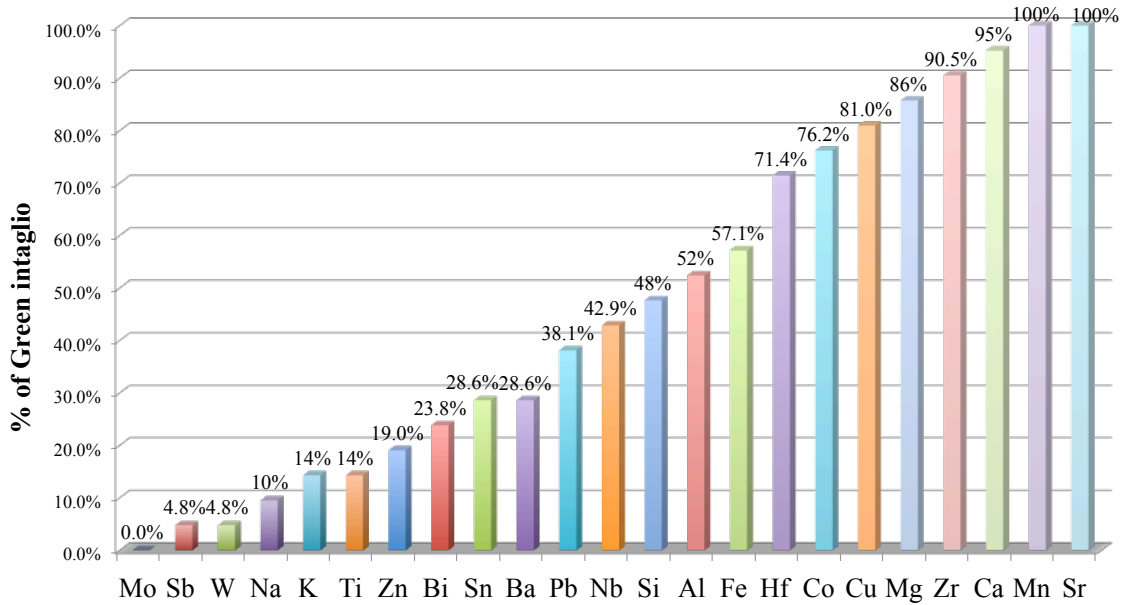


Figure 77. Bar graph showing the list of elements detected in green intaglio samples.

4.6.7 Purple Intaglio Printing Inks

Four of the intaglio samples were purple in color. Four elements, Ca, Cu, Zn, Sr and Ba were present in all of these purple intaglio samples. Some elements from the element menu like Na, Ti, Sb, Pb and Bi were completely absent. Figure 78 shows the list of the detected and the undetected elements.

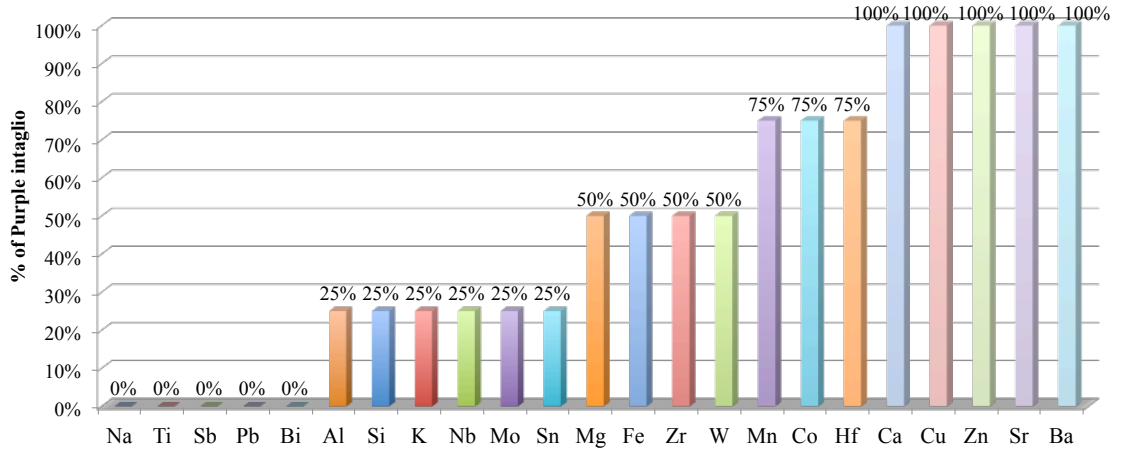


Figure 78. Bar graph showing the list of elements detected in purple intaglio.

4.6.8 Maroon Intaglio Printing Inks

Three of the intaglio samples were maroon in color. Six elements, Mg, Mn, Cu, Sr, Zr, and Hf were detected in all of the maroon intaglio samples. One third of the samples had Al, Fe, Zn, and Bi while Ca, Co, Nb, and Pb were detected in two-thirds of the samples. Figure 79 shows the list of the elements detected in maroon intaglio samples.

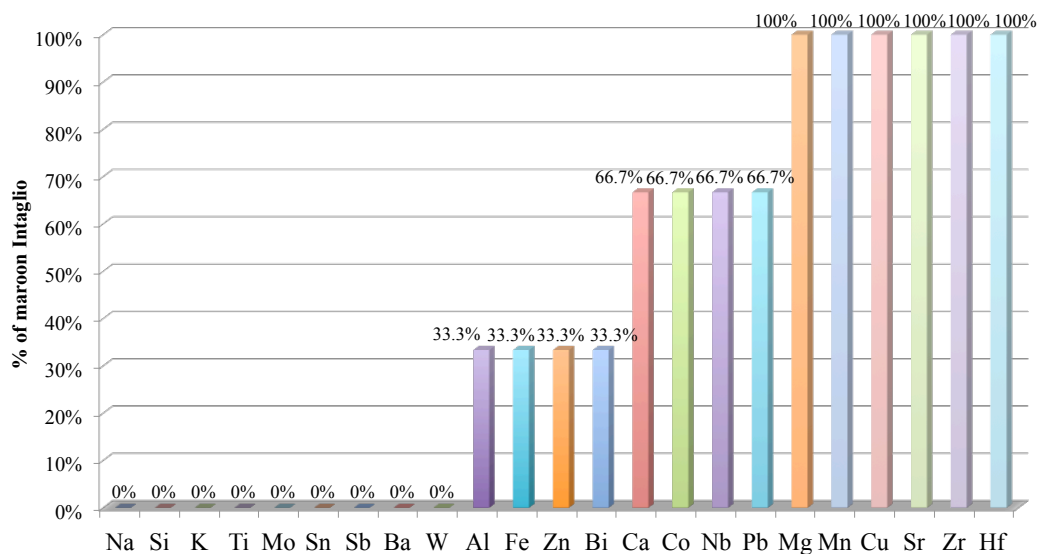


Figure 79. Bar graph showing the list of elements detected in maroon intaglio inks.

4.6.9 Orange Intaglio Printing Inks

Two of the intaglio samples were orange colored. A total of 16 elements were detected in this subset. All the orange intaglio contained Mg, Al, Ca, Mn, Co, Sr, and Zr. Elements like Na, Si, Fe, Cu, Zn, Nb, Hf, and Pb were detected in 50% of the samples. Some elements like K, Ti, Mo, Sn, Sb, Ba, and W were completely absent in this subset. Figure 80 shows the list of the elements present in orange intaglio samples.

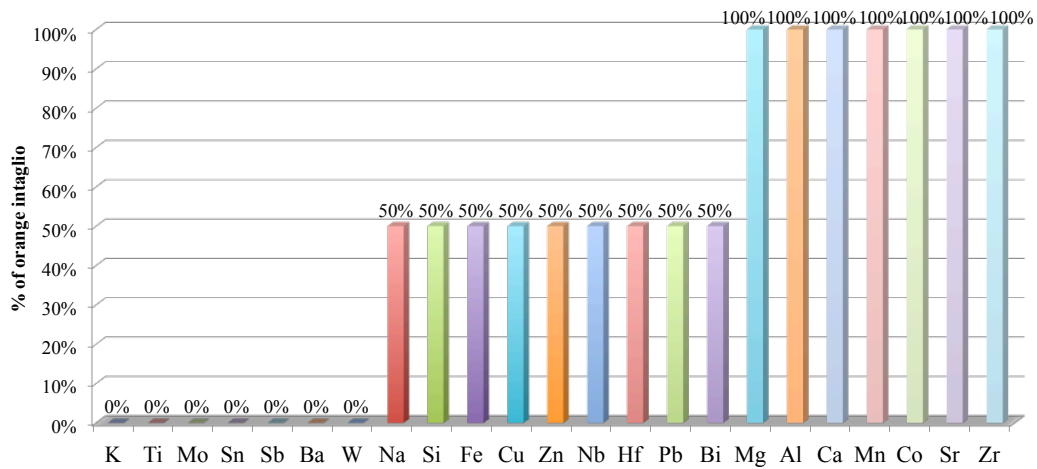


Figure 80. Bar graph showing the list of elements detected in orange intaglio samples.

4.6.10 Overall Discrimination for Intaglio Printing Inks

Spectral Overlay comparison was able to distinguish 3653 pairs of intaglio inks out of 3653 possible combinations. The discrimination was the highest compared to all other three printing inks. Only two pairs were indistinguishable using LA-ICP-MS.

These two pairs are listed in Table 26.

Table 26. List of indistinguishable intaglio pairs by LA-ICP-MS.

Indistinguishable pairs	Source	Common elements detected
10IT Vs. 11 IT	Ukraine (2011)	Mg, Al, Ca, Mn, Co, Sr, Zr, Hf
35IT Vs. 36IT	Italy (2002)	Mg, Ca, Ti, Mn, Co, Cu, Zr, Nb, Hf

All the duplicate controls were correctly associated providing 100% correct association. Table 27 summarizes the overall discrimination for intaglio printing inks by Spectral Overlay.

Table 27. Overall discrimination capability of LA-ICP-MS for the analysis of intaglio printing inks.

# Samples	86
# Samples from different sources	86 (3655 comparison pairs)
Duplicate controls from same sources	3 quality controls, 3 duplicate controls (6 comparison pairs)
% Discrimination	99.95% (3653 out of 3655)
% False exclusions	0% (0 out of 6)
% False inclusions	0.05% (2 out of 3655)

Spectral Overlay and One –Way ANOVA were used to study the association of controls. For two controls OF 04 and OF 06, ⁵⁵Mn and ⁵⁹Co were monitored. Spectral Overlay showed no difference between the duplicates run on different days as shown in Figures 81 and 82. One Way ANOVA with Tukey’s HSD test also showed no significant difference within these controls. Figure 83 and Figure 84 are the One Way ANOVA plots showing a significant difference in Mn and Co concentration in the two controls (IT 04 and IT 06), but no significant difference within the controls.

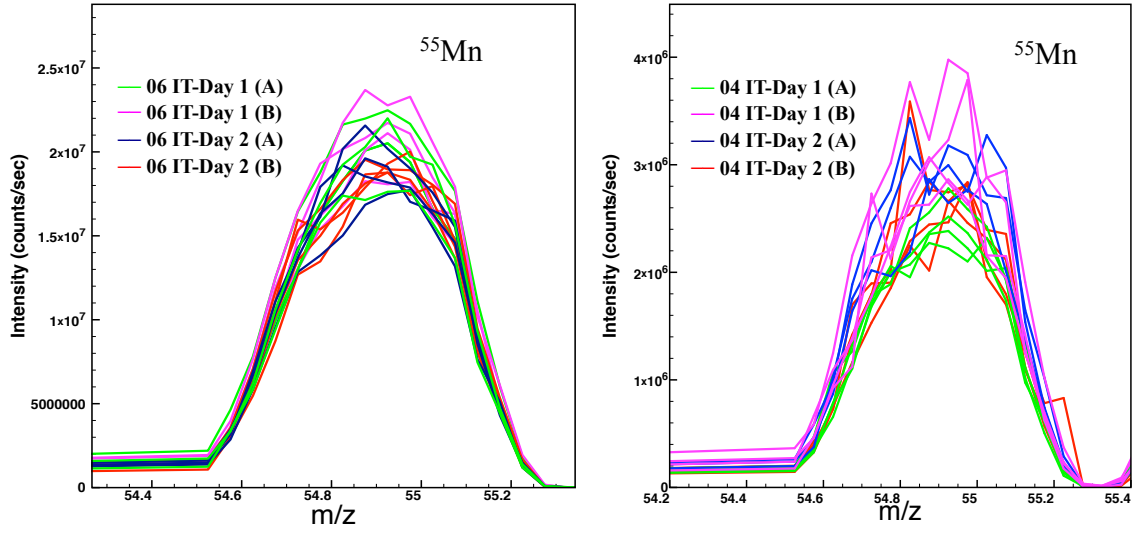


Figure 81. Spectral Overlay comparison for two Intaglio Controls on the right (IT 06) and left (IT 04) by Mn.

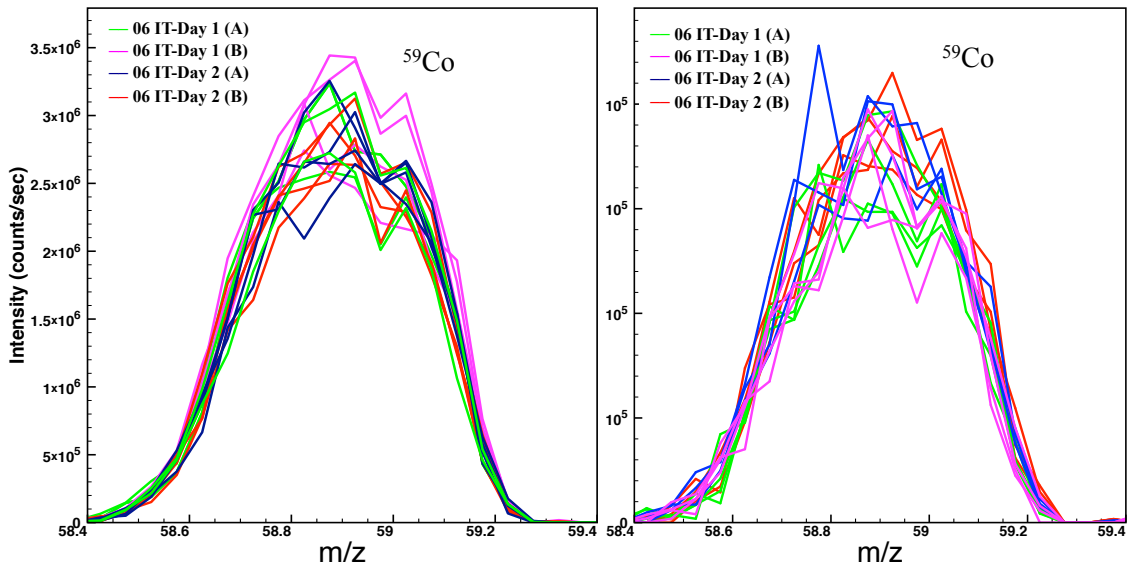


Figure 82. Spectral Overlay comparison for two intaglio controls (IT 06 on right and IT 04 on left) by Co.

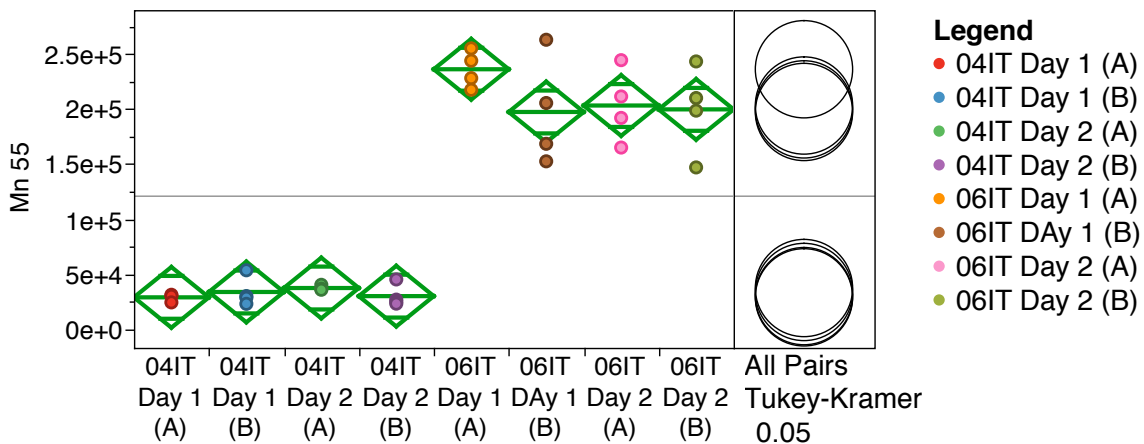


Figure 83. One Way ANOVA with Tukey's HSD test for the analysis of ^{55}Mn in intaglio controls.

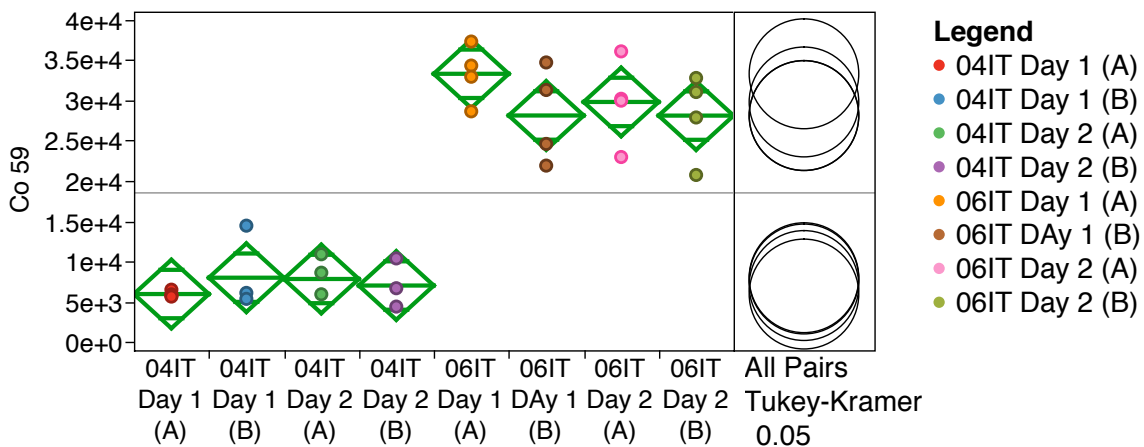


Figure 84. One Way ANOVA with Tukey's HSD test for the analysis of ^{59}Co in intaglio controls.

4.6.11 Multivariate Analysis of Intaglio Printing Inks

Principal Component Analysis and Linear Discriminant Analysis were performed for the multivariate analysis of intaglio printing inks.

4.6.11.1 Principal Component Analysis of Intaglio Printing Inks

Principal Component Analysis of 86 different intaglio printing inks was performed. The integrated areas of all the elements, which were at least three times the background.

The PCA plot obtained from only the first two principal components is shown in Figure 85. Some of the intaglio printing inks are well classified (For e.g., IT 58 shown as green cross marks in the upper first quadrant). The first three PC explained 43.3% of the total variance.

Table 28. PCA scores for the first three Principal Components in intaglio inks.

PC1	PC2	PC3	Cumulative variance
18.50%	14.70%	10.10%	43.30%

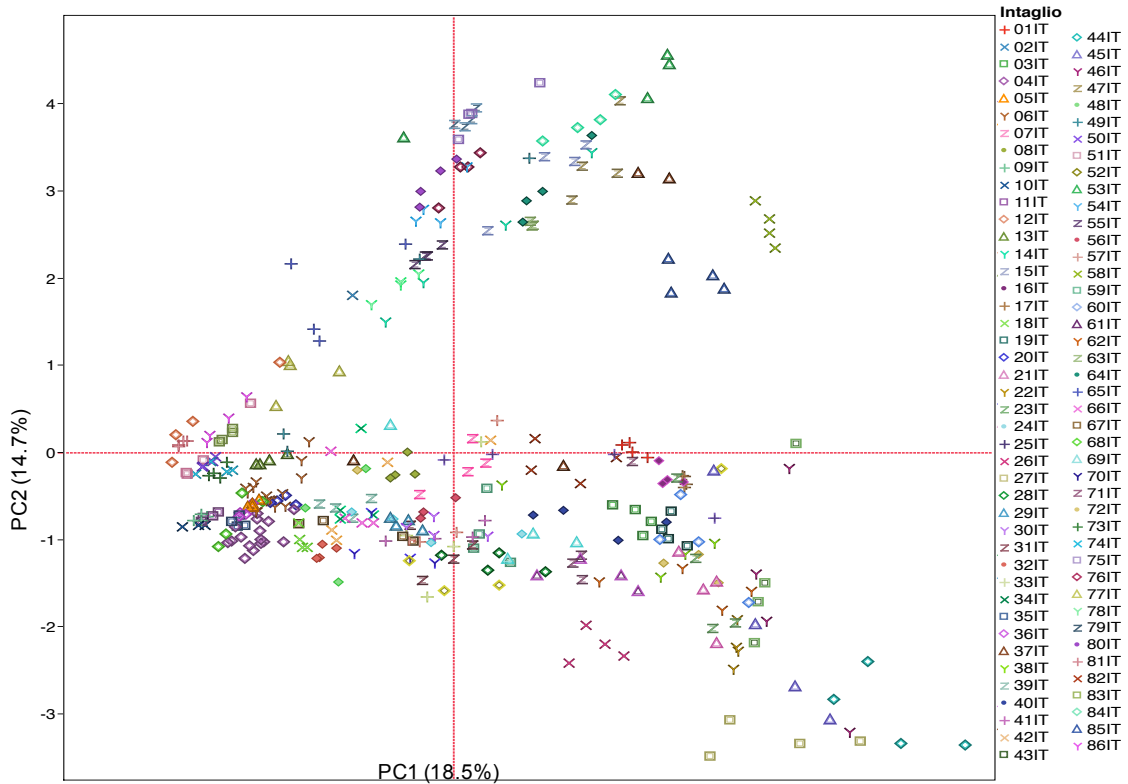


Figure 85. Two-dimensional PCA plot for intaglio printing inks by LA-ICP-MS.

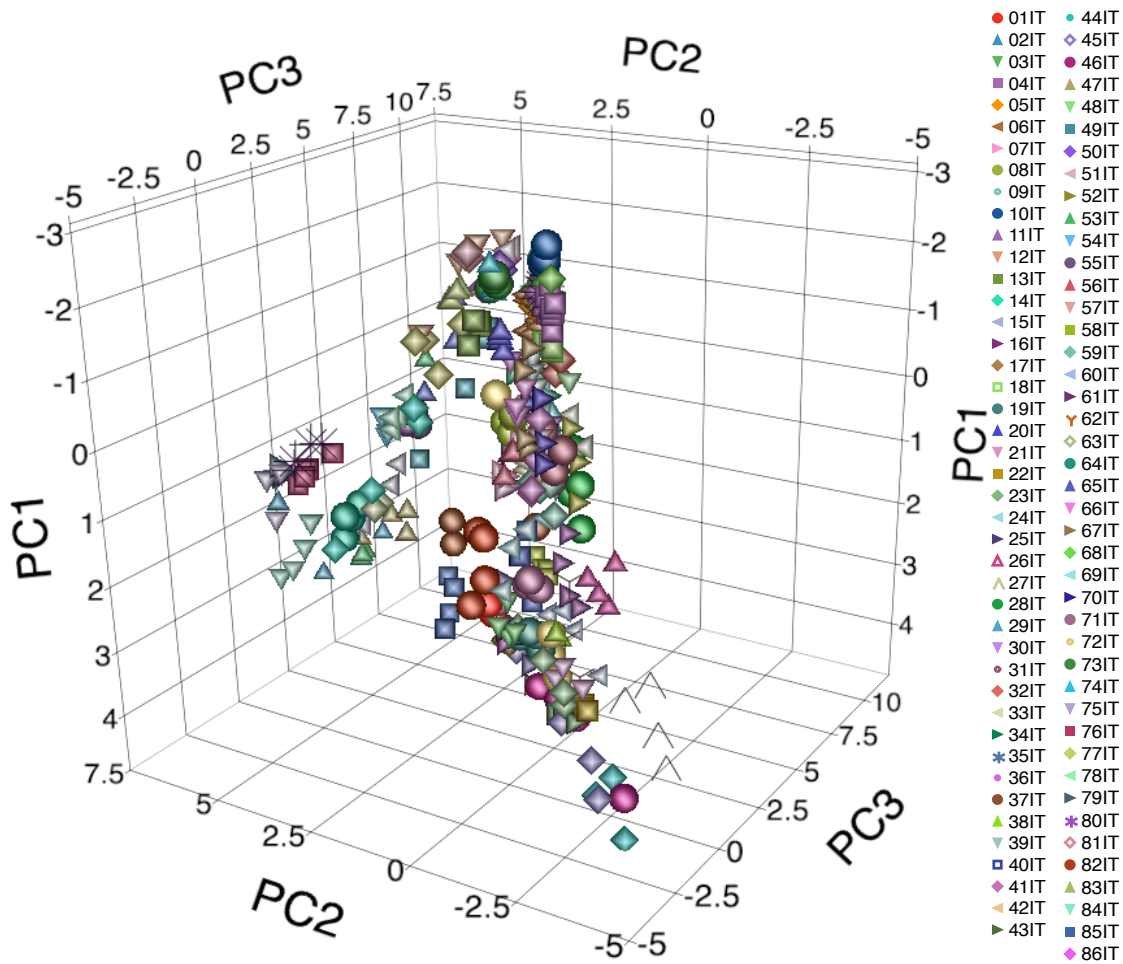


Figure 86. Three-dimensional PCA plot for intaglio printing inks by LA-ICP-MS.

The three dimensional PCA shows classification of 86 intaglio inks as shown in Figure 86. Some intaglio inks can be seen clustered separately from other inks. For example, IT 27 has a distinct group at the bottom right of the plot as shown in Figure 85. The PCA plot in Figure 85 based on the source (country) of intaglio inks provides a clear visualization of the ink. Intaglio inks from same country are clustered together. For example, intaglio ink from South Korea (green rectangles) is clustered together as shown in Figure 87 and Figure 88.

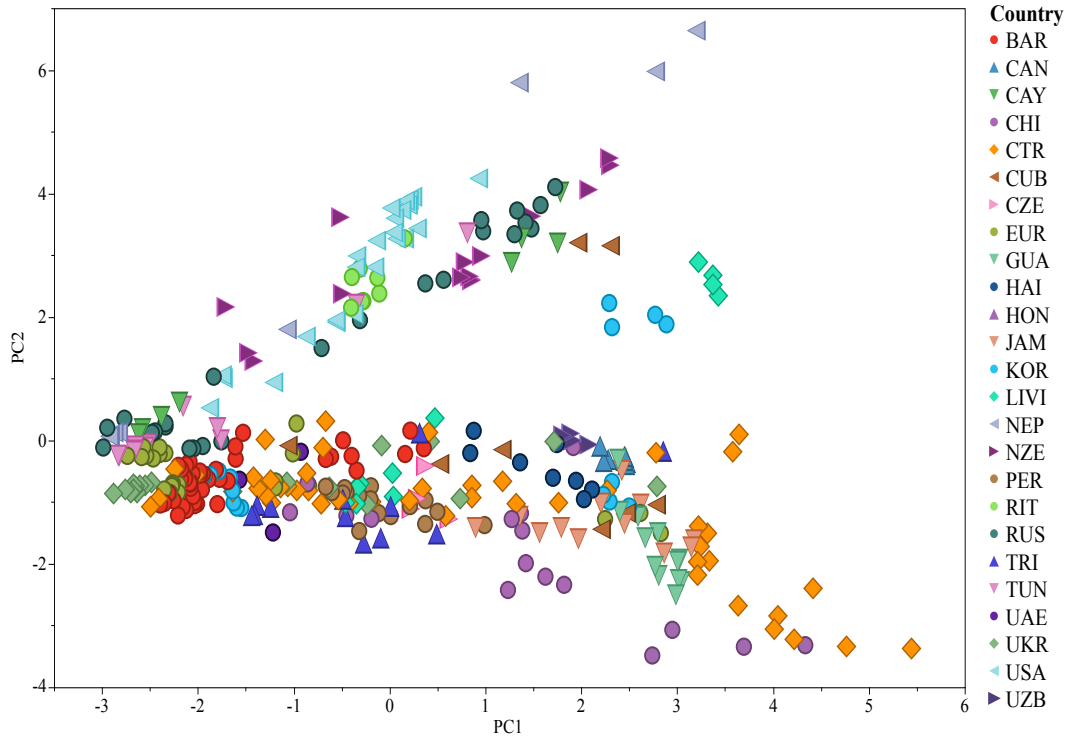


Figure 87. Two-dimensional PCA plot obtained from LA-ICP-MS data for intaglio samples by country.

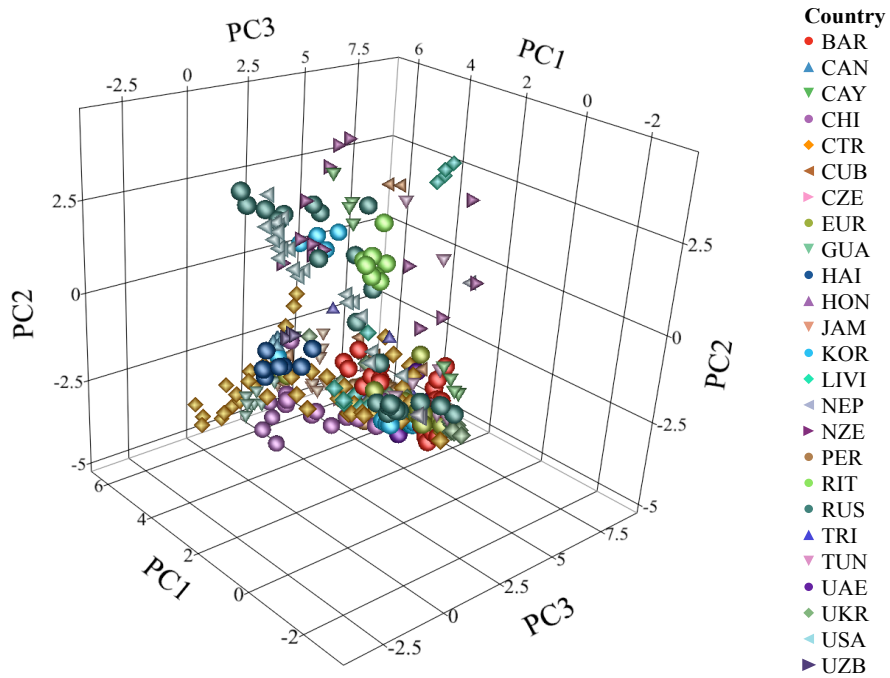


Figure 88. Three-dimensional PCA plot for intaglio inks by country.

4.6.11.2 Linear Discriminant Analysis of Intaglio Printing Inks

Linear Discriminant Analysis discriminated most of the intaglio pairs. Only seven pairs of intaglio inks were misclassified as shown in Table 29. The controls that were used to study inter day and intra day variation were also shown as misclassified (correct association). Table 29 is the confusion matrix that shows the list of intaglio printing ink pairs that were misclassified by LDA

Table 29. List of intaglio printing ink pairs misclassified by LDA.

Misclassified pairs	Source
06IT Vs. 11IT	Barbados (2007) Vs. Ukraine (2011)
29IT Vs. 30IT	Peru (2009)
32IT Vs. 33IT	Trinidad and Tobago (2006)
35IT Vs. 36IT	Italy (2002)
66IT Vs. 69 IT	Costa Rica (2000)
73IT Vs. 74 IT	Italy (2013)
74IT Vs. 81IT	Italy (2013) Vs. Nepal (2009)

Most of these pairs were of the same source and were manufactured in the same year. Figure 89 shows that 71% of the misclassified pairs were from the same country and were manufactured in the same year, while 29% of the misclassified pairs were from different countries and were manufactured in different years.

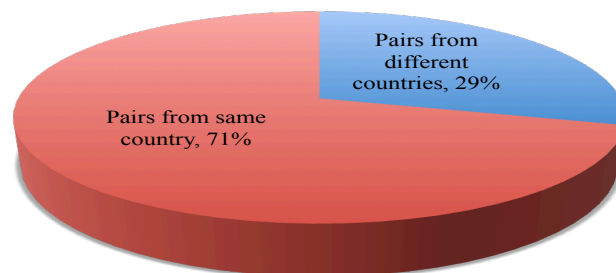


Figure 89. Pie chart showing the percentage of misclassified pairs from different sources.

There was some agreement between Spectral Overlay and LDA. One of the two pairs that was not distinguishable by Spectral Overlay was also misclassified by LDA. Table 30 lists that common pair.

Table 30. Common intaglio pairs indistinguishable by Spectral Overlay and LDA.

Common indistinguishable pairs	Source	Common elements detected
35IT Vs. 36IT	Italy (2002)	Mg, Ca, Ti, Mn, Co, Cu, Zr,

4.6.11.3 Partial Least Square Discriminant Analysis of Intaglio Printing Inks

Two duplicate controls were used for the Partial Least Square Discriminant Analysis. These two duplicate controls were IT 04 and IT 06. Twelve replicates of each of these duplicates were searched through the intaglio database containing 88 inks. Both of these intaglio duplicates were correctly associated as shown in Figure 90 and Figure 91. This resulted in 100% correct association of duplicate controls.

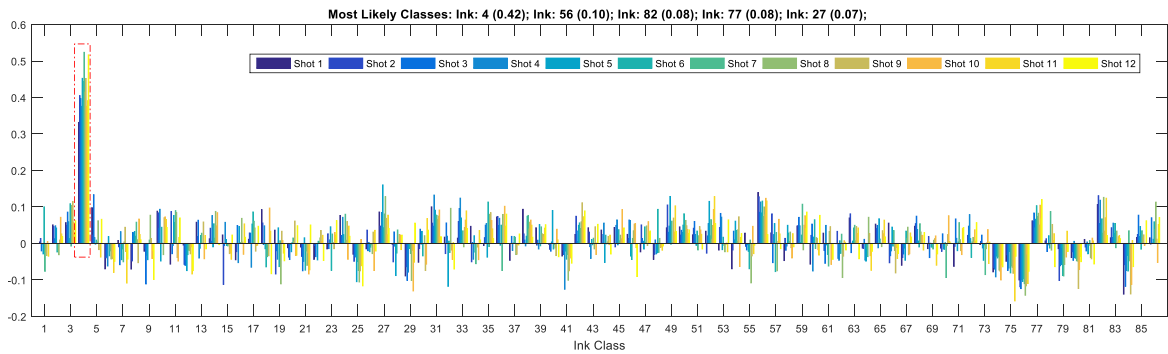


Figure 90. PLS-DA plot for IT 04 showing the correct association in the ink database.

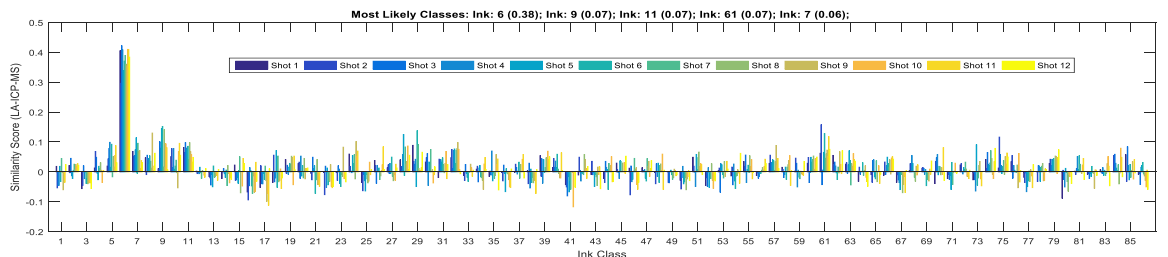


Figure 91. PLS-DA plot for IT06 showing the correct association in the ink database.

4.6.11.4 K-Nearest Neighbor Analysis of Intaglio Printing Inks

Of the two controls used, one of the controls was not correctly associated with itself in the database. This provided 50% correct association by K-NN analysis. Figure 92 shows the correct association of one of the intaglio controls using K-NN algorithm.

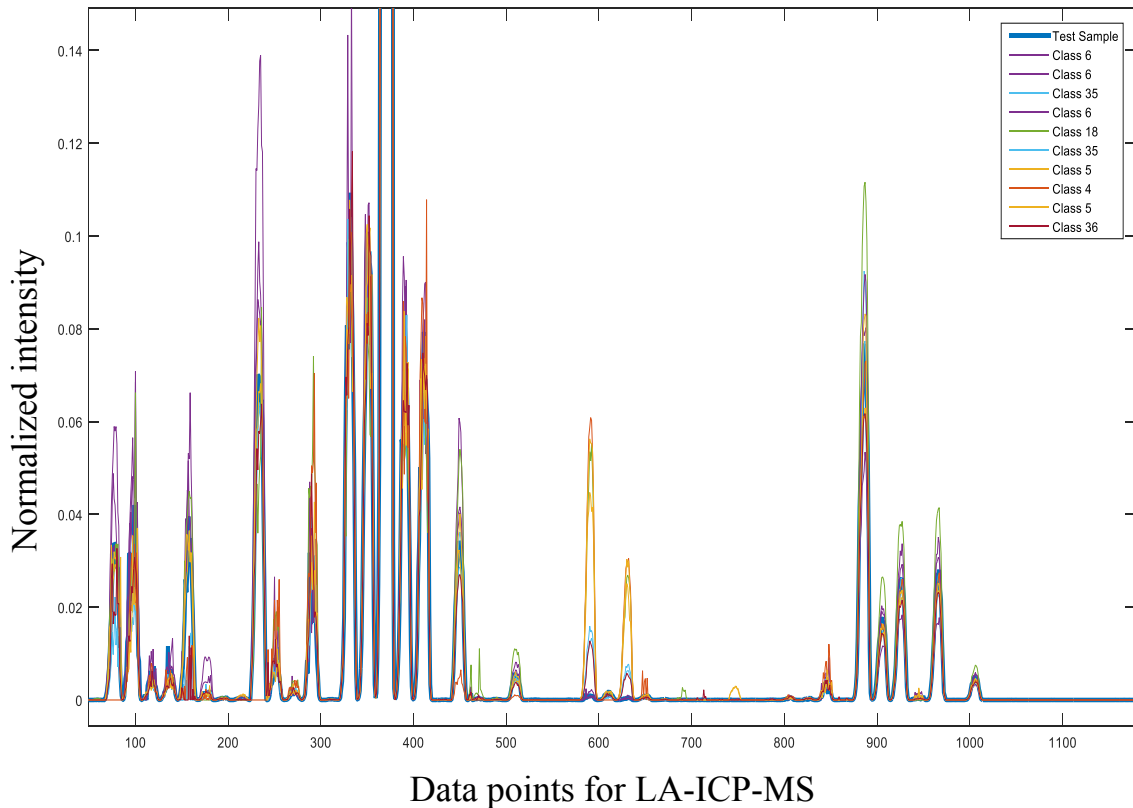


Figure 92. K-NN plot for IT06 showing the correct association with itself in the ink database.

4.7 Canonical Discriminant Analysis of Intaglio Printing Inks

Canonical Discriminant Analysis is a supervised algorithm used to classify objects based on their characteristic features. The group membership of the objects is known prior to analysis. This is a dimension reduction technique, which minimizes the dimension of the study by extracting useful features from a set of variables, in the form of

discriminant functions. The first function (canonical component 1) is built to maximize the group differences⁶¹. The next functions (Canonical 2, Canonical 3.) are built to be orthogonal to the first, and still maximize group differences. The process of extracting canonical components can be repeated until the number of canonical components equals the number of original variables or the number of classes minus one, whichever is smaller⁶¹.

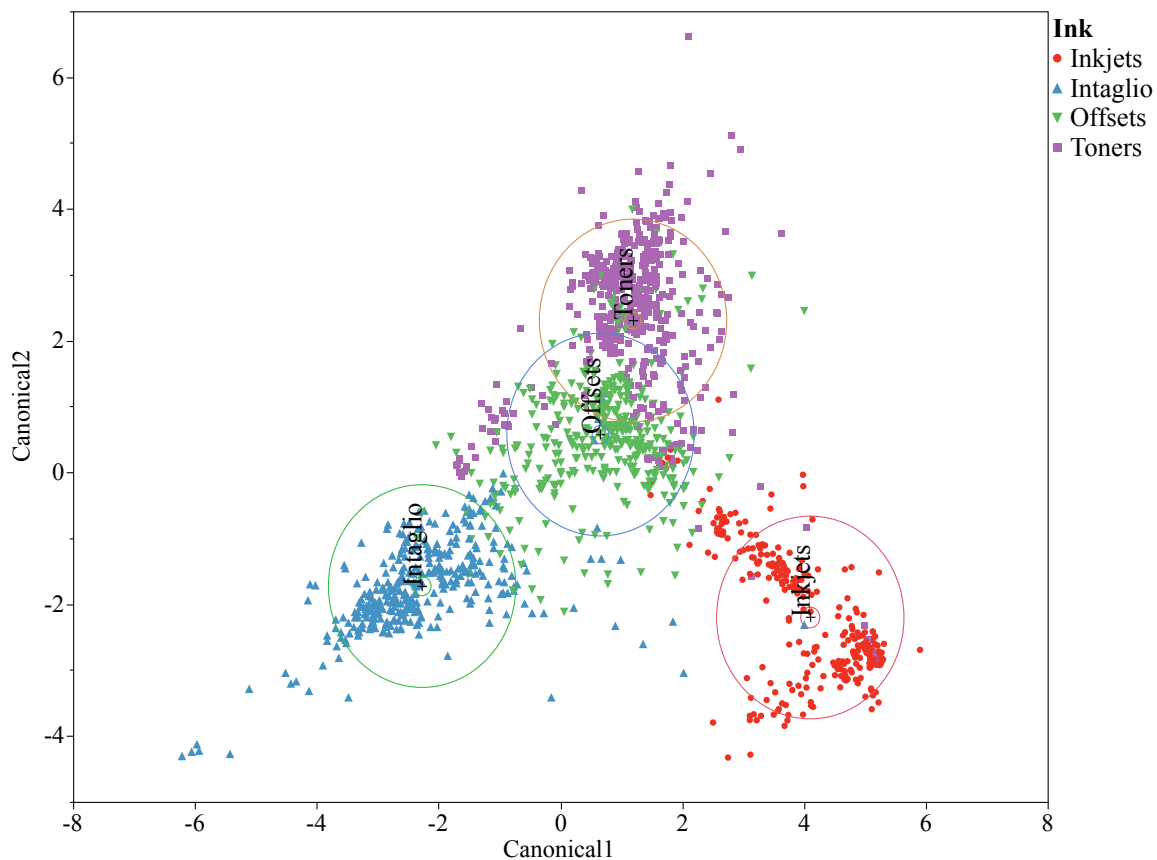


Figure 93. Two-dimensional Canonical Plot for 391 ink samples from four different groups.

The number of functions derived is equal to $\max N-1$ (for four printing ink types, there will be a maximum of three Canonical Components). Figure 93 is a two-dimensional Canonical Plot for 319 printing inks using the LA-ICP-MS spectrum. It

shows that four different types of inks, which differ in their morphology, and the way in which the ink is deposited, can be classified into four distinct classes using LA-ICP-MS. Some overlapping between the two different ink groups (toners and offsets) can be visualized in figure 93. The use of different chemical agents as taggants, and additives make some of the inks different from its group (for example addition of Molybdenum in toners, as charge controlling agent). Intaglio inks can be seen to be the least overlapping inks in the figure. This is due to the fact that, intaglio inks have various elements, which are not present in toners, inkjets or offset inks.

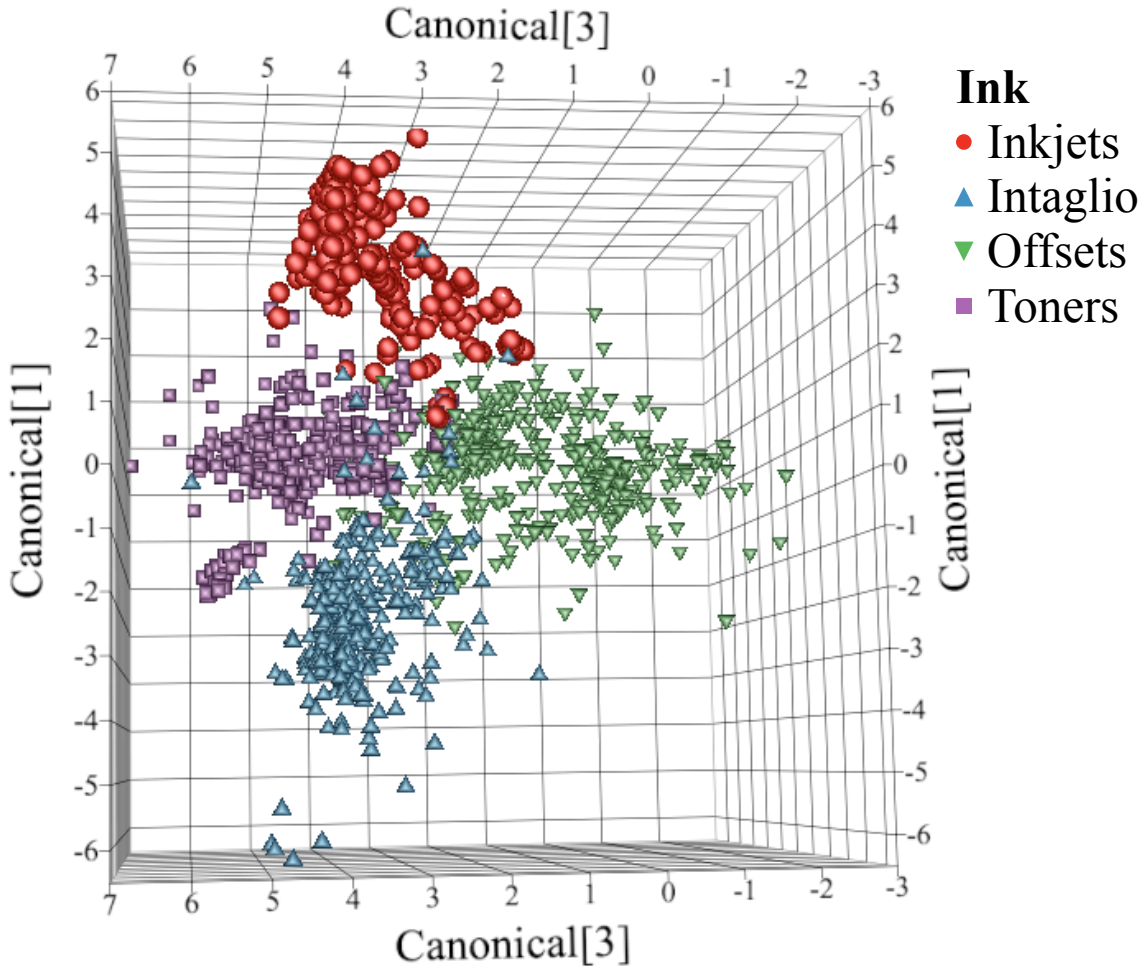


Figure 94. Three-dimensional Canonical plot for 319 different types of inks.

4.8 Conclusion

LA-ICP-MS provided discrimination greater than 99% for all four types of inks. The elemental characterization of four different types of printing inks was successful using this tool. A very good association of the controls used was also detected. Both Spectral Overlay and Statistical analysis showed a good discrimination between inks originating from different sources, while showing a correct association between the inks sharing the same origin. Table 31 summarizes the discrimination potential of LA-ICP-MS for all four different types of inks.

Table 31. Overall discrimination of four inks by LA-ICP-MS⁶.

	Inkjet	Toner	Intaglio	Offset
# Samples	78	76	86	79
# Samples from different sources	78	76	86	79
# Comparison Pairs	3003	2850	3655	3081
Duplicate Controls	0	20	3	16
Quality controls	3	4	3	7
Total Comparison pairs for controls	3	26	6	37
% Discrimination	99.6% (2990/3003)	99.1% (2825/2850)	99.95% (3653/3655)	99.8% (3075/3081)
% False exclusions	0% (0/3)	7.7% (2 out 26)	0% (0/6)	0 (0/37)
% False inclusions	0.4% (11/3003)	0.9% (25/2850)	0.05% (2/3655)	0.2% (6/3081)

Chapter 5. Analysis of Ink Samples by LIBS

LIBS was also used for elemental detection of inks. LIBS provided multiple lines for comparison for different elements. Figure 95 shows a typical LIBS spectrum of a standard sample containing 10,000ppm concentration of different elements like Na, Mg, Al, Ti, K, Ti, Mn, Fe, Cu, Zn, Sr, and Pb.

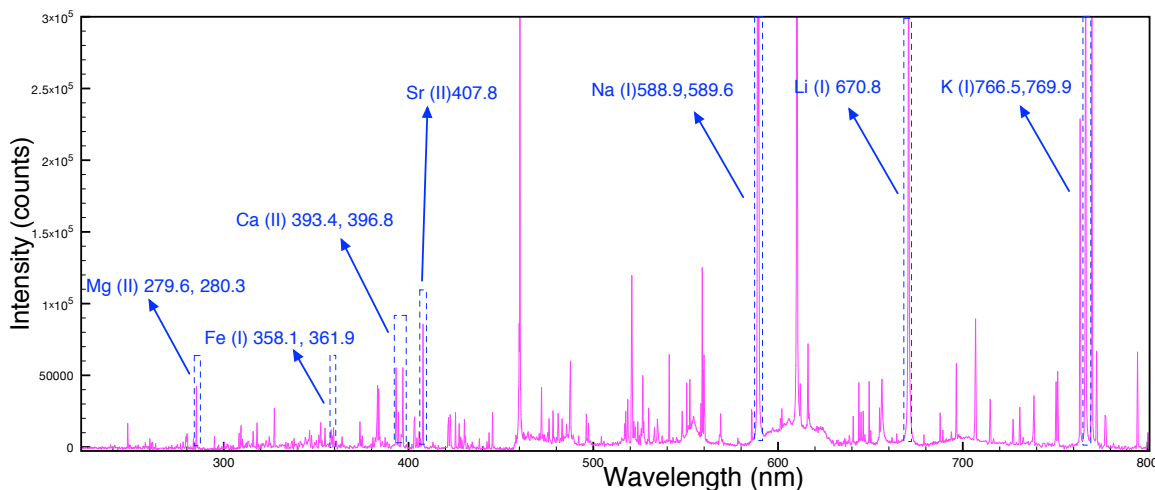


Figure 95. A LIBS spectrum for a 10,000ppm standard sample.

5.1 Instrumentation of LIBS

The LIBS instrument used for the analysis of printing inks was a RT 100HP system from Applied Spectra, Fremont, CA. This LIBS system consisted of an IR laser with a 1064nm ns-Nd:YAG laser and a Czerny Turner spectrograph (Princeton Instruments, NJ) with an ICCD detector (Gen II, Andor Technology, CT) and dual grating turret (operated at 2400 grooves/mm). This system also had an automated X-Y-Z stage that could be moved in three different directions with a speed range from 1-20 $\mu\text{m/s}$.

5.2 Sample Preparation for Analysis by LIBS

The intaglio regions were first confirmed using Keesing Documentchecker (Keesing reference systems Inc.) and for further verification a microscope was used. The sample was carefully handled with dedicated gloves and was affixed to the sample stage using a double-sided tape. Figure 96 shows a section of the intaglio ink that was analyzed by using LIBS.

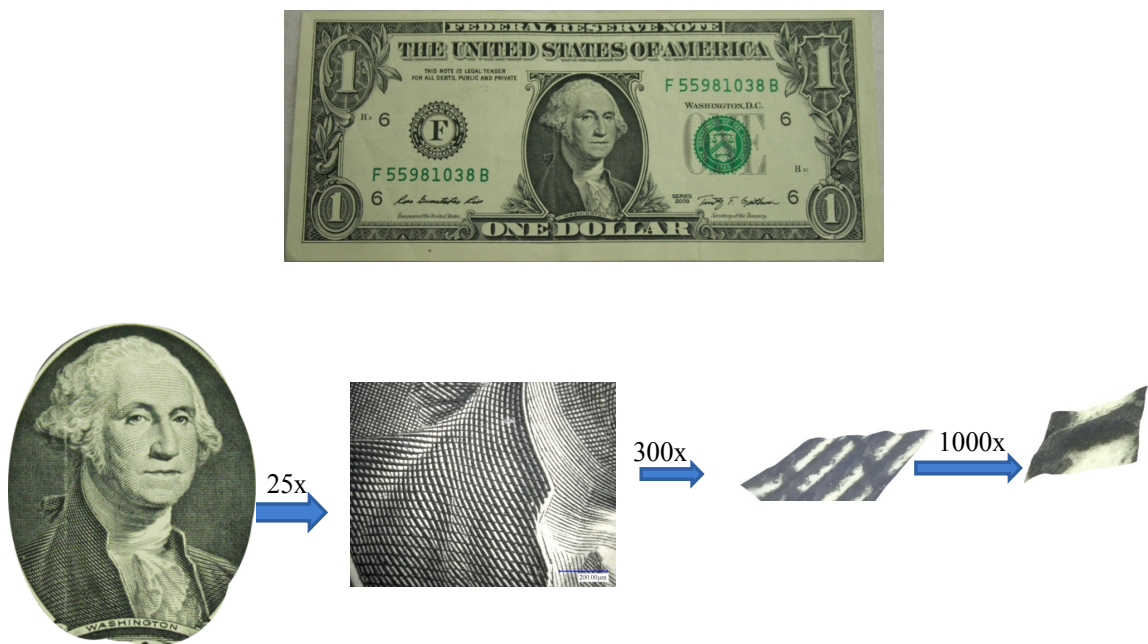


Figure 96. Intaglio ink present in a United States banknote.

5.3 Optimization of LIBS for the Analysis of Inks

The optimization protocol for the analysis of inks by LIBS was very similar to LA-ICP-MS. The optimization was based on the signal intensity, signal to noise ratio and the extent of paper contribution. To minimize the damage to the paper fibers, low laser energy (20%) was used as higher energy resulted in significant paper contribution as shown in figure 97¹¹.

A line scan mode was suitable for the ink analysis as the spot mode caused more damage to the paper. A spot size of $350\mu\text{m/s}$ was used to account for any sample heterogeneity. Different laser frequencies ranging from 1 to 10 Hz were tested. Similarly the scan speed was also varied from $10\mu\text{m/s}$ to $30\mu\text{m/s}$. A high laser frequency resulted in more damage to the paper, so the scan speed was also varied accordingly to minimize the impact of laser on the paper fibers.

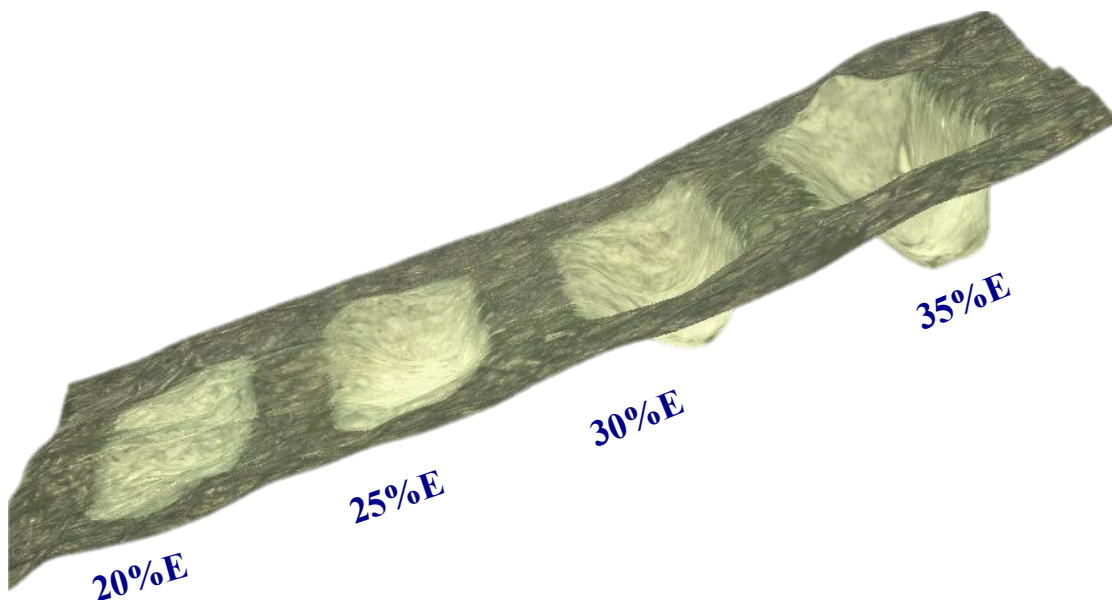


Figure 97. Effect of increasing laser energy and the extent of paper damage¹¹.

5.3.1 Use of Argon as an Ambient Gas

The use of different gases like Argon, Helium has been reported in literature^{23,24,76}. In the present study Argon was used as an ambient gas to increase the signal intensity. It was found that the use of Argon gas increased the signal in LIBS by approximately four times as shown in figure. The flow of Argon gas had also effect in the precision of the measurement as shown in figure 99. It was found that at lower flow rate

the precision was low. Figure 99 shows that precision is poor at a flow rate of 0.5L/min compared to those at higher flow rates. The overall optimized parameters for the analysis of intaglio inks are tabulated in table 32.

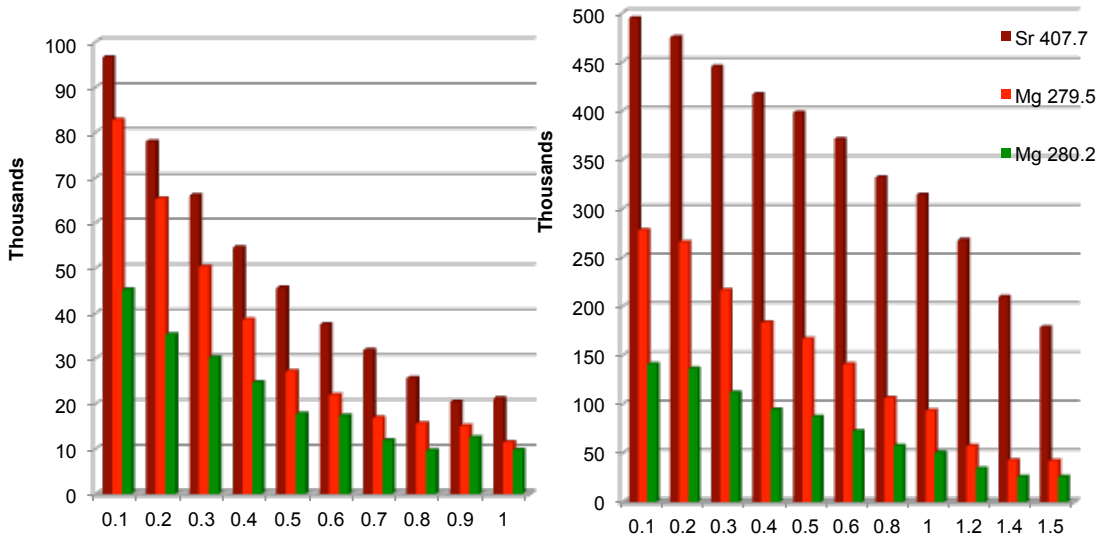


Figure 98. Effect of Helium (left) and Argon (right) as ambient gas on the intensity of emission lines in LIBS.

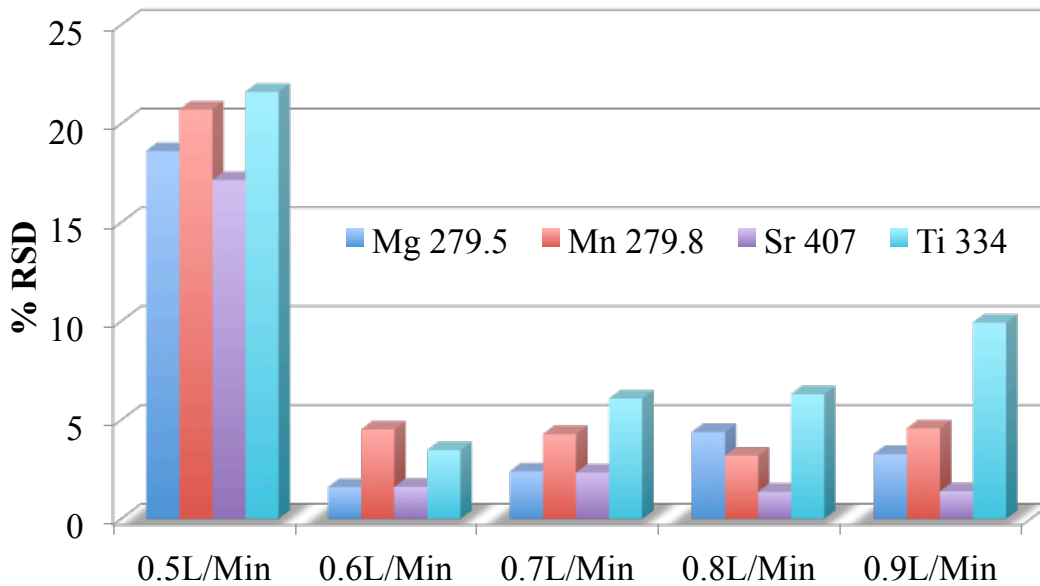


Figure 99. Effect of Argon gas flow on the precision of peak intensity in LIBS.

Table 32. Optimized parameters for the analysis of intaglio inks by LIBS.

Parameters	Intaglio
Ablation mode	Single line
Laser spot size	350 μ m
Frequency	2 Hz
Laser energy	20% (4.1mJ)
Ablation rate	25 μ m/s
Gate Delay	1 μ s
Argon flow in the cell	0.7L/min
Number of shots	100
Length of line	1.25mm

5.4 Data Analysis of LIBS for the Analysis of Printing Inks (Intaglio)

Aurora data analysis software was used for the detection and confirmation of LIBS emission lines. Several elements were detected using LIBS. The analysis of paper was also done. Various elements were also present in paper. Those elements that were significantly higher (at least 3 times) than paper, were only reported as detected. The list of elements that were detected in intaglio inks is tabulated in Table 33. Figure 100 shows the overlay of two spectra (ink and paper). All the emission lines in red color are from ink while the ones in cyan color are from paper. The confirmation of these elements was done through the LIBS and NIST database. Most of the elements had more than two interference free emission lines. The presence of more than two emission lines with no interferences and highest intensities confirmed the presence of an element. Figure 101 shows the confirmation of Ti in inks through the detection of multiple emission lines.

Table 33. List of elements detected by standalone LIBS.

Elements detected	Emission lines (nm)
Ca	393.3 (II), 396.8 (II)
Mg	517.3 (I), 516.7 (I)
Ti	332.3(I), 334.9 (II), 334.2 (I)
Cu	324.3 (I), 327.4 (I)
Na	588.9 (I), 589.6 (I)
Fe	356.5 (I), 357.0 (I), 358.2 (I)
Mn	358.7 (I), 360.9 (I)
Si	390.5(I), 288.1 (I)
Zn	330.3 (I), 472.2 (I)

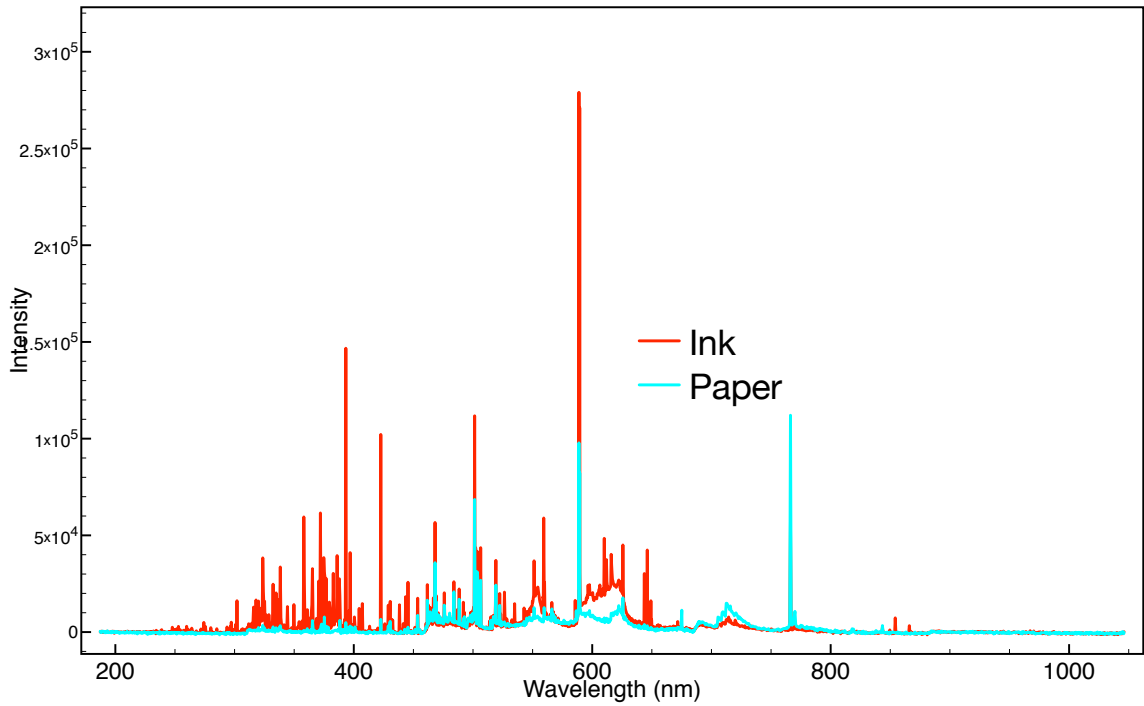


Figure 100. LIBS spectra for ink and paper.

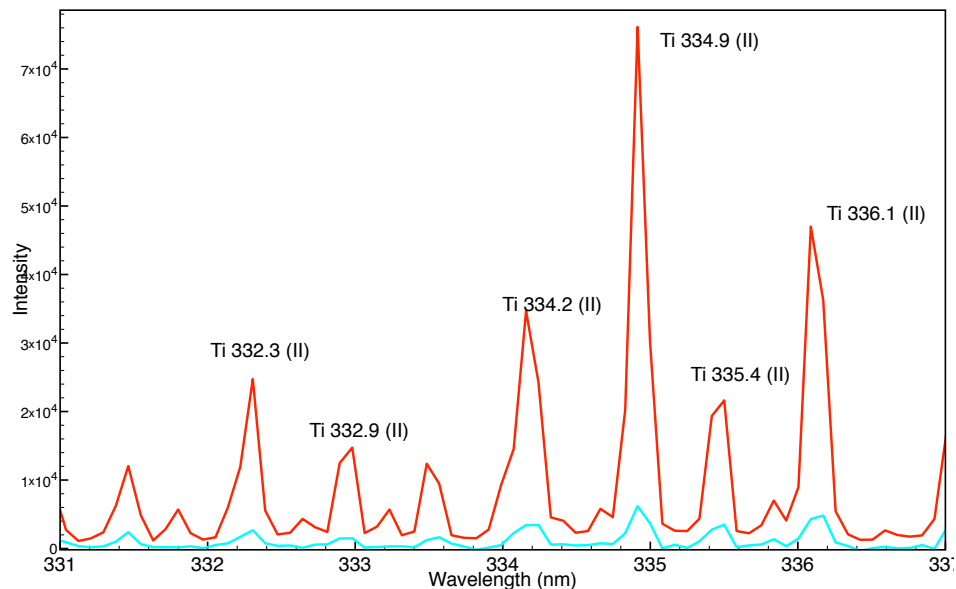


Figure 101. Multiple Ti emission lines detected by LIBS in intaglio ink.

Most of the peaks in the LIBS spectrum were identified to be from Ca. The paper also contained Ca, but the relative intensity of Ca in the paper was very low as compared to the ink as shown in Figure 102.

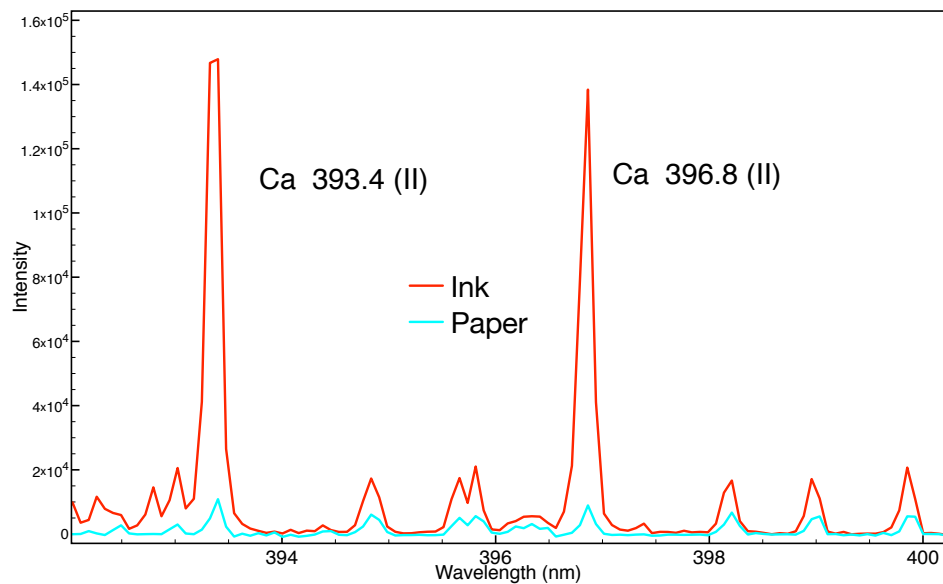


Figure 102. Ca emission lines detected in ink and paper by LIBS.

5.4 Conclusion

LIBS provided information about the major and minor elements present in ink. Some elements like K were also present in the paper. For the confirmation of the elements in inks, paper background cannot be ignored. For qualitative analysis, only those elements are considered which are at least three times higher than in the paper. Elements have multiple emission lines; hence, there are chances of overlapping of emission lines (interferences) from different elements. Only those lines that are free from interferences can be considered for comparison purposes. LIBS analysis of intaglio inks provided good information about the different kind of elements present in the inks and was used to create an elemental menu for LA-ICP-MS.

Chapter 6. Analysis of Printing Inks by Tandem LIBS/LA-ICP-MS and Normalization Study

Most of the contents in this chapter have already been published⁴¹ [<http://dx.doi.org/10.1016/j.sab.2014.11.011>]. The operating conditions for LIBS and LA-ICP-MS are different as they operate under different principles. They have to be optimized differently when operated in standalone mode in comparison to tandem mode. For example, the most important factor for LIBS is the efficient excitation of the atomic and ionic species and their subsequent correct timing for the optical collection of the emission lines; while for ICP-MS, the production of sub-micron sized particles with efficient particle transport to the ICP plays the most critical role. Also, the ionization of the particles in ICP depends on the particle size, as smaller particles ionize better than the large chunks. LIBS is also affected by the ambient gas environment, which determines the shape, size and life duration of the microplasma. The ideal conditions for tandem LIBS/LA-ICP-MS should result in long and stable microplasma for LIBS, with a fine and uniform aerosol travelling with uniform velocity to the ICP-plasma^{19,26}. When LIBS and LA-ICP-MS are operated in tandem mode, different instrumental conditions have to be optimized to achieve a balanced state with compromised analytical signals compared to their optimum signals when performed in standalone modes. LA-ICP-MS has sensitivity that is at least one order of magnitude higher than LIBS, so the approach was to first optimize the acquisition parameters for LIBS and then re-optimize the parameters for the tandem mode. This resulted in sacrificing some ICP-MS sensitivity to obtain

simultaneous information with considerable precision (less than 10% RSD for LIBS and less than 5% RSD for LA-ICP-MS).

6.1 Sample selection for Tandem LIBS/LA-ICP-MS Analysis

For each of the four printing ink types, the samples were chosen from the set of 319 inks. These pairs were selected because they exhibited a similar elemental profile when analyzed by standalone LA-ICP-MS. This subset of inks consisted of 9 black toners, 10 inkjets, 13 offsets, and 12 intaglio printing inks as shown in Figure 103.

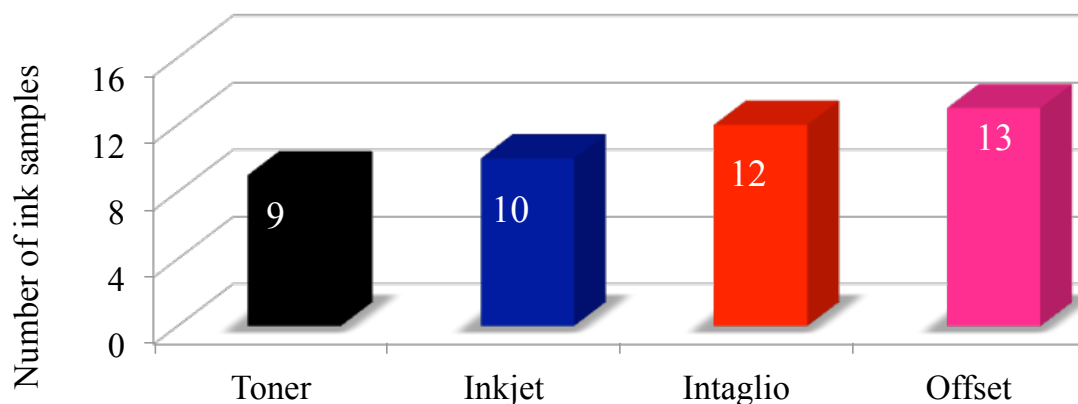


Figure 103. Bar graph showing the distribution of four printing inks for the tandem LIBS/LA-ICP-MS study.

6.2 Analysis of toner printing inks by tandem LIBS/LA-ICP-MS

Nine black toners out of 77 toners were selected for the tandem analysis. All these pairs had the same set of elements and were of the same concentration. Table 32 shows the list of all the toner printing inks included in this subset for tandem LIBS/LA-ICP-MS study. Standalone LA-ICP-MS was able to detect only Mn and Fe in eight of these toners (~89%), while in one of the pairs, only Ti, Zr, Nb, Sn, and Hf was detected. Five of the samples were from HP brand. Two of the toners belonged to RC brand while there was

one toner each from TS and SH brand as shown in table 34. Table 35 shows the list of the toner pairs that had a very similar LA-ICP-MS elemental profile. Ten of the indistinguishable pairs had a common HP brand.

Table 34. List of toner pairs used for the tandem LIBS/LA-ICP-MS study.

Toners	Brand
TN12	HP
TN13	HP
TN17	HP
TN18	HP
TN19	HP
TN52	RC
TN53	RC
TN57	TS
TN77	SH

Table 35. List of toner pairs that were indistinguishable by LA-ICP-MS.

Indistinguishable	Elements detected by LA-ICP-MS	Source (Brand)
TN 12 and TN 13	Mn, Fe	HP
TN 12 and TN 17	Mn, Fe	HP
TN 12 and TN 18	Mn, Fe	HP
TN 12 and TN 19	Mn, Fe	HP
TN 12 and TN 77	Mn, Fe	HP and SH
TN 13 and TN 17	Mn, Fe	HP
TN 13 and TN 18	Mn, Fe	HP
TN 13 and TN 19	Mn, Fe	HP
TN 17 and TN 18	Mn, Fe	HP
TN 17 and TN 19	Mn, Fe	HP
TN 18 and TN 19	Mn, Fe	HP
TN 52 and TN 53	Ti, Zr, Nb, Sn, Hf	RC

6.2.1 Optimization of Tandem LIBS/LA-ICP-MS for the Analysis of Toners

The parameters measured for the optimization of tandem LIBS/LA-ICP-MS were signal intensity, signal to noise ratio (S/N), precision (%RSD) and the extent of paper damage. It is desired to use maximum laser energy to ablate the ink off the paper with minimal destruction to the paper substrate. With the increase in the laser energy, the signal intensity also increased, but it also increased the paper contribution as shown in figure 97. A variation of laser energy starting from 10% to 80% was studied. With laser energy lower than 20%, background noise dominated the spectrum, in addition to suppression of peaks at lower wavelength. The laser energy that was optimum for toners was found to be 70% (37.6 J/cm²). A 200µm laser spot size was chosen to account for any sample heterogeneity. Table 36 shows the list of optimized parameters for the analysis of toners by tandem LIBS/LA-ICP-MS⁴¹.

Table 36. Optimized parameters for the analysis of toners by tandem LIBS/LA-ICP-MS.

Parameters	Toners
Ablation mode	Single line
Laser spot size	200 µm
Frequency	1.8Hz
Laser energy	70% (13mJ)
Ablation rate	40µm/s
Gate Delay	0.8µs
Argon flow in the cell	0.6L/min

6.2.2 Results from the Tandem LIBS/LA-ICP-MS Analysis of Toners

The data normalization for LA-ICP-MS was done by dividing the intensity of each element by the total sum of the peaks of the elements in the spectrum as described in Chapter 4.1. LA-ICP-MS with a quadrupole mass analyzer suffers from isobaric and polyatomic interferences. The detection of Ca in toners is difficult because of the isobaric interference from Argon at mass 40 (^{40}Ar) and the presence of polyatomic interferences, such as $^{39}\text{Ar}^1\text{H}$, formed in the ICP. Less abundant isotopes like ^{44}Ca (2.1% abundance) are difficult to detect at lower concentrations. Similarly, ^{28}Si has a major interference from $^{14}\text{N}^{14}\text{N}$. Therefore, this isotope had to be avoided and the less abundant isotope ^{29}Si (4.7% abundance) had to be monitored during the analysis in the mass spectrum. Multiple emission lines for these elements (Ca and Si) were detected by LIBS with very few interference in the emission spectrum. Tandem LIBS/LA-ICP-MS analysis of toners provided valuable information about Ca, Si and Na as well. Na proved to be a good emitter in LIBS and could be detected in most of the toner inks. Figure 104 shows the detection of Si in one of the pairs that was indistinguishable by standalone LA-ICP-MS.

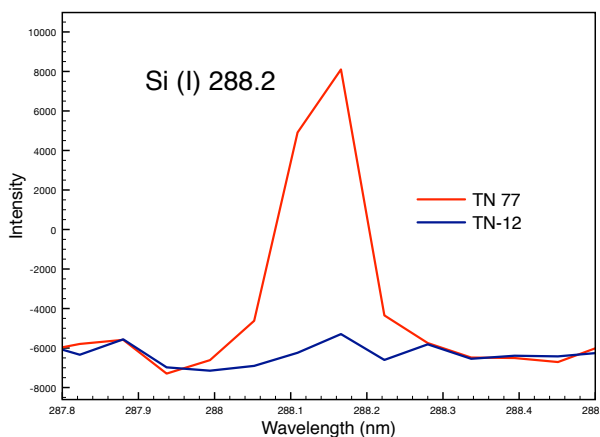


Figure 104. Si peaks for TN 12 and TN 77 detected in LIBS spectrum⁴¹.

LA-ICP-MS was able to detect more elements than LIBS because of the its sensitivity. Table 37 lists all the elements that were detected by LA-ICP-MS and LIBS when performed in tandem mode. The additional elements detected by LIBS are in bold.

Table 37. List of elements detected in toners by LA-ICP-MS and LIBS in tandem mode⁴¹.

Toners	Brand	Elements detected by LA-ICP-MS	Elements detected by LIBS
TN12	HP	Na, Mg, Fe, Mn, Zn, Sr, Ba	Na, Ca, K, Fe
TN13	HP	Mn, Fe	Na, Ca
TN17	HP	Mn, Fe	Na, K, Fe, Mn
TN18	HP	Mn, Fe	Na, Ca, K
TN19	HP	Mn, Fe	Na, Ca
TN52	RC	Ti, Zr, Nb, Sn, Hf	Na, K, Ca, Ti,
TN53	RC	Ti, Zr, Nb, Sn, Hf	Na, Si, Ti, Ca
TN57	TS	Ti, Sr, Zr, Sn, Hf	Na, Si, K, Ca, Ti
TN77	SH	Mn, Fe	Na, Si, Ca, Mn, Fe

Similarly, Ca and K were also detected in most of the pairs. Silicon was detected in two of the toner pairs and provided additional discrimination for these pairs. The presence of additional elements in LIBS spectrum was confirmed on the basis of detection of more than two emission lines for that element. Table 35 shows the list of additional elements detected by LIBS that contributed in discrimination of those indistinguishable pairs.

6.2.3.3 Multivariate Analysis of the Tandem LIBS/LA-ICP-MS data for Toners

The multivariate analysis of toners was performed using PCA, LDA and cluster analysis. The performance of LIBS, the performance of LA-ICP-MS and their fusion are analyzed independently and compared.

6.2.3.1 Principal Component Analysis of Toners by LA-ICP-MS Spectrum

The application of PCA to the integrated areas of different elements detected in ink resulted in classification of the inks. Figure 105 and Figure 106 show the two-dimensional and three-dimensional PCA plots for toners using the data from LA-ICP-MS only. The first three Principal Components explained a total of 80.2% of variance, as shown in Table 38.

Table 38. Variances explained by the first three Principal Components.

Principal Components	PC1	PC2	PC3	Cumulative
Variance Explained	42.7%	29.3%	8.3%	80.3%

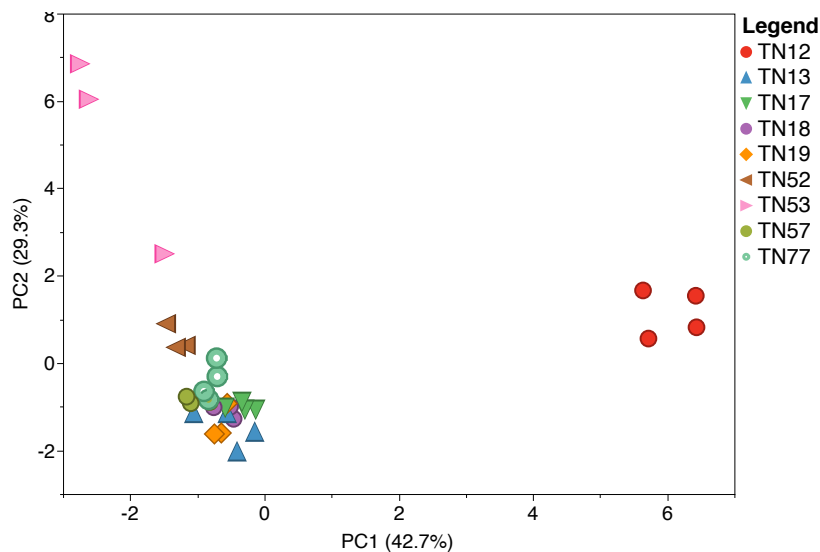


Figure 105. Two-dimensional PCA plot for toners from data obtained by LA-ICP-MS.

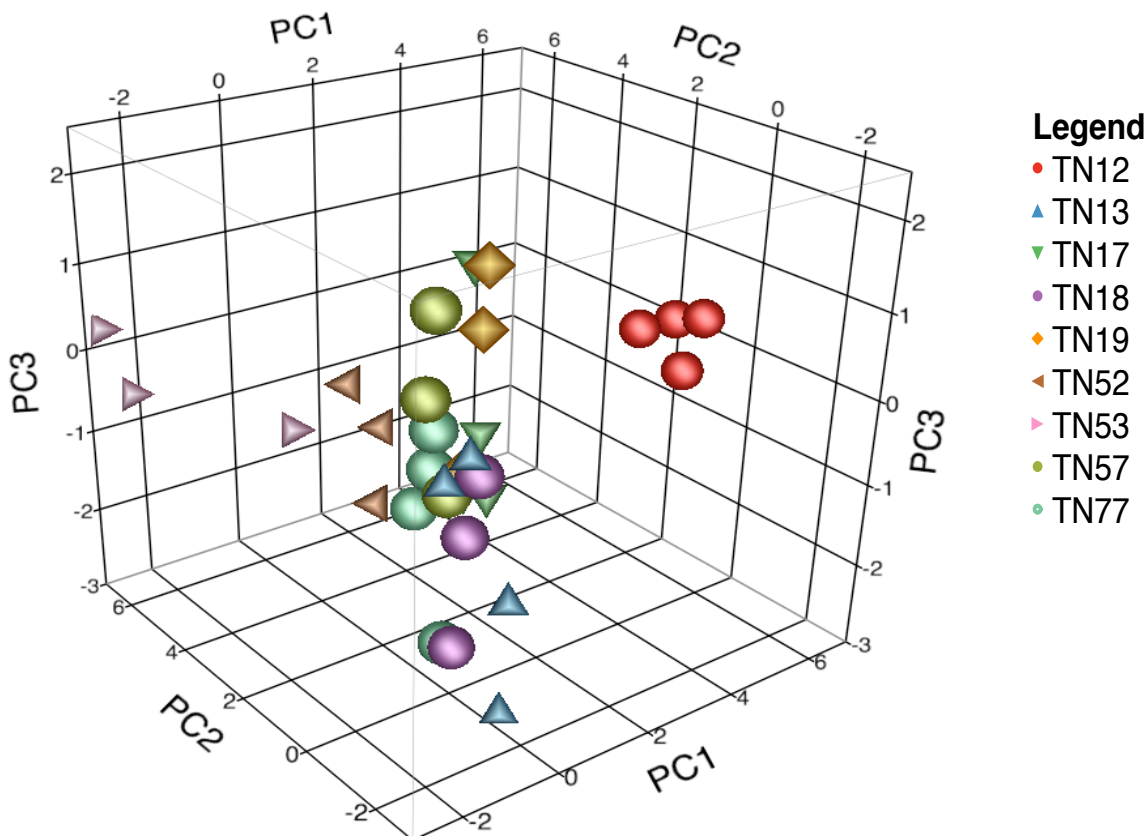


Figure 106. Three-dimensional PCA plot using data obtained from LA-ICP-MS.

6.2.3.2 Principal Component Analysis of Toners by LIBS Spectrum

A fewer elements were detected by LIBS as compared to LA-ICP-MS. The peak area of these detected elements were integrated and used as variables for PCA. The first three Principal Components explained a total of 70.9% variance, which is less than that obtained from LA-ICP-MS. Table 39 lists the percentage of variance explained by each of the first three Principal Components. Figure 107 and Figure 108 show the two-dimensional and three-dimensional PCA plots for toners using LIBS spectrum.

Table 39. Variances explained by the first three PCs (LIBS).

Principal Components	PC1	PC2	PC3	Cumulative
Variance Explained	35.6	23.1	12.2	70.9

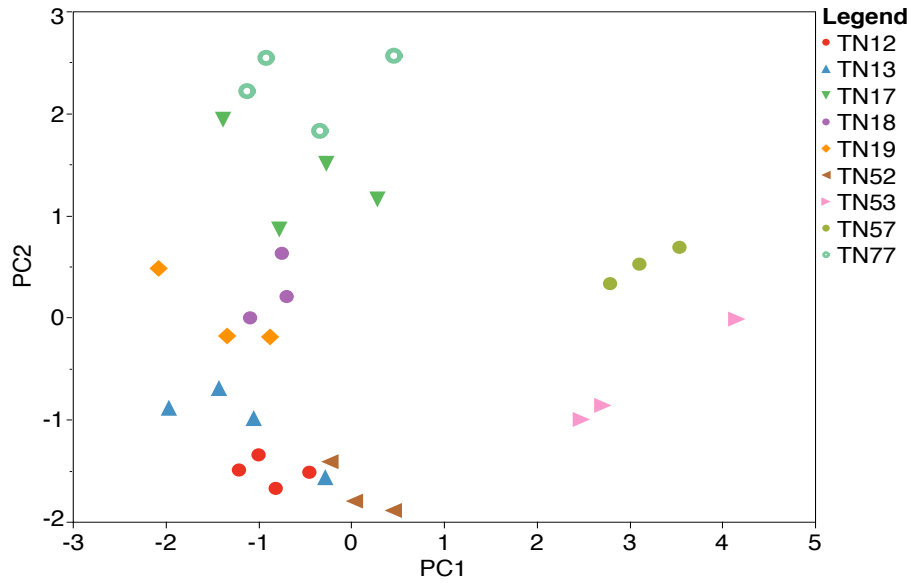


Figure 107. Two-dimensional PCA plot for toners using data obtained from LIBS.

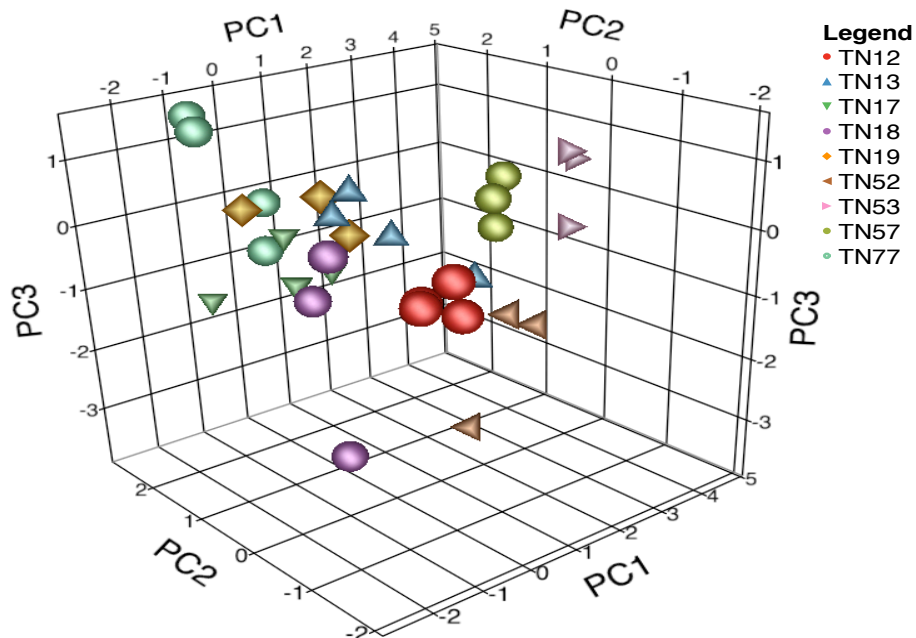


Figure 108. Three-dimensional PCA plot for toners obtained by using LA-ICP-MS data.

6.2.3.3 Principal Component Analysis of Toners by the Fusion of LIBS and LA-ICP-MS Spectrum

The fusion of LIBS and LA-ICP-MS provided some additional discrimination and better classification. Because of the correlation between some of the variables in LIBS and LA-ICP-MS the total percentage of variance explained by the Principal Components did not significantly increase. Replicates of same toner inks are grouped together as shown by the ellipses in Figure 109. Figure 109 and Figure 110 show the two-dimensional and three-dimensional PCA plots for toners after the data fusion of LIBS and LA-ICP-MS. The first three PCs explained 70.1% of the total variance as shown in Table 40.

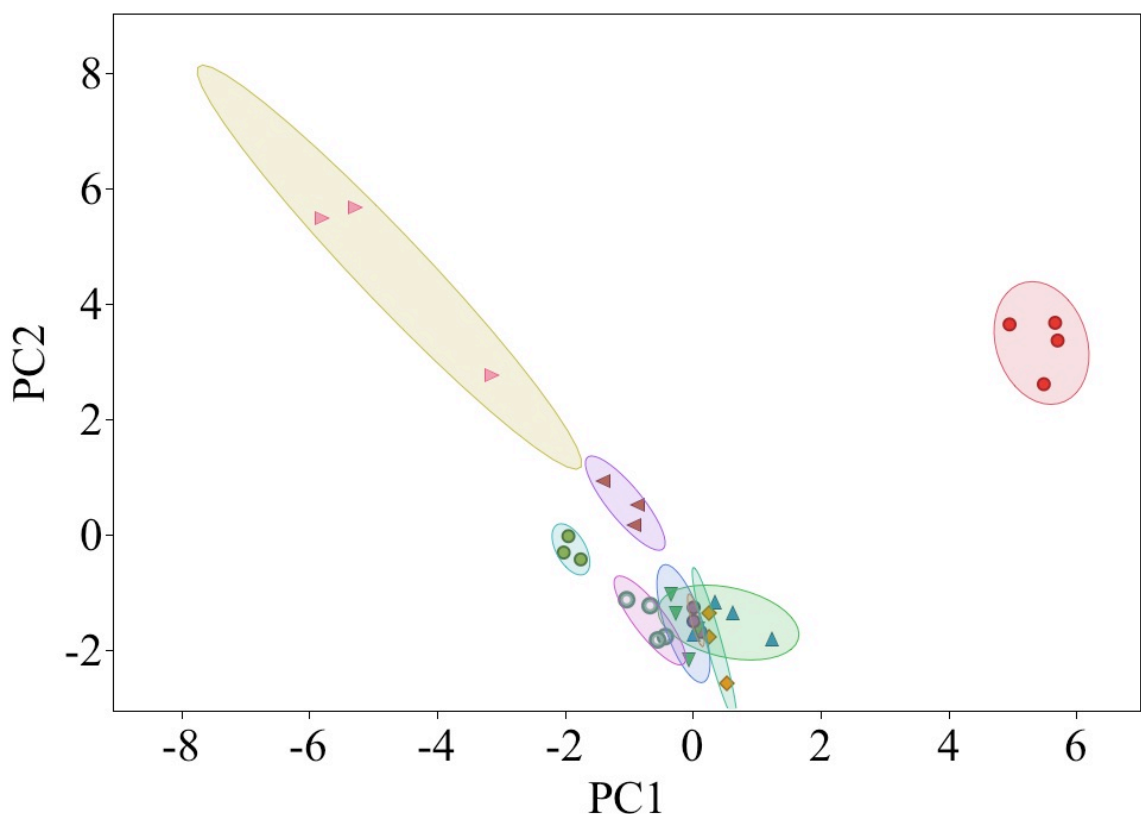


Figure 109. Two-dimensional PCA plot for toners after fusion of LIBS and LA-ICP-MS.

Table 40. Variances from the first three PCs after the fusion of LIBS and LA-ICP-MS.

Principal Components	PC1	PC2	PC3	Cumulative
Variance Explained	28.9	23.5	17.7	70.1

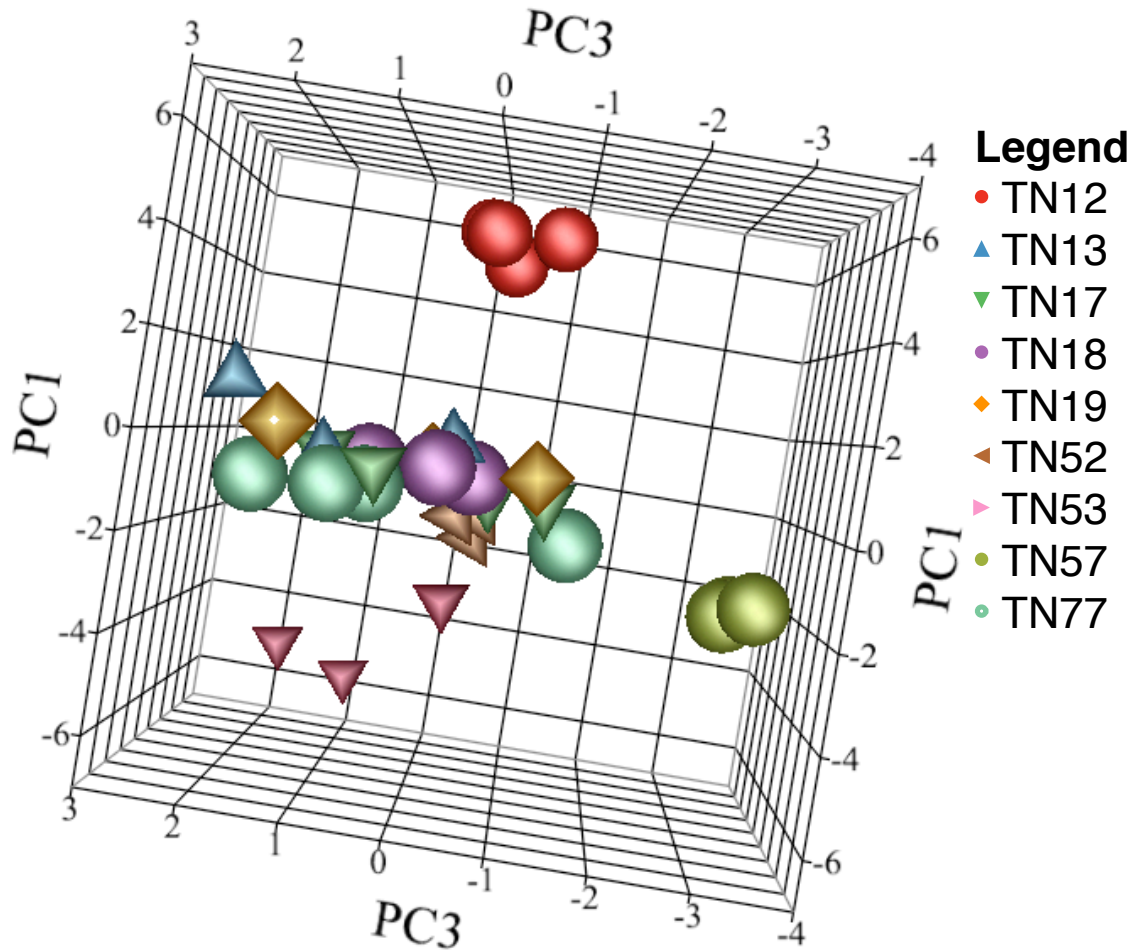


Figure 110. Three-dimensional PCA plot obtained after the fusion of LIBS and LA-ICP-MS.

6.2.3.4 Linear Discriminant Analysis of Toners by LIBS

LIBS provided an excellent discrimination for toner samples. Only one of the pairs was not correctly classified. Table 41 is a confusion matrix showing the correct classification

(35 pairs) and 1 misclassification of toners. The pair that was incorrectly classified by LDA is shown in Table 42.

Table 41. Confusion matrix obtained from LDA of toners using LIBS only

Toners	TN12	TN13	TN17	TN18	TN19	TN52	TN53	TN57	TN77
TN12	4	0	0	0	0	0	0	0	0
TN13	1	3	0	0	0	0	0	0	0
TN17	0	0	4	0	0	0	0	0	0
TN18	0	0	0	3	0	0	0	0	0
TN19	0	0	0	0	3	0	0	0	0
TN52	0	0	0	0	0	3	0	0	0
TN53	0	0	0	0	0	0	3	0	0
TN57	0	0	0	0	0	0	0	3	0
TN77	0	0	0	0	0	0	0	0	4

Table 42. Misclassified toner pair by LDA using data from LIBS.

Misclassified/Indistinguishable Pairs	Color	Brand
12TN vs. 13TN	Black	HP

The same toner pair was also indistinguishable by Spectral Overlay using standalone LA-ICP-MS. They were of same color and also from the same brand as listed in Table 42.

6.2.3.5 Linear Discriminant Analysis of Toners by LA-ICP-MS

Linear Discriminant Analysis of toners using LA-ICP-MS also provided an excellent discrimination. Only one pair was misclassified out of possible 36 possible combinations. Table 43 is a confusion matrix that shows the correctly classified pairs and the incorrectly classified pair. The toner pair that was incorrectly classified is listed in Table 44. Toner 13 and toner 18 were both black and belonged to same HP brand. This pair was also indistinguishable by Spectral Overlay using standalone LA-ICP-MS.

Table 43. Confusion matrix from LDA for toners using LA-ICP-MS only.

Row	TN12	TN13	TN17	TN18	TN19	TN52	TN53	TN57	TN77
TN12	4	0	0	0	0	0	0	0	0
TN13	0	3	0	1	0	0	0	0	0
TN17	0	0	4	0	0	0	0	0	0
TN18	0	0	0	3	0	0	0	0	0
TN19	0	0	0	0	3	0	0	0	0
TN52	0	0	0	0	0	3	0	0	0
TN53	0	0	0	0	0	0	3	0	0
TN57	0	0	0	0	0	0	0	3	0
TN77	0	0	0	0	0	0	0	0	4

Table 44. Misclassified toner pair by LDA using data from LA-ICP-MS only.

Misclassified/Indistinguishable Pairs	Color	Brand
0013TN vs. 0018TN	Black	HP

6.2.3.6 Linear Discriminant Analysis of Toners by the Fusion of LIBS and LA-ICP-MS

The fusion of LIBS and LA-ICP-MS provided a 100% correct discrimination of toner printing inks. Table 45 is the confusion matrix showing the correct classification of all nine toner inks.

Table 45. Confusion matrix from LDA for toners after fusion of LIBS and LA-ICP-MS.

Toners	TN12	TN13	TN17	TN18	TN19	TN52	TN53	TN57	TN77
TN12	4	0	0	0	0	0	0	0	0
TN13	0	4	0	0	0	0	0	0	0
TN17	0	0	4	0	0	0	0	0	0
TN18	0	0	0	3	0	0	0	0	0
TN19	0	0	0	0	3	0	0	0	0
TN52	0	0	0	0	0	3	0	0	0
TN53	0	0	0	0	0	0	3	0	0
TN57	0	0	0	0	0	0	0	3	0
TN77	0	0	0	0	0	0	0	0	4

6.2.3.7 Canonical Discriminant Analysis of Toners by Tandem LIBS/LA-ICP-MS

Canonical Discriminant Analysis produces Canonical Components that provides maximum separation among different groups. Figure 111 shows the two-dimensional Canonical plot obtained using LIBS, LA-ICP-MS and the fusion of LIBS and LA-ICP-MS. The fusion of LIBS and LA-ICP-MS provided clear separation of groups as shown in Figure 111 and Figure 112. The replicates of the same ink are clustered together while the separation between different ink groups is maximized.

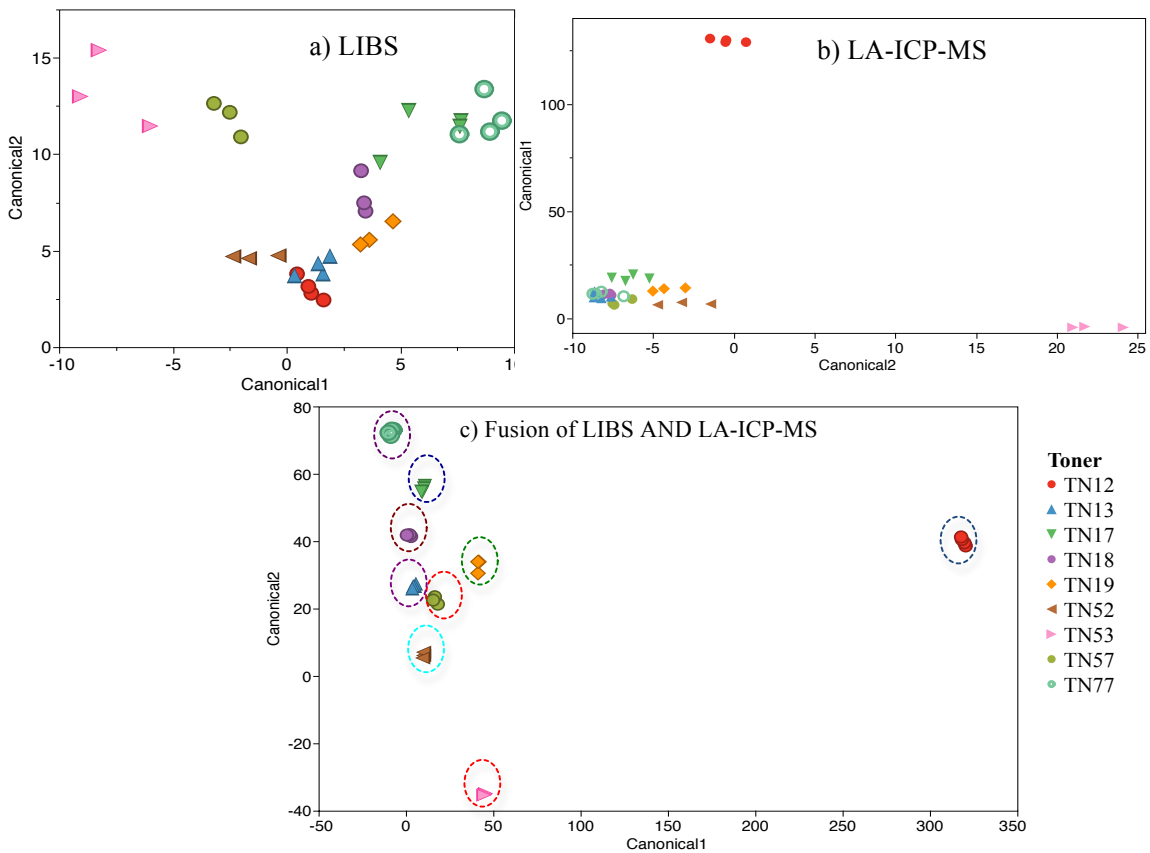


Figure 111. Canonical plots for toners using a) LIBS b) LA-ICP-MS and c) fusion of LIBS and LA-ICP-MS.

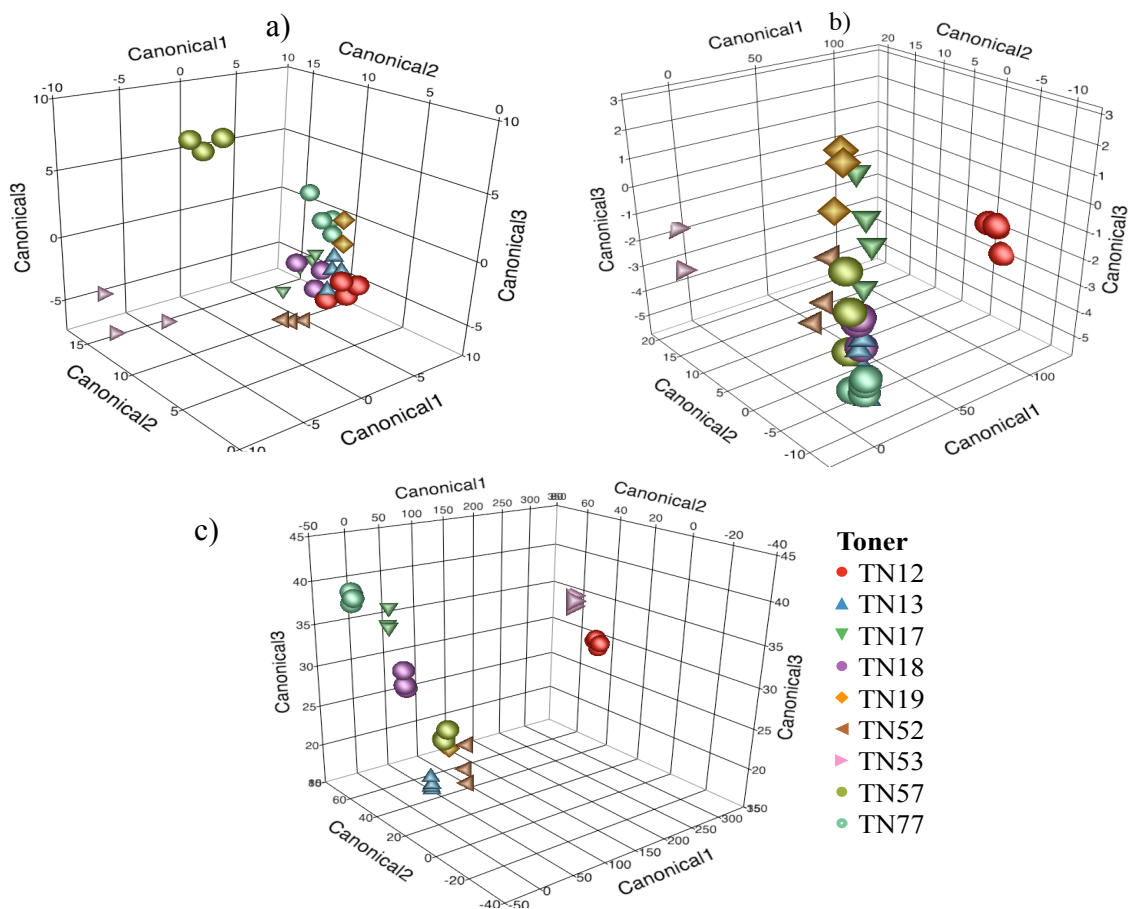


Figure 112. Three-dimensional Canonical Plot for toners using a) LIBS b) LA-ICP-MS, c) fusion of LIBS and LA-ICP-MS.

6.2.3.8 Cluster Analysis of Toners by Tandem LIBS/LA-ICP-MS

Cluster Analysis helps to visualize which pairs are similar and which pairs are different. It clusters the similar inks together while separating them from different inks. Figure 113 is a Hierarchical Cluster Analysis plot for toners using LIBS, LA-ICP-MS and fusion of LIBS and LA-ICP-MS. This plot shows that the fusion has grouped the replicates of the same ink together. The same color in the cluster shows correct association and different colors in the same cluster means that there is some misclassification or incorrect association. For example, TN 13 in LIBS (a) is very similar

to TN 18 and TN 19 while it looks similar to TN 18, TN 19, 57,77 in LA-ICP-MS (b), the fusion clusters all the four replicates to one group which is close to TN 18 and 19 only.

Toner 13, 18 and 19 are all from the same HP manufacturer.

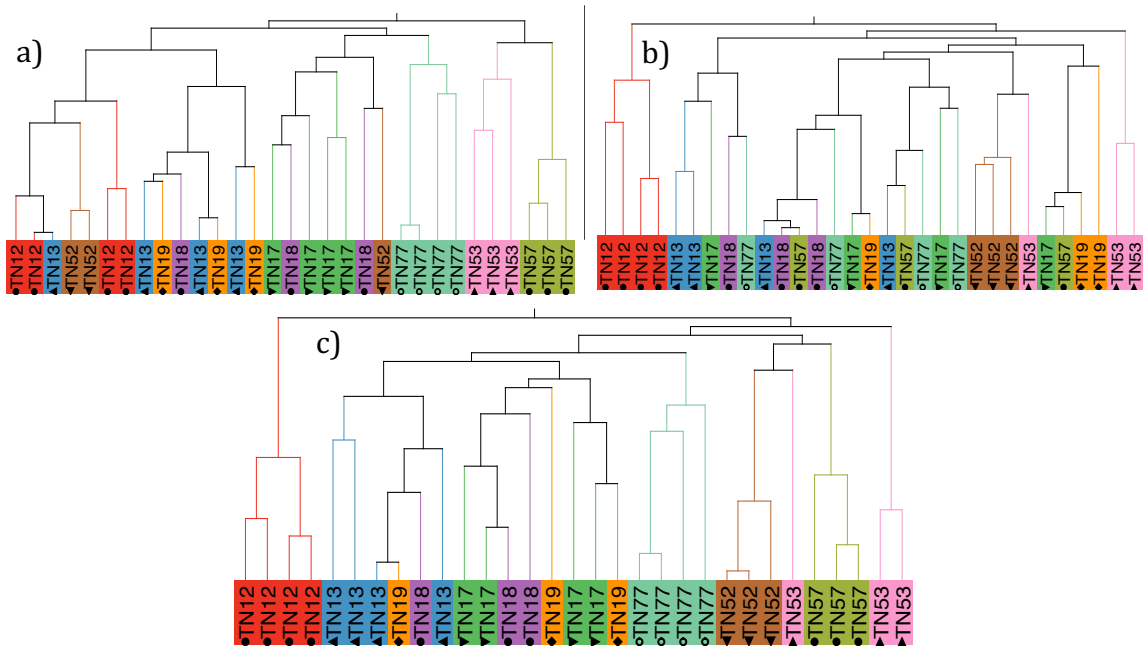


Figure 113. Hierarchical cluster Analysis for toners using a) LIBS b) LA-ICP-MS c) Fusion of LIBS and LA-ICP-MS.

Another way of presenting the clusters is using the constellation plot. The ink samples are arranged as the endpoints. The lines drawn from the points represent the proximity between different clusters. Shorter lines show smaller differences while longer lines show greater variation between the samples. Figure 114 shows the constellation plot for toners for LIBS, LA-ICP-MS and the fusion of LIBS and LA-ICP-MS.

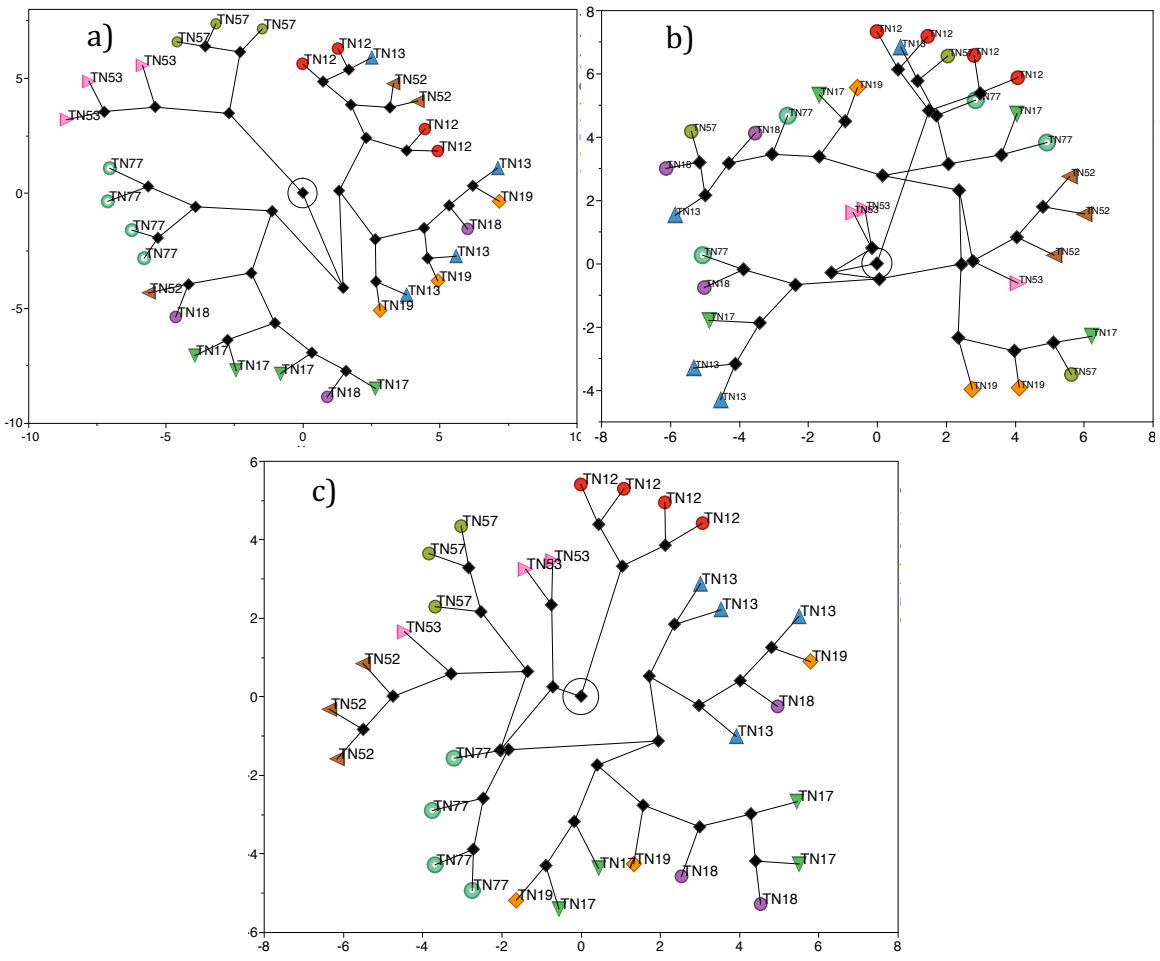


Figure 114. Constellation plot for toners using a) LIBS b) LA-ICP-MS and c) fusion of LIBS and LA-ICP-MS.

6.3 Analysis of Inkjet Printing Inks by Tandem LIBS/LA-ICP-MS

Ten inkjets of four different colors (CMYK) belonging to six different brands were used for the tandem study. Out of these 45 possible pairs, 4 pairs were not distinguishable by standalone LA-ICP-MS. Table 46 shows the list of inkjet inks used for the tandem LIBS/LA-ICP-MS study.

Table 46. List of inkjet printing inks used for the tandem LIBS/LA-ICP-MS study.

Inkjet	Brand	Color
IN 01	BR	Black
IN 04	CN	Yellow
IN 05	CN	Magenta
IN 09	EP	Magenta
IN 10	EP	Yellow
IN 40	HP	Cyan
IN 56	KD	Black
IN 57	KD	Black
IN 66	BR	Cyan
IN 70	SH	Cyan

The four pairs of inkjet printing inks, which were indistinguishable by standalone LA-ICP-MS, are listed in Table 47.

Table 47. List of indistinguishable inkjet pairs when analyzed by standalone LA-ICP-MS.

Indistinguishable pairs (LA-ICP-MS)	Source	Color
IN 4 and IN 9	CN vs. EP	Yellow vs. Magenta
IN 4 and IN 10	CN vs. EP	Yellow
IN 9 and IN 10	EP	Magenta vs. Yellow
IN 56 and IN 57	KD	Black

6.3.1 Optimization of Tandem LIBS/LA-ICP-MS for the Analysis of Inkjets

Inkjet printing inks were challenging to analyze by laser ablation due to their relative thin layer embedded onto the paper fibers. Different laser parameters in addition to the carrier gas flow, gate delay and scanning speed, were optimized. Relatively lower laser energy (40%) was used for inkjet inks. Table 48 summarizes the optimized parameters for the analysis of inkjet samples by tandem LIBS/LA-ICP-MS.

Table 48. Optimized parameters for the analysis of inkjets by tandem LIBS-LA-ICP-MS.

Parameters	Inkjets
Ablation mode	Single line
Laser spot size	200 μm
Frequency	0.8Hz
Laser energy	40% (7.8mJ)
Ablation rate	50 $\mu\text{m/s}$
Gate Delay	0.1 μs
Argon flow in the cell	0.9L/min

6.3.2 Results for the Tandem LIBS/LA-ICP-MS Analysis of Inkjets

Elements like Ca and K were detected by LIBS in inkjet inks. These elements are difficult to detect by a quadrupole ICP-MS due to the isobaric and polyatomic interferences formed inside the ICP. Figure 115 shows the detection of K emission lines in an inkjet sample (IJ 9) while being absent in IJ 10, and thus providing additional discrimination.

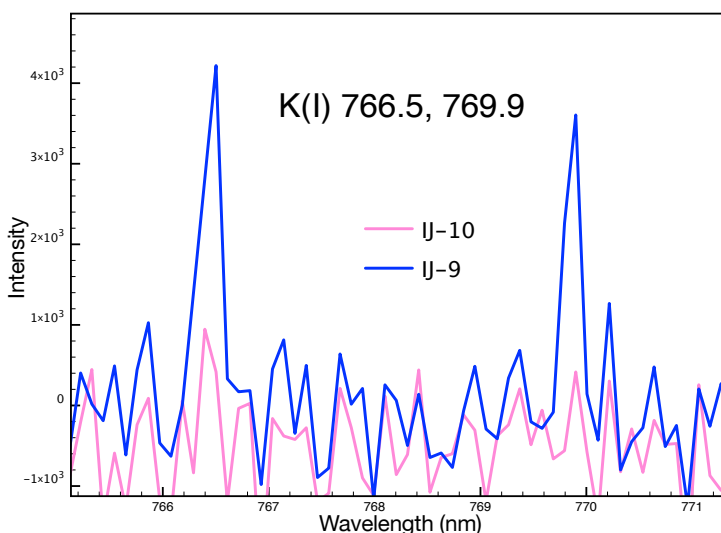


Figure 115. K peaks for IJ 9 and IJ 10 detected by LIBS⁴¹.

Sodium was detected in all of these inkjet inks by LA-ICP-MS, while Li was detected in only one of the inkjet printing inks. Additional elements detected by LIBS were K, and Ca as shown in bold in Table 49.

Table 49. List of elements detected by LIBS and LA-ICP-MS in inkjets in tandem mode.

Inkjet	Brand	Color	Elements detected	Elements detected
IN 01	BR	Black	Li, Na, K	Li, Na, K
IN 04	CN	Yellow	Na	Na, Ca
IN 05	CN	Magenta	Na	Na, Ca, K
IN 09	EP	Magenta	Na	Na
IN 10	EP	Yellow	Na	Na
IN 40	HP	Cyan	Na, Cu, S	Na
IN 56	KD	Black	Na, Al, K	Na, K
IN 57	KD	Black	Na, Al, K	Na, K
IN 66	BR	Cyan	Na, S, Cu	Na, K, Cu
IN 70	SH	Cyan	Na, S, Cu	Na, K, Cu

Four pairs of inks were indistinguishable when analyzed by LA-ICP-MS alone. For these pairs, LIBS provided additional discrimination through the detection of elements like Ca and K.

6.3.3 Multivariate Analysis of the Tandem LIBS/LA-ICP-MS data for Inkjets

Principal Component Analysis (PCA) and Linear Discriminant Analysis were performed on the data obtained from LIBS and LA-ICP-MS. The detected elements in LIBS and LA-ICP-MS were integrated and combined for the multivariate analysis.

6.3.3.1 Principal Component Analysis of Inkjets by LA-ICP-MS

Only five elements were detected in this subset by LA-ICP-MS. Principal Component Analysis of inkjets using the five variables can be visualized through Figure

116 and Figure 117. The first three Principal Components were able to explain 74.4% of the total variance in this subset as listed in Table 50.

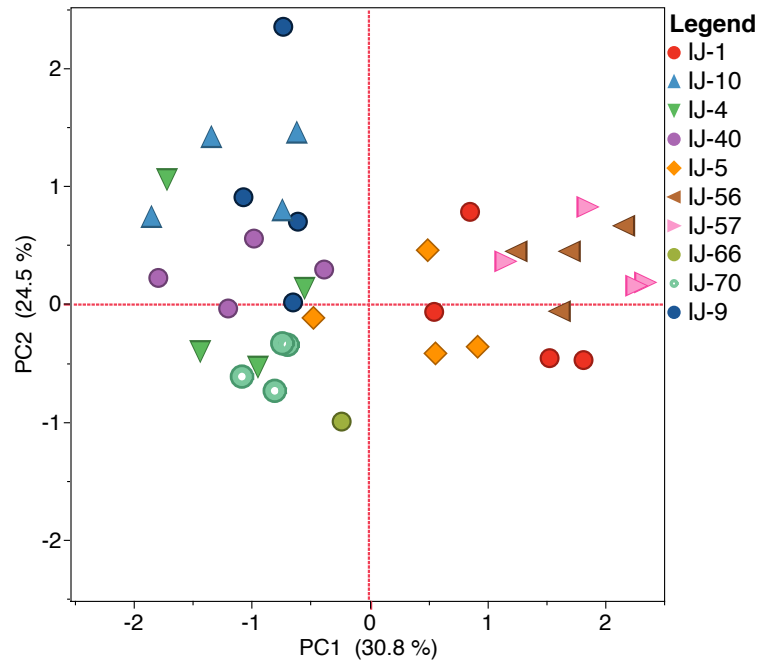


Figure 116. Two-dimensional PCA plot for inkjets by LA-ICP-MS.

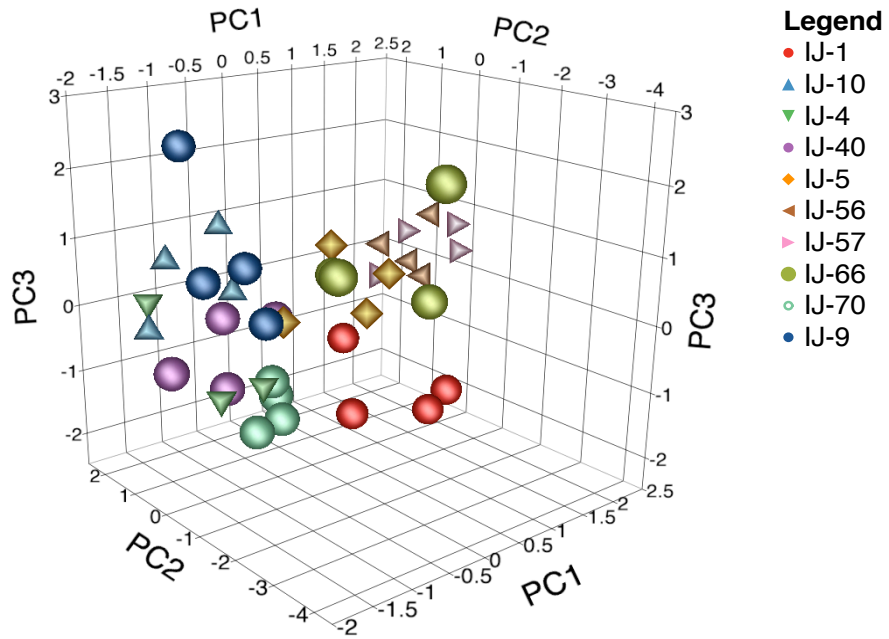


Figure 117. Three-dimensional PCA plot for inkjets by LA-ICP-MS.

Table 50. Variances explained by first three PCs using LA-ICP-MS.

Principal Components (PCs)	PC1	PC2	PC3	Cumulative
Variance explained	30.8%	24.5%	19.1%	74.4%

6.3.3.2 Principal Component Analysis of Inkjets by LIBS

Four elements were detected in inkjet printing inks using LIBS. The four variables Na, K, Ca, and Cu were used for the Principal Component Analysis. The classification can be visualized through 2d and 3d PCA plots in Figure 118 and Figure 119 respectively. The first three Principal Components explained 74.5% of the total variance for inkjets as shown in Table 51.

Table 51. Variances explained by the first three PCs.

Principal Components (PCs)	PC1	PC2	PC3	Cumulative
Variance explained	64.3%	19.9%	12.1%	96.3%

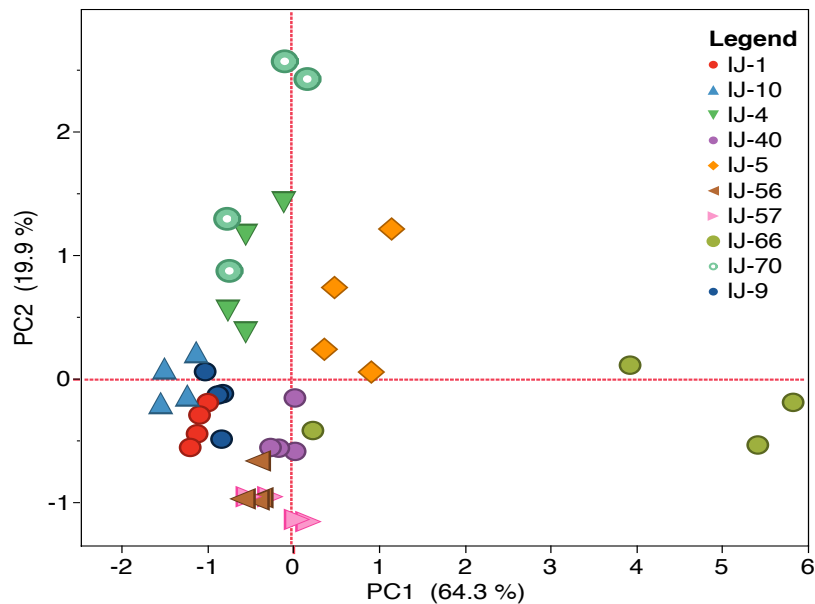


Figure 118. Two-dimensional PCA plot for inkjets using LIBS.

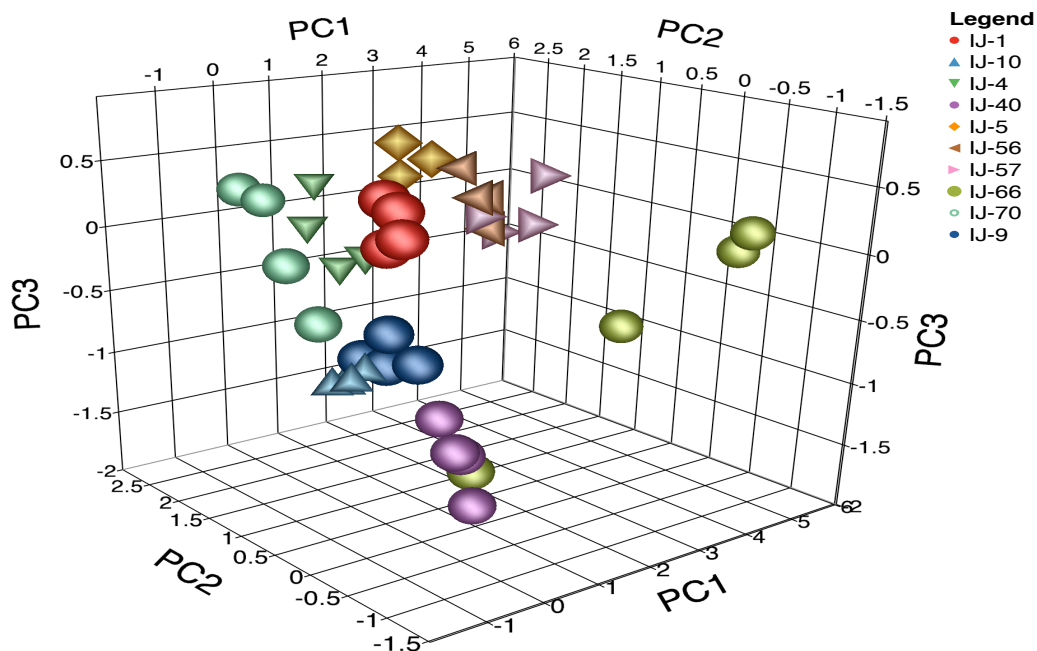


Figure 119. Three-dimensional PCA plot for inkjets using LIBS.

6.3.3.3 Principal Component Analysis of Inkjets by the Fusion of LIBS and LA-ICP-MS

The fusion of LIBS and LA-ICP-MS provided a distinct classification of inkjet inks. The pairs that had similar elemental composition were grouped together. For example, two inkjets 56 and 57 are clustered very close to each other as shown in Figure 120 and Figure 121. These two inks indistinguishable using the standalone LA-ICP-MS. Similarly, inkjet 9 and 10 are also clustered together which also have similar elemental profile. A total of nine elements (four from LIBS and five from LA-ICP-MS) were used for the PCA analysis. The first three Principal Components explained a total of 77.2% of the total variance as shown in Table 52.

Table 52. Variances explained by the first three PCs after the fusion of LIBS and LA-ICP-MS

Principal Components (PCs)	PC1	PC2	PC3	Cumulative variance
Variance explained	40.7%	22.3%	13.2%	77.2%

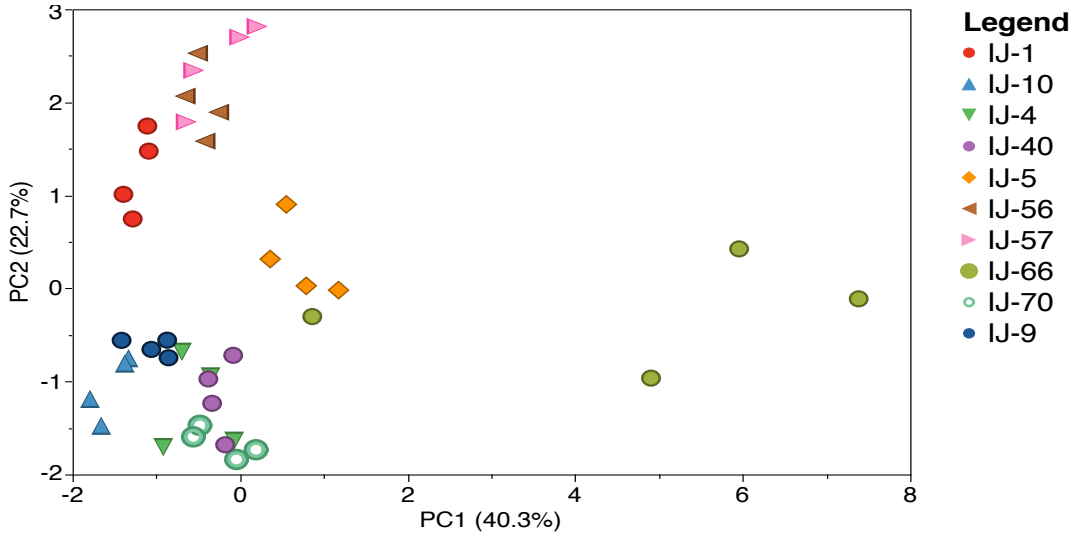


Figure 120. Two-dimensional PCA plot for inkjets from the fusion of LIBS and LA-ICP-MS.

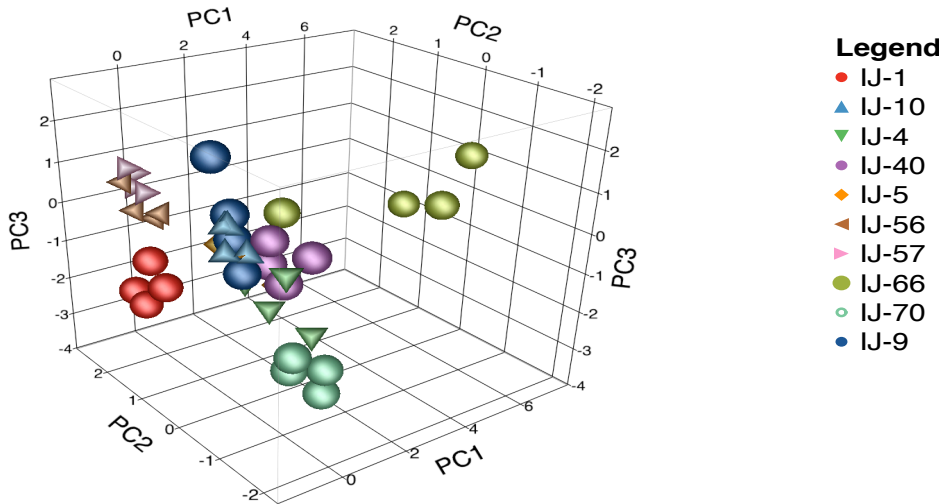


Figure 121. Three-dimensional PCA plot for inkjets from the fusion of LIBS and LA-ICP-MS.

6.3.3.4 Linear Discriminant Analysis of Inkjet Printing Inks by Tandem LIBS/LA-ICP-MS

The Linear Discriminant Analysis was first performed individually with LIBS and LA-ICP-MS, and compared to the fusion of LIBS and LA-ICP-MS.

6.3.3.4.1 Linear Discriminant Analysis using LA-ICP-MS for inkjets

Linear Discriminant Analysis with leave one out cross validation was performed on the data obtained from LIBS spectrum to separate the groups based on their discriminant functions. LDA correctly discriminated 39 pairs out of 45 pairs. This provided 86.7% correct discrimination as shown in Table 53. Linear Discriminant Analysis also provided canonical variables that best separated the groups. Figure 122 and Figure 123 provide the two-dimensional and three-dimensional canonical plots respectively showing the different groups for inkjets.

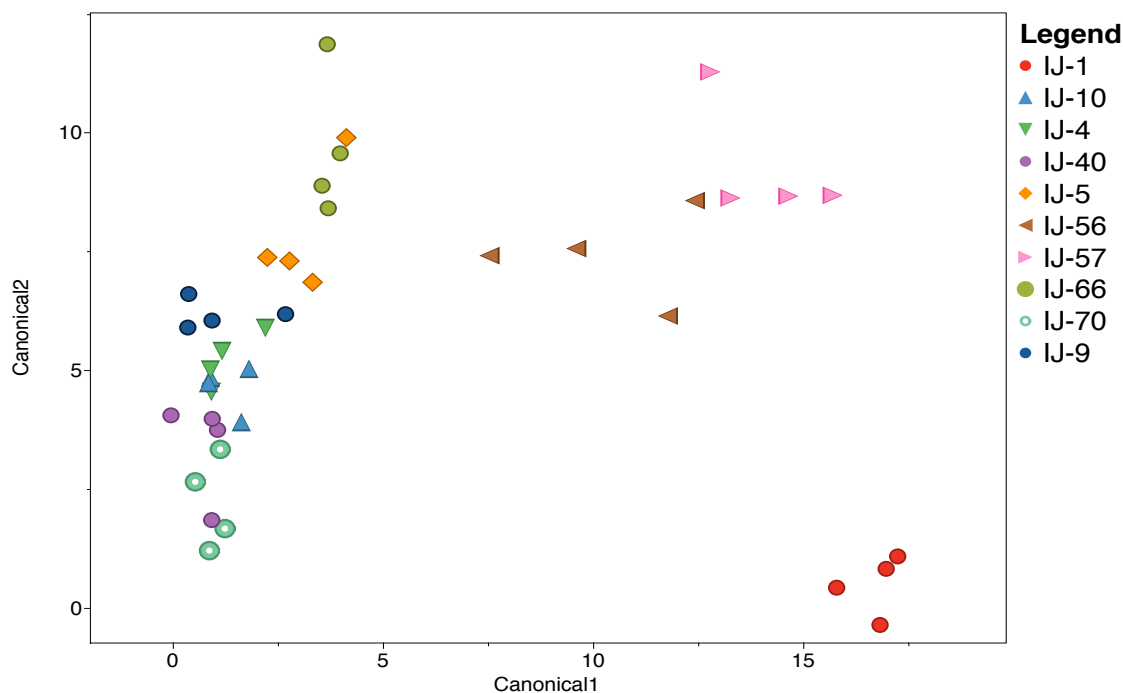


Figure 122. Two-dimensional Canonical Plot for inkjets from LA-ICP-MS data.

Table 53. Confusion matrix from LDA for inkjets using LA-ICP-MS.

INKJET	IJ-1	IJ-10	IJ-4	IJ-40	IJ-5	IJ-56	IJ-57	IJ-66	IJ-70	IJ-9
IJ-1	4									
IJ-10	0	3								
IJ-4	0	1	3							
IJ-40	0	0	0	3						
IJ-5	0	0	0	0	4					
IJ-56	0	0	0	0	0	4				
IJ-57	0	0	0	0	0	0	4			
IJ-66	0	0	0	0	1	0	0	3		
IJ-70	0	0	0	1	0	0	0	0	3	
IJ-9	0	0	1	0	0	0	0	0	0	3

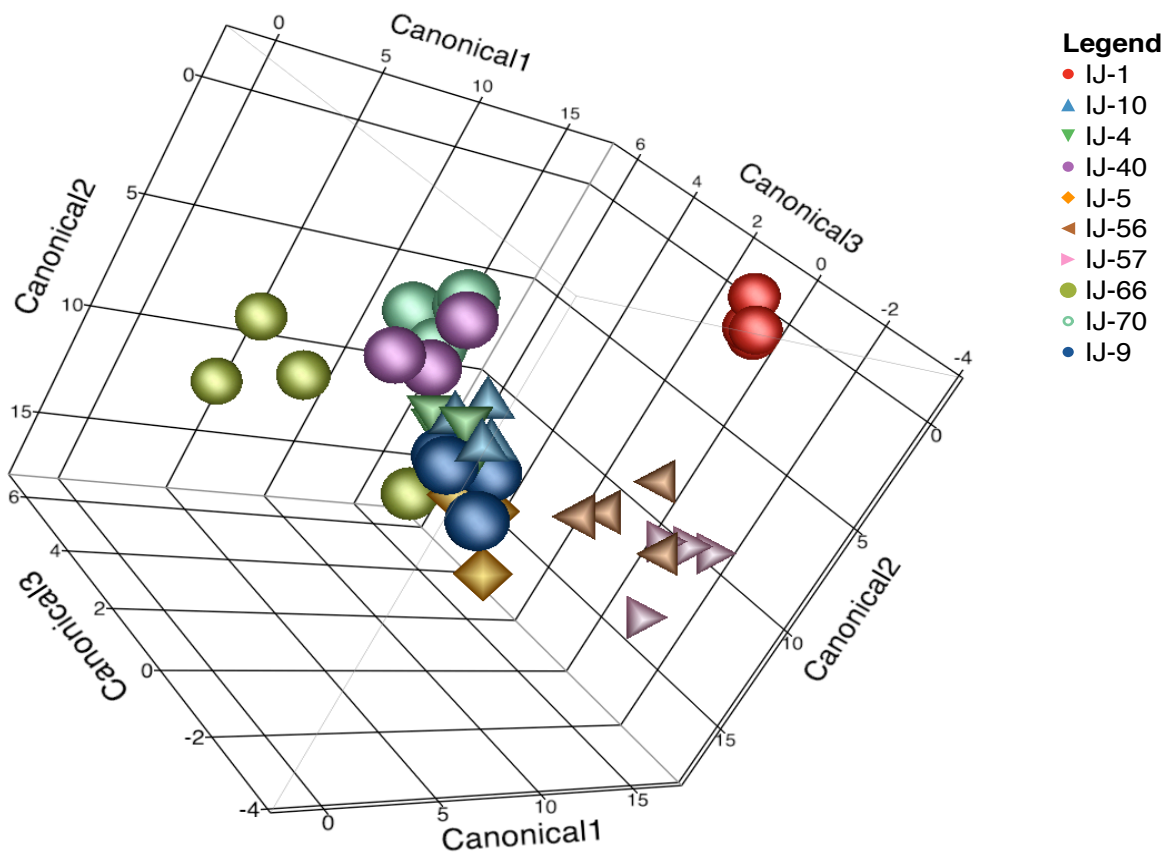


Figure 123. Three-dimensional Canonical plot for inkjets based on LA-ICP-MS spectrum.

6.3.3.4.2 Linear Discriminant Analysis Using LIBS for Inkjets

The elements detected by LIBS were used for the linear Discriminant Analysis. LDA using LIBS data only showed 8 misclassified pairs, resulting 82.3% correct discrimination of the inkjet pairs. Table 54 is the tabulated confusion matrix obtained after LDA using data from LIBS only.

The canonical plots shown in Figure 124 and Figure 125 show classification of 10 different inkjets. Inkjets with very similar elemental profile are grouped very close to each other. For example IJ 56 and IJ 57 can be seen to be very closely related as shown in Figure 124 and 125. Similarly IJ 1 is grouped separately from other inks.

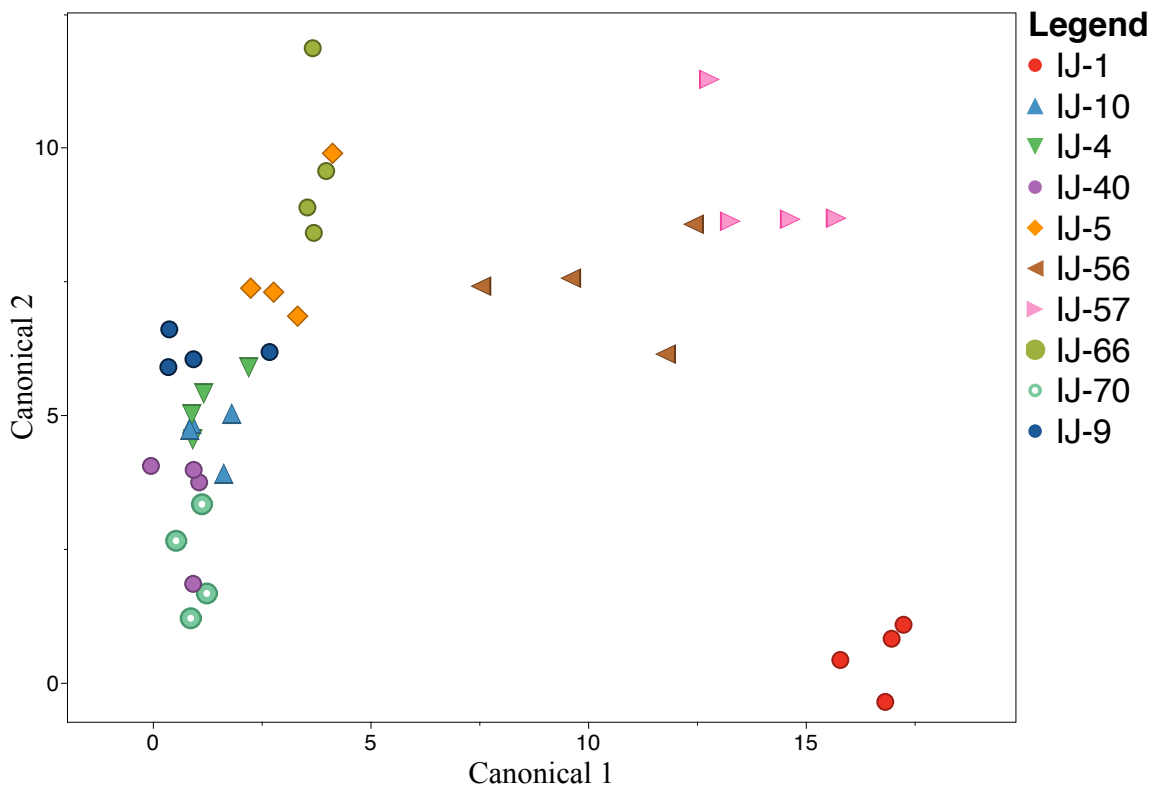


Figure 124. Two-dimensional PCA plot for inkjets using LIBS data.

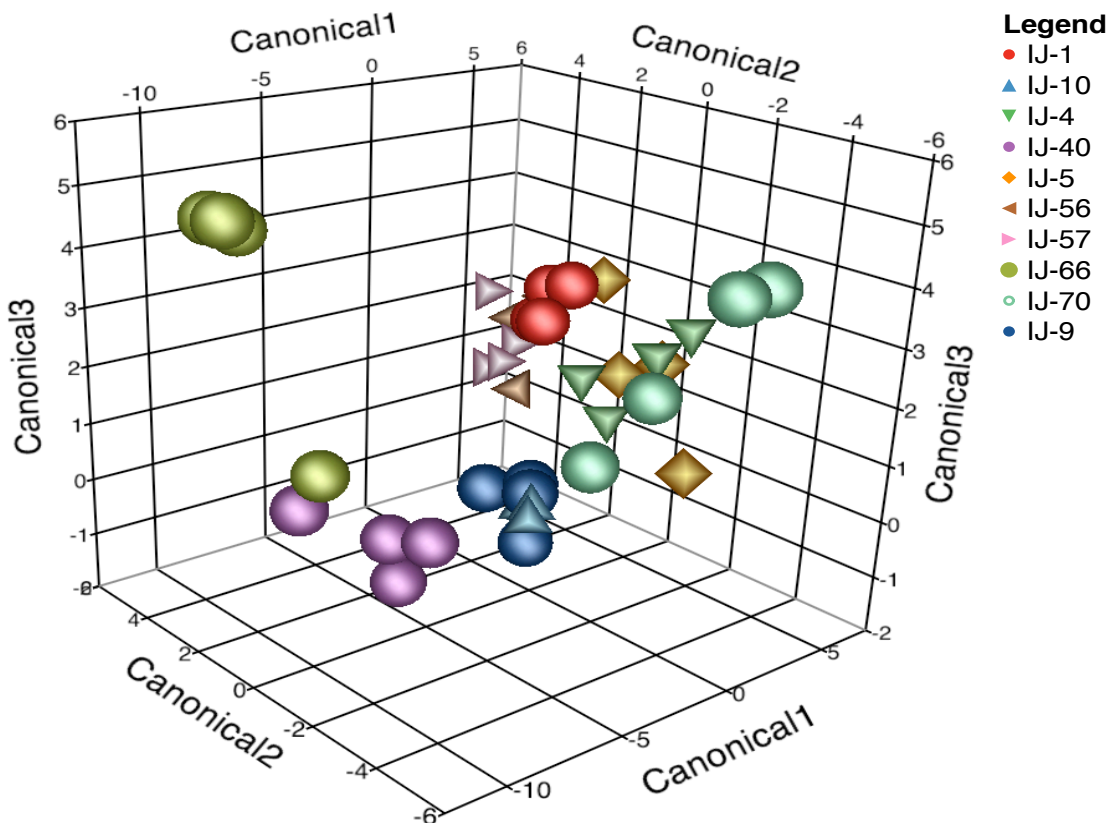


Figure 125. Three-dimensional Canonical plot for inkjets by LIBS.

Table 54. Confusion matrix from LDA for inkjets using LIBS.

Inkjet	IJ-1	IJ-10	IJ-4	IJ-40	IJ-5	IJ-56	IJ-57	IJ-66	IJ-70	IJ-9
IJ-1	4	0	0	0	0	0	0	0	0	0
IJ-10	0	2	0	0	0	0	0	0	0	0
IJ-4	0	0	4	0	0	0	0	0	0	0
IJ-40	0	0	0	3	0	0	0	0	0	0
IJ-5	0	0	0	0	4	0	0	0	0	0
IJ-56	0	0	0	0	0	3	0	0	0	0
IJ-57	0	0	0	0	0	1	3	0	0	0
IJ-66	0	0	0	1	0	0	0	3	0	0
IJ-70	0	1	0	0	0	0	0	0	3	0
IJ-9	0	1	0	0	0	0	0	0	0	3

6.3.3.5 Linear Discriminant Analysis of Inkjets by the Fusion of LIBS and LA-ICP-MS

The elements detected from the two sensors were merged and the discriminant analysis was performed again. The combination provided an increased correct classification rate. All the 10 inks were correctly classified as shown in Table 55. The canonical plots shown in Figure 126 and 127 also illustrate a distinct classification compared to the individual performance of two sensors.

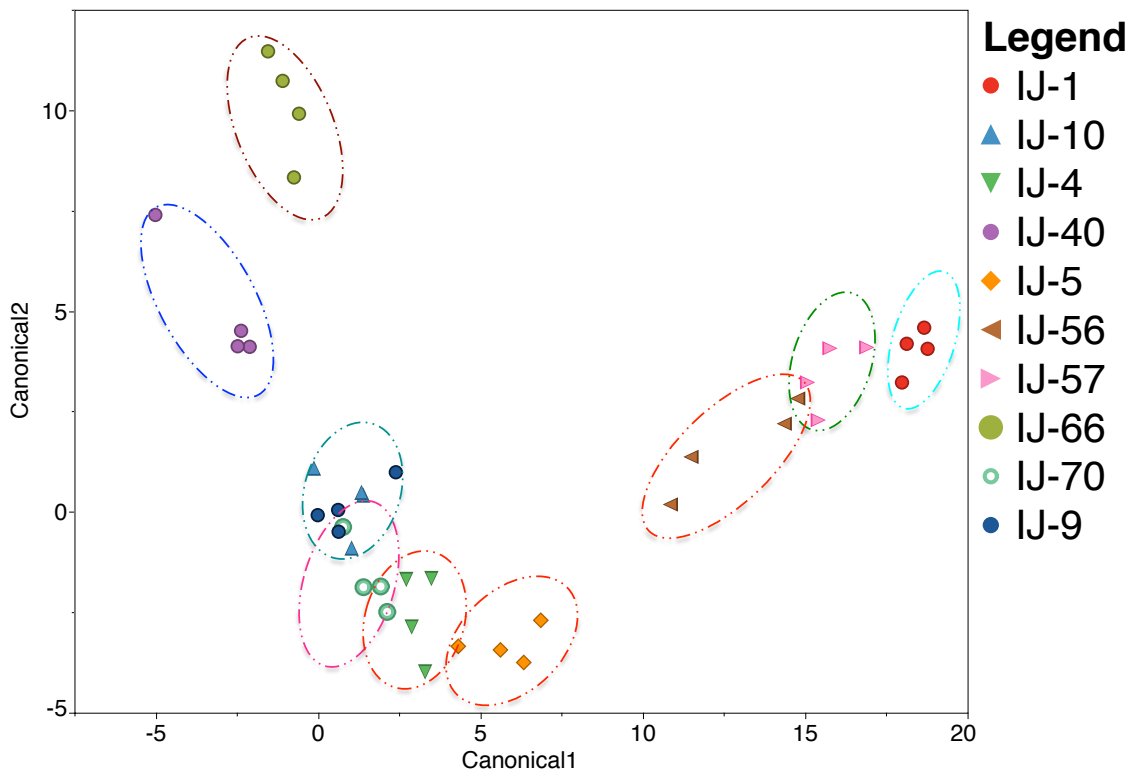


Figure 126. Two-dimensional Canonical Plot for inkjets from the fusion of LIBS and LA-ICP-MS.

Table 55. Confusion matrix from LDA for inkjets after data fusion of LIBS and LA-ICP-MS.

Row	IJ-1	IJ-10	IJ-4	IJ-40	IJ-5	IJ-56	IJ-57	IJ-66	IJ-70	IJ-9
IJ-1	4	0	0	0	0	0	0	0	0	0
IJ-10	0	4	0	0	0	0	0	0	0	0
IJ-4	0	0	4	0	0	0	0	0	0	0
IJ-40	0	0	0	4	0	0	0	0	0	0
IJ-5	0	0	0	0	4	0	0	0	0	0
IJ-56	0	0	0	0	0	4	0	0	0	0
IJ-57	0	0	0	0	0	0	4	0	0	0
IJ-66	0	0	0	0	0	0	0	4	0	0
IJ-70	0	0	0	0	0	0	0	0	4	0
IJ-9	0	0	0	0	0	0	0	0	0	4

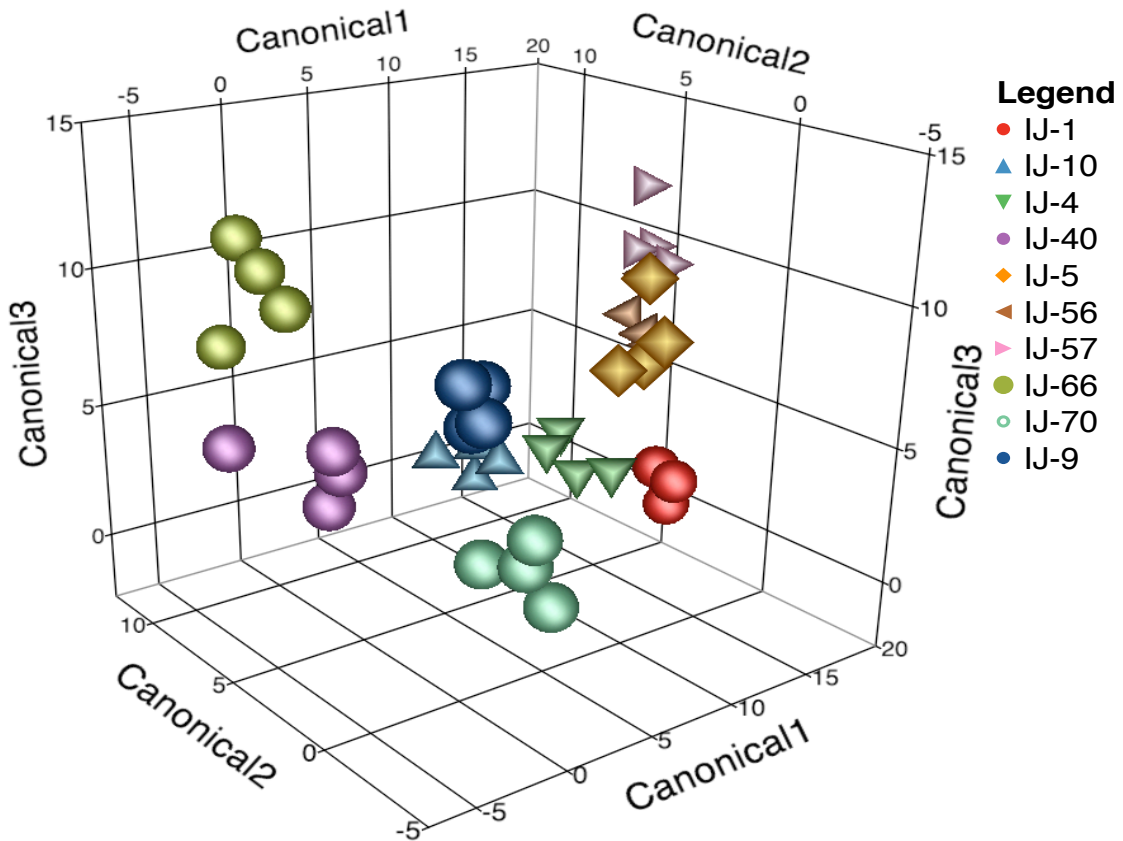


Figure 127. Three-dimensional Canonical plot for inkjets after data fusion of LIBS and LA-ICP-MS.

6.3.3.6 Cluster Analysis for Inkjet Printing Inks

Cluster Analysis was performed on the inkjet printing inks using LIBS and LA-ICP-MS spectrum. The comparison was made between the cluster analysis by LIBS and LA-ICP-MS. Finally these two cluster analyses were compared to the analysis by fusion of LIBS and LA-ICP-MS. Figure 128 shows the hierarchical cluster analysis by LIBS (on the left), LA-ICP-MS (on the right) and by fusion of LIBS and LA-ICP-MS (on the bottom). Presence of two or many colors in the same cluster shows incorrect association, whereas the presence of same color for a certain cluster means the correct association. Figure 128 shows that IJ 70 is clustered with IJ 40 by LIBS (a) and also by LA-ICP-MS (b), but the fusion shows that all the replicates of IJ 70 are clustered together.

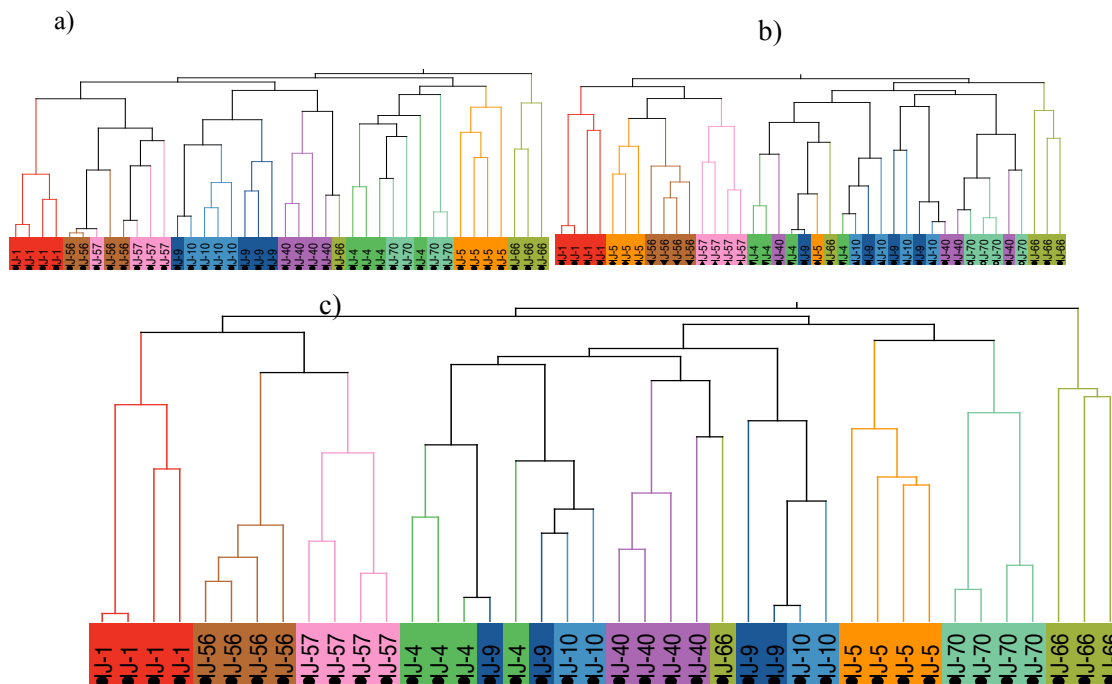


Figure 128. Hierarchical cluster analysis for inkjets by a) LIBS b) LA-ICP-MS c) fusion of LIBS and LA-ICP-MS.

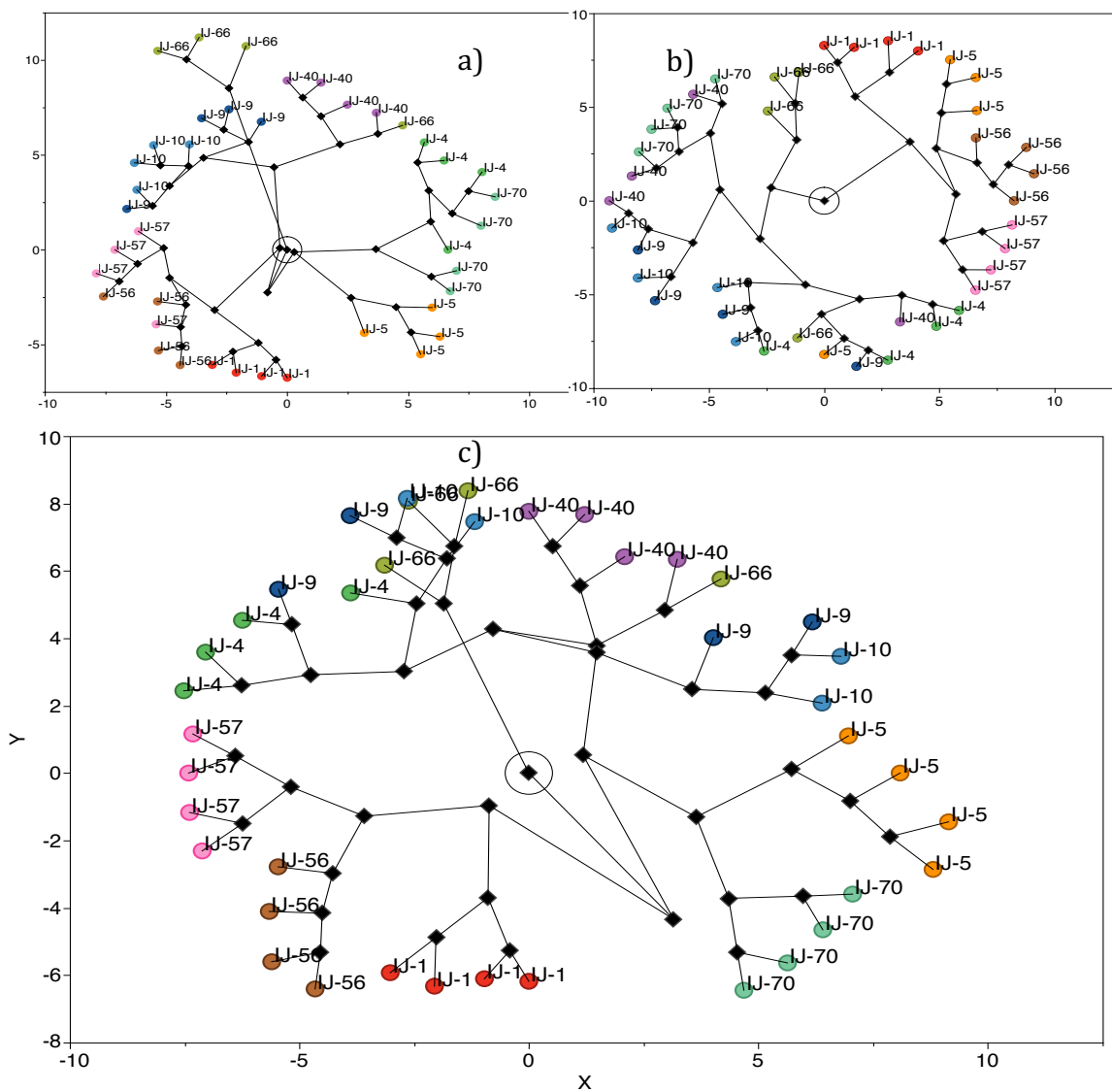


Figure 129. Constellation plot for inkjets by a) LIBS b) LA-ICP-MS c) fusion of LIBS and LA-ICP-MS.

Figure 129 is a constellation plot showing that the replicates of the same inks are branched closer while different replicates are farther from the joint. The constellation plot for the fusion shows better clustering of the replicates belonging to the same ink compared to LIBS and LA-ICP-MS alone.

6.4 Analysis of Intaglio Printing Inks by Tandem LIBS/LA-ICP-MS

A total of 12 intaglio printing inks were selected from the set of 86 intaglio inks. This subset contained all those pairs that were not distinguishable by standalone LA-ICP-MS. Table 56 shows the list of intaglio printing inks that were used for the tandem study. All of these inks were from bank notes that were collected from different countries. The inks were selected on the basis of the similar LA-ICP-MS elemental profile.

Table 56. List of intaglio inks selected for tandem LIBS/LA-ICP-MS study.

Intaglio	Color	Country
IT 4	Dark Green	Argentina
IT 6	Dark Magenta	Barbados
IT 9	Black	Ukraine
IT 10	Red	Ukraine
IT 11	Gold	Ukraine
IT 27	Red	Honduras
IT 33	Maroon	Trinidad and Tobago
IT 35	Brown	Europe (Italy)
IT 36	Brown	Europe (Italy)
IT 40	Green	Costa Rica
IT 44	Green	Costa Rica
IT 50	Dark Blue	Tunisia

Four pairs of these inks had very similar elemental profile when analyzed by standalone LA-ICP-MS. These pairs are listed in Table 57.

Table 57. List of indistinguishable pairs for standalone LA-ICP-MS.

Intaglio	Color	Country
IT 10	Red	Ukraine
IT 11	Gold	Ukraine
IT 35	Brown	Europe (Italy)
IT 36	Brown	Europe (Italy)

6.4.1 Optimization of Tandem LIBS/LA-ICP-MS for the Analysis of Intaglio Printing Inks

The optimization process was similar to toners and inkjets. First LIBS was optimized, then the tandem system was re-optimized with parameters that worked best for both LIBS and LA-ICP-MS. Due to the relative thickness of intaglio ink over paper, higher laser energy (2.1mJ) was used. The optimized parameters for the analysis of intaglio inks by tandem LIBS/LA-ICP-MS are listed in Table 58.

Table 58. Optimized parameters for the analysis of intaglio inks by tandem LIBS/LA-ICP-MS.

Parameters	Intaglio
Ablation mode	Single line
Laser spot size	200 μm
Frequency	4 Hz
Laser energy	20% (4.1mJ)
Ablation rate	30 $\mu\text{m/s}$
Gate Delay	0.1 μs
Argon flow in the cell	0.75L/min

6.4.2 Results from Tandem LIBS/LA-ICP-MS Analysis of Intaglio Printing Inks

For these indistinguishable pairs LIBS was able to detect elements like K, which suffered from isobaric interference from ^{40}Ar and also from polyatomic interference ($^{39}\text{Ar}^1\text{H}$). K was able to discriminate one of the two indistinguishable pairs as shown in Figure 130. LA-ICP-MS was able to detect a larger number of elements compared to LIBS. Table 59 lists the additional elements detected by LIBS (in bold).

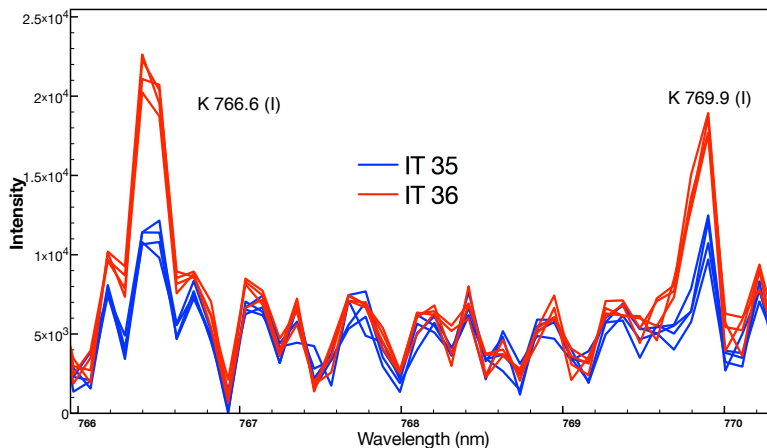


Figure 130. Spectral Overlay of two intaglio samples discriminated by K emission lines in LIBS spectrum⁴¹.

Table 59. List of elements detected by LA-ICP-MS and additional elements detected by LIBS for intaglio printing inks.

Intaglio	Elements detected by LA-ICP-MS	Elements detected by LIBS
IT 4	Mg, Ca, Ti, Mn, Co, Cu, Sr, Zr, Hf	Ca
IT 6	Mg, Al, Mn, Fe, Co, Zr, Hf	Mg, Ca
IT 9	Mg, Al, Ca, Mn, Fe, Co, Sr, Zr, Hf	Na, Ca, K
IT 10	Mg, Al, Ca, Mn, Co, Sr, Zr, Hf	Na, K
IT 11	Mg, Al, Ca, Mn, Co, Sr, Zr, Hf	Na, K
IT 27	Mg, Ca, Mn, Fe, Co, Sr, Zr, Nb, Hf	ND
IT 33	Mg, Mn, Co, Cu, Sr, Zr, Nb, Hf, Pb	ND
IT 35	Mg, Ca, Ti, Mn, Co, Cu, Zr, Nb, Hf	Na, K
IT 36	Mg, Ca, Ti, Mn, Co, Cu, Zr, Nb, Hf	Na, Ca, K
IT 40	Mg, Ca, Mn, Fe, Co, Cu, Sr, Zr, Nb, Hf,	Mg, Ca
IT 44	Mg, Ca, Mn, Cu, Sr, Zr, Nb, Hf, Pb, Bi	Na, Ca, K
IT 50	Ca, Ti, Mn, Fe, Cu, Sr, Mo, Sb	Na, Ca

6.4.3 Multivariate Analysis of Intaglio Printing Inks by Tandem LIBS/LA-ICP-MS

Principal Component Analysis, Linear Discriminant Analysis and Cluster Analysis were performed on the data obtained from two sensors. Analysis was done for the individual sensors and also for the fusion of the two sensors.

6.4.3.1 Principal Component Analysis of intaglio printing inks by LIBS

A total of six elements were detected by LIBS in this subset of intaglio inks. These six elements namely Na, Mg, K, Ti and Sr were used for the PCA analysis. The two dimensional and three dimensional PCA plots for intaglio inks show that most of the inks are very similar and are not distinctly classified by LIBS as shown in Figure 131 and Figure 132.

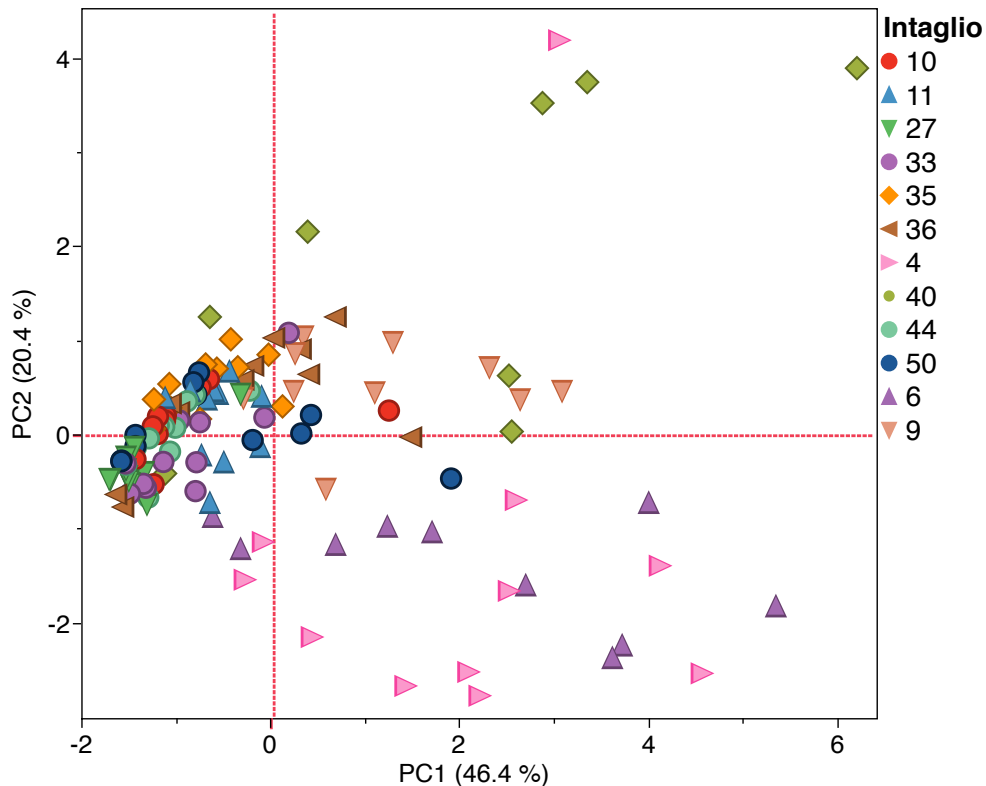


Figure 131. Two-dimensional PCA plot for intaglio inks by LIBS.

Table 60 shows that the first three Principal Components explained the 81.6% of the total variance for intaglio inks.

Table 60. Variances explained by the first three PCs for intaglio inks by LIBS.

Principal Components	PC1	PC2	PC3	Cumulative
Variance Explained (%)	46.4%	20.4%	14.8%	81.6%

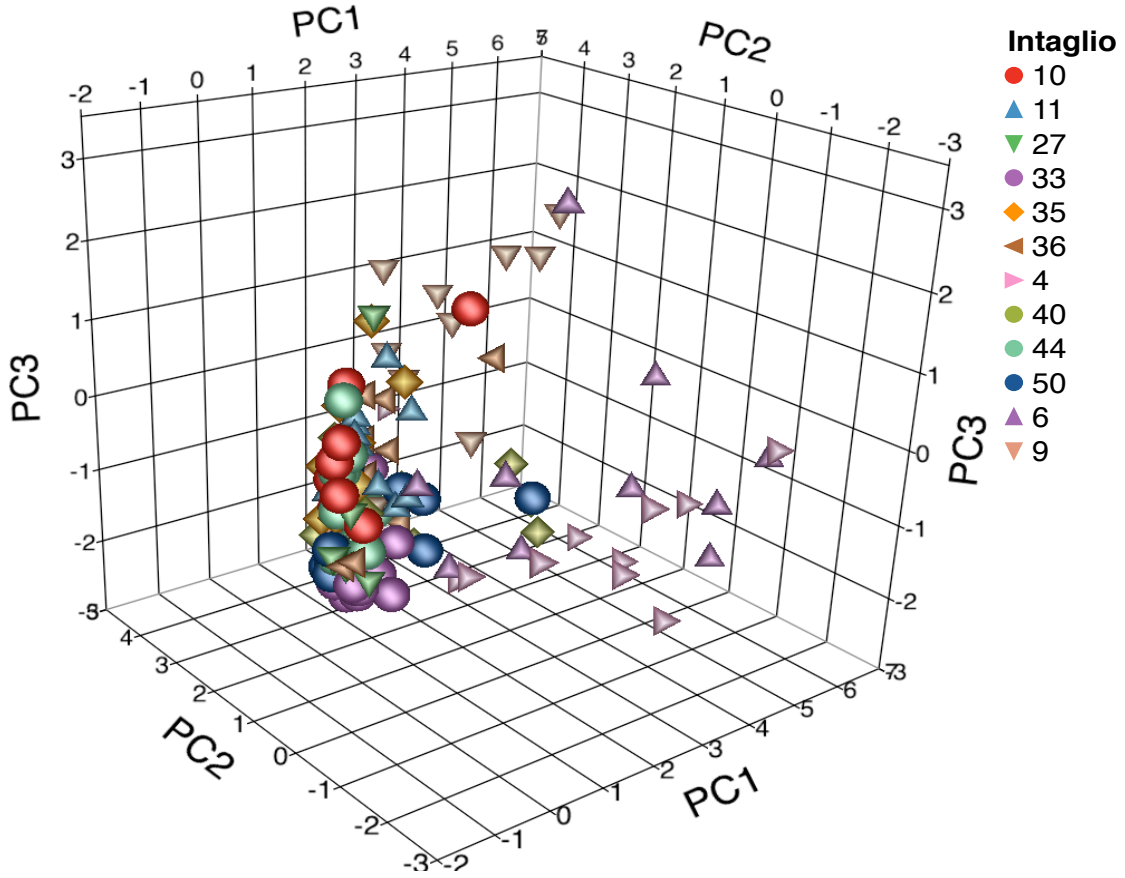


Figure 132. Three-dimensional PCA plot for intaglio printing inks by LIBS.

6.4.3.2 Principal Component Analysis of Intaglio Printing Inks by LA-ICP-MS

Most of the intaglio inks had similar elemental profile as shown in Table 57. The PCA plots in Figure 133 and Figure 134 also showed that most of the similar inks were

classified together. However, IT 50 was found to be different from other inks. This is because IT 50 contains elements like Mo and Sb, while these elements were completely absent in other intaglio inks. Similarly, IT 40 and IT 44 contained element Bi, which was found to be absent in other inks. These two inks are also separated from rest of the other intaglio inks and are classified closer to each other, as shown in Figure 133 and Figure 134. The first three Principal components explained 72.5% of the total variance as shown in Table 61.

Table 61. Variances explained by first three PCs for intaglio inks by LA-ICP-MS.

Principal Components	PC1	PC2	PC3	Cumulative Variance
Variance Explained (%)	44.9%	15%	12.6%	72.5%

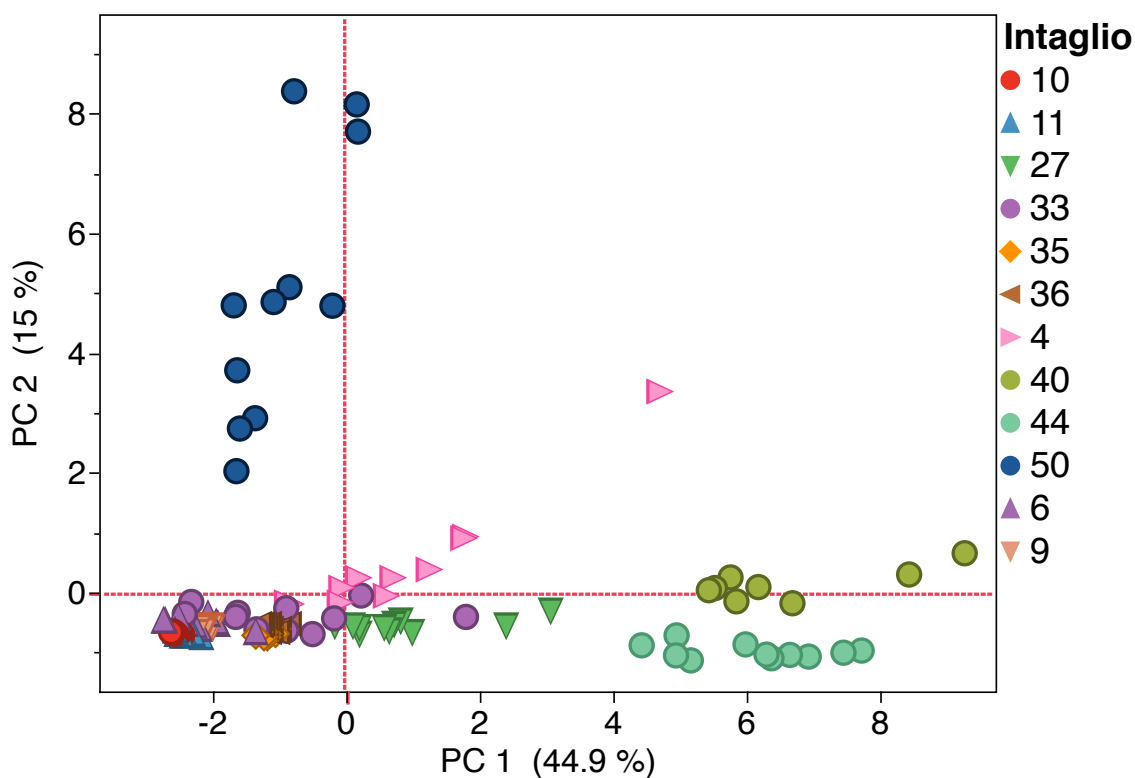


Figure 133. Two-dimensional PCA plot for intaglio by LA-ICP-MS.

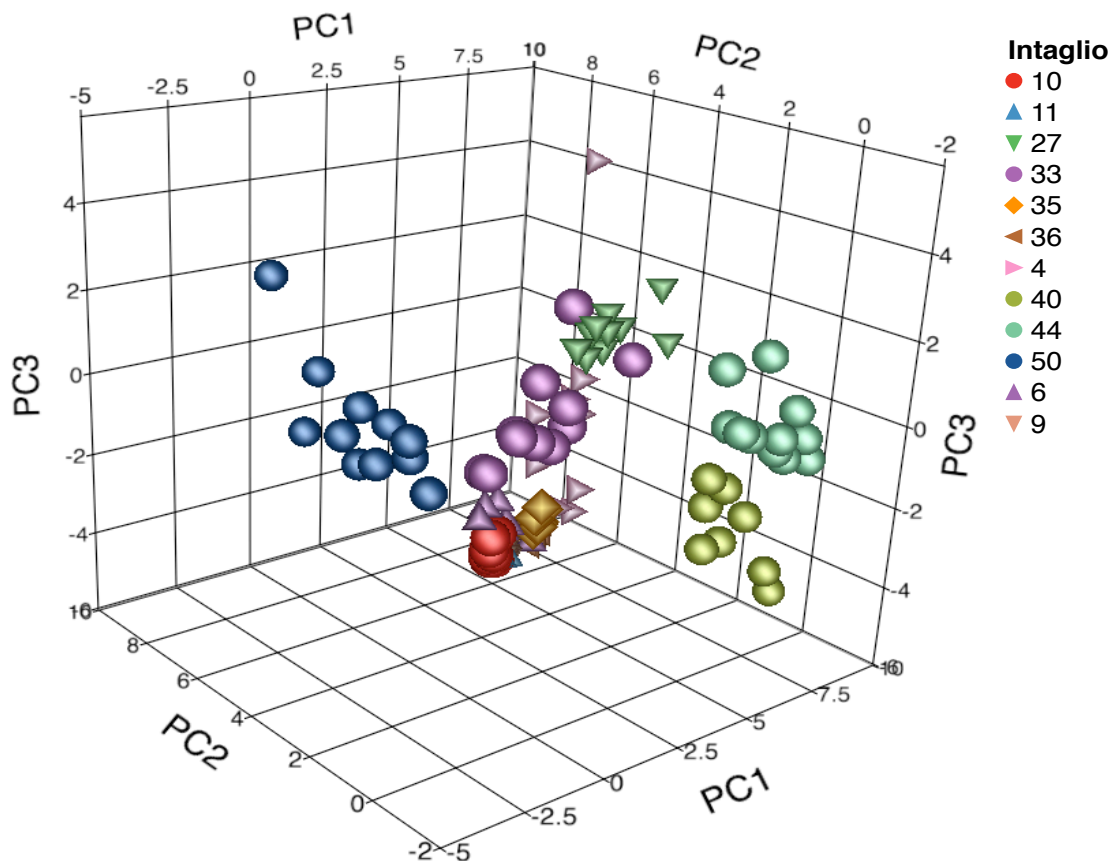


Figure 134. Three-dimensional PCA plot for intaglio by LA-ICP-MS.

6.4.3.3 Principal Component Analysis of Intaglio Printing Inks by the Fusion of LIBS and LA-ICP-MS

The fusion of LIBS and LA-ICP-MS was performed by combining the elements detected by the two sensors. Figure 135 and Figure 136 represent the two-dimensional and three-dimensional PCA plots obtained after the fusion of LIBS and LA-ICP-MS respectively.

Table 62. Variances explained by first three PCs after fusion of LIBS and LA-ICP-MS.

Principal Components	PC1	PC2	PC3	Cumulative Variance
Variance Explained (%)	35.7%	13.4%	12.1%	62.2%

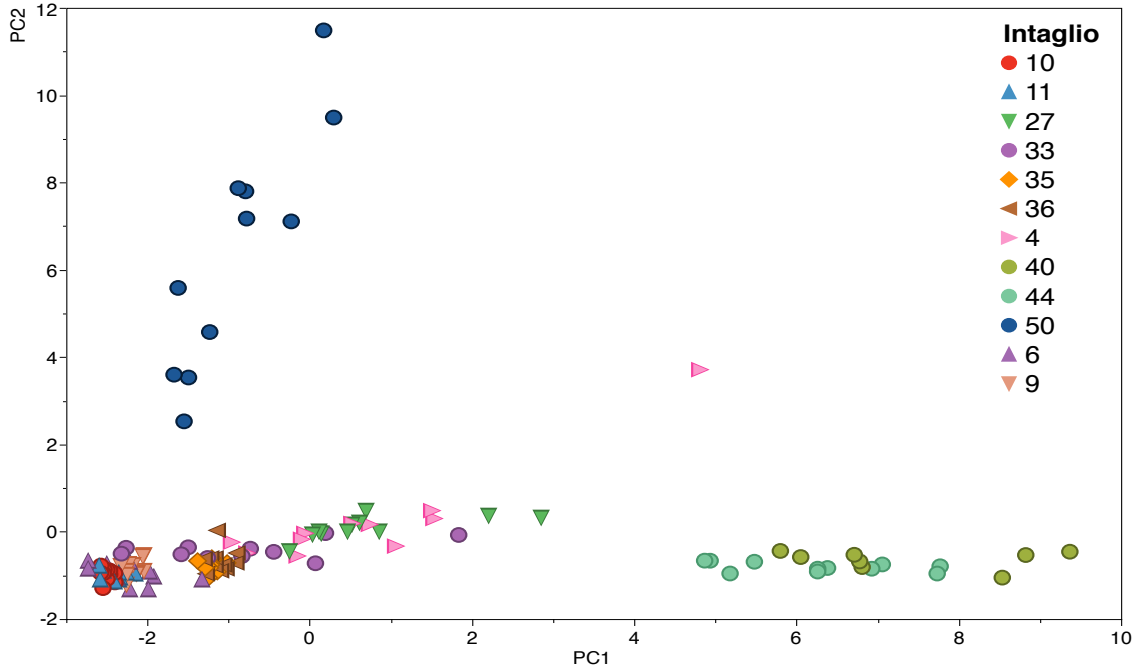


Figure 135. Two-dimensional PCA plot for intaglio after the fusion of LIBS and LA-ICP-MS.

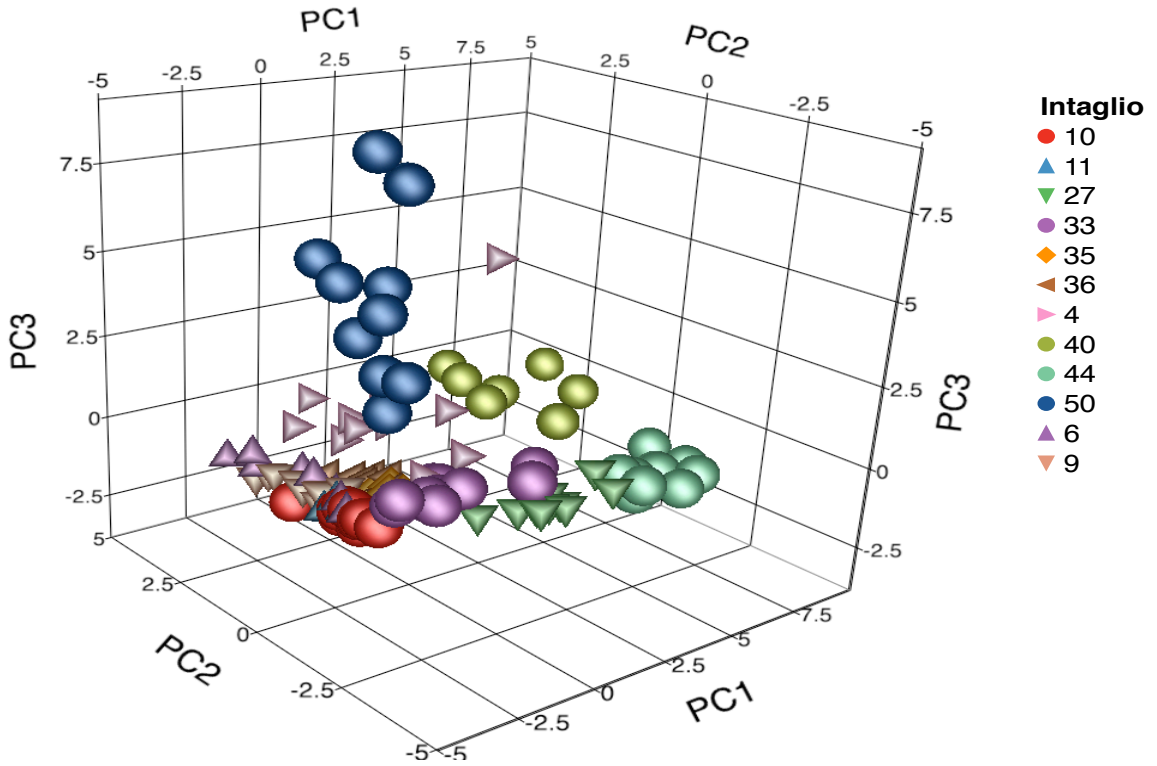


Figure 136. Three-dimensional PCA plot for intaglio after the fusion of LIBS and LA-ICP-MS.

6.4.3.4 Linear Discriminant Analysis of Intaglio Printing Inks by LIBS

Out of 66 pairs, 25 pairs were misclassified by LIBS. Table 63 is the confusion matrix obtained from Linear Discriminant Analysis of intaglio inks. The misclassified intaglio samples are labeled as 1, while the correctly associated are labeled as 0.

Table 63. Confusion matrix for intaglio printing inks by LDA using LIBS.

IT	IT10	IT11	IT27	IT33	IT35	IT36	IT4	IT40	IT44	IT50	IT6	IT9
IT10	0											
IT11	1	0										
IT27	0	0	0									
IT33	0	0	0	0								
IT35	0	0	0	0	0							
IT36	0	0	0	0	0	0						
IT4	0	0	0	1	0	0	0					
IT40	0	0	0	0	0	0	0	0				
IT44	0	0	0	0	0	0	0	0	0			
IT50	0	0	0	0	0	0	0	0	0	0		
IT6	0	0	0	1	0	1	0	0	0	0	0	
IT9	0	0	0	0	0	0	0	0	0	0	0	0

6.4.3.5 Linear Discriminant Analysis of Intaglio Printing Inks by LA-ICP-MS

Out of 66 pairs, 4 pairs were misclassified by LA-ICP-MS. Table 64 is the confusion matrix obtained from Linear Discriminant Analysis of intaglio inks. Misclassified intaglio samples are labeled as 1, while the correctly associated are labeled as 0 in the table.

Table 64. Confusion matrix for intaglio by LDA using LA-ICP-MS.

IT	IT10	IT11	IT27	IT33	IT35	IT36	IT4	IT40	IT44	IT50	IT6	IT9
IT10	0											
IT11	1	0										
IT27	0	0	0									
IT33	0	0	0	0								
IT35	0	0	0	0	0							
IT36	0	0	0	0	0	0						
IT4	0	0	0	1	0	0	0					
IT40	0	0	0	0	0	0	0	0				
IT44	0	0	0	0	0	0	0	0	0			
IT50	0	0	0	0	0	0	0	0	0	0		
IT6	0	0	0	1	0	1	0	0	0	0	0	
IT9	0	0	0	0	0	0	0	0	0	0	0	0

6.4.3.6 Linear Discriminant Analysis of Intaglio Printing Inks after the Fusion of LIBS and LA-ICP-MS

Out of 66 possible pairs, only 1 pair was misclassified by the fusion of LIBS and LA-ICP-MS. Table 65 is the confusion matrix obtained from Linear Discriminant Analysis of intaglio inks. In the table, misclassified intaglio samples are labeled as 1, while the correctly associated are labeled as 0. The fusion of LIBS and LA-ICP-MS resulted in improvement in the classification of intaglio printing inks by Linear Discriminant Analysis. The Canonical plots from linear Discriminant Analysis also showed more distinct grouping of the intaglio inks after the fusion of the two sensors as shown in Figure 137 and Figure 138.

Table 65. Confusion matrix from LDA for intaglio after fusion of LIBS and LA-ICP-MS.

Intaglio	IT1	IT11	IT27	IT33	IT35	IT36	IT4	IT40	IT44	IT50	IT6	IT9
IT10	0											
IT11	1	0										
IT27	0	0	0									
IT33	0	0	0	0								
IT35	0	0	0	0	0							
IT36	0	0	0	0	0	0						
IT4	0	0	0	0	0	0	0					
IT40	0	0	0	0	0	0	0	0				
IT44	0	0	0	0	0	0	0	0	0			
IT50	0	0	0	0	0	0	0	0	0	0		
IT6	0	0	0	0	0	0	0	0	0	0	0	
IT9	0	0	0	0	0	0	0	0	0	0	0	0

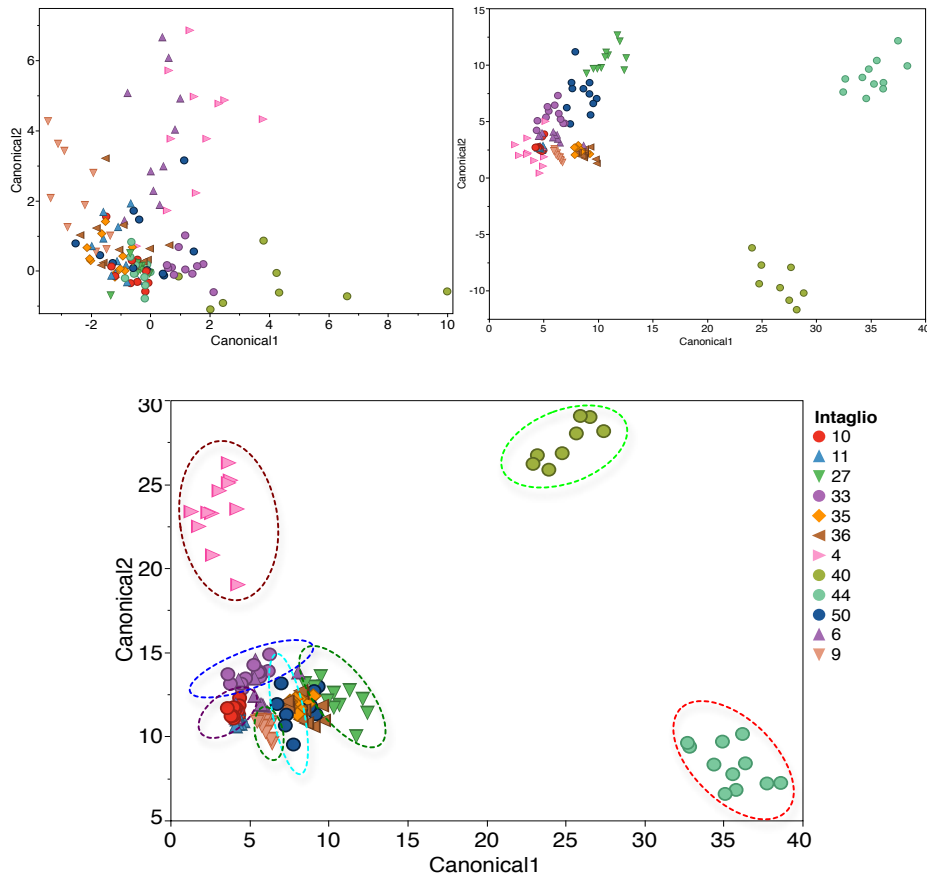


Figure 137. Two dimensional Canonical plot for intaglio by LIBS (top left), LA-ICP-MS (top right) and the fusion of LIBS and LA-ICP-MS (bottom).

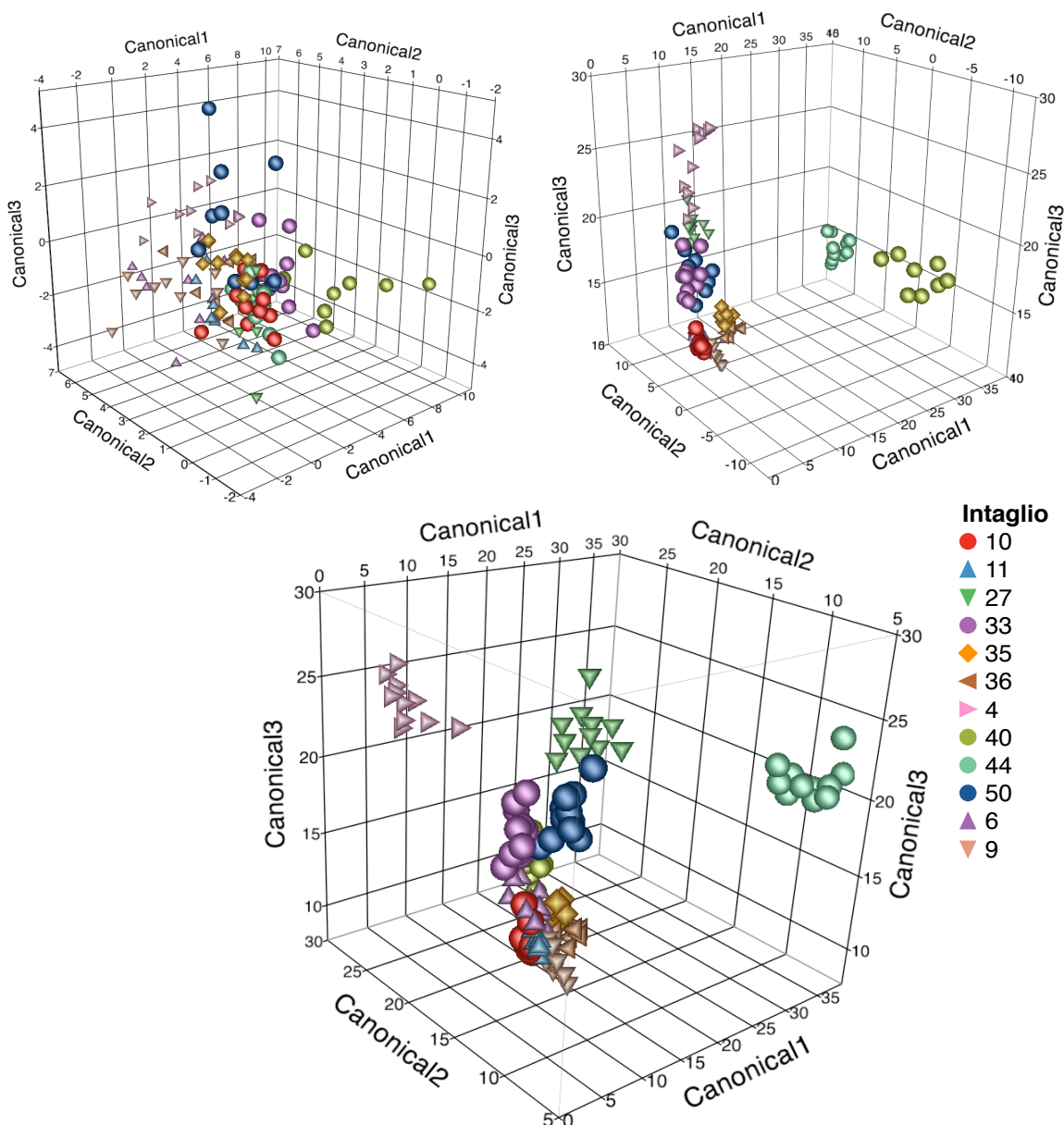


Figure 138. Three-dimensional Canonical plot for intaglio by LIBS (top left), LA-ICP-MS (top right) and the fusion of LIBS and LA-ICP-MS (bottom).

6.4.3.7 Cluster Analysis of Intaglio Printing Inks by Tandem LIBS- LA-ICP-MS

Hierarchical cluster analysis was performed on intaglio printing inks based on elements detected by LIBS and LA-ICP-MS. As expected, LA-ICP-MS performed better

than LIBS in cluster analysis. Figure 139 shows the performance of each sensor and the performance of the fusion. Presence of more than one color in a cluster indicates incorrect inclusion of different intaglio samples. The clusters obtained after fusion of LIBS and LA-ICP-MS show that similar intaglio inks (same color in the cluster) are clustered closer.

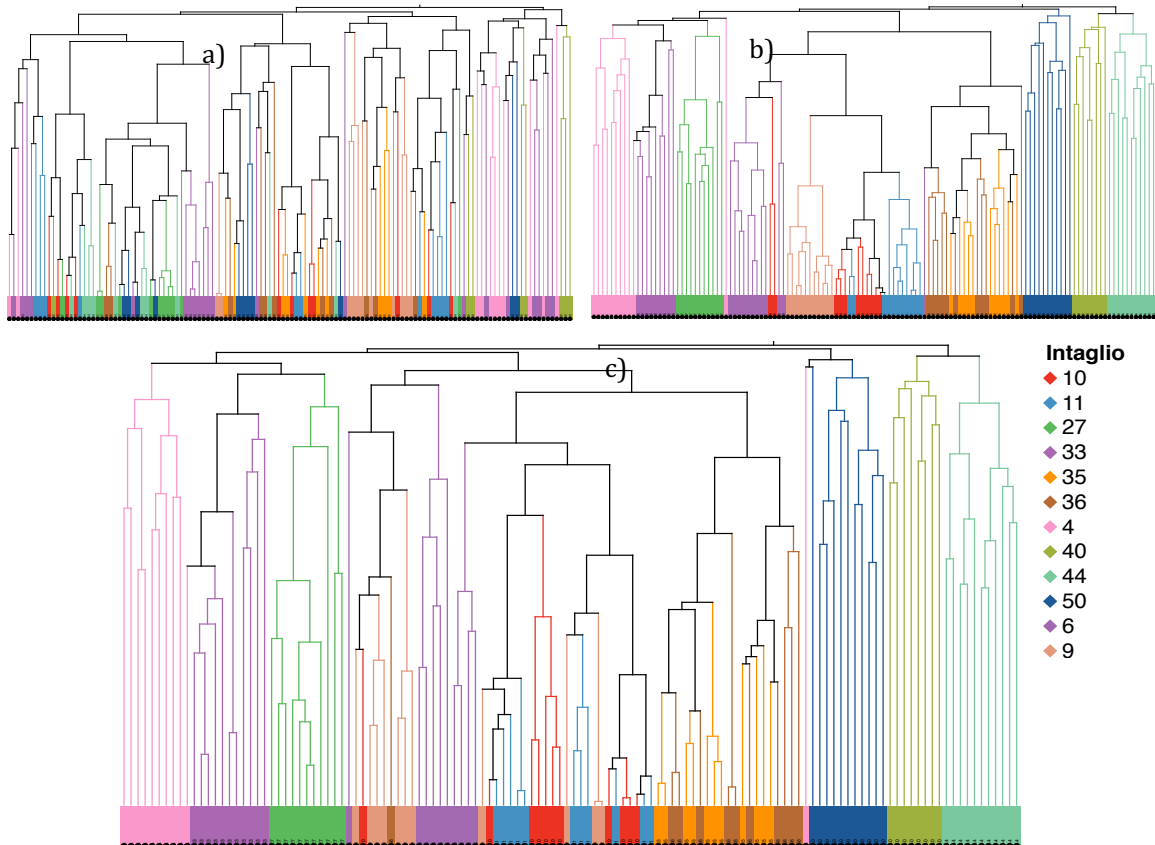


Figure 139. Hierarchical cluster analysis for intaglio inks by a) LIBS b) LA-ICP-MS c) Fusion of LIBS and LA-ICP-MS.

Another way of performing cluster analysis is through the use of constellation plot. Figure 140 shows the constellation plot obtained from LIBS, LA-ICP-MS and the fusion of LIBS and LA-ICP-MS. The endpoints in Figure 136 (a) have replicates of different intaglio inks in the same branch showing incorrect clustering of intaglio inks.

The intaglio inks IT 4 and IT 40, for example, are clustered incorrectly with IT 5 and 60 in LIBS (top-left), while they have separate clusters in the fusion (bottom). This indicates that the fusion of LIBS and LA-ICP-MS performs better than the two individual sensors.

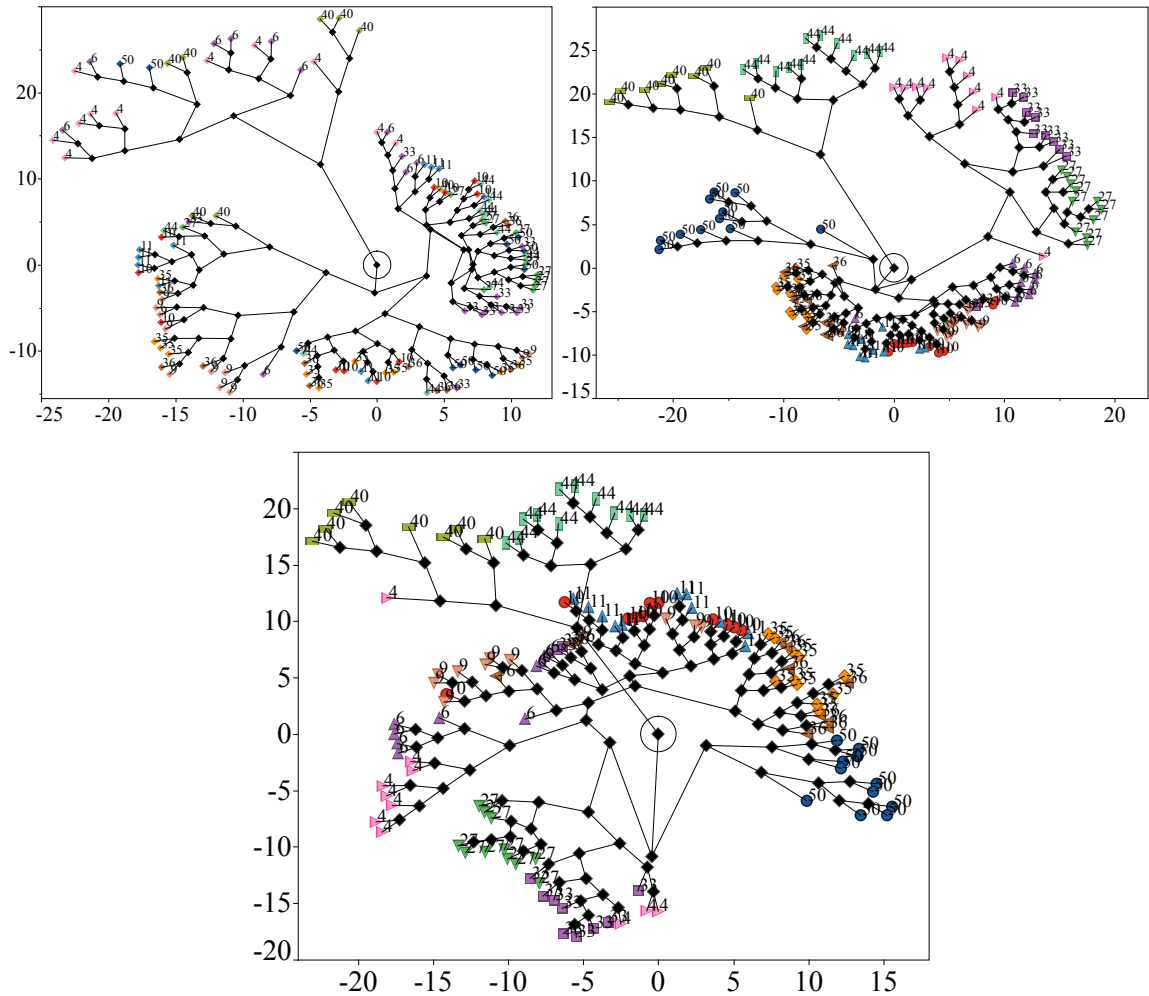


Figure 140. Constellation plot for intaglio inks by LIBS (top-left), LA-ICP-MS (top-right) and fusion of LIBS and LA-ICP-MS (bottom).

6.5 Analysis of Offset Printing Inks by Tandem LIBS/LA-ICP-MS

A total of 13 offset printing inks were used for the tandem LIBS/LA-ICP-MS study. These inks were from six different manufacturers and they were of different colors as shown in Table 66. These offset printing inks were from five different brands.

Table 66. List of offset printing inks used for tandem LIBS/LA-ICP-MS study.

Offset	Source	Color
OF 18	SC	Cyan
OF 21	GI	Black
OF 27	GI	Yellow
OF 47	LIVI	Green
OF 50	USPB	Blue/Pink/Orange Lines
OF 65	UB	Cyan
OF 71	SC	Yellow
OF 73	SC	Cyan
OF 74	SC	Magenta
OF 75	SC	Yellow
OF 76	SC	Black
OF 77	SC	Cyan
OF 78	SC	Magenta

In this subset of offset printing inks, six pairs were indistinguishable using LA-ICP-MS alone. These pairs are listed in Table 67.

Table 67. List of indistinguishable pairs of offset inks when analyzed by LA-ICP-MS

Offset	Source	Color
OF 21 Vs. OF 27	GI	Black Vs. Yellow
OF 47 Vs. OF 50	LIVI Vs. USB	Green vs. Blue/Pink/Orange Lines
OF 18 Vs. OF 65	SC Vs. UB	Cyan
OF 71 Vs. OF 75	SC	Yellow
OF 73 Vs. OF 77	SC	Cyan
OF 74 Vs. OF 78	SC	Magenta

6.5.1 Optimization of Tandem LIBS/LA-ICP-MS for the Analysis of Offset Inks

Like inkjets, the offset inks are also embedded on paper. A number of parameters including the laser energy, the frequency of the laser shots, gate delay, and scanning speed had to be optimized for both LIBS and LA-ICP-MS. Table 68 lists the optimized parameters for the analysis of offset printing inks using tandem LIBS/LA-ICP-MS.

Table 68. Optimized parameters for the analysis of offsets by tandem LIBS/LA-ICP-MS.

Parameters	Offset
Ablation mode	Single line
Laser spot size	200 μm
Frequency	4 Hz
Laser energy	20% (4.1mJ)
Ablation rate	30 $\mu\text{m/s}$
Gate Delay	0.1 μs
Argon flow in the cell	0.7L/min

6.5.2 Results from Tandem LIBS/LA-ICP-MS Analysis of Offset Printing Inks

Additional elements like Ca, K, and Si were detected by LIBS. These elements were very helpful in discriminating the six pairs of the indistinguishable inks listed in Table 69. It can be seen in Figure 141 two offset inks, OF 21 and OF 27, both have Ca in them, but the concentration of Ca is different in these two inks, which is reflected by their intensities. Different elements detected by LIBS and LA-ICP-MS in the tandem analysis of offset printing inks is tabulated in Table 69. The additional elements detected by LIBS are in bold.

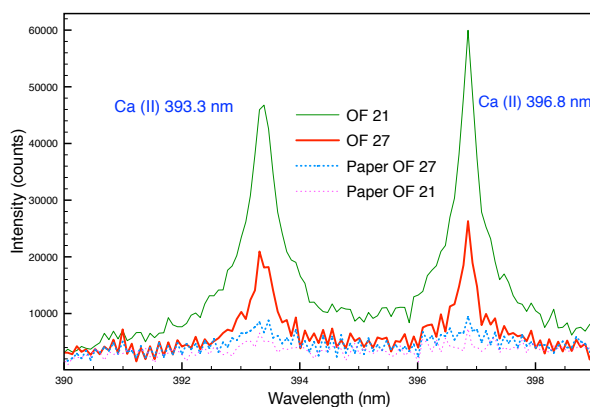


Figure 141. Spectral Overlay of Ca emission lines obtained through LIBS spectrum for two offset printing inks⁴¹.

Table 69. List of elements detected in offset printing inks by LIBS and LA-ICP-MS in tandem mode⁴¹.

Offset	Elements detected by LA-ICP-MS	Elements detected by LIBS
OF 18	Mn, Co, Cu	Na, Ca
OF 21	Mn, Co, Sn	Ca
OF 27	Mn, Co, Sn	Ca
OF 47	ND	Na, Ca, K
OF 50	ND	Na
OF 65	Mn, Co, Cu	Na
OF 71	Mg, Al	Na
OF 73	Mg, Cu	Mg, Ca, Cu, Si
OF 74	Mg, Al, Sr, Ba	Na, Mg, Ca, Si
OF 75	Mg, Al	Na, Si, Ca
OF 77	Mg, Cu	Na, Ca
OF 78	Mg, Al, Sr, Ba	Ca, Sr

6.5.3 Multivariate Analysis of Offset Printing Inks by tandem LIBS/LA-ICP-MS

Principal Component Analysis, Linear Discriminant Analysis, and Cluster Analysis were performed on the data obtained from two sensors: LIBS and LA-ICP-MS. Performance of these two sensors was compared with each other, and with the fusion of the two sensors.

6.5.3.1 Principal Component Analysis of Offset Printing Inks by LIBS

Figure 142 and Figure 143 represent the two-dimensional and three-dimensional PCA plots for offset printing inks using LIBS. Some offset samples are classified distinctly apart from the other offset inks. For example, offset 73 and offset 21 are

classified in different regions from the other offset samples. The first three Principal Components provided 62.2% of the total variance as shown in Table 70.

Table 70. Variances explained in offset samples by first three PCs using LIBS

Principal Components	PC1	PC2	PC3	Cumulative Variance
Variance Explained (%)	57.3%	27%	12.4%	92.4%

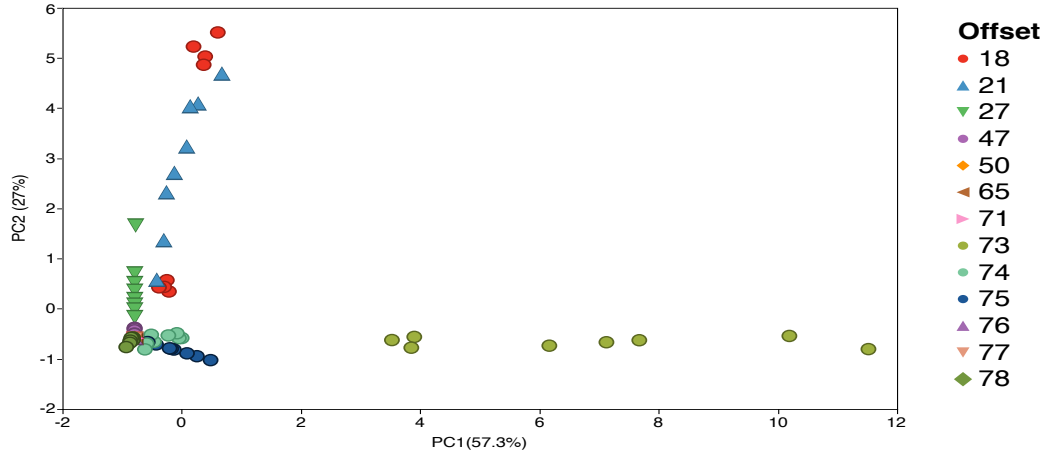


Figure 142. Two-dimensional PCA plot for offset samples by LIBS.

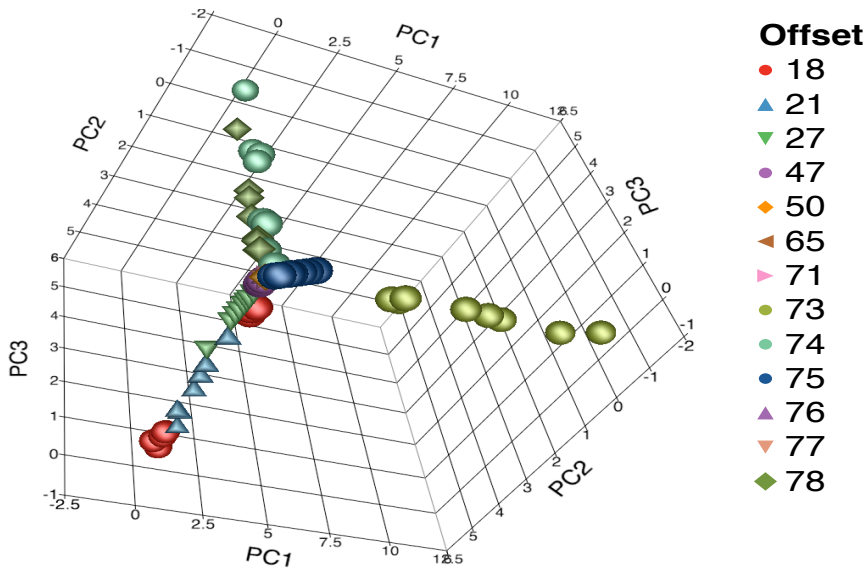


Figure 143. Three-dimensional PCA plot for offset samples by LIBS.

6.5.3.2 Principal Component Analysis of Offset Printing Inks by LA-ICP-MS

Figure 137 and Figure 138 represent the two-dimensional and three-dimensional PCA plots for offset printing inks using LA-ICP-MS, respectively. Some offset samples are classified distinctly apart from the others. For example, OF 76 and OF 73 are classified in different regions from the other offset samples as shown in Figure 144 and Figure 145. The first three Principal Components explained 79.9% of the total variance as shown in Table 71.

Table 71. Variances explained in offset samples by first three PCs using LA-ICP-MS.

Principal Components	PC1	PC2	PC3	Cumulative Variance
Variance Explained (%)	35.8%	24.9%	19.2%	79.9%

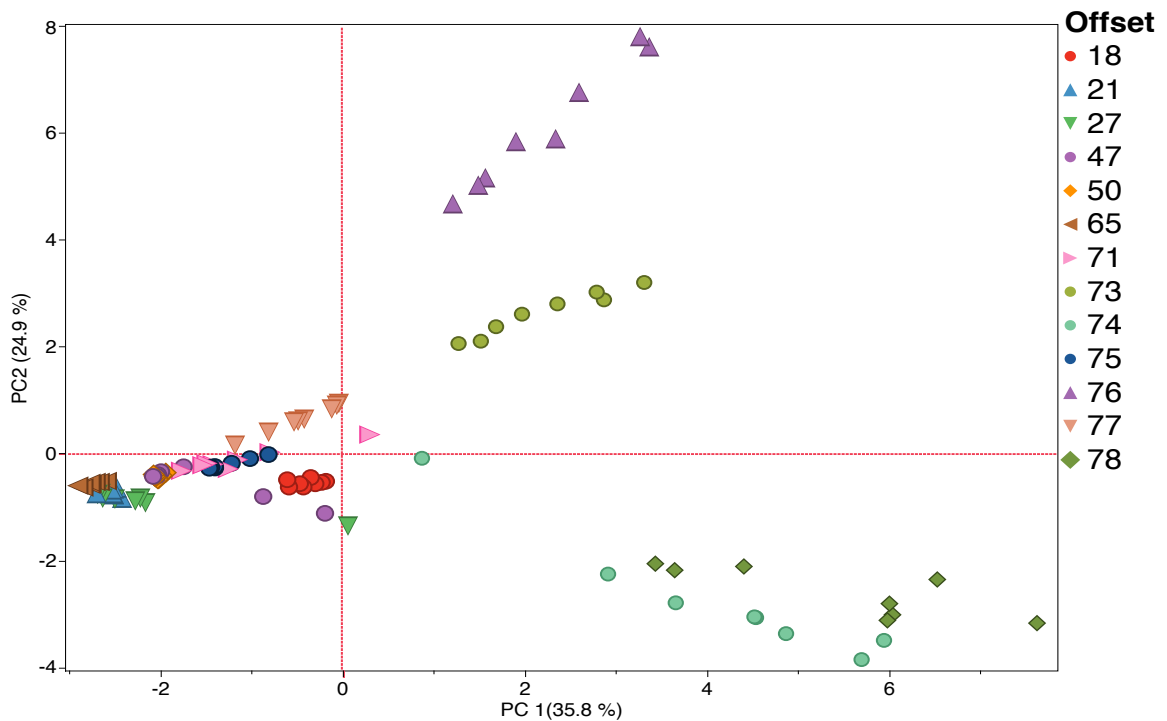


Figure 144. Two-dimensional PCA plot for offset samples after fusion of LIBS and LA-ICP-MS.

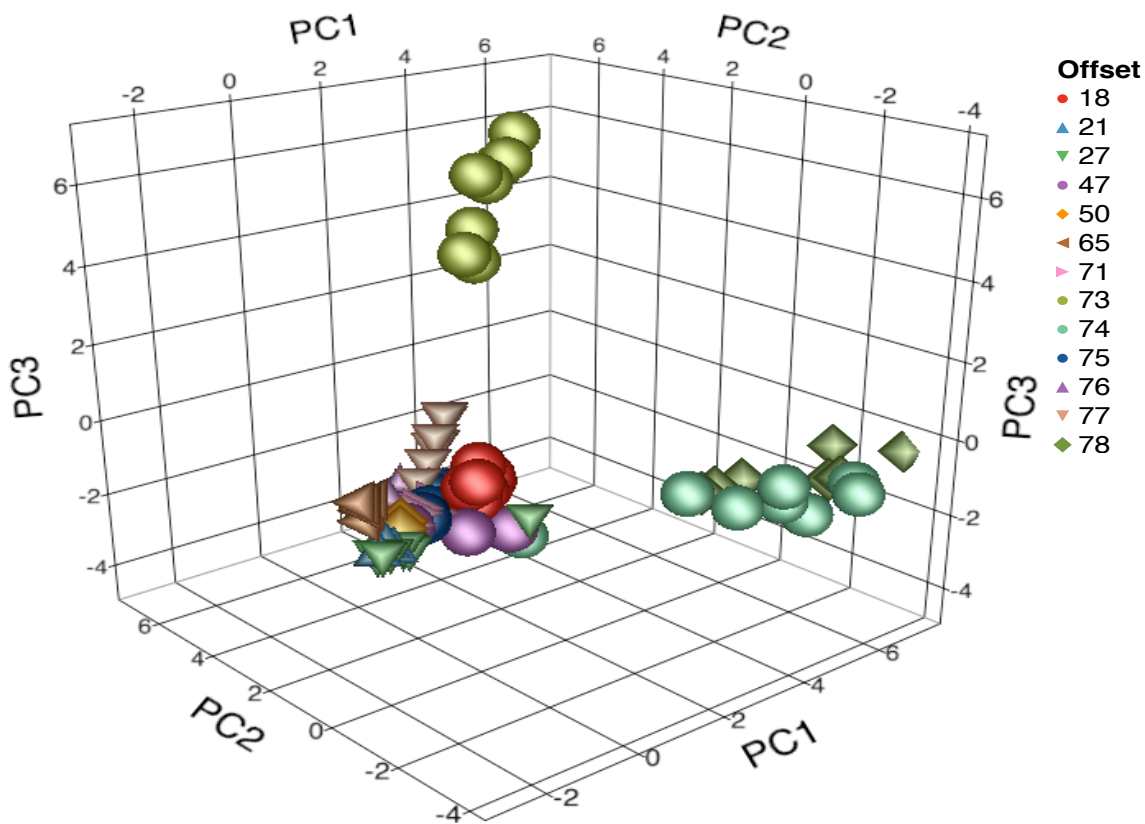


Figure 145. Three-dimensional PCA plot for offset samples after fusion of LIBS and LA-ICP-MS.

6.5.3.3 Principal Component Analysis of Offset Printing Inks by tandem LIBS/ LA-ICP-MS

Figure 146 and Figure 147 represent the two-dimensional and three-dimensional PCA plots for offset printing inks obtained after the fusion of LIBS and LA-ICP-MS. The first three PCs provided 79.9% of the total variance as shown in Table 72.

Table 72. Variances explained in offset samples by first three PCs after fusion of LIBS and LA-ICP-MS

Principal Components	PC1	PC2	PC3	Cumulative Variance
Variance Explained (%)	28.9%	23.5%	17.7%	70.1%

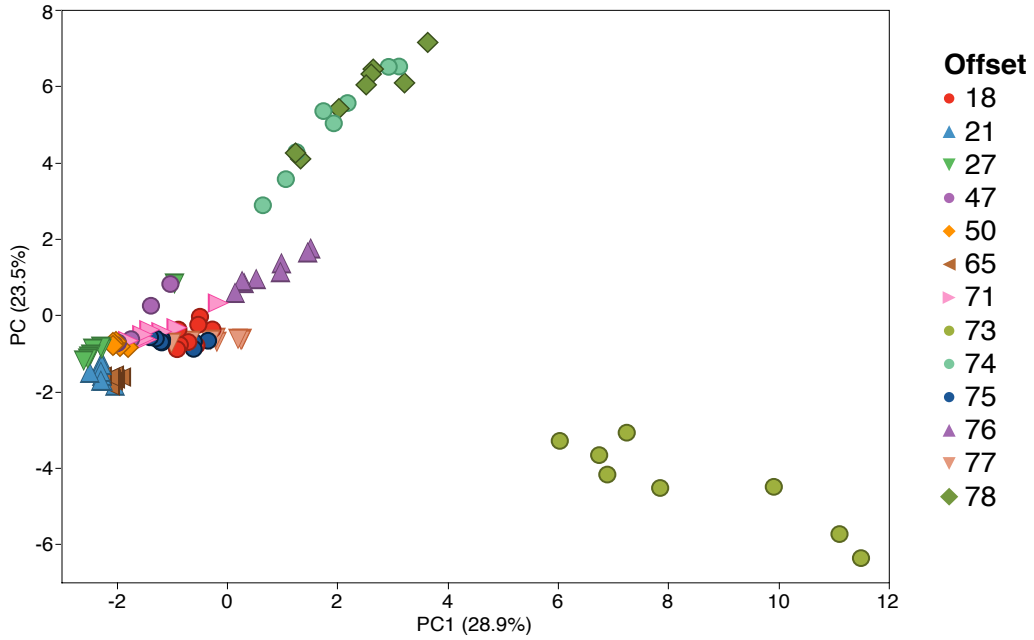


Figure 146. Two-dimensional PCA plot for offset inks from the fusion of LIBS and LA-ICP-MS.

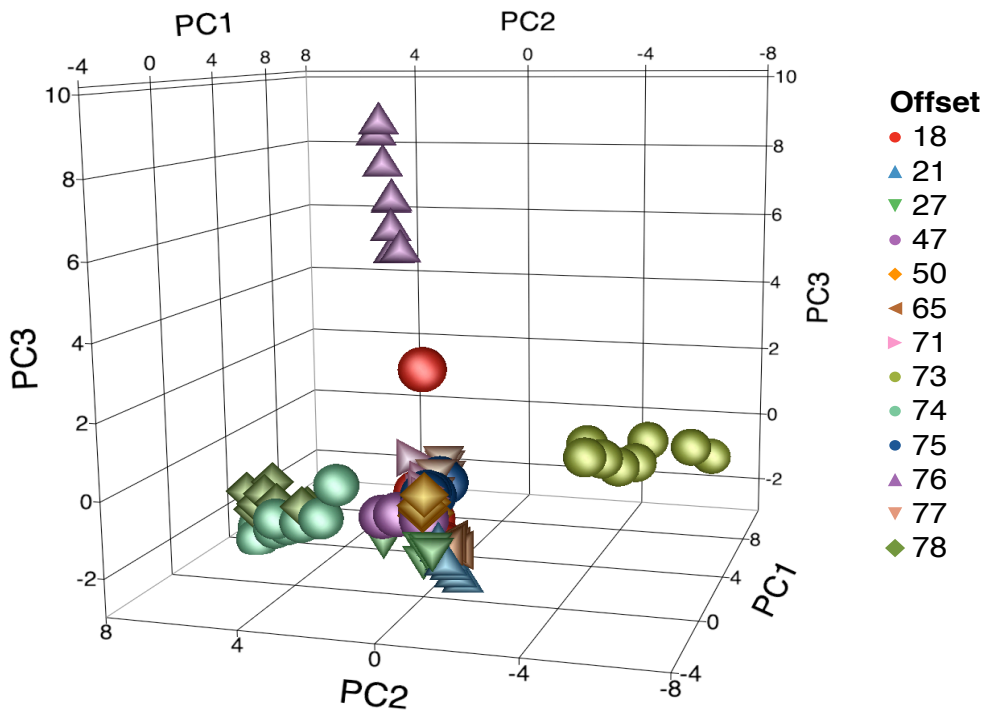


Figure 147. Three-dimensional PCA plot for offset inks after fusion of LIBS and LA-ICP-MS.

6.5.3.4 Linear Discriminant Analysis of Offset Printing Inks by LIBS

A total of 12 pairs were incorrectly classified by LDA using the elements from LIBS only. This provided 15.4% misclassification, or a correct classification of 84.6%. Table 73 is the confusion matrix obtained from linear discriminant analysis using LIBS. The digit ‘0’ indicates correct classification while ‘1’ indicates misclassification.

Table 73. Confusion matrix from LDA for offset samples by LIBS

OF	OF18	OF21	OF27	OF47	OF50	OF65	OF71	OF73	OF74	OF75	OF76	OF77	OF78
OF18	0												
OF21	1	0											
OF27	0	0	0										
OF47	0	1	0	0									
OF50	0	0	1	1	0								
OF65	0	0	0	0	1	0							
OF71	0	0	0	0	1	0	0						
OF73	0	0	0	0	0	0	0	0					
OF74	0	0	0	1	1	0	0	0	0				
OF75	0	0	0	0	1	0	0	0	0	0			
OF76	0	0	0	0	1	0	0	0	0	0	0		
OF77	0	0	0	0	1	0	0	0	0	0	0	0	
OF78	0	0	0	0	1	0	0	0	0	0	0	0	0

6.5.3.5 Linear Discriminant Analysis of Offset Printing Inks by LA-ICP-MS

A total of 5 pairs were incorrectly classified by LDA using the elements from LA-ICP-MS only. This provided 6.4% misclassification, or a correct classification of 93.6%. Table 74 is the confusion matrix obtained from linear discriminant analysis using LA-ICP-MS data. The digit ‘0’ indicates correct classification while ‘1’ indicates misclassification.

Table 74. Confusion matrix for offset inks from LDA by LA-ICP-MS.

OF	OF18	OF21	OF27	OF47	OF50	OF65	OF71	OF73	OF74	OF75	OF76	OF77	OF78
OF18	0												
OF21	0	0											
OF27	0	1	0										
OF47	0	0	0	0									
OF50	0	0	0	1	0								
OF65	0	0	0	1	0	0							
OF71	0	0	0	0	0	0	0						
OF73	0	0	0	0	0	0	0	0					
OF74	0	0	0	0	0	0	0	0	0				
OF75	0	0	0	1	0	0	1	0	0	0			
OF76	0	0	0	0	0	0	0	0	0	0	0		
OF77	0	0	0	0	0	0	0	0	0	0	0	0	
OF78	0	0	0	0	0	0	0	0	0	0	0	0	0

6.5.3.6 Linear Discriminant Analysis of Offset Printing Inks after the Fusion of LIBS and LA-ICP-MS

A total of two pairs were incorrectly classified by LDA using the elements from the fusion of LIBS and LA-ICP-MS.

Table 75. Confusion matrix for offset inks from LDA after fusion of LIBS and LA-ICP-MS.

OF	OF18	OF21	OF27	OF47	OF50	OF65	OF71	OF73	OF74	OF75	OF76	OF77	OF78
OF18	0												
OF21	0	0											
OF27	0	0	0										
OF47	0	0	0	0									
OF50	0	0	0	1	0								
OF65	0	0	0	0	0	0							
OF71	0	0	0	0	0	0	0						
OF73	0	0	0	0	0	0	0	0					
OF74	0	0	0	0	0	0	0	0	0				
OF75	0	0	0	0	0	0	1	0	0	0			
OF76	0	0	0	0	0	0	0	0	0	0	0		
OF77	0	0	0	0	0	0	0	0	0	0	0	0	
OF78	0	0	0	0	0	0	0	0	0	0	0	0	0

The Linear Discriminant Analysis provided 2.6% misclassification, or a correct classification of 97.4%. Table 75 is the confusion matrix obtained from linear discriminant analysis after the data fusion. The digit ‘0’ indicates correct classification while ‘1’ indicates misclassification.

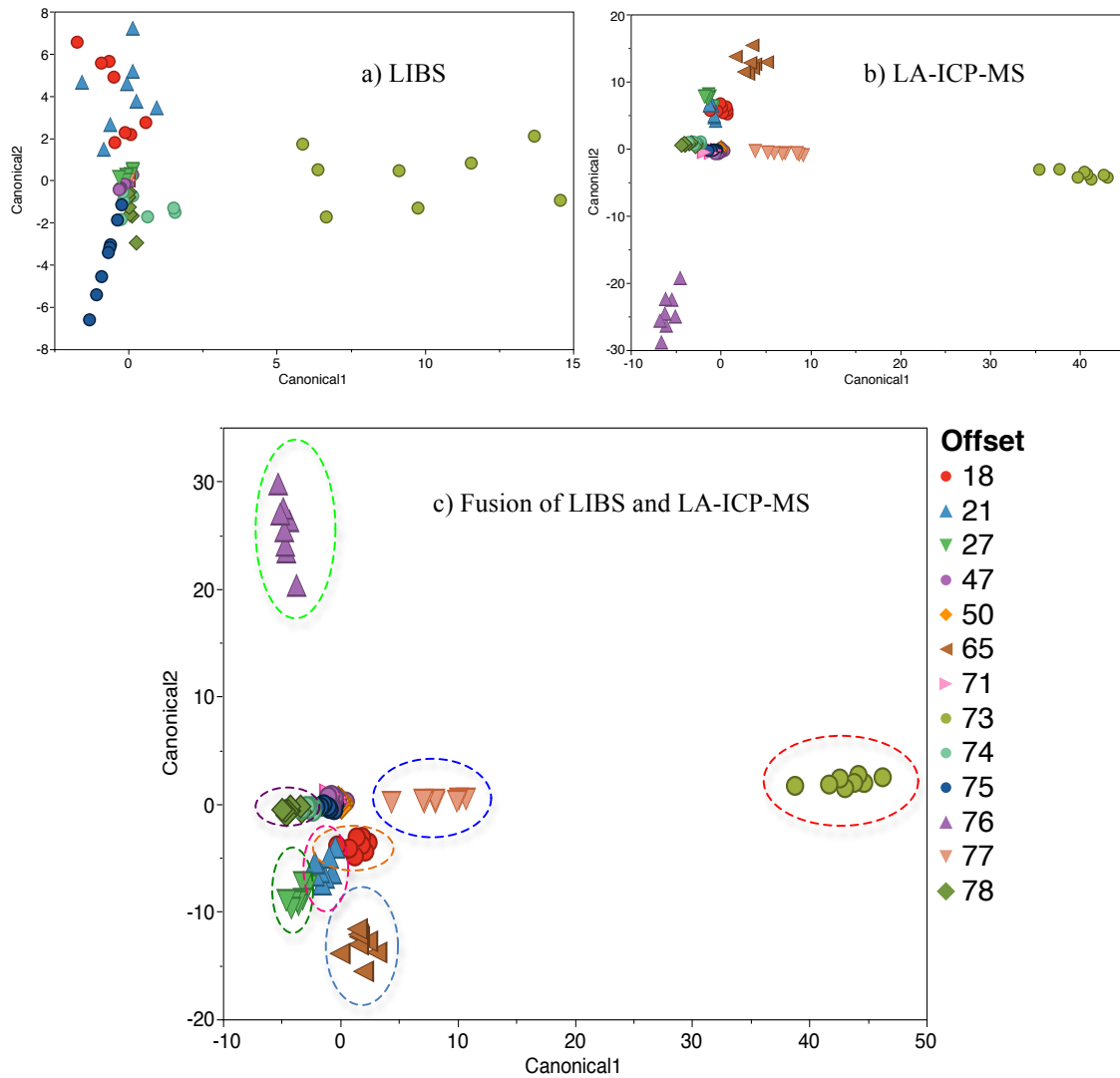


Figure 148. Two dimensional Canonical plot for offset samples by a) LIBS b) LA-ICP-MS c) fusion of LIBS and LA-ICP-MS.

The canonical plots obtained from the discriminant analysis show that the classification is better after the fusion of LIBS and LA-ICP-MS. Figure 148 and Figure

149 are the two dimensional and three dimensional canonical plots for LIBS (a), LA-ICP-MS (b), and after the fusion of LIBS and LA-ICP-MS (c). Different offset inks are shown inside ellipses in Figure 148(c), which indicates that, the fusion of LIBS and LA-ICP-MS provides better classification than the individual sensors.

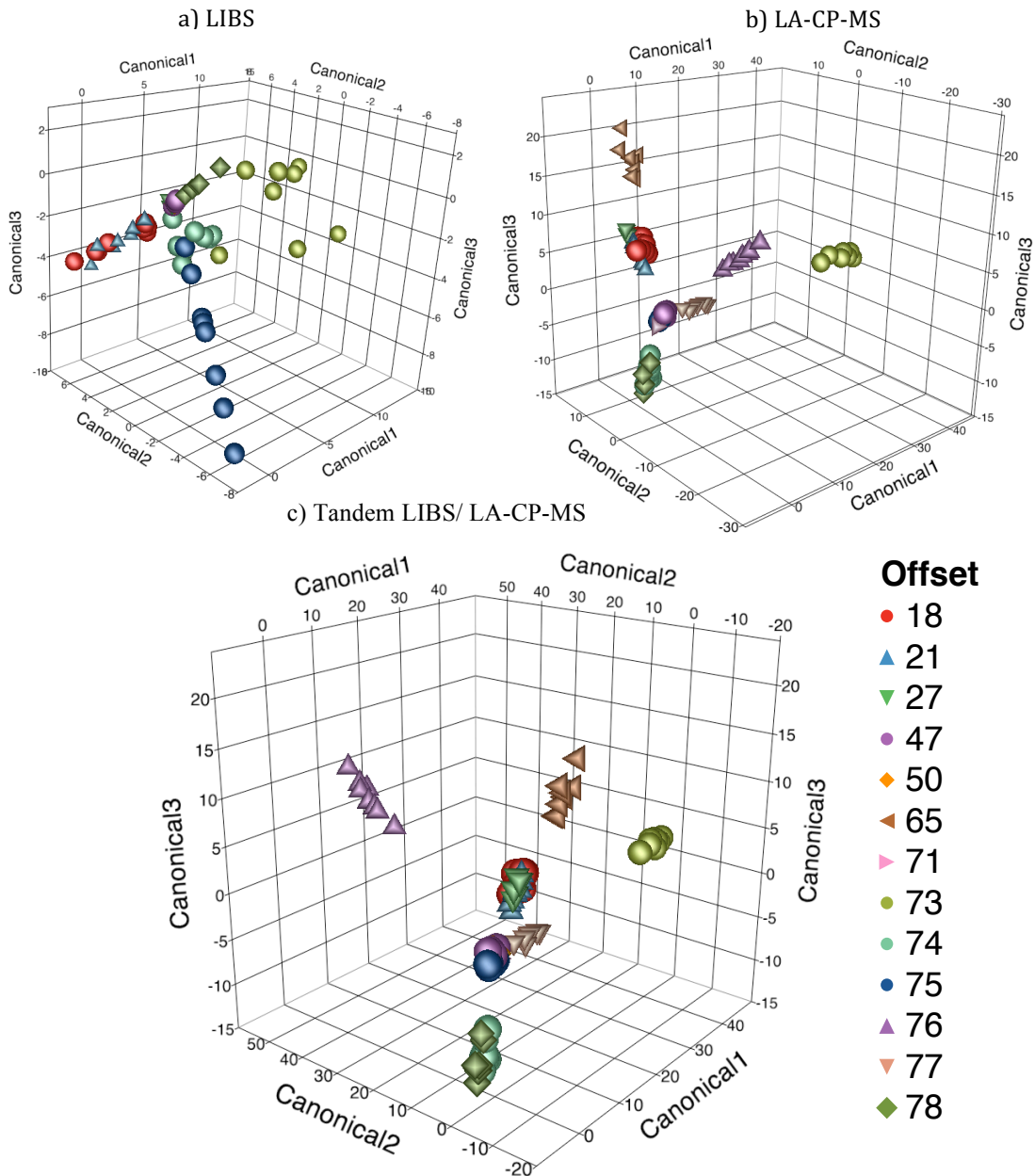


Figure 149. Three dimensional Canonical plot for offset samples by a) LIBS b) LA-ICP-MS c) fusion of LIBS and LA-ICP-MS.

6.5.3.7 Cluster Analysis of Offset Printing Inks by LIBS

Hierarchical cluster analysis was performed on the data obtained from LIBS and LA-ICP-MS to evaluate their performances individually and in comparison to the fusion of LIBS and LA-ICP-MS. Figure 150 (c) shows the hierarchical cluster plot for the fusion. The fusion classifies the offset ink samples with less misclassification (same colored lines) compared to LIBS (a) and LA-ICP-MS (b).

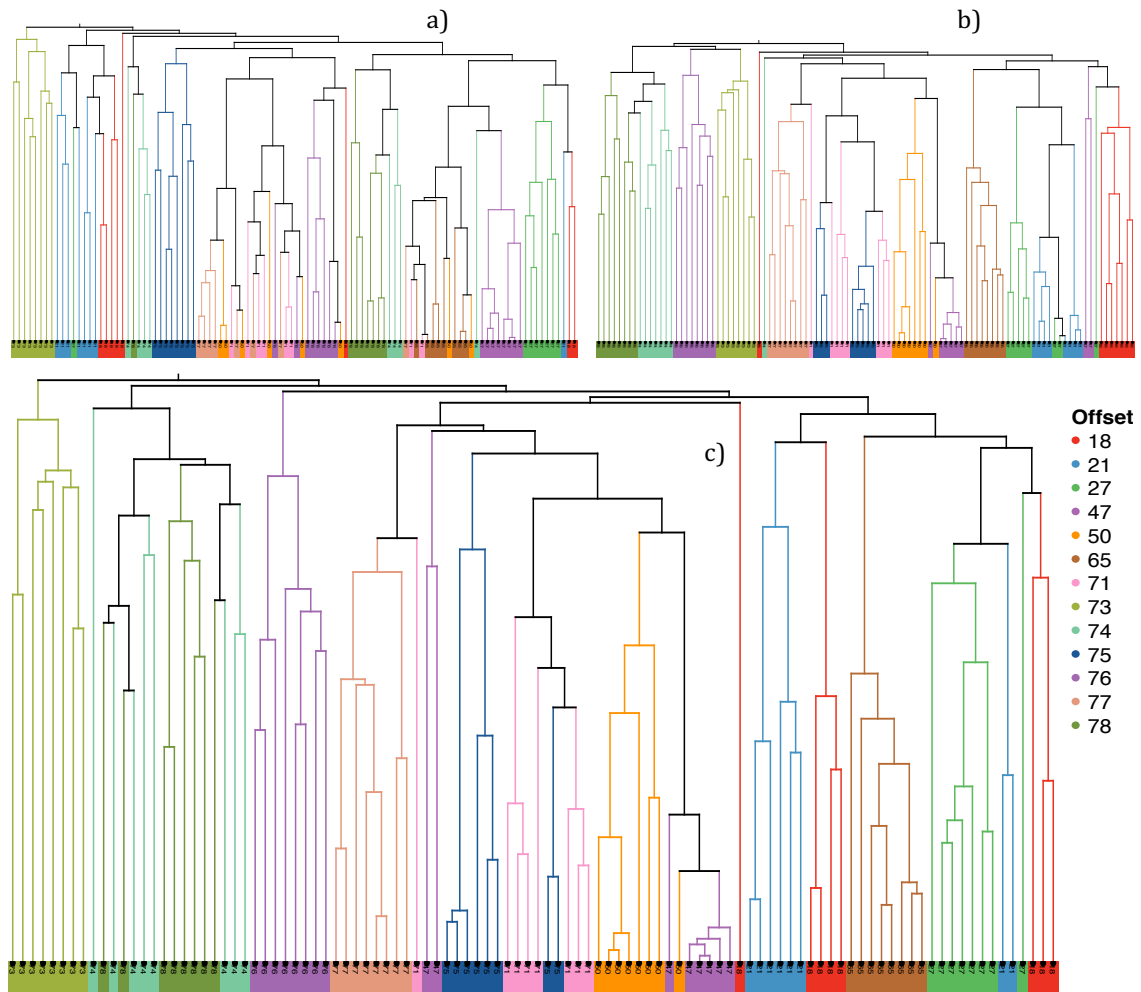


Figure 150. Hierarchical cluster analysis of offset samples by a) LIBS b) LA-ICP-MS c) fusion of LIBS and LA-ICP-MS.

Figure 150 is the constellation plot obtained from LIBS (a), LA-ICP-MS (b), and fusion of LIBS and LA-ICP-MS (c). OF 18 and OF 21 are branched in the same joint in the constellation plot for LIBS, similarly, OF 21 and OF 27 are clustered together in the plot for LA-ICP-MS, while they are well classified in their own joints after the fusion of LIBS and LA-ICP-MS. This is an example showing the utility of fusion of LIBS and LA-ICP-MS for the correct classification of offset printing inks.

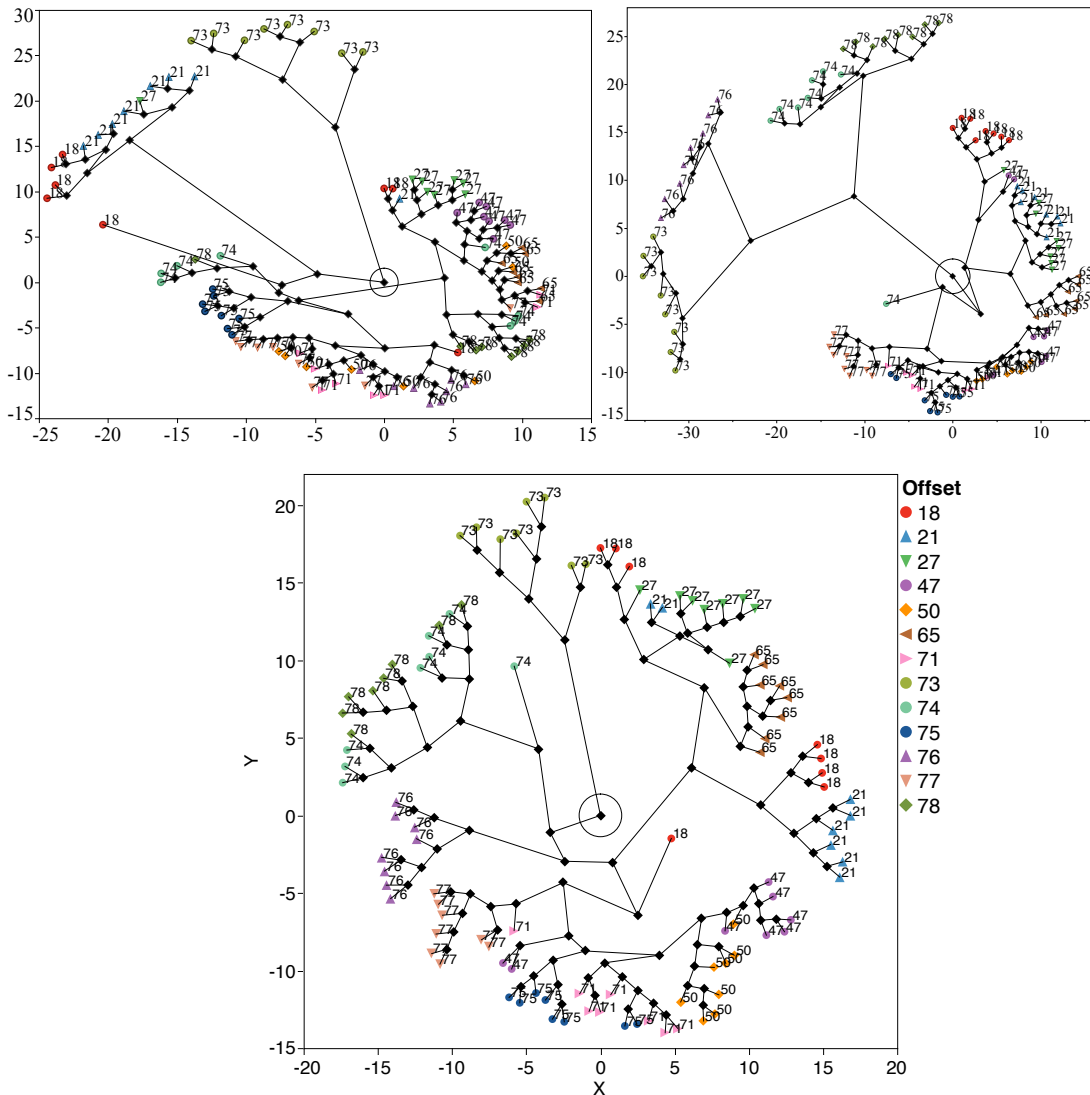


Figure 151. Constellation plot for offset samples by a) LIBS b) LA-ICP-MS c) fusion of LIBS and LA-ICP-MS.

6.6 Analysis of Controls in Tandem LIBS/LA-ICP-MS Study

Besides discrimination, association of the samples originating from the same source was also studied. Both Spectral Overlay and One-Way ANOVA showed no significant difference between the controls. Two controls were used for this study. One of the controls was an offset sample, OF 74, while the other control was 5,000ppm of Sr solution spiked on paper.

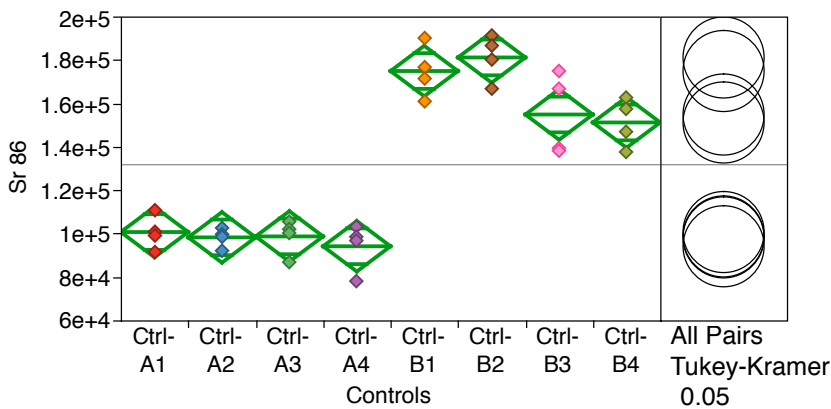


Figure 152. One-Way ANOVA for two controls for ^{86}Sr from mass spectrum.

One-Way ANOVA with Tukey's HSD test showed a significant difference between the two controls while no significant difference within the two controls.

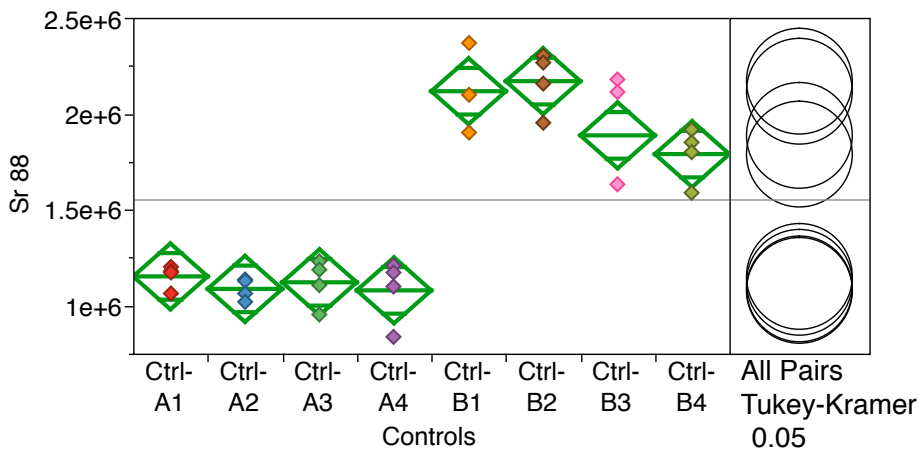


Figure 153. One-Way ANOVA for two controls for ^{88}Sr from mass spectrum.

Similar to mass spectrum, the emission spectrum from LIBS also produced spectra indistinguishable from each other for the same two controls. Figure 152 and Figure 153 are the One-Way ANOVA plots using the integrated peak areas of ^{86}Sr , and ^{88}Sr respectively from the mass spectrum.

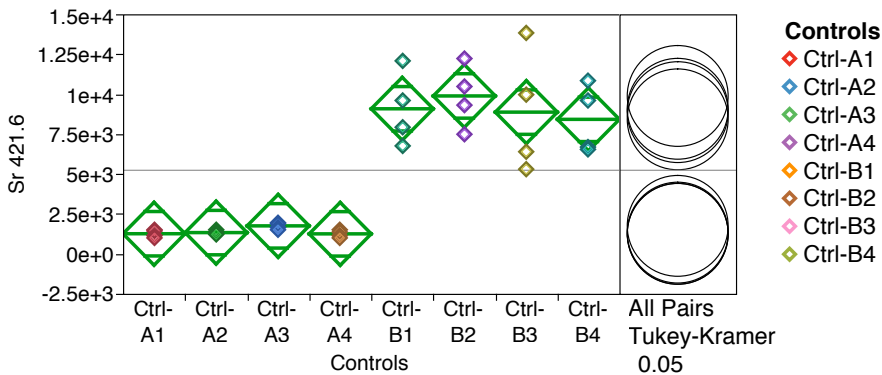


Figure 154. One-Way ANOVA for two controls for Sr 421nm emission line from LIBS.

The two emission lines at 407.8nm and 421.6nm provided unambiguous identification of Sr. One-Way ANOVA with Tukey’s HSD test was used to determine if there was any significant difference between the two. Figure 154 and Figure 155 show the One-Way ANOVA plots for two Sr controls. No significant difference was found between the controls providing a 100% correct association.

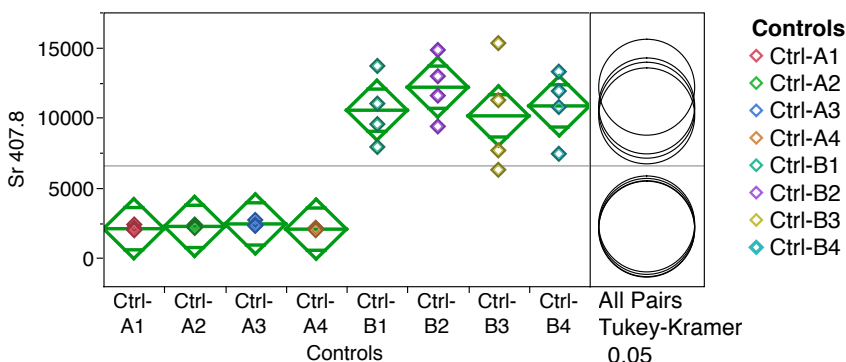


Figure 155. One Way ANOVA for two controls based on Sr 407.8nm emission line from LIBS.

6.7 Calibration Curves and Limit of Detections

The lack of standard reference materials for inks makes their quantitative analysis by LIBS and LA-ICP-MS a challenging task. A paper substrate (Whatman 42) that had only a few elements in low concentrations was chosen as a substrate. Standard solutions of different concentrations ranging from 100 to 1000ppm were prepared. One microliter of the standard solution was spiked on paper. The paper was left to dry overnight. Tandem LIBS/LA-ICP-MS was performed on the dried samples⁴¹.

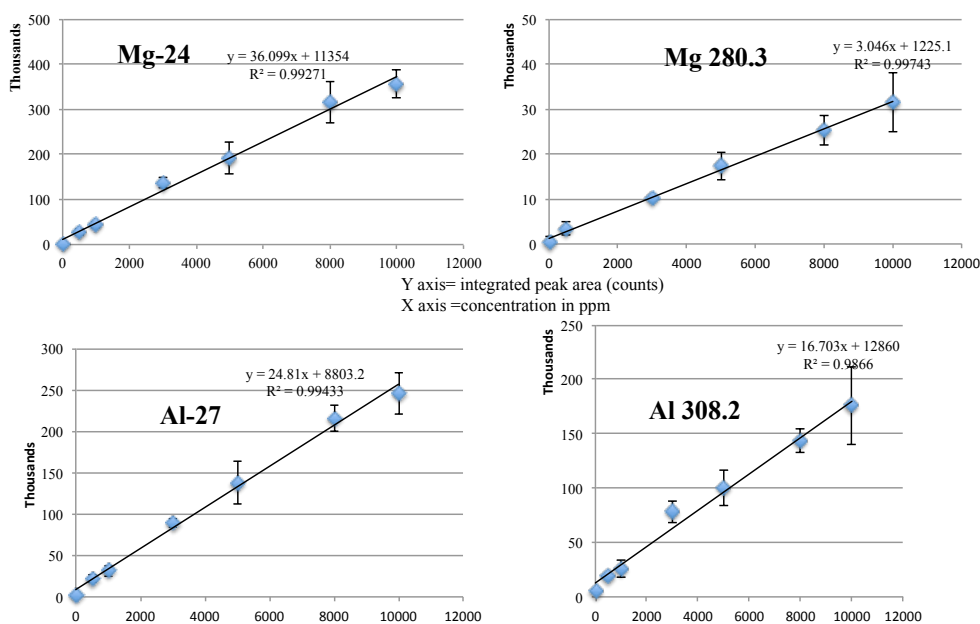


Figure 156. Calibration curves for Mg (top) and Al (bottom) from LA-ICP-MS and LIBS respectively in the tandem mode.

Calibration curves were built taking the integrated peak areas of the elements for both LIBS and LA-ICP-MS. These integrated areas were background subtracted prior to calibration curve analysis. The calibration curves for most of the elements were linear and reproducible. The R square values were higher than 0.97 for all elements as shown in Figure 156. The relative standard deviation was less than 10% for all of the elements.

The limits of detections were calculated as three times the standard deviation of blank. The obtained limits of detections ranged from subparts per million to parts per million for both LIBS and LA-ICP-MS as shown in Table 76⁴¹.

Table 76. Limits of detection for LIBS and LA-ICP-MS in tandem mode⁴¹.

Element	LA-ICP-MS (ppm)	LIBS (ppm)
Li	0.7	3.4
Na	79.2	36.4
Mg	17	32
Al	29.3	102.8
K	33.8	7.7
Ca	393.9	58.3
Mn	0.6	133.5
Fe	30.3	190.9
Ni	1.2	150.4
Co	0.2	38
Cu	9.9	61.3
Zn	5.5	94.3
Sr	4	7.2

The limits of detection for LA-ICP-MS obtained in tandem mode are at least one order of magnitude higher, as compared to the previous studies performed by using the standalone LA-ICP-MS¹⁰. The reason for this is the loss in the sensitivity of LA-ICP-MS due to the compromised parameters, so as to obtain a balanced situation for both LIBS and LA-ICP-MS. As expected, the obtained limits of detection for LA-ICP-MS were lower than LIBS for most of the elements. For some of the elements like K and Ca the limits of detection for LIBS are lower than that of LA-ICP-MS. This is because the most abundant isotopes have isobaric and polyatomic interferences from Argon, so the least abundant isotopes ³⁹K, and ⁴²Ca had to be used. Sr proved to be a good emitter in LIBS, and also was able to be detected in trace level in ICP-MS.

6.8 Data Fusion Using Machine Learning Algorithm and Chemometrics

Data fusion was accomplished using software developed by Covar Technology in collaboration with Applied Spectra. The software used was LIA-GUI (Laser Induced Acoustics, Graphic User Interface), which is available as MATLAB source code. The software utilizes Machine Learning algorithm and chemometrics for data fusion. The data fusion for LIBS and LA-ICP-MS was performed by taking the mean of the outputs of the PLSDA classifier for LIBS and LA-ICP-MS⁶. The following three steps were involved for the data fusion of LIBS and LA-ICP-MS.

- 1) PLS-DA (classifier) LIBS = PLS-DA (LIBS spectrum)
- 2) PLS-DA (classifier) LA-ICP-MS = PLS-DA (LA-ICP-MS) spectrum
- 3) Fusion Value = mean (PLSDA classifier LIBS spectrum, PLSDA classifier LA-ICP-MS spectrum)

Figure 157 shows an example of data fusion between LIBS and LA-ICP-MS. The database was populated with 17 offset samples for the tandem LIBS/LA-ICP-MS fusion study. Each sample had eight replicates. Four replicates were used to create a reference library while the remaining four were used as test samples.

The values on the 'X' axis of figure 157 refer to the inks present in the database. The length of the bars corresponds to the similarity score for a particular ink in x-axis. The higher the value of similarity index in y-axis, the more likely the reference sample would a 'match' to the test sample. The test sample in figure 157 is OF 74. OF 74 and OF 78 are two samples from the same manufacturer called Sunchemicals. They both are Magenta colored and have same set of elements when analyzed by standalone LA-ICP-MS. LIBS was found to be better at discriminating while being poor at associating the

similar inks together, while LA-ICP-MS was found to perform better in associating the inks sharing common origin and having similar elemental profile.

Test Sample OF-74

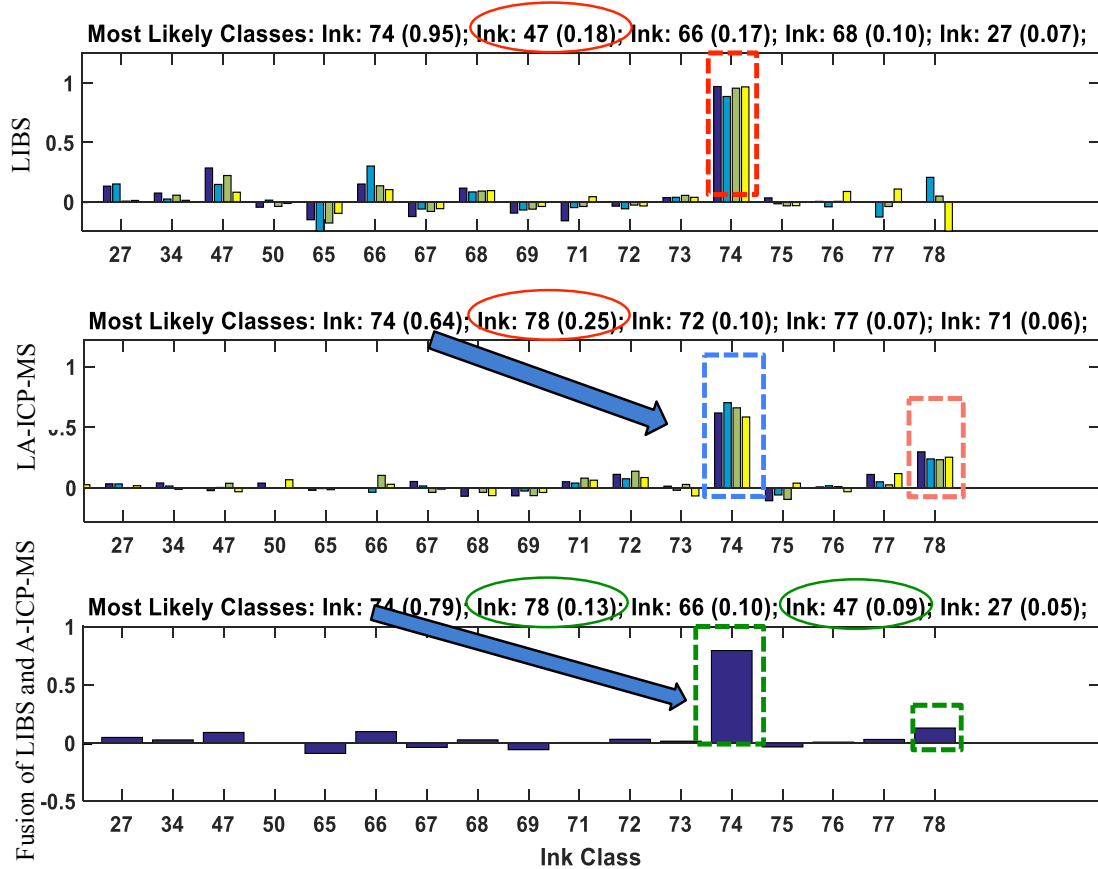


Figure 157. PLSDA plot showing the discrimination by LIBS (top), LA-ICP-MS (middle) and the fusion of LIBS and LA-ICP-MS (bottom).

The fusion also maximizes the separation between the two closely related pairs. OF-47 with a similarity score of 0.18 is found to be the second closest match to the test sample OF 74 by LIBS analysis, but the similarity score decreases to 0.09 for OF 47 after fusion. Similarly, the closely related sample OF-78, with a similarity score of 0.25 when analyzed by LA-ICP-MS alone, has a decreased score of 0.13 after the fusion. Thus the

fusion has helped to maximize the separation between the two closely related pairs and provide an unambiguous identification of the test sample.

6.8 Overall Results from Tandem LIBS/LA-ICP-MS Study of Printing Inks

LIBS and LA-ICP-MS have been successfully used in tandem for the first time for the analysis of printing inks. Qualitative and semi- quantitative tandem LIBS-LA-ICP-MS methods have been developed, optimized, and tested for the elemental and isotopic analysis of printing inks. For those particular printing inks, having similar elemental LA-ICP-MS profile, LIBS was successful to detect those elements that were difficult to monitor using the quadrupole ICP-MS⁴¹.

All the four sets of inks have different elemental compositions that largely depend on the source of manufacture. The results show that major, minor, and trace elements present in the ink samples can serve as discriminators. LIBS provided complementary information to LA-ICP-MS through the detection of those elements that suffer from isobaric and polyatomic interferences in quadrupole ICP-MS.

For those samples known to produce indistinguishable LA-ICP-MS spectra (very similar formulations), the ability of LIBS to detect the major and minor elements can provide additional discrimination over a discrimination using only LA-ICP-MS. LIBS has higher detection limits, meaning that it cannot detect elements at trace level. LA-ICP-MS can overcome this weakness by detecting trace elements. The combination has proved to be mutually beneficial and more representative for the elemental characterization of printing inks. The overall result is summarized in Table 77.

Table 77. Overall discrimination for LIBS and LA-ICP-MS and their fusion for four printing ink types⁴¹.

		% Discrimination		
Ink type	Number of samples	LIBS	LA-ICP-MS	Tandem (fusion of) LIBS/LA-ICP-MS
Toners	9 (36 comparison pairs)	100%	66.60%	100%
Inkjets	10 (45 comparison pairs)	97.80%	91.10%	100%
Offsets	13 (78 comparison pairs)	92.42%	90.90%	100%
Intaglios	12 (66 comparison pairs)	87.88%	96.97%	98.50%

6.9. Normalization of LA-ICP-MS Spectrum Using LIBS Spectrum

LIBS and LA-ICP-MS have been successfully used for the chemical analysis of different materials of forensic interest. Both of these laser based analytical tools when used in tandem have synergistic effect. LIBS provides multiple interference free emission lines for elements that suffer from isobaric and polyatomic interferences in a quadrupole mass analyzer (for e.g., Ca, Si, K, Fe) while LA-ICP-MS can detect trace elements that are beyond the detection limits of LIBS, in addition to providing isotopic information, thus both techniques complement each other when used in tandem. The major disadvantages of LA-ICP-MS are the shot to shot laser fluctuations which alters the ablation yield and increases the Relative Standard Deviations (RSDs) making the quantitative analysis very difficult. Similarly, for LIBS in addition to the laser shot to shot fluctuation, instability of the spectroscopic plasma signals, is another issue which also makes the quantitative study by LIBS very challenging. In the present study, NIST

glass standards (NIST 610, 612, 1831, FGS1 and FGS2) have been analyzed for the first time by tandem LIBS-LA-ICP-MS. The present study shows another important utility of a tandem LIBS/LA-ICP-MS where the LA-ICP-MS signal obtained from ^{29}Si (element present at the highest concentration) can be used for the normalization of LIBS data. Similarly, one of the emission lines from an element, having low self-absorption coefficient in the LIBS spectrum (Si 288.1nm), can be used as an internal standard to normalize LA-ICP-MS spectrum.

6.9.1 Optimization of Tandem LIBS/LA-ICP-MS for the Analysis of Glass Samples

Different parameters for glass were optimized for the tandem LIBS/LA-ICP-MS study. Similar to the tandem analysis of printing inks, parameters like laser output energy, gate delay, scanning speed, carrier gas flow were optimized. The most important parameter for LIBS was finding the correct gate delay, as it affects both the signal intensity, and the signal to noise ratio. Parameters were optimized based on their intensities, signal to noise ratio, and the precision. Figure 158 shows that a gate delay of $0.1\mu\text{s}$ provides the highest intensities for elements like Na, Al, K, Ca and Fe. Signal intensities in LA-ICP-MS were not affected by the change in gate delay.

It was found that use of Argon gas increased the signal intensities in LIBS about four times compared to when no gas or air was used. Higher flow of Argon gas was favorable for LIBS, but signal suppression in LA-ICP-MS was detected at higher flows. The optimized gas flow was found to be 0.6L/min for LA-ICP-MS as shown in Figure 159.

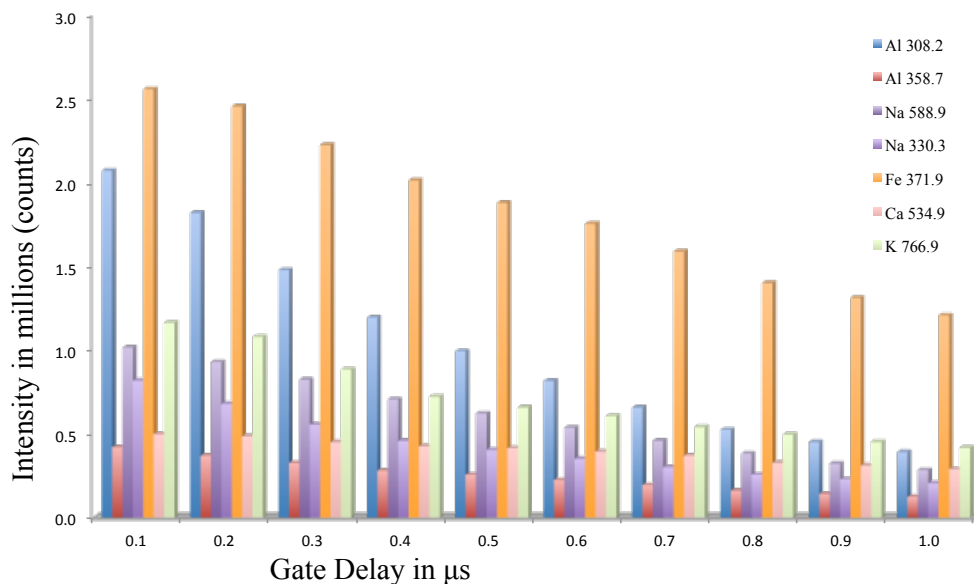


Figure 158. Variation of emission intensities with gate delay for LIBS.

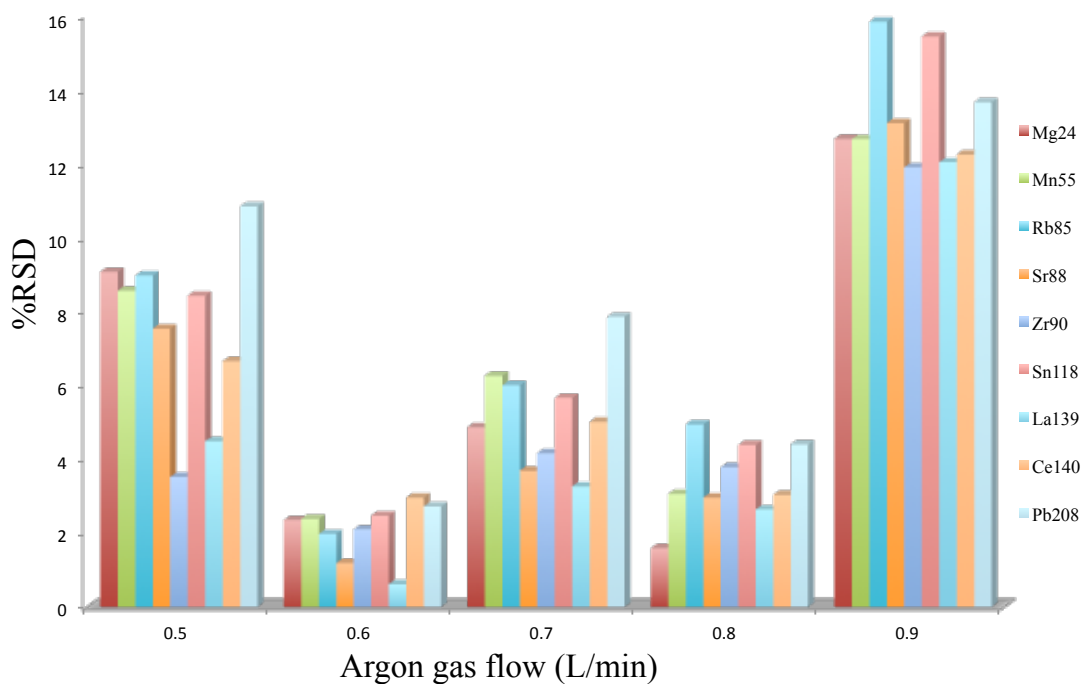


Figure 159. Optimization of Helium gas flow through precision analysis.

The optimized parameters for the analysis of glass by tandem LIBS/LA-ICP-MS are summarized in Table 78.

Table 78. Optimized parameters for the analysis of glass by tandem LIBS/LA-ICP-MS.

Laser energy	20%
Frequency	5 Hz
Spot size	200um
Ablation rate	150um/s
Gate Delay	0.1us
Ar flow rate	0.6/0.6 Lmin-1
Number of shots	168

6.9.2 Silicon as an Internal Standard

Silicon is present in high percentage in glass in the form of Silicon dioxide. More than 70% of the total glass is composed of Silicon dioxide. Any change in the laser energy is accompanied by the similar change in the amount of Silicon removed from the glass. Thus the mass of different elements removed from the glass is correlated to the mass of Silicon removed during the laser ablation. Figure 160 shows the correlation between different elements like Al, K, Mg and Sr with Si for NIST 1831.

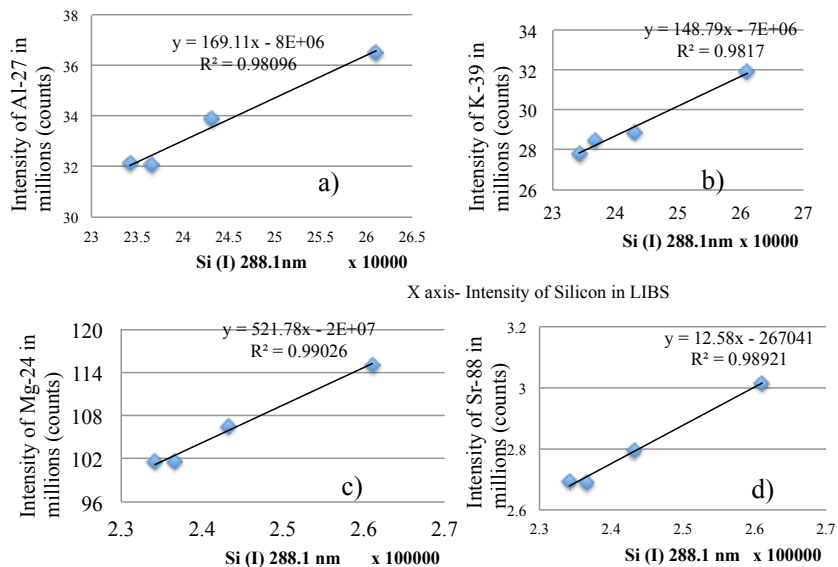


Figure 160. Correlation plot for a) ^{27}Al b) ^{39}K c) ^{24}Mg d) ^{88}Sr with Si (I) 288.1 line.

6.9.3 Normalization of LA-ICP-MS Spectra Using Si 288.1nm

Silicon emission line at 288.1nm was used to monitor the amount of Si ablated from glass. All the peaks in the mass spectrum were normalized to Si 288.1nm. The precision was improved for LA-ICP-MS (RSDs' below 5% for most of the elements) maintaining a good linearity in the calibration curves (R^2 values > 0.95). The concentration of Hafnium was close to detection limit, so the precision was found to be the least for it as shown in figure 161. The values in parentheses in X axis are the concentration of respective elements in ppm. The differences in precision before and after normalization are shown in Figure 161.

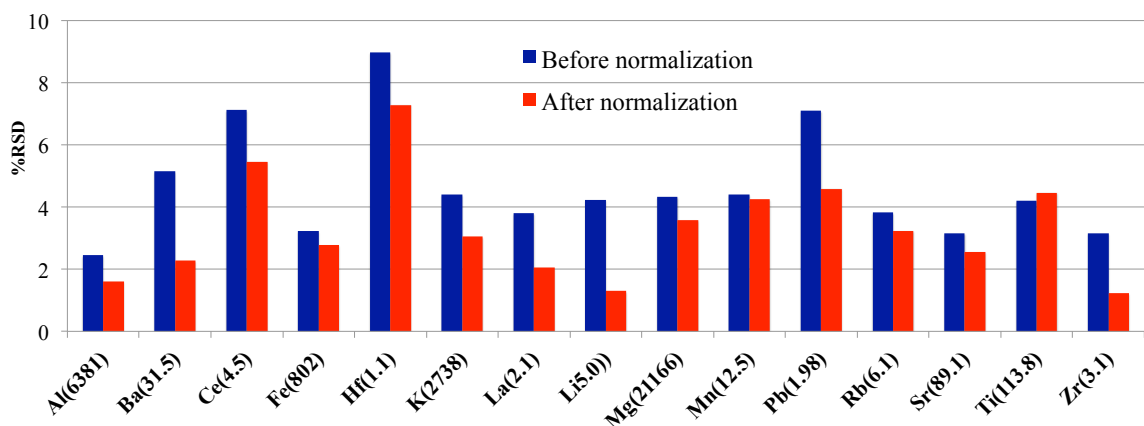


Figure 161. Bar graph showing the Relative Standard Deviations before and after normalization for elements in mass spectrum for NIST 1831.

Similar results were also obtained for NIST 610 glass standards as shown in Figure 162.

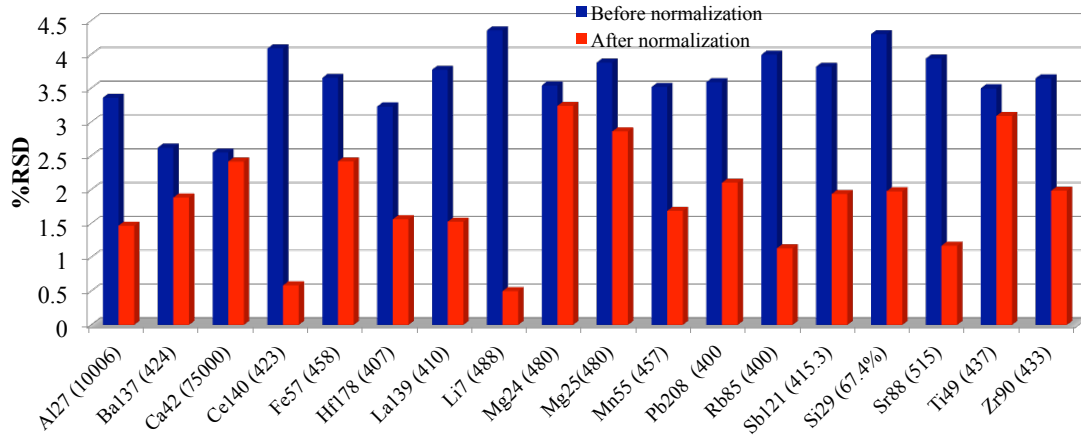


Figure 162. Bar graph showing the Relative Standard Deviations before and after normalization for elements in mass spectrum for NIST 610.

6.9.4 Comparison with the Standard Test Method for Glass Analysis by LA-ICP-MS

The RSD's obtained after normalization were compared to those obtained from Standard Test Method for Determination of Trace Elements in Soda-Lime Glass Samples Using Laser Ablation Inductively Coupled Plasma Mass Spectrometry for Forensic Comparisons also known as E2927⁷⁷.

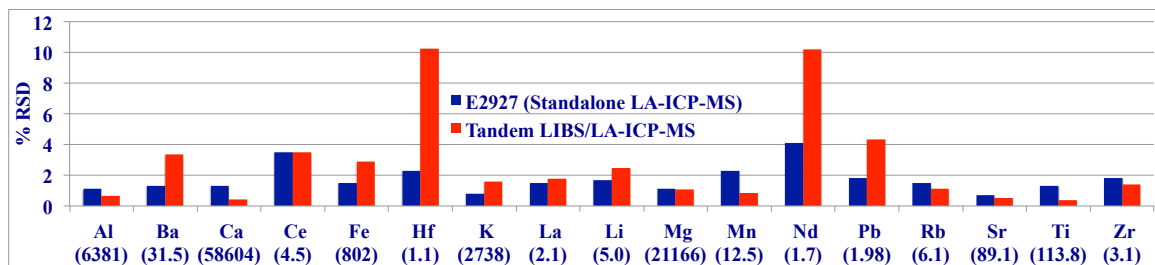


Figure 163. Comparison of RSDs obtained from Tandem method with the Standard method for NIST 1831 by LA-ICP-MS.

It can be seen from Figure 163 and Figure 164 that RSDs are below 5% for all of the elements in tandem mode for both NIST and FGS glass standards. The precision obtained after normalization to LIBS are comparable to those obtained from the standard method for the analysis of glass using LA-ICP-MS.

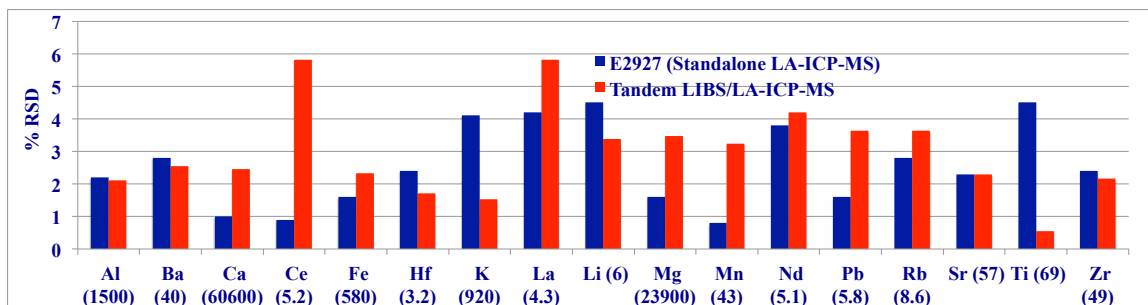


Figure 164. Comparison of RSDs obtained from Tandem method with the Standard method for FGS1 glass analysis.

The precision for LIBS was below 6% for most of the elements in the tandem mode. Figure 165 shows the precision in terms of RSD for different elements in NIST and FGS glass standards by LIBS in the tandem mode.

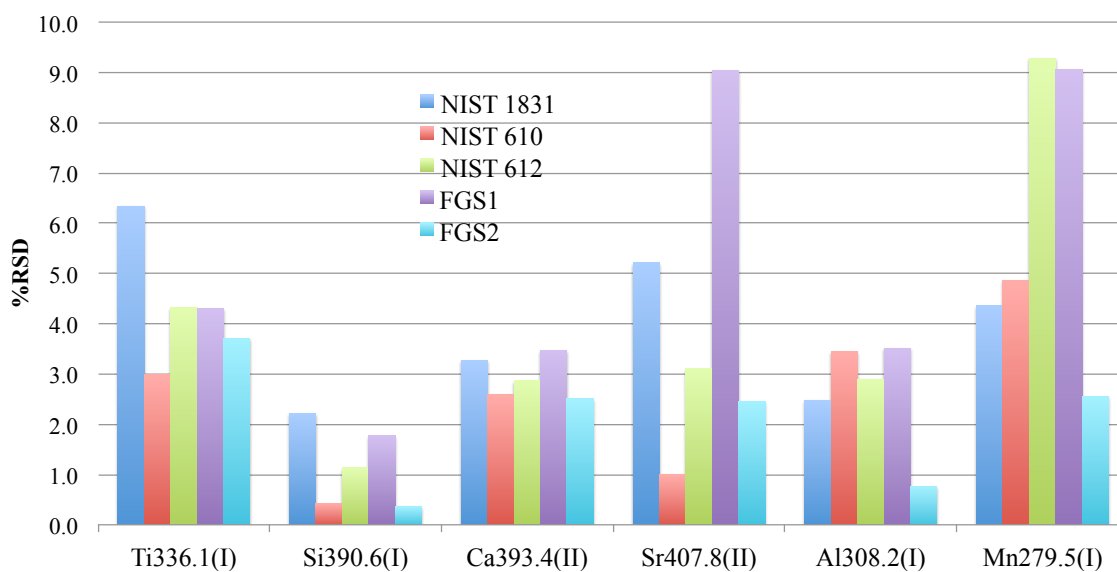


Figure 165. Bar graph showing the Relative Standard Deviations for elements in LIBS spectrum for NIST and FGS glass standards.

6.9.5 Conclusion

Shot to shot fluctuations in laser energy is one of the primary factors for sacrificing precision for both LIBS and LA-ICP-MS. Silicon, being the most abundant element in glass, served as a good internal standard for normalization of both LIBS and LA-ICP-MS spectrum. The precision was improved for LA-ICP-MS (RSDs' below 5% for most of the elements) maintaining a good linearity in the calibration curves (R^2 values > 0.95). The precision obtained by normalization using tandem LIBS-LA-ICP-MS when compared to the ASTM method for glass analysis (E2927) by LA-ICP-MS (standalone) was found to be comparable for some of the elements. Similarly, RSDs' were found to be below 6% for most of the elements in LIBS spectrum proving that the tandem method is mutually beneficial for both LIBS and LA-ICP-MS.

Chapter 7. Contamination Study Using Tandem LIBS/LA-ICP-MS

Sodium and Potassium are two important elements for discriminating printing inks. However, these elements are also present in human sweat and can be transferred to the ink samples if they are not handled with care. This can lead to erroneous results and false discrimination. In order to evaluate the effect of contamination on inks by manipulation with bare hands and sweated hands, a contamination study was performed for printing inks. The contaminated inks were subjected to the tandem LIBS-LA-ICP-MS using the optimized parameters for the respective inks types and compared with the uncontaminated samples.

7.1 Sample Preparation

Two printing inks, an inkjet (IN 47), and a toner (TN 21) were used for the contamination study. For inkjet ink, 5 μ l of the liquid ink was deposited on Whatman paper (Grade 42) and was left for drying at room temperature. For toner, a small amount of toner powder was carefully rolled on to a paper substrate, mounted over a glass slide, and was allowed to melt at 180 degree centigrade. The melted ink was then homogeneously smeared around the Whatman paper. These two untouched inks (NT) were then contaminated in two different ways. One way of contaminating the inks was by touching them with bare hands from multiple people (MT), and the other way of contamination was through the application of sweat from a marathon runner after running five miles (ST).

7.2 Method Optimization

The optimized parameters are listed in Table 79. The listed optimized parameters provided the best values for signal, signal to noise ratio, precision, and also resulted in minimum damage to the paper substrate. Data normalization was achieved by dividing the peak intensity at each data point by the sum of the total intensities of all the data points in the spectrum.

Table 79. Optimized parameters for the analysis of toners and inkjets by tandem LIBS/LA-ICP-MS.

Parameters	Inkjets	Toners
Ablation mode	Single line	Single line
Laser spot size	200 μm	200 μm
Frequency	0.8Hz	1.8Hz
Laser Energy	40% (7.8mJ)	70% (13mJ)
Ablation rate	50 $\mu\text{m/s}$	40 $\mu\text{m/s}$
Gate Delay	0.1 μs	0.8 μs
Argon flow in the cell	0.90L/min	0.60L/min

7.3 Results and Discussion

The combination of LIBS and LA-ICP-MS in a single set up resulted in two distinct fingerprint spectra providing information from atomic/ionic emissions and isotopic composition (m/z) for each ink sample. The concentration of ^{23}Na was found to be different for both toners and inkjets handled in three different ways as shown in Figure 166. It was found to be present in the highest concentration in the inks heavily contaminated with sweat followed by the ink handled with many hands. Similarly, K was

detected by LIBS and found to be at higher concentrations in both the contaminated inks (MT and ST) as compared to the untouched ones (NT) as shown in Figure 167.

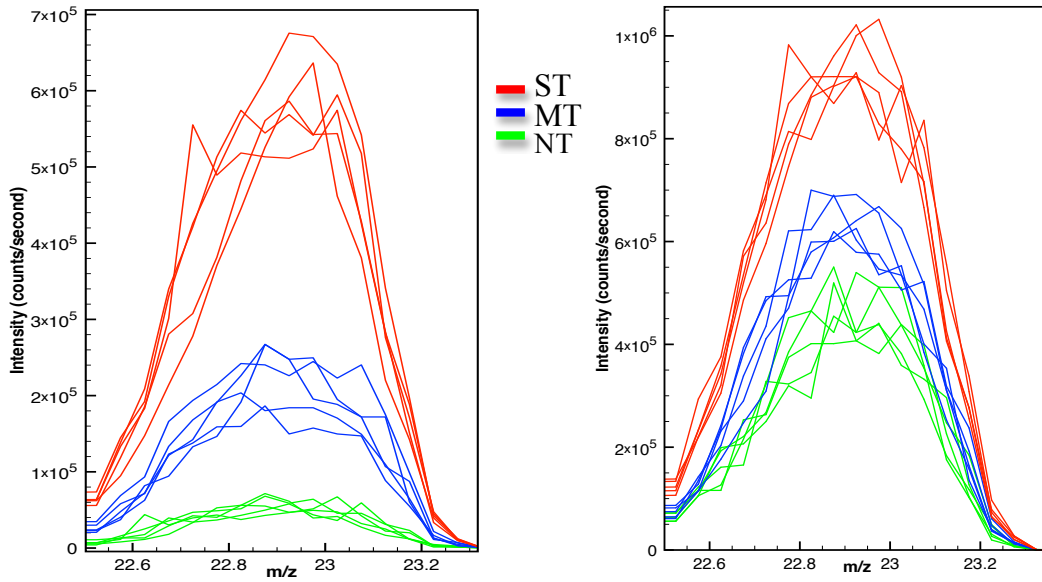


Figure 166. Spectral Overlay of ²³Na peaks for contaminated and clean toners (right) and inkjets (left).

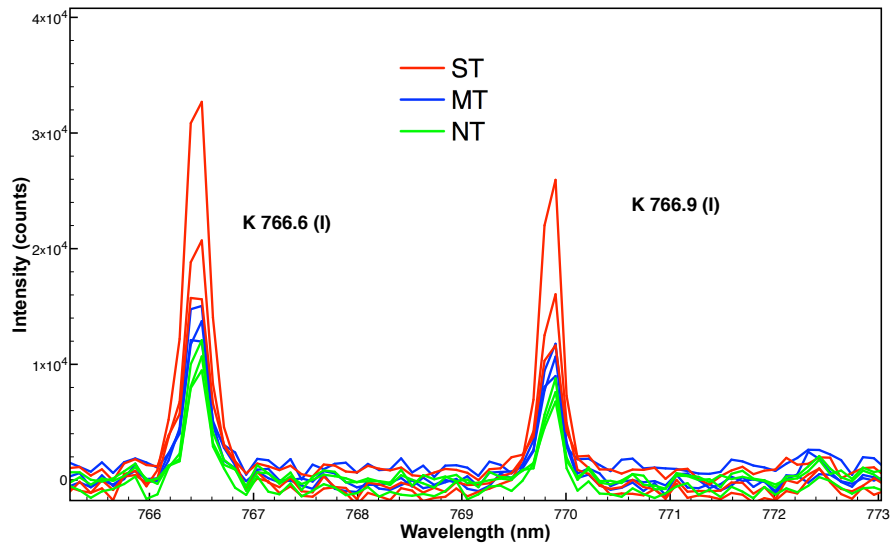


Figure 167. Spectral Overlay of K emission lines for contaminated and clean toners.

Since normalization of all the peaks was done using the sum of all the peaks in the spectra, a significant decrease in the intensity of other elements was detected in the spectra, a significant decrease in the intensity of other elements was detected in the contaminated inks due to the increase in ^{23}Na concentration. Figure 168 shows the intensity of ^{48}Ti for the three ink types, which is found to be very high in the untouched inks (NT), as it has low ^{23}Na concentration, while other inks (MT and ST) have lower intensities of ^{48}Ti due to their high ^{23}Na concentration.

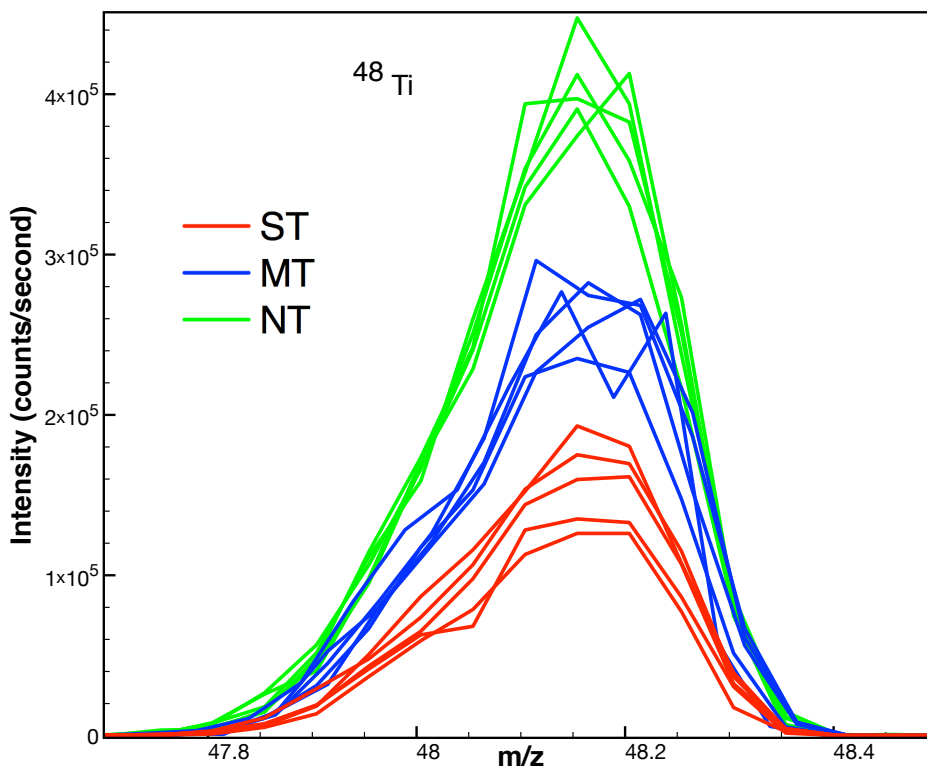


Figure 168. Variation of ^{48}Ti peaks in contaminated and pristine toners.

On removing the contribution from ^{23}Na and ^{39}K , ^{48}Ti was found to have similar peak profile for NT, MT and ST inks. The Spectral Overlay plot shows that all the replicates of NT, MT and ST inks overlap with each other after the removal of these contaminants as shown in figure 169.

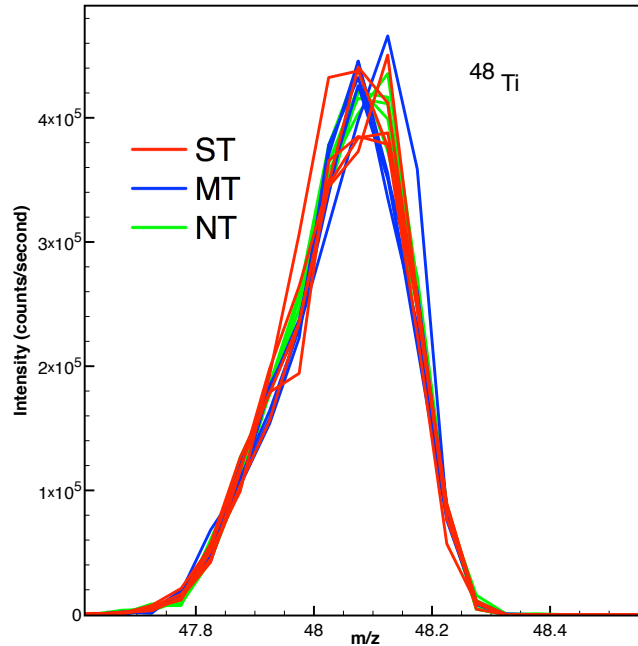


Figure 169. Ti peaks in contaminated and clean toners after removing the contribution from Na and K.

7.4 Statistical Analysis of Contaminated and Clean Printing Inks

One Way-ANOVA, Principal Component Analysis, Canonical Correlation analysis were performed on the contaminated and untouched inks for comparison. These tests detected significant differences between the three types of inks.

7.4.1 One-Way ANOVA for Contaminated and Clean Printing Inks

One-Way ANOVA with Tukey's HSD test was performed on these three types of inks. One Way ANOVA with Tukey's HSD test revealed significant difference between these inks based on the concentration of Na as shown in Figure 170 and 171 for toners and inkjets respectively.

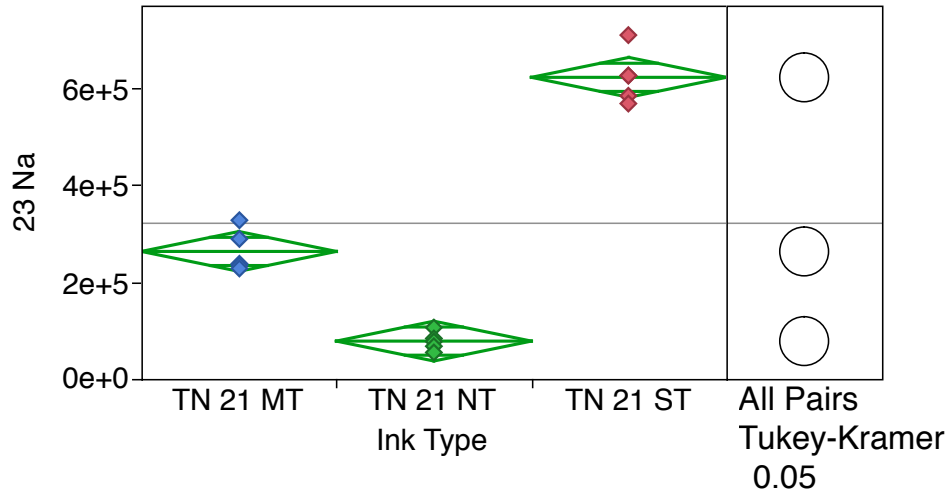


Figure 170. One Way ANOVA plot for contaminated and clean toner by ^{23}Na .

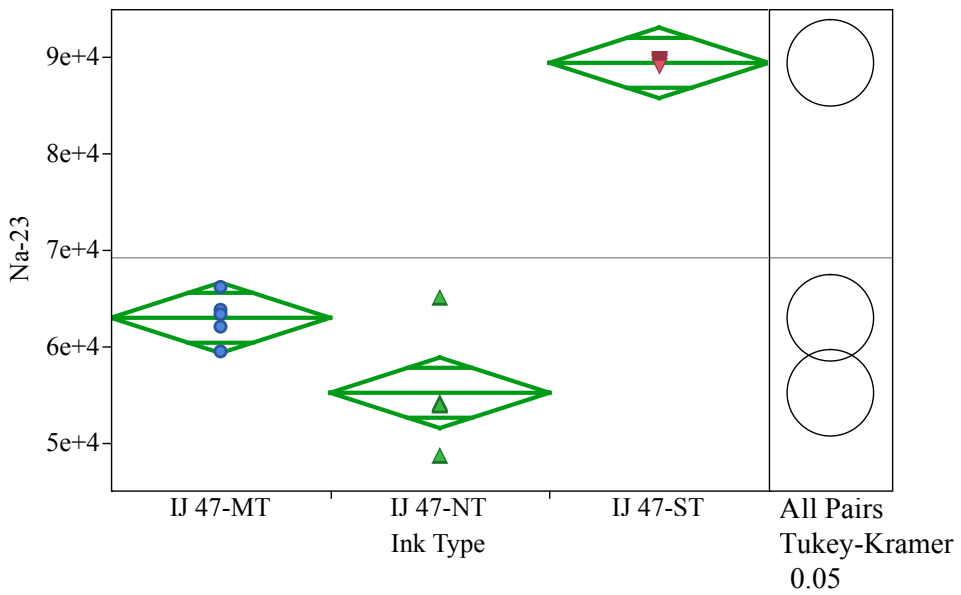


Figure 171. One Way ANOVA plot for contaminated and clean inkjet samples by ^{23}Na .

Similarly, concentration of Ti in the three types of inks was found to be different. One-Way ANOVA with Tukey's HSD test showed a significant difference in the concentration of Ti among the three inks. It was found to be in the highest concentrations in clean samples compared to the contaminated ones as shown in Figure 172.

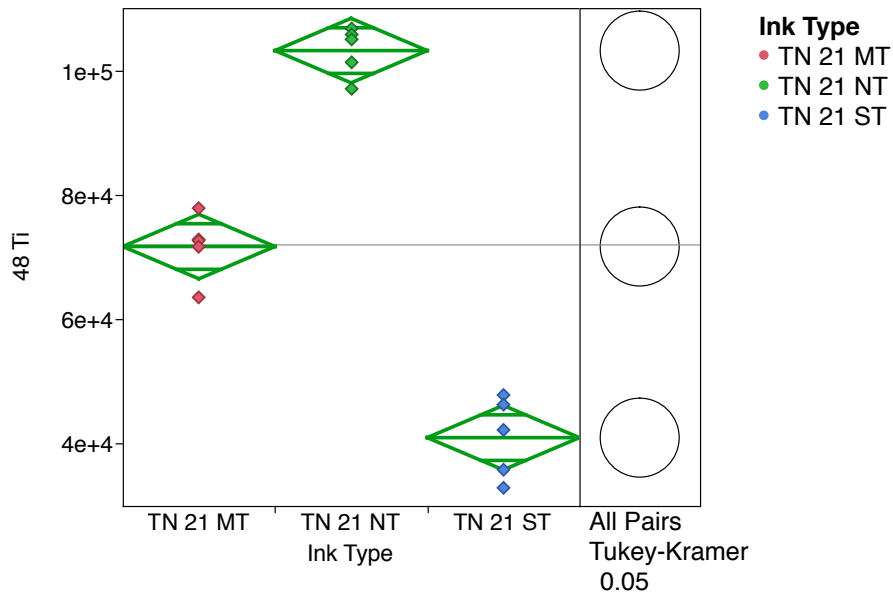


Figure 172. One Way ANOVA plot for contaminated and clean toner inks by ^{48}Ti .

After removing the contribution from Na and K, Ti peaks in all the three types of inks were found to be similar and no significant difference between them was detected as shown in Figure 173. It suggested that, the presence of Na and K as contaminants can affect the concentration of other elements.

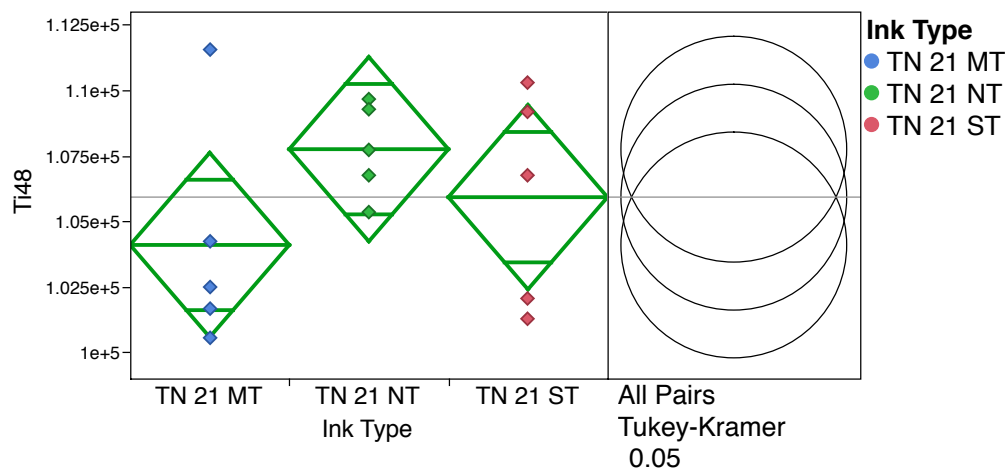


Figure 173. One Way ANOVA plot for contaminated and clean toner inks by ^{48}Ti after removing the contribution from Na and K.

7.4.2 Principal Component Analysis of Contaminated and Clean Printing Inks

PCA was performed after the data fusion of LIBS and LA-ICP-MS for all the three types of inks. PCA also showed a clear separation of three distinct classes of inks as shown in Figure 174. The three ellipses in Figure 174 indicated three different classes of same inkjet 47.

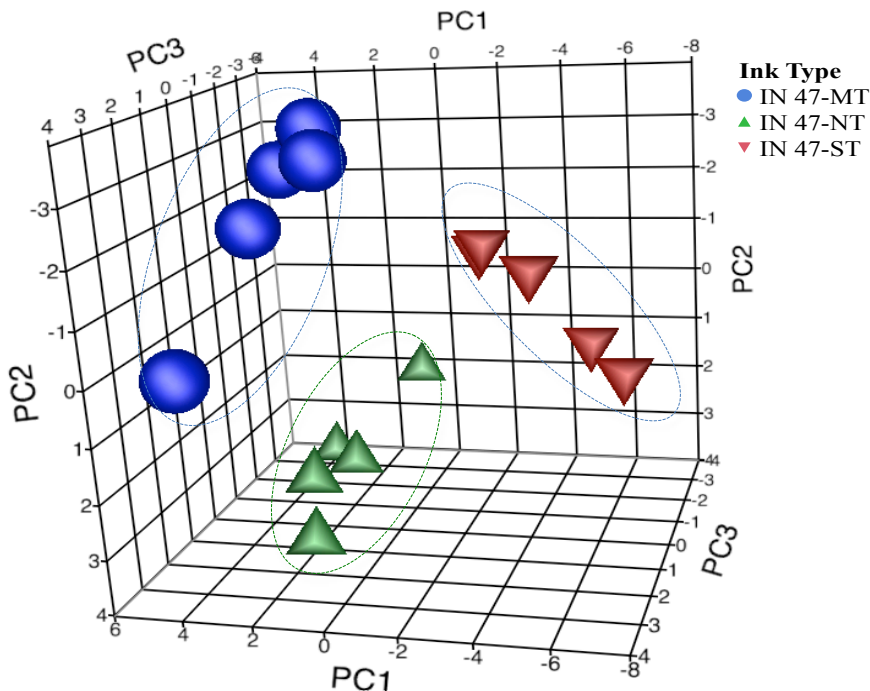


Figure 174. Three-dimensional PCA plot for contaminated and clean inkjets.

7.4.3 Cluster Analysis for contaminated and clean printing inks

Hierarchical Cluster analysis was performed on the contaminated and clean printing inks. Three separate clusters were detected for three differently contaminated inks as shown in Figure 175. This suggested that contamination might cause the misclassification of the ink when elements like Na and K are used for the discrimination purpose.

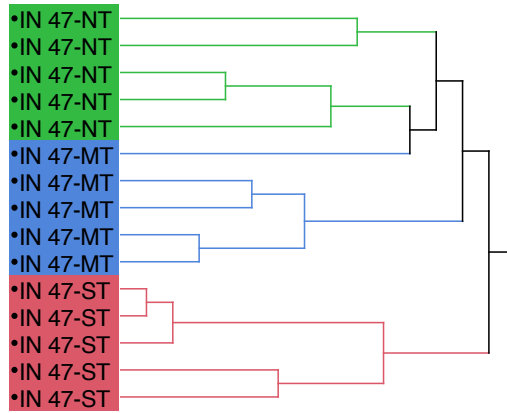


Figure 175. Hierarchical cluster analyses for contaminated and clean inkjet printing inks.

7.4.3 Canonical Correlation Analysis of Contaminated and Clean Printing Inks

The canonical analysis was performed after data fusion of LIBS and LA-ICP-MS for the contaminated and clean inks. Figure 176 represents the three dimensional Canonical plot for toners and inkjets. Six distinct classes can be seen in the canonical plot for two types of inks, Inkjet 47 and TN 21.

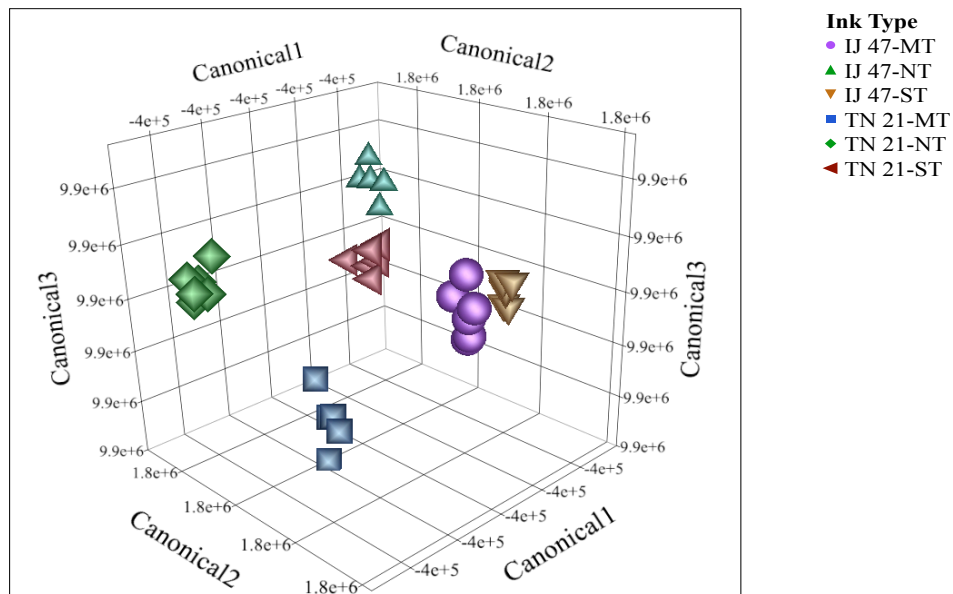


Figure 176. Three-dimensional Canonical Plot for toners and inkjets.

7.5 Conclusion

The present study shows that both Na and K could be incorporated into inks through contamination. These elements shouldn't be taken into account for discrimination purposes if the inks are handled with bare hands or are contaminated with sweat. The results from contamination study showed a significant difference in the intensities of Na and K for the three inks. One-Way ANOVA also showed a distinct effect of contamination from other elements like Ti. Principal Component Analysis (PCA) analysis also showed three distinct classes of manipulated inks. The examination of contaminated inks suggests that these elements should be closely monitored and avoided for discrimination purposes, unless their magnitude of difference is significantly larger from the observed threshold level of hand-manipulation contamination, and therefore can be attributed to truly differences in their formulations. In the present study of four different types of printing inks (319 total) the contamination of the inks was carefully avoided. Toners and inkjets were either printed or extracted in the purest form from the inner ink cartridge using dedicated gloves and clean sample preparation area. For intaglio and offset printing inks, the paper background was also subtracted. The rationale behind the paper subtraction was that any contamination in the ink is also followed by the contamination in the paper. Thus the subtraction of paper background ensured the subtraction of any possible contaminants in the ink.

Chapter 8. Summary

Toners, inkjets, intaglio and offset printing inks were found to have different elemental composition depending upon their source of manufacture. Major, minor and trace elements present in these ink samples serve as good discriminators when a high degree of certainty is sought. A total of 319 different inks were analyzed by standalone LA-ICP-MS. It provided information about the major, minor, and trace elements that were present in the printing inks. LA-ICP-MS itself provided more than 99% discrimination for four different types of inks.

Due to the higher detection limits of LIBS compared to LA-ICP-MS, it was able to provide information mainly about the major and minor elements present in inks. The detection of trace elements by LA-ICP-MS and the simultaneous detection of major and minor elements (which suffer from isobaric and polyatomic interference in ICP), by using LIBS proved to be a useful concept for the representation of an overall chemical profile of printing inks. A novel tool that combines the benefits of two individual sensors (LIBS and ICP-MS) was successfully set up and used for the analysis of printing inks for the first time. Successful development, optimization, and testing of qualitative and semi-quantitative tandem LIBS-LA-ICP-MS methods were performed for the elemental and isotopic analysis of four different types of printing inks. Particularly, for those samples known to produce indistinguishable LA-ICP-MS spectra (very similar chemical formulations), the tandem method provided rich elemental information by exploiting the ability of LIBS to detect the major and minor elements that suffered from interferences in LA-ICP-MS. This resulted in additional discrimination over a discrimination using

standalone LA-ICP-MS. For the four different types of inks, it was found that the application of LIBS was successful to overcome the spectral interferences of ICP-MS for the elements K, Ca, Si, and Fe, which proved to be good discriminators. The synergy between LIBS and LA-ICP-MS has provided complementary information, and enhanced the discrimination for all four types of inks.

Contamination of inks can significantly alter the results of ink analysis. Elements like Na and K, which are present in human sweat, could be transferred to ink by contact. Spectral Overlay and Multivariate Statistical Analysis both showed a significant difference in the concentration of these elements in contaminated inks. The concentration of other elements present in the inks was also affected as a consequence of contamination. The examination of contaminated inks suggested that elements like Na and K have to be closely monitored before using them for discrimination purposes.

The present study illustrates another important utility of tandem LIBS/LA-ICP-MS where the signal of one of the elements present in higher concentration in LIBS can be used to normalize the LA-ICP-MS spectra. The precision was improved after normalization. This also ameliorates the laser (energy) shot to shot fluctuation during the laser ablation and enhances the precision of the measurement.

In summary, LIBS and LA-ICP-MS, despite their inherent limitations have been used as standalone sensors for the discrimination of a variety of matrices including printing inks. The fusion of these two sensors into a single setup not only ameliorated the drawbacks of both techniques but also provided additional discrimination.

8.1 Future Directions of the Research Work

In the present research, printing inks and papers were analyzed by LIBS, LA-ICP-MS and tandem LIBS/LA-ICP-MS. The use of controls for each type of printing ink and their correct association validated the consistent instrument performance and the normalization of the spectrum to the total sum of the peaks addressed the matrix effects to some extent. However, the use of an internal standard or matrix match standards, would have resulted a more quantitative analysis of the inks.

The analysis of four different types of inks, namely toners, inkjets, intaglio and offsets showed that different kinds of elements are present in each of these four inks. These elements can be used to create an element menu for the ink standards. Matrix matched standard for printing inks and the use of a suitable internal standard that behaves in a similar way, as the analyte of interest would be the future work for this project. In the present study, all the inks were paper background subtracted to remove the paper contribution and also to avoid the contamination. It was hypothesized that any contamination in the ink is also followed by the contamination on paper; however, ink and paper are two different types of matrices. To better understand the extent of contamination on ink and paper a more detailed study of contamination of the individual matrices (ink and paper) is recommended for future work.

REFERENCES

1. Klockenkämper, R.; Von Bohlen, A.; Moens, L., Analysis of pigments and inks on oil paintings and historical manuscripts using total reflection x-ray fluorescence spectrometry. *X-ray Spectrometry* **2000**, *29* (1), 119-129.
2. Zięba-Palus, J.; Kunicki, M., Application of the micro-FTIR spectroscopy, Raman spectroscopy and XRF method examination of inks. *Forensic Science International* **2006**, *158* (2), 164-172.
3. Kaur, N.; Jasuja, O. P.; Singla, A. K., Thin layer chromatography of computer printer ribbon inks. *Forensic Science International* **1992**, *53* (1), 51-60.
4. Polk, D.; Attard, A.; Giessen, B., Forensic characterization of papers. II: determination of batch differences by scanning electron microscopic elemental analysis of the inorganic components. *Journal of Forensic Sciences* **1977**, 524-533.
5. Egan, W. J.; Galipo, R. C.; Kochanowski, B. K.; Morgan, S. L.; Bartick, E. G.; Miller, M. L.; Ward, D. C.; Mothershead II, R. F., Forensic discrimination of photocopy and printer toners. III. Multivariate statistics applied to scanning electron microscopy and pyrolysis gas chromatography/mass spectrometry. *Analytical and Bioanalytical Chemistry* **2003**, *376* (8), 1286-1297.
6. Trejos, T.; Torrión, P.; Corzo, R.; Raeva, A.; Subedi, K.; Williamson, R.; Yoo, J.; Almirall, J., A novel forensic tool for the characterization and comparison of printing ink evidence: development and evaluation of a searchable database using data fusion of spectrochemical methods. *Journal of Forensic Sciences (Accepted and in Press)* **2015**.
7. Ikezawa, S.; Wakamatsu, M.; Ueda, T. In *Quantitative analysis of silver nanoparticle ink using laser-induced breakdown spectroscopy*, Sensing Technology (ICST), 2011 Fifth International Conference on, IEEE: **2011**; pp 1-5.
8. Koenig, A., Direct Elemental Analyses of Ink on Paper by Laser Ablation ICP-MS. *Laser* **2003**, *24* (88Sr), 12C.
9. Oujja, M.; Vila, A.; Rebollar, E.; García, J.; Castillejo, M., Identification of inks and structural characterization of contemporary artistic prints by laser-induced breakdown spectroscopy. *Spectrochimica Acta Part B: Atomic Spectroscopy* **2005**, *60* (7), 1140-1148.
10. Trejos, T. Evaluation of the Evidential Value of the Elemental Composition of Glass, Ink and Paper by Laser-Based Micro-Spectrochemical Methods. **2012**.
11. Trejos, T.; Corzo, R.; Subedi, K.; Almirall, J., Characterization of toners and inkjets by laser ablation spectrochemical methods and Scanning Electron Microscopy-

Energy Dispersive X-ray Spectroscopy. *Spectrochimica Acta Part B: Atomic Spectroscopy* **2014**, 92 (0), 9-22.

12. Trejos, T.; Flores, A.; Almirall, J. R., Micro-spectrochemical analysis of document paper and gel inks by laser ablation inductively coupled plasma mass spectrometry and laser induced breakdown spectroscopy. *Spectrochimica Acta Part B: Atomic Spectroscopy* **2010**, 65 (11), 884-895.

13. Cerrai, E.; Trucco, R. *ON THE "MATRIX EFFECT" IN LASER SAMPLED SPECTROCHEMICAL ANALYSIS*; CISE, Milan: **1968**.

14. Marich, K. W.; Carr, P. W.; Treytl, W. J.; Glick, D., Effect of matrix material on laser-induced elemental spectral emission. *Analytical Chemistry* **1970**, 42 (14), 1775-1779.

15. Mohamed, W. T. Y.; Askar, A., Study of the matrix effect on the plasma characterization of heavy elements in soil sediments using LIBS with a portable Echelle spectrometer. *Progress in Physics* **2007**, 46.

16. Choi, S.-J.; Lee, K.-J.; Yoh, J. J., Quantitative laser-induced breakdown spectroscopy of standard reference materials of various categories. *Applied Physics B* **2013**, 113 (3), 379-388.

17. Theriault, G. A.; Bodensteiner, S.; Lieberman, S. H., A real-time fiber-optic LIBS probe for the in situ delineation of metals in soils. *Field Analytical Chemistry & Technology* **1998**, 2 (2), 117-125.

18. Cremers, D. A.; Multari, R. A.; Knight, A. K., Laser-induced Breakdown Spectroscopy. *Encyclopedia of Analytical Chemistry* **2000**.

19. Cremers, D. A.; Radziemski, L. J., *Handbook of Laser-induced Breakdown spectroscopy*. John Wiley: **2006**.

20. Singh, J. P.; Thakur, S. N., *Laser-induced Breakdown Spectroscopy*. Elsevier: **2007**.

21. Griem, H. R., *Principles of Plasma Spectroscopy*. Cambridge University Press: **2005**; Vol. 2.

22. ANDRZEJ W. MIZIOLEK, V. P., ISRAEL SCHECHTER, , *LASER-INDUCED BREAKDOWN SPECTROSCOPY (LIBS), Fundamentals and Applications*. Cambridge University Press: New York, **2006**.

23. Zeng, X.; Mao, S. S.; Liu, C.; Mao, X.; Greif, R.; Russo, R. E., Plasma diagnostics during laser ablation in a cavity. *Spectrochimica Acta Part B: Atomic Spectroscopy* **2003**, *58* (5), 867-877.
24. Corsi, M.; Cristoforetti, G.; Giuffrida, M.; Hidalgo, M.; Legnaioli, S.; Palleschi, V.; Salvetti, A.; Tognoni, E.; Vallebona, C., Three-dimensional analysis of laser induced plasmas in single and double pulse configuration. *Spectrochimica Acta Part B: Atomic Spectroscopy* **2004**, *59* (5), 723-735.
25. Thomas, R., *Practical guide to ICP-MS : a tutorial for beginners*. Third edition. ed.; CRC Press, Taylor & Francis Group: Boca Raton, **2013**; p xxvii, 418 pages.
26. Montaser, A., *Inductively Coupled Plasma Mass Spectrometry*. Wiley: **1998**.
27. Taylor, H. E., *Inductively Coupled Plasma-mass Spectrometry: Practices and Techniques*. Academic Press: **2001**.
28. Dawson, P. H., *Quadrupole mass spectrometry and its applications*. Elsevier: **2013**.
29. Hahn, O.; Malzer, W.; Kanngiesser, B.; Beckhoff, B., Characterization of iron- gall inks in historical manuscripts and music compositions using x- ray fluorescence spectrometry. *X-Ray Spectrometry* **2004**, *33* (4), 234-239.
30. Claybourn, M.; Ansell, M., Using Raman spectroscopy to solve crime: inks, questioned documents and fraud. *Science & Justice* **2000**, *40* (4), 261-271.
31. Giancane, G.; Valli, L.; Imperio, E., Spectral characterization of postage stamps printing inks by means of Raman spectroscopy. *Analyst* **2015**.
32. Heudt, L.; Debois, D.; Zimmerman, T. A.; Köhler, L.; Bano, F.; Partouche, F.; Duwez, A.-S.; Gilbert, B.; De Pauw, E., Raman spectroscopy and laser desorption mass spectrometry for minimal destructive forensic analysis of black and color inkjet printed documents. *Forensic Science International* **2012**, *219* (1), 64-75.
33. Hoehse, M.; Paul, A.; Gornushkin, I.; Panne, U., Multivariate classification of pigments and inks using combined Raman spectroscopy and LIBS. *Analytical and Bioanalytical Chemistry* **2012**, *402* (4), 1443-1450.
34. Kuptsov, A. H., Applications of Fourier transform Raman spectroscopy in forensic science. **1994**.
35. Vila, A.; Jawhari, T.; Garcia, J. F., A non-destructive characterization of stratigraphies in contemporary prints using micro-Raman spectroscopy. *Journal of Raman Spectroscopy* **2007**, *38* (10), 1267-1273.

36. Siegel, J.; Allison, J.; Mohr, D.; Dunn, J., The use of laser desorption/ionization mass spectrometry in the analysis of inks in questioned documents. *Talanta* **2005**, *67* (2), 425-429.
37. Maurice, S.; Wiens, R.; Saccoccio, M.; Barraclough, B.; Gasnault, O.; Forni, O.; Mangold, N.; Baratoux, D.; Bender, S.; Berger, G., The ChemCam instrument suite on the Mars Science Laboratory (MSL) rover: science objectives and mast unit description. *Space Science Reviews* **2012**, *170* (1-4), 95-166.
38. Menut, D.; Fichet, P.; Lacour, J. L.; Rivoallan, A.; Mauchien, P., Micro-laser-induced breakdown spectroscopy technique: a powerful method for performing quantitative surface mapping on conductive and nonconductive samples. *Applied Optics* **2003**, *42* (30), 6063-6071.
39. Lu, Y.; Zorba, V.; Mao, X. L.; Zheng, R. E.; Russo, R. E., UV fs-ns double-pulse laser induced breakdown spectroscopy for high spatial resolution chemical analysis. *Journal of Analytical Atomic Spectrometry* **2013**, *28* (5), 743-748.
40. Guirado, S.; Fortes, F. J.; Lazic, V.; Laserna, J. J., Chemical analysis of archeological materials in submarine environments using laser-induced breakdown spectroscopy. On-site trials in the Mediterranean Sea. *Spectrochimica Acta Part B-Atomic Spectroscopy* **2012**, *74-75*, 137-143.
41. Subedi, K.; Trejos, T.; Almirall, J., Forensic analysis of printing inks using tandem Laser Induced Breakdown Spectroscopy and Laser Ablation Inductively Coupled Plasma Mass Spectrometry. *Spectrochimica Acta Part B-Atomic Spectroscopy* **2015**, *103*, 76-83.
42. Kula, A.; Król, M.; Wietecha-Posłuszny, R.; Woźniakiewicz, M.; Kościelniak, P., Application of CE-MS to examination of black inkjet printing inks for forensic purposes. *Talanta* **2014**, *128* (0), 92-101.
43. Kula, A.; Wietecha-Posłuszny, R.; Pasionek, K.; Krol, M.; Wozniakiewicz, M.; Koscielniak, P., Application of laser induced breakdown spectroscopy to examination of writing inks for forensic purposes. *Science & Justice* **2014**, *54* (2), 118-125.
44. Dolgin, B.; Chen, Y. H.; Bulatov, V.; Schechter, I., Use of LIBS for rapid characterization of parchment. *Analytical and Bioanalytical Chemistry* **2006**, *386* (5), 1535-1541.
45. Elsherbiny, N.; Nassef, O. A., Wavelength dependence of laser induced breakdown spectroscopy (LIBS) on questioned document investigation. *Science & Justice* **2015**.

46. Lennard, C.; El-Defar, M. M.; Robertson, J., Forensic application of laser-induced breakdown spectroscopy for the discrimination of questioned documents. *Forensic Science International* **2015**, *254*, 68-79.
47. Metzinger, A.; Rajkó, R.; Galbács, G., Discrimination of paper and print types based on their laser induced breakdown spectra. *Spectrochimica Acta Part B: Atomic Spectroscopy* **2014**, *94*, 48-57.
48. Wagner, B.; Bulska, E., On the use of laser ablation inductively coupled plasma mass spectrometry for the investigation of the written heritage. *Journal of Analytical Atomic Spectrometry* **2004**, *19* (10), 1325-1329.
49. Wagner, B.; Garbos, S.; Bulska, E.; Hulanicki, A., Determination of iron and copper in old manuscripts by slurry sampling graphite furnace atomic absorption spectrometry and laser ablation inductively coupled plasma mass spectrometry. *Spectrochimica Acta Part B-Atomic Spectroscopy* **1999**, *54* (5), 797-804.
50. Chesson, L. A.; Tipple, B. J.; Barnette, J. E.; Cerling, T. E.; Ehleringer, J. R., The potential for application of ink stable isotope analysis in questioned document examination. *Science & Justice* **2015**, *55* (1), 27-33.
51. Corzo, R.; Subedi, K.; Trejos, T.; Almirall, J., Evaluation of the Forensic Utility of Scanning Electron Microscopy-Energy Dispersive Spectroscopy and Laser Ablation-Inductively Coupled Plasma-Mass Spectrometry for Printing Ink Examinations. *Journal of Forensic Sciences* **2015**, *Accepted and in Press*.
52. Szyrkowska, M.; Czerski, K.; Paryjczak, T.; Parczewski, A., Ablative analysis of black and colored toners using LA-ICP-TOF-MS for the forensic discrimination of photocopy and printer toners. *Surface and Interface Analysis* **2010**, *42* (5), 429-437.
53. Latkoczy, C.; Ghislain, T., Simultaneous LIBS and LA-ICP-MS analysis of industrial samples. *Journal of Analytical Atomic Spectrometry* **2006**, *21* (11), 1152-1160.
54. Fernandez, A.; Mao, X.; Chan, W.; Shannon, M.; Russo, R., Correlation of spectral emission intensity in the inductively coupled plasma and laser-induced plasma during laser ablation of solid samples. *Analytical Chemistry* **1995**, *67* (14), 2444-2450.
55. Kaiser, J.; Galiová, M.; Novotný, K.; Červenka, R.; Reale, L.; Novotný, J.; Liška, M.; Samek, O.; Kanický, V.; Hrdlička, A., Mapping of lead, magnesium and copper accumulation in plant tissues by laser-induced breakdown spectroscopy and laser-ablation inductively coupled plasma mass spectrometry. *Spectrochimica Acta Part B: Atomic Spectroscopy* **2009**, *64* (1), 67-73.

56. Chirinos, J. R.; Oropeza, D. D.; Gonzalez, J. J.; Hou, H. M.; Morey, M.; Zorba, V.; Russo, R. E., Simultaneous 3-dimensional elemental imaging with LIBS and LA-ICP-MS. *Journal of Analytical Atomic Spectrometry* **2014**, 29 (7), 1292-1298.
57. Leach, R., The Printing Ink Manual.: 4th Edition. In *The Printing Ink Manual*, 4th ed.; SPRINGER VERLAG GMBH: **1988**.
58. Halko, D. J., Ink additives for improved ink-jet performance. Google Patents: **1991**.
59. Montermann, W. A., Printing ink with anti-skinning agent. Google Patents: **1957**.
60. Magdassi, S., *The Chemistry of Inkjet Jets*. World Scientific Publishing Company, Incorporated: **2009**.
61. Kipphan, H., *Handbook of Print Media: Technologies and Production Methods*. Springer: **2001**.
62. Marshall, A.; Hudd, A. L., Ink composition. Google Patents: **1994**.
63. Magdassi, S., Ink requirements and formulations guidelines. *The chemistry of inkjet inks. New Jersey-London-Singapore: World Scientific* **2010**, 19-41.
64. Govindarajalu, B., In *Computer Architecture and Organization*, McGraw-Hill Education (India) Pvt Limited: **2010**.
65. Nagabhushana, S., *Lasers and Optical Instrumentation*. I.K. International Publishing House Pvt. Limited: **2010**.
66. Griffiths, A., *Prints and Printmaking: An Introduction to the History and Techniques*. University of California Press: **1996**.
67. National Research Council . Committee on Next-Generation Currency, D.; Sincerbox, G. T., In *Counterfeit Deterrent Features for the Next-Generation Currency Design*, National Academy Press: Washington, DC, **1993**.
68. Beebe, K. R., *Chemometrics: A Practical Guide*. **1998**.
69. Siegel, J., *Forensic Chemistry: Fundamentals and Applications*. Wiley: **2016**.
70. Miller, J. N.; Miller, J. C., *Statistics and Chemometrics for Analytical Chemistry*. Pearson Education: **2005**.
71. Everitt, B. S.; Landau, S.; Leese, M.; Stahl, D., *Cluster Analysis*. Wiley: **2011**.

72. Gambogi, J., Zirconium and Hafnium. In *Minerals Yearbook, 2008, V. 1, Metals and Minerals*, U.S. Government Printing Office: **2011**; pp 85-2.
73. Lehmann, U.; Stadler, U. L.; Mamak, M.; Knischka, R., Tungsten oxides as ir absorbers for nir curing, laser welding etc. Google Patents: **2014**.
74. Adel, J.; Czech, E., Finely divided blue molybdenum oxide. Google Patents: **1996**.
75. Laden, P., *Chemistry and Technology of Water Based Inks*. Springer Netherlands: **2012**.
76. Russo, R. E.; Suen, T. W.; Bol'shakov, A. A.; Yoo, J.; Sorkhabi, O.; Mao, X.; Gonzalez, J.; Oropeza, D.; Zorba, V., Laser plasma spectrochemistry. *Journal of Analytical Atomic Spectrometry* **2011**, 26 (8), 1596-1603.
77. E2927-13, A., *Standard Test Method for Determination of Trace Elements in Soda-Lime Glass Samples Using Laser Ablation Inductively Coupled Plasma Mass Spectrometry for Forensic Comparisons*. **2013**; Vol. 14.02.

VITA

KIRAN SUBEDI
Born in Nepal, Pokhara

Email: ksube001@fiu.edu, keasans@gmail.com

EDUCATION

- Masters in Physical Chemistry from Tribhuvan University, Nepal, 2009
- Presidential Fellowship at Florida International University, 2011
- Doctoral Candidate in Chemistry with a Forensic Track (2011- Present), at Florida International University, Miami, Florida, USA
- Best Oral Presentation in LIBS at SCIX, Nevada, Reno, 2014
- Best Scientific Exhibition Award at World Forensic Festival (IAFS), South Korea, 2014
- Dissertation Year Fellowship at Florida International University, 2015

PRESENTATIONS AND PUBLICATIONS

1. Kiran Subedi, Tatiana Trejos, Jose Almirall (01/06/2014-01/11/2014), “Forensic analysis of printing inks using tandem LIBS and LA-ICP-MS” Poster session presented at Winter Plasma Conference, Amelia Island, Florida, USA.
2. Trejos, T.; Corzo, R.; Subedi, K.; Almirall, J., Characterization of toners and inkjets by laser ablation spectrochemical methods and Scanning Electron Microscopy-Energy Dispersive X-ray Spectroscopy. *Spectrochimica Acta Part B: Atomic Spectroscopy* 2014, 92, 9-22.
3. Kiran Subedi, Tatiana Trejos, Jose Almirall (09/27/2014-10/02/2014), “Application of tandem LIBS/LA-ICP-MS for the analysis of printing inks using multivariate statistical tools and data fusion.” (Best Oral Presentation in LIBS at SCIX, Nevada, Reno).
4. Kiran Subedi, Tatiana Trejos, Jose Almirall (10/12/2014-10/18/2014), “Application of tandem LIBS/LA-ICP-MS for the forensic analysis of printing

inks”. Poster session presented at World Forensic Festival (IAFS), Seoul, South Korea. (Best Scientific Exhibition Award).

5. Kiran Subedi, Tatiana Trejos, Jose Almirall (01/22/2015-01/25/2015), “A study on the effect of document contamination from handling in the forensic analysis of printing inks using tandem LIBS/LA-ICP-MS.” Poster session presented at American Society for Mass Spectrometry (ASMS), Hilton Clearwater Beach, Florida.
6. Subedi, K.; Trejos, T.; Almirall, J., Forensic analysis of printing inks using tandem LIBS and LA-ICP-MS. *Spectrochimica Acta Part B: Atomic Spectroscopy* 2015, *103*, 76-83.
7. Corzo, R.; Subedi, K.; Almirall, J., Evaluation of the Forensic Utility of Scanning Electron Microscopy-Energy Dispersive Spectroscopy and Laser Ablation-Inductively Coupled Plasma-Mass Spectrometry for Printing Ink Examinations, *Journal of Forensic Sciences* (In Press).
8. Trejos, T.; Torrión P.; Corzo, R.; Raeva A.; Subedi, K.; Williamson R.; Yoo, J.; Almirall, J., A novel forensic tool for the characterization and comparison of printing ink evidence: development and evaluation of a searchable database using data fusion of spectrochemical methods, *Journal of Forensic Sciences* (In Press).